SWITCHABLE ASSEMBLY OF STABLE ORDERED MOLECULAR LAYERS:
TOWARDS A REVERSIBLE BIOSENSOR PLATFORM

Dem Fachbereich Chemie der Universität Dortmund

zur Erlangung des akademischen Grades eines

Doktor der Naturwissenschaften

(Dr. rer. Nat.)

vorgelegte Dissertation

von:

M. Sc. Ravindra R. Deshmukh

Geboren am 11.09.1975

In Jalana, Indien

Betreuer: Priv. Doz. Dr. Börje Sellergren

Koreferrent: Univ.-Prof. Dr. Roland Winter

Universität Dortmund, Institut für Umweltforschung

March 2006

ACKNOWLEDGMENTS

I take this opportunity to convey my deepest sense of gratitude to all those who helped me in my thesis work.

First and foremost, I would like to thank my supervisor, *PD Dr. Börje Sellergren* for giving me the opportunity to work in the field of *Self-Assembled Monolayers* (SAMs) and for constant support and guidance throughout this work.

I also thank *Prof. Dr. Michael Spiteller*, Head, INFU, for the nice atmosphere and working environment during this thesis work.

I would like to thank *Dr. Andrew J. Hall*, *Dr. Eric Schillinger, Dr. Marco Emgenbroich* and *Dr. Francesca Lanza-Sellergren* for creative guidance, invaluable help and friendly discussions during the work. Very special thanks to *Dr. Jeroen Verhage* (specially for the crate of Hövels, which has driven me to finish my thesis in time!!!!) for helpful discussions and constructive suggestions during thesis writing.

My special thanks to *Dr. F. Katzenberg* for contact angle measurements, *Dr. J. Baranski, and Dr. Ioana Pera* for Atomic Force Microscopy measurements and *Robert Stonies* for gold evaporations.

I would like to thank especially all the members of Sellergren group (present and former) featuring in no particular order as such, *Dr. Sandra Pati*, Dr. *Panagiotis Manesiotis, Dr. Maria-Magdalena Titirici, Dr. Yasumasa Kenekiyo, Carla Aureliano, Filipe Vilela, Cristiana Borrelli, Issam Lazraq, Bettina Hofmann, Kim Schwarzkopf, Anupkumar,* for nice working atmosphere and for their wonderful advices and support during my stay in the group.

I would like to thank my teachers *Prof. M.N. Deshpande, Dr. R. J. Lahoti, Dr. K.V. Srinivisan, Dr. U. R. Kalkote and Dr. S.R Bhusare* for their helpful guidance during my early stages of the research work.

Last but definitely not the least; I owe my immense gratitude to my parents for their continuous support, blessings and their encouragement throughout my research work.

Table of contents

1 Zusammenfassung

In dieser Doktorarbeit wird das Design, die Synthese und die schrittweise Konstruktion von Self-Assembled Monolayers (selbstorganisierte Monoschichten, SAMs) *via* nicht-kovalenten Interaktionen auf Goldoberflächen beschrieben. Diese SAMs sind nützlich zur Konstruktion einer Biosensor Plattform.

Molekülen interagieren mit anderen Molekülen durch schwache Wechselwirkungen (0.1-5 kcal mol^{-1}), sowie Wasserstoffbrücken, Van-der-Waals-Kräfte, oder Dispersionskräfte. Diese sind zusammen bekannt als 'nicht-kovalente' Interaktionen. Solche Interaktionen spielen eine wichtige Rolle in fundamentalen biologischen Prozessen, wie z.B. der Faltung von Proteinen oder des Expression von Genen und deren Transskription.

Der Hauptteil dieser Arbeit beschäftigt sich mit der Konstruktion einer reversibelen Version eines Biosensor- Chips durch nicht-kovalente Interaktionen. Zu Beginn ist demonstriert, wie α,ω-bis(4-amidinophenoxy)alkane reversibele mono-und doppelschichten auf Thiol-SAM's, welche carboxyl-funktionalisiert wurden, auf Gold bilden. Zur Erweiterung des Repertoires frei liegenden Gruppen auf den amphiphylen SAMs, haben wir eine Serie von ω-funktionalisierten α-(4-amidinophenoxy)alkan Amphiphylen hergestellt. Anschließend haben wir die Formation von Monoschichten auf Mercaptohexadecansäure (MHA) funktionalisierten SAMs auf Goldoberflächen beobachtet.

Die Kopfgruppeninteraktionen zwischen der negativ geladenen Carboxylat-Oberfläche (Protonen Akzeptor) und den positiv geladenen Amidinium-Amphiphylen (Protonen Donor) bilden bei alkalischem pH Wert (pH 9) ein gezieltes, zyklisches und stabiles Netzwerk von Wasserstoffbrücken.

Da diese Selbstorganisationen durch den pH bestimmt werden, wollten wir die Originaloberfläche mit Säuregruppen durch Änderung des pH-Wertes zurück bekommen. Hierbei haben wir beobachtet, dass bei einer Senkung des pHs von pH 9 zu pH 3 die amphiphyle Schicht komplett von der Carboxylat-Oberfläche abgerissen wird. Die Reversibilität der Sensorplatform ist also erreicht.

Desweiteren haben wir beobachtet dass die Schichtdicke bei Senkung des pH-Werts abnimmt. Dies entspricht dem Grad der Ionisierung der Carboxylgruppen auf der Goldoberfläche.

Die Regeneration der Oberfläche kann also durch Änderung des pH-Werts erreicht werden. Eine verschmutzte Oberfläche kann einfach durch Senkung des pH Werts weggewaschen werden und neu gebildet werden.

Die direkte Formation der Amphiphyl Schicht auf der Oberfläche und die Deformation dieser Schicht wurde mit *in situ*-Ellipsometry beobachtet. Es gibt Übereinstimmung zwischen der beobachteten Schichtdicke und der maximalen Schichtdicke. Dies deutet auf eine dicht-gepackte Monoschicht auf der COOH-Oberfläche hin. Um mehr Informationen über die Schichtdicke zu bekommen wurden Luft-Ellipsometrie- und Rasterkraft-Mikroskopie- (AFM) Experimente durchgeführt. Die Resultate waren in Übereinstimmung mit den *in situ*-Ellipsometrie-Experimenten.

Reflexions-Absorptions-Infrarot-Spektroskopie (RAIR) Experimente von Ein-Komponenten- und Zwei-Komponenten- Amphiphylschichten zeigten die charakteristischen Peaks aller funktionellen Gruppen in den selbst-organisierten Monoschichten. Das RAIR Experiment war in Übereinstimmung mit dem Transmissionsspektrum, was auf die Anwesenheit der amphiphylen Schicht auf dem COOH SAM deutet.

Die asymmetrische CH_2-Streckungsspitze bei 2917 cm^{-1}, die in nahezu allen amphiphylen Schichten beobachtet wurde, deutet auf die Anwesenheit einer kristallinen und geordneten amphiphylen Schicht.

Kontaktwinkel-Experimente zeigten, dass hydrophobe Oberflächen geformt werden. Die zuerst hydrophile Oberfläche (KW = 10° ± 5°) wird umgewandelt in eine weniger hydrophobe Oberfläche durch Selbst-Assemblierung des ω-funktionalisierten α-4-amidinophenoxy)alkan-Amphiphyls in acht Schritten.

Der wichtigste Teil dieser Dissertation beschreibt die Konstruktion der "schaltbaren Assemblierung stabiler und geordneter molekularer Schichten, hin zu reversibelen Biosensor-Plattformen".

Das ω-Biotin funktionalisierte Amphiphyl war auf der Schicht mit Carboxylsäure Kopfgruppen selbstorganisiert. Anschließend wurde Streptavidin (SA) auf der Biotin-Oberfläche immobilisiert um die Biosensor-Aktivität zu bestimmen. Eine sehr geringe Konzentration von Streptavidin (500 nM) konnte mit Luft-Ellipsometrie und RAIR Spektroskopie noch nachgewiesen werden. Basierend auf RAIR Spektren vor und nach Protein-Adsorption und Waschen mit Boratpuffer (pH 9) wird gezeigt, dass die ω-Biotin funktionalisierten Amphiphyl-Schichten beim Streptavidin Austausch stabil sind. Sowohl eine kristalline Struktur wurde in der Schicht wahrgenommen, als auch die Anwesenheit der Amid I -und Amid II- Banden des Streptavidins.

Zur Erhaltung einer maximalen Anzahl von Biotingruppen auf der Oberfläche und zur Minimierung nicht-spezifischer Adsorption des Streptavidins, wurde das ω-Biotin funktionalisierte Amphiphyl verdünnt mit ω-hydroxyl funktionalisierten SAMs.

Eine maximale Bindung von Streptavidin (47 Å ± 4 Å) wurde bei einem Gehalt von 25% Biotin erhalten. Bei einem steigenden Gehalt von Biotin wurde eine Abnahme der Schichtdicke des Streptavidin beobachtet.

Die beobachtete Schichtdicke der Proteinmoleküle auf einem Hydroxyl-terminierten SAM, einebloßen Goldschicht und einem MHA terminierten SAM zeigt, dass die nicht-spezifische Bindung von Streptavidin unerheblich war.

Eine Senkung des pH-Wertes auf der Oberfläche ergibt das Säure funktionalisierte SAM auf der Goldoberfläche, welches erneut benutzt werden kann für neue Experimente.

2 Summary

In this thesis are described the design, synthesis and stepwise construction of reversible versions of self-assembled monolayers (SAMs) on gold surfaces via non-covalent interactions and subsequent use of this system for the construction of biosensor platforms.

Molecules can interact with other molecules through weak interactions (0.1 - 5 kcal mol^{-1}), such as hydrogen bonding, van der Waals, or dispersive forces, which are collectively known as *non-covalent* interactions. Such interactions play a key role in fundamental biological processes, such as protein folding or the expression and transfer of genetic information.

Throughout this work, the main efforts were focused towards the construction of a reversible version of biosensor chips via *non-covalent* interactions. Previously we have demonstrated that *α,ω*-bis(4-amidinophenoxy)alkanes reversibly form mono and bi-layers on carboxylic acid functionalized thiol SAMs on gold. In order to extend the repertoire of exposed head groups in the amphiphilic SAMs, we have synthesized a series of *ω*-functionalized *α*-(4-amidinophenoxy)alkane amphiphiles and studied their monolayer formation on mercaptohexadecanoic acid (MHA) functionalized SAMs on gold surfaces.

The head group interactions between the negatively charged carboxylate surfaces (COO^{-}, proton acceptor) and positively charged amidinium amphiphiles (proton donor) leading to the cyclic, directed, and stable hydrogen-bonded network was driven by a basic (pH 9) borate buffer.

As these assemblies were pH driven, we thought to reconstruct the original acid functionalized sensor platform by changing the pH. Hence, by lowering the pH of the surrounding medium of the system form the original pH 9 to pH 3, the amphiphilic layer was completely removed from the acid surface and a reversible version of a sensor platform was achieved. We have also observed that the layer thickness decreases with decreasing pH in a manner reflecting the degree of ionization of the carboxylic acid groups on the gold surfaces.

The pH switching ability of these formed amphiphiles leads to the regeneration of a single sensor surface upon fouling.

The live formation and disassembly of the amphiphilic assembly on the acid terminated SAMs was studied using *in situ* ellipsometry. The agreement between the observed layer thicknesses upon addition of the corresponding amphiphiles and the maximum length (estimated length) of the molecules suggests that the amphiphiles form closely packed monolayers on the carboxylate surfaces. To obtain more information on the layer thickness, air ellipsometry and atomic force microscopy were performed and the results were corroborated with those obtained from *in situ* ellipsometry.

Infrared Reflection Absorption Spectroscopy (IRAS) study of single component and mixed component amphiphilic layers showed that the characteristic peaks for all functionalities in the SAMs were comparative to their transmission spectrum (KBr pellets) indicating the presence of the amphiphilic layers on the acid terminated SAMs. In almost all spectra, the CH_2 asymmetric stretch at ~ 2917 cm^{-1} of the assembled SAMs on the acid surfaces shows the presence of a crystalline and ordered amphiphilic layer. The wetting properties of the surfaces were characterized by contact angle (CA) measurements. The less hydrophobic surfaces was obtained by converting original ω-functionalized acid surfaces (CA ~10°, ±5°) into ω-functionalized α-(4-amidinophenoxy)alkane amphiphile surfaces (CA ~70-75°, ±5°) by self-assembly.

The most important part of this thesis describes the stepwise construction of the "*switchable assembly of stable, ordered molecular layers: Towards a reversible biosensor platform*". To achieve this, we have synthesized an ω-functionalized biotinylated amphiphile in a total of eight steps.

The ω-biotin functionalized amphiphile was subjected to monolayer formation on acid terminated SAMs. Onto these self-assembled layers, streptavidin (**SA**) was immobilized to detect the biosensor activity. A very low concentration of **SA** (**500 nM**) was detected using air ellipsometry and IRAS. Based on the IRAS spectra recorded after protein adsorption and rinsing of the surfaces with borate buffer

pH 9, the ω-biotin functionalized amphiphilic layer appeared stable with respect to protein (**SA**) exchange.

Furthermore, the crystalline-like nature of the layer and the presence of amide I and amide II bands of the added protein in SAMs were detected.

To maximize surface density of the biotin-terminated amphiphile for the selective recognition of protein **SA**, and to minimize the non-specific adsorption of the protein, the ω- biotin functionalized amphiphile was diluted with ω-hydroxy terminated SAMs.

We also observed a maximum binding of streptavidin (47 ±4 Å) at a biotin content of 25%, with a gradual decrease in the thickness of the adsorbed **SA** film as the composition of biotin was increased.

The obtained layer thicknesses of the protein **SA** molecule on hydroxy terminated SAMs, on bare gold and on MHA terminated SAMs showed that non-specific binding of **SA** was negligible.

The acidification of the above surfaces yields the acid functionalized (MHA) SAMs on the gold surface, which in return can be *reused* for subsequent measurements.

3 Introduction

3.1 *Self-assembled monolayers*

One of the most exciting aspects of thin organic films is the interdisciplinary nature of the area, forming bridges between the fields of physics, chemistry and biology. The most common methods for forming supported organic films are the **Langmuir-Blodgett** and **self-assembly techniques,** with their primary difference being that they produce physisorbed and chemisorbed monolayars, respectively.

Self-assembly is a tremendously useful technique that is found in almost every area of molecular science. Examples of natural systems that self-assemble include single stranded DNA that self-assembles into duplexes, phospholipids that self-assemble into lipid bilayers and long chains of amino acids that self-assemble into proteins with a defined three-dimensional shape.

Molecules can interact with other molecules through weak interactions (0.1 - 5 kcal mol^{-1}), such as hydrogen bonding, van der Waals, or dispersive forces, which are collectively known as *non-covalent* interactions. Such interactions play a key role in fundamental biological processes, such as protein folding or the expression and transfer of genetic information. Especially, H-bonds have an enormous impact on our daily life.

Self-assembled monolayers (SAMs) are molecular assemblies that are formed spontaneously by the immersion of an appropriate substrate into a solution of an active surfactant in an organic solvent [1, 2]. There are several types of SA methods that yield organic monolayers. These include the addition of organosilanes to hydroxylated surfaces (SiO_2 on Si, Al_2O_3 on Al, glass, etc.) [3- 14], alkanethiols to gold [15-23], silver [24] and copper [25-27], dialkyl sulfides to gold [28], dialkyl disulfides to gold [29], alcohols and amines to platinum [28], and carboxylic acids to aluminum oxide [30-32] and silver [33].

From an energetic viewpoint, a self-assembling surfactant molecule can be divided into three parts (Figure 3.1). The first part is the head group, which provides the most exothermic process, i.e., chemisorption on the substrate surface. The very strong molecular-substrate interactions result in an apparent pinning of the head group to a specific site on the surface through a chemical bond. This can be a covalent Si-O bond in the case of alkyltrichlorosilanes on hydroxylated surfaces; a covalent, slightly polar, Au-S bond in the case of alkanethiols on gold; or an ionic $-CO_2^-$ Ag^+ bond in the case of carboxylic acids on AgO/Ag. As a result of the exothermic head group-substrate interactions, molecules try to occupy every available binding site on the surface and, in this process; they push away molecules that have already adsorbed leading to the formation of crystalline molecular assemblies.

Interchain van der Waals and electrostatic interactions

Surface group

Alkyl or derivatized alkyl group

Surface active headgroup

Chemisorption at the surface

Surface
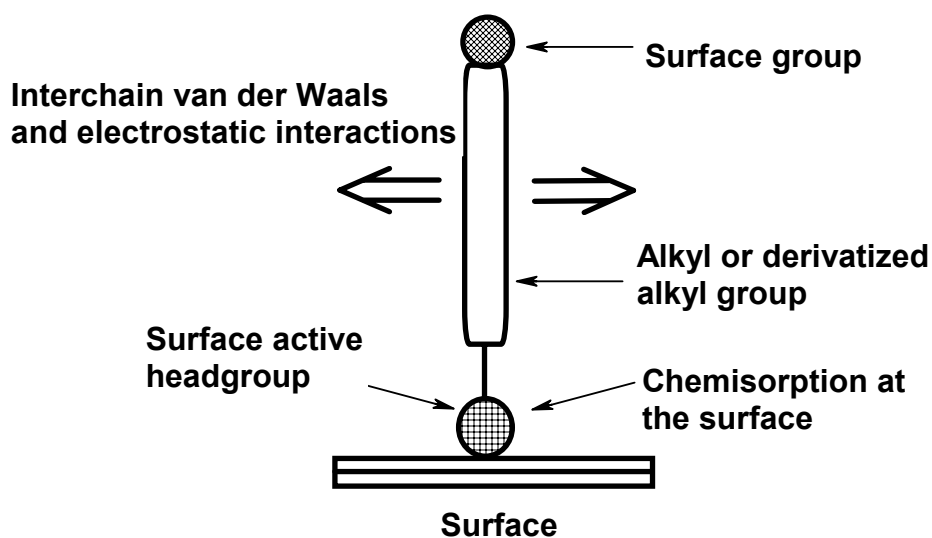
Figure 3.1: A Schematic view of the forces in a self-assembled monolayer.

The second molecular part is the alkyl chain, the first and most important process in the formation of SAMs is *chemisorption.* Only after molecules are put in place on the surface can formation of an ordered and closely packed assembly begin. Van der Waals interactions are the main forces in the case of the simple alkyl chains. On the other hand, when a polar bulky group is substituted into the alkyl

chain, there are also long-range electrostatic interactions that, in some cases, are energetically more important than the Van der Waals attractions.

The third part is the terminal functionality, which, in the case of a simple alkyl chain, is a methyl (CH_3) group. These surface groups are thermally disorderd at room temperature, as is apparent from helium diffraction [25] and FTIR studies [34] in the case of methyl terminated monolayers, and from surface reorganization studies in the case of hydroxyl terminated monolayers [35].

The term *order* is used to describe molecular assemblies with translational symmetry, i.e., a two-dimensional crystalline-like monolayer. The term "close packing" is usually associated with the density of crystalline poly(ethylene).

In the field of self-assembly, the structure and bonding of organic molecules adsorbed to metal surfaces may be investigated using different surface sensitive techniques such as Infrared Reflection Absorption Spectroscopy (**IRAS**), Contact angle measurements, atomic force microscopy (AFM), ellipsometry, surface plasmon resonance (SPR), Neutron reflectativity, and cyclic voltametry (CV) are the few techniques which surface chemist uses in laboratory to analyze the surfaces.

SAMs of functionalized alkanethiols on gold surfaces hold great promise for applications in several different areas. Some examples of suggested and implemented applications are molecular recognition, SAMs as model substrates and biomembrane mimetics in studies of biomolecules at surfaces, selective binding of enzymes to surfaces, chemical force microscopy, metallization of organic materials, corrosion protection, molecular crystal growth, alignment of liquid crystals, pH-sensing devices, patterned surfaces on the μm scale, electrically conducting molecular wires and photoresists.

References

[1] Bigelow, W. C., Pickett, D. L., Zisman, W. A., *J. Colloid Interface Sci.* **1946,** 1, 513.

[2] Zisman, W. A., *Adv. Chem. Ser.* **1964,** 43, 1 .

[3] Sagiv, J., *J. Am. Chem. Soc.* **1980,** 102, 92.

[4] Maoz, R., Sagiv J., *J. Colloid Interface Sci.* **1984,** 100, 465

[5] Gun, J., Iscovici, R., Sagiv J., *J. Colloid Interface Sci.* **1984,** 101, 201

[6] Gun, J., Sagiv, J., *J. Colloid Interface Sci.* **1986,** 112, 457.

[7] Finklea, H. O., Robinson, L. R., Blackburn, A., Richter, B., Allara, D., Bright, T., *Langmuir* **1986,** 2, 239.

[8] Cohen, S R., Naaman, R., Sagiv, J., *J. Phys. Chem.* **1986,** 90, 3054.

[9] Maoz, R., Sagiv, J., *Thin Solid Films* **1985,** 132, 135.

[10] Maoz, R., Sagiv, J., *Langmuir* **1987,** 3, 1045.

[11] Netzer, L., Iscovici, R., Sagiv, J., *Thin Solid Films* **1983,** 99, 235.

[12] Netzer, L., Sagiv., J. *J. Am. Chem. Soc.* **1983,** 105, 674.

[13] Tillman, N., Ulman, A., Schildkraut, J. S., Penner, T. L., *J. Am. Chem. Soc.* **1988,** 111, 6136.

[14] Tillman, N., Ulman, A., Penner, T. L., *Langmuir* **1989,** 5, 101.

[15] Bain, C. D., Troughton, E. B., Tao, Y., Evall, J., Whitesides, G. M., Nuzzo, R. G., *J. Am. Chem. Soc.* **1989,** 111, 321.

[16] Porter, M. D., Bright, T. B., Allara, D. L,, Chidsey, C. E. D., *J. Am. Chem. Soc.* **1987,** 109, 3559.

[17] Nuzzo, R. G., Dubois, L. H., Allara, D. L., *J. Am. Chem. Soc.* **1990,** 112, 558.

[18] Rubinstein, I., Steinberg, S., Tor, Y., Shanzer, A., Sagiv, J., *Nature* **1988,** 332, 426.

[19] Whitesides, G. M., Laibinis, P. E., *Langmuir* **1990,** 6, 87.

[20] Chidsey, C. E. D., Loiacono, D. N., *Langmuir* **1990,** 6, 709.

[21] Chidsey, C. E. D., Liu, G. Y., Rowntree, P., Scoles, G., *J. Chem. Phys.* **1989,** 91, 4421.

[22] Bain, C. D., Whitesides, G. M., *J. Am. Chem. Soc.* **1989,** 111, 7164.

[23] Strong, L., Whitesides, G. M., *Langmuir* **1988,** 4, 546.

[24] Ulman, A., *J. Mat. Ed.* **1989,** 11, 205.

[25] Stewart. K. R., Whitesides, G. M., Godfried, H. P., Silvera, I. F., *Surf. Sci.* **1986,** 57, 1381.

[26] Blackman, L. C. F., Dewar, M. J. S., *J. Che,. Soc.* **1957,** 171.

[27] Blackman, L. C. F., Dewar, M. J. S., Hampson, H., *J. Appl. Chem.* **1957,** 7, 160.

[28] Troughton, E. B., Bain, C. D., Whitesides, G. M., Nuzzo, R. G., Allara, D. L., Porter, M. D., *Langmuir* **1988,** 4, 365.

[29] Nuzzo, R. G., Fusco, F. A., Allara, D. L., *J. Am. Chem. Soc.* **1987,** 109, 2358.

[30] Allara, D. L., Nuzzo, R. G., *Langmuir* **1985,** 1, 45.

[31] Allara, D. L., Nuzzo, R. G., *Langmuir* **1985,** 1, 52.

[32] Ogawa, H., Chihera, T., Taya, K., *J. Am. Chem. Soc.* **1985,** 107, 1365.

[33] Schlotter, N. E., Porter, M. D., Bright, T. B., Allara, D. L., *Chem. Phys. Lett.* **1986,** 132, 93.

[34] Nuzzo, R. G., Kprenic, E. M., Dubois, L. H., *J. Chem. Phys.* **1990,** 93, 767.

[35] Evans, S. D., Ulman, A., Sharma, R., *Langmuir* **1991,** 7, 15.

3.2 Preparation of gold surfaces

From an experimental point of view, gold is among the easiest of materials to use as a substrate. Unlike many other metals, gold does not readily oxidize or contaminate upon exposure to the atmosphere. Gold films can be handled with a minimal amount of precautions and do not require specialized facilities, such as clean rooms. For example, gold films that have been exposed to the variety of airborne contaminants found in a typical organic chemistry laboratory can reused. High quality SAMs can be routinely obtained, as thiols and disulfides displace these weakly adsorbed materials during the assembly of the SAM.

The most commonly employed method for generating gold surfaces is the evaporation of gold onto a relatively flat substrate to produce a thin film (~ 1000 to 2000 Å). Such preparations are conducted within a vacuum chamber that is capable of achieving a pressure less than 10^{-6} torr. The passage of an electrical current through a metal target is used to heat the gold to a temperature where the source material evaporates and deposits onto the substrates (the evaporation rate in our case was 0.3 nm/s). Generally this procedure is accomplished either by applying a voltage across a tungsten filament that supports the source material or by applying an electron beam directly to the material. The evaporation system shown in Figure 3.2 is a common apparatus in materials science, physics and electrical engineering departments, and gold is one of the easier materials to evaporate in such systems. Particular advantages of this procedure are that one can generate gold surfaces of relatively large areas (> 100 cm^2) inexpensively and that the resulting gold films are extremely pure. We have used glass substrates because they are relatively flat. As the level of adhesion between the deposited gold film and the glass support is relatively weak; a 20 nm layer of chromium was used to enhance the adhesion. A requirement for adhesion by these materials is that the vacuum is maintained between evaporation of the adhesion layer and the gold; this procedure requires that the evaporation chamber contains two individually addressable evaporation sources.
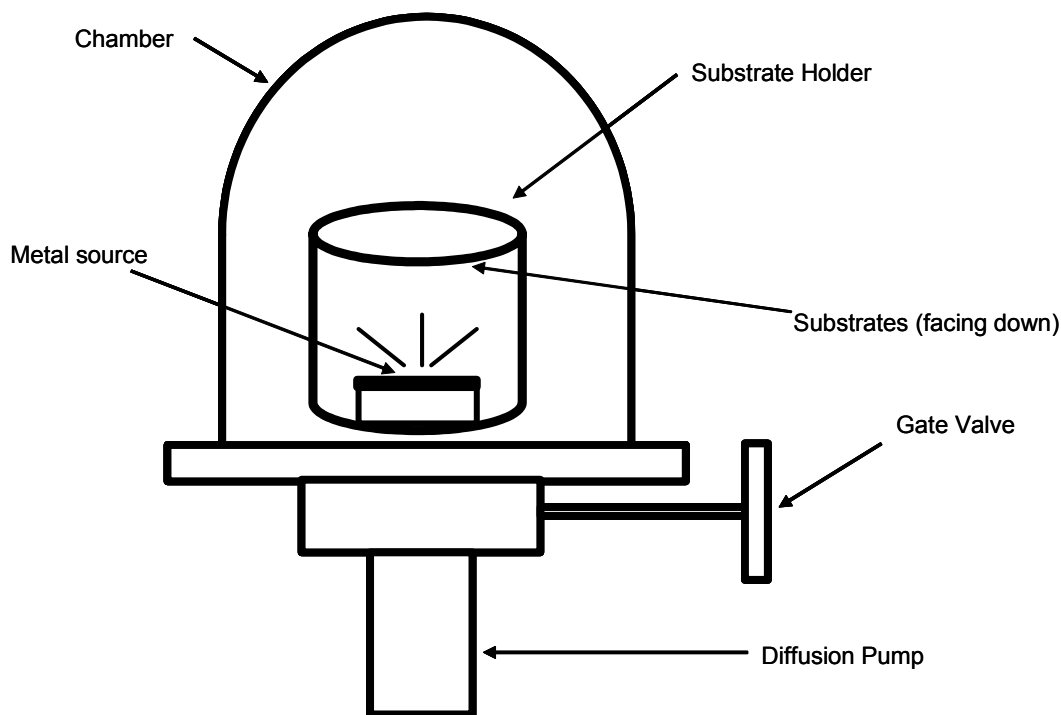
Figure 3.2: Schematic illustration of a typical evaporation system used for the preparation of gold substrates.

Nuzzo *et al.* [1] showed that gold layers prepared by evaporation at room temperature are polycrystalline and have a predominately (111) texture. An increasingly popular substrate in these studies is an epitaxial gold layer supported on mica. [2]. Mica has a layered structure and the act of simply peeling apart the mica sheets can reveal large surface areas that are atomically flat. The crystallinity and morphology of the gold films that form on mica are dependent on the temperature of the mica during the deposition [3]. For example, gold evaporated onto mica held at room temperature contains Au(111) crystallites that are ~ 50 nm in diameter; this structure is essentially identical to that which forms when gold is evaporated at room temperature onto glass substrates.
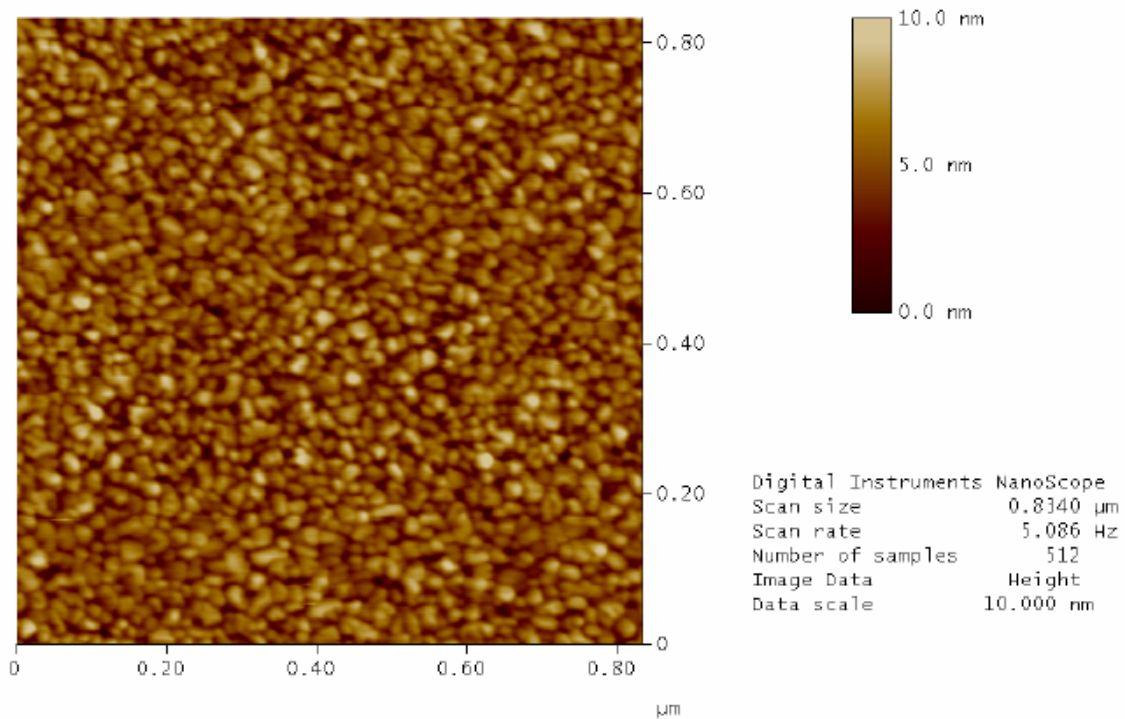
Figure 3.3: Topographic image of a gold surface obtained using atomic force microscopy. The gold surface was prepared by the sequential evaporation of 20 Å of chromium and 1000 Å of gold onto a freshly cleaved mica surface at room temperature.

3.3 Synthesis of self-assembled monolayers of alkanethiols

Sulfur and selenium compounds have a strong affinity to transition metal surfaces. This is probably because of the possibility to form multiple bonds with surface metal clusters. The number of reported surface active organosulfur compounds that form monolayers on gold has increased in recent years. The most studied, and probably most understood SAM is that of alkanethiolates on Au(111) surfaces.

For the study of surface properties, SAMs must fulfil the following requirements: 1) to be strongly attached to the substrate and, therefore, chemically and thermally stable, (2) to be homogeneous and closely packed, and (3) to allow a diverse range of surface functional groups to be present. Alkanethiols readily give **homogeneous, ordered,** and **chemically** and **mechanically** stable SAMs and hence provide an excellent model system for study.

During the last two decades, much progress has been made in the preparation of self-assembled monolayers on different substrates. The greatest operational challenge that the materials' chemist faces in this research area is often in accessing the molecular precursors needed for preparing the chemically diverse surfaces available by the assembly of thiols onto gold. The commercially available thiols are primarily limited to unsubstituted short-chained alkanethiols $(CH_3(CH_2)_nSH$; n=0 to 8) and unsubstituted long-chained alkanethiols $(CH_3(CH_2)_{2n-1}SH$; n=5 to 9) that produce low-energy methyl surfaces. Short-chained alkanethiols $(HS(CH_2)_nX$; n=1,2 for X=COOH, CO_2CH_3, $CO_2CH_2CH_3$ and n=2 for X=NH$_2$ and OH) and related disulfides, which may not form highly organized structures due to limited interchain packing, various aromatic thiols that achieve limited intermolecular packing on the surfaces and $α,ω$-alkanedithiols $(HS(CH_2)_nSH$; n=2 to 9) that form disorganized films comprising structures with one or both thiols adsorbed to the gold surface. Biological species, such as lipoic acid, cysteine, and dithiothreitol provide commercially available materials for derivatizing the gold surface with thiols that contain polar functionalities.

Porter *et al.* [4] reported that, the formation of densely packed, crystalline hydrocarbon monolayers requires the use of alkanethiols with typically greater than twelve methylene units and a tail group that is smaller than the cross-sectional area of the polymethylene chain. Bulky tail groups, although increasingly popular for synthetic reasons, would not be expected to form the highly organized, densely packed assemblies associated with the assembly of longer-chained alkanethiols. Their primary role is to provide a point of attachment to the gold surface via chemisorption processes and their level of organization depends greatly on the nature and packing abilities of the species extending away from the surface.

In the literature, the types of organosulfur compounds that have been adsorbed onto gold exhibit a broad diversity. For many of these compounds, they can be grouped into categories based on their skeleton (alkyl or aromatic groups), types of substitution (small, bulky, electroactive, etc.), and associated properties (crystalline packing, polymerizable, reactive, etc.). The following section provides an overview of the chemical structures that have been assembled onto gold along with a discussion of their properties and utility.

Because of their high level of packing, *n*-Alkanethiols containing small terminal groups enable the formation of densely packed, often crystalline, self-assembled monolayers on gold. Such films are useful in studying barrier properties [5] friction [6], adsorption [7, 8], multilayer formation [9-14], and wetting phenomena [15-18]. Examples of the terminal moieties in this category include CH_3, OH, COOH, $CONH_2$, and CO_2CH_3, where the cross-sectional diameter of the tail group is smaller than that for the polymethylene chain (~ 20 Å) [19] and its size should not interfere with the packing of the hydrocarbon chains. With these tail groups, the monolayer expresses a two-dimensional sheet of homogeneous organic functionality at its exposed surface. These surfaces provide useful models for fundamental studies of organic systems such as polymers, as a detailed understanding of their surface chemistry is complicated by their heterogeneity, both in terms of composition and structure.

In our previous reports for the formation of well ordered acid functionalized SAMs, we have observed that not all alkanethiols assemble onto gold and form highly organized assemblies [20]. In addition to the requirement that the tail group size not interfere with the packing of the hydrocarbon chains, the length of the hydrocarbon chain also plays a role in structuring the assembly [20]. Using complementary techniques, Porter *et al.* determined that shorter-chained assemblies ($HS(CH_2)_nCH_3$; n ≤ 11) are more disordered than longer chained alkanethiolate monolayers (n ≥ 15) [4]. The longer-chained thiols form a fully extended, trans zigzag structure on gold with the hydrocarbons tilted at an angle of ~ 30° from the surface normal which is shown in the Figure 3.4
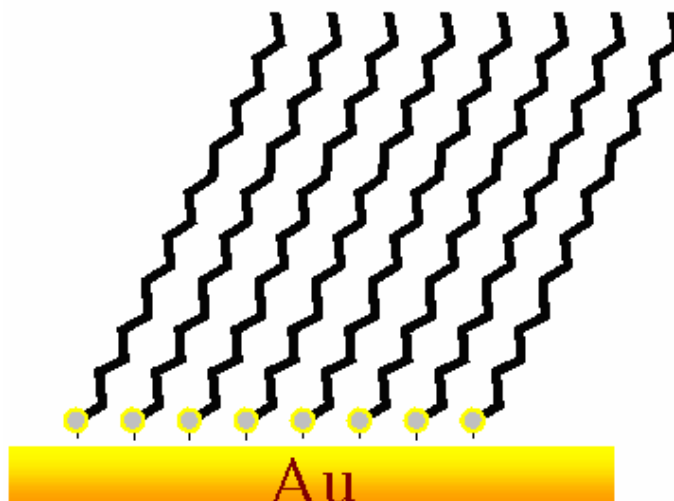
Figure 3.4: Self-assembled monolayers of octadecanethiol on gold surface.

For the shorter-chained thiols, the level of interchain attraction is lower and diminishes the degree of order for these assemblies. These systems are still highly organized but contain a greater density of gauche conformers than those prepared from longer-chained adsorbates.

The ability to tailor the exposed surface of the monolayer by selection of the tail group on the alkanethiol provides great advantages in the studies of various interfacial properties such as wetting, friction, adhesion, and adsorption. For example, monolayers formed from $HS(CH_2)_{15}X$ generate a surface with **high** (X= COOH), *intermediate* (X= OCH_3), or *low* (X= CH_3) energy surface, with free energies that depend on the chemical constituency of the terminal group [18, 21]. In this straightforward manner, surfaces with varying surface energies may be produced by appropriate choice of terminal group. The alkyl-based monolayers are extremely convenient systems for producing such structures because a diverse collection of tail groups can be incorporated synthetically into the alkyl framework with relative ease. The following section explores the diversity of tail groups that have been expressed at the surface of monolayers supported on gold and focuses on the relationship between molecular structure and surface free energy, as determined from wetting measurements.

3.4 Terminal groups that produce high energy surfaces

The thiols-on-gold methodology is perhaps the most versatile system of self-assembled monolayers, as it offers the ability to form high-energy surfaces with relative simplicity. The only constraints are that the tail groups do not interact strongly with the gold substrate or react with thiols [18]. The assembly of alkanethiols can lead to surfaces that expose OH, COOH, $CONH_2$, $B(OH)_2$, and PO_3H_2 groups which are all wetted by water. The wetting properties for above surfaces formed by the assembly of thiols onto gold were reported previously and they are summarized in Table 3.1 [θ (H_2O) < 15°].

Polar terminal groups can provide reactive sites for further derivatization of a monolayer surface. The formation of multilayer structures on surfaces terminating in carboxylic acids [9, 12], phosphonic acids [10, 11], and alcohols [13, 23-24] have been well described. In addition, OH, COOH, and NH_2 surfaces can provide anchoring sites for the covalent immobilization of various molecules.

3.5 Terminal groups that produce surfaces with intermediate energies

Alkanethiols terminating with halogens [18], nitriles [5], and ether groups [18, 16] produce SAMs with intermediate surface energies. Despite the polarities associated with these functionalities, these surfaces are much less hydrophilic than those that contain hydrogen bond-donating fuctional groups (OH, COOH, and $CONH_2$). Methyl capped polar functionalities such as methyl esters, acetates and amides, exhibit similar wettabilities to SAMs exposing nitriles or halides.

3.6 Terminal groups that produce low energy surfaces

As for other self-assembling systems, alkyl thiols and disulfides that terminate in nonpolar groups, adsorb onto gold and produce low-energy surfaces that have hydrophobic and oleophobic characteristics [4, 18, 25]. SAMs prepared from alkanethiols that expose methyl group at their surface shows the highly hydrophobic surfaces. As a result of their dense packing, robust behavior, and hydrophobic nature, these SAMs provide useful model substrates for determining the oriented structure of surfactants at the interface between water and hydrophobic surfaces [27].

Surface energy	Surface Head Group	θ (H_2O) Advancing	Reference
High-Energy Surfaces	-COOH	< 15	17, 18, 21
	-CONH$_2$	< 15	21
	-OH	< 15	21, 17
Intermediate-Energy Surfaces	-Br	83	17
	-S$_2$(CH$_2$)$_{11}$NH$_2$)$_2$	51	79
	-S$_2$(CH$_2$)$_{12}$NH$_2$)$_2$	59	79
	-CN	60	17, 5
	-COOCH$_3$	67	18, 21
	-OCH$_3$	74	16, 18
Low-Energy Surfaces	-CH$_3$	115	17
	-O(CH$_2$)$_2$CH$_3$	105	16

Table 3.1: Wetting properties of SAMs on gold formed from alkanethiols.

3.7 Use of polar surface for covalent and non-covalent attachment

Terminally substituted alkanethiol SAMs with polar tail groups have provided reaction centers for the attachment of various species to gold. Alkanethiols terminating in COOH and OH groups are among the most synthesized organosulfur compounds [18, 21, 28] and they produce SAMs amenable to further chemical modification. Recently, Wöll *et al.* [29] demonstrated that COOH functionalized SAMs could be transformed into their carboxylate anion (COO⁻) by using 0.0 2 M $HS(CH_2)_{15}X$ where X= COOH, in pure ethanol. The generation of negatively charged carboxylate (COO⁻) surfaces was achieved due to the presence of a small amount of NaOH present in the ethanol. They also stated that although NaOH is not soluble in pure ethanol, ethanol regularly contains small amount of water which is sufficient to solve the small amount of NaOH.

We have already demonstrated that carboxylate anion terminated SAMs could be used for the successful non-covalent immobilization of *α,ω*-(4-amidinophenoxy)alkanes [20, 32] and subsequent adsorption of molecules like phosphate biomolecules [30] and oligonucleotides on them [31]. The COOH terminated SAMs have also been utilized for covalently immobilizing biomolecules such as cytochrome C [33], proteins [34], and antibodies [35] on gold surfaces.

SAMs of OH-terminated alkanethiols have also been used in surface modification reactions. Tillman and Ulman chemisorbed octadecyltrichlorosilane $(CH_3(CH_2)_{17}SiCl_3)$ onto SAMs of $HS(CH_2)_{11}OH$ on gold where the thiols provided a hydroxylated surface for attachment [24]. Hydroxylated surfaces readily react with trifluoroacetic anhydride to form the corresponding trifluoroacetate, with phosphorus oxychloride $(POCl_3)$ to form a phosphate surface and with chlorosulfonic acid $(ClSO_2OH)$ to form a sulfate surface. Lofas and Johnsson have reacted alcohol-terminated SAMs on gold with epichlorohydrin; which gives an ethylene oxide surface that allowing attachment of a dextran matrix to the gold film as part of a biosensor system [52].

The use of photochemistry for selective surface modification of SAMs has been demonstrated, e.g. aryl azide [36, 37] and benzophenone derivatives [35] have been used in the formation of photo patterned surfaces. Photochemical modification of SAMs has also been achieved using stilbene derivatives where isomerization between the trans- and cis- forms produced controllable differences in wettability [38].

SAMs have also been served as nucleation sites for the formation of electro active polymers by presenting attached monomer units at their surfaces. Recently, SAMs derived from pyrrole-containing alkanethiols were used to form two-dimensional polymers on gold by direct electrochemical polymerization of the SAM and to grow thicker poly(pyrrole) films on gold by electro polymerization of the SAM with pyrrole [39, 40].

3.8 Alkanethiols containing aromatic structures

The structural diversity of substituted *n*-alkanethiolate SAMs on gold extends beyond the simple, purely polymethylene-based systems. These other compounds have been useful for studying such phenomena as wetting [53, 54], electron transfer [55], protein adsorption [56], molecular recognition [57], and sensing [58]. Most either contain a polymethylene chain that links the thiol group with a complex tail group or they include an aromatic group that is located within the usual *n*-alkanethiol framework.

3.9 Self-assembled monolayer as biosensor platform

Biosensors are increasingly being employed within biotechnology and pharmaceutical studies to investigate the interactions between proteins and between potential drug molecules and their receptors. Biosensors consist of two principal components: a transducer that converts a chemical or biochemical signal into a readable electrical signal, and a chemical interface that ascertains a selective chemical response.

The use of SAMs in this field of research is rapidly growing. In particular, many biomedical fields apply SAMs as an interface-layer between a metal surface and a solution or vapour. These days researcher emphasis on uniform, mixed and functionalized monolayers applied for immobilization of biological components including (oligo-)nucleotides, proteins, antibodies and receptors as well as polymers.

As biomolecules provide high selectivity, antibodies, enzymes, nucleic acids or biological systems (receptors, whole cells) have already been exploited in biosensors, in which a biological sensing element is integrated with an electrochemical, optical transducer [59, 60]. Lu *et al* [61] showed that the direct immobilization of biomolecules by physisorption process on the surfaces was achieved and was subsequently applied in microtiterplate immunoassays.

SAM technology is most advantageous for electrochemical, Surface Plasmon Resonance (SPR) and (electrochemical) Quartz Crystal Microbalance (QCM) sensors. Modifying a sensor surface with SAMs generates model systems with a specific property or function. Collison M *et al*. used carboxylic acid-terminated SAM [$HS(CH_2)n COOH$ with n = 15 or 11] to immobilize cytochrome -c [62]. Redox enzymes linked to SAMs have been studied by Creager and Olsen [63]. A versatile and useful biotin-functionalized SAM has been presented by Ringsdorf and coworkers [64, 65]. They showed that when (strept)avidin was bound to above biotin functionalized monolayer; a biotinylated antibody (anti-hCG) could then be immobilized on the same surface.

3.10 *Switchable surfaces*

Interest in the reliable detection and quantification of potentially harmful or physiologically-active chemical agent at robust interface has grown very high during last two decades. While emphasizing on robustness of the surface, one should also consider the high selectivity, and most importantly, the *re-usability* of the same interface. As Self-ssembled Monolayers (SAMs) are chemisorbed in nature, once they are formed on the metal surfaces, they are non changeable and commonly non-reusable. Recently Choi *et al*. [78] reported the design of self-

assembled surfaces which exhibit dynamic changes in interfacial properties such as wettability in response to an electrical potential. In the same report, they have shown that the originally hydrophilic surfaces can be converted into the moderately hydrophobic surfaces by subjecting these SAM to the electrical potential (Figure 3.5). Thus, without altering the chemical identity of the SAMs, reversible switching surfaces can be prepared.
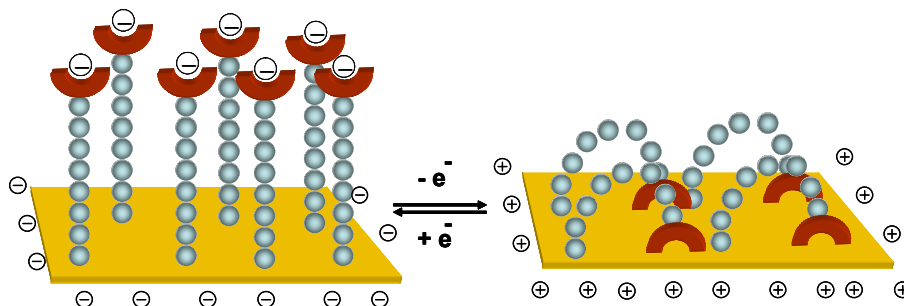
Figure 3.5: Idealized representation of transition between straight (hydrophilic) and bent (hydrophobic) molecular conformations.

Most of the natural processes occur in aqueous medium. Hence, we thought to have self-assembled monolayers which could be used in aqueous medium. Generally, the formation of SAMs occurs in organic solvents like ethanol and THF. The perfect example in this class is carboxylic acid {SH-$(CH_2)_x$-COOH (X=10 to 15)} terminated self-assembled monolayers on gold surface. The important idea behind using the carboxylic acid terminated SAMs is that these SAMs could act as host molecule at the surface interface for a guest molecules that is positively charged (Figure 3.6). Amidines are known to form pH sensitive interactions with carboxylate ion (COO$^-$) in aqueous medium [20, 30-31].
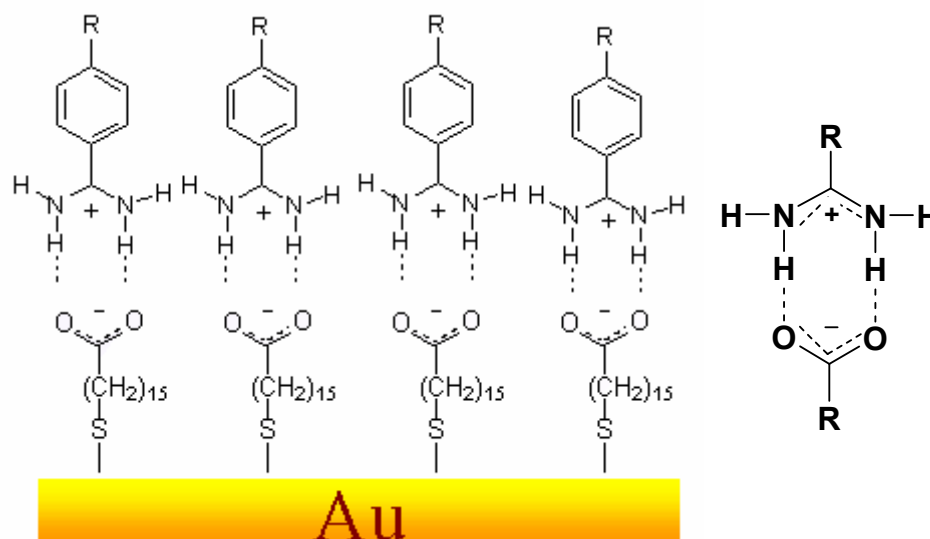
Figure 3.6: Schematic representation of carboxylate and amidinium ion interaction on the gold surface.

3.11 The amidinium-carboxylate ion pair

It is well reported in literature that carboxylate and amidinium or guanidinium ions form strong, cyclic, directed hydrogen bonded ion pairs (Scheme 3.1). The guanidinium-carboxylate binding mode, with its strong binding interactions, is ubiquitous in enzyme-substrate binding as well as in the stabilization of protein tertiary structures via internal salt bridges [66-68].
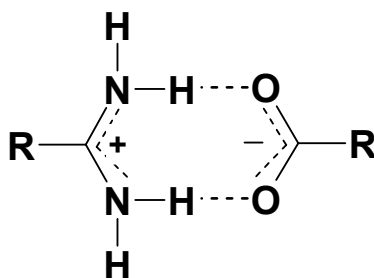
Scheme 3.1: Schematic representation of cyclic, hydrogen-bonded ion pairs formed between amidines and oxoacids.

These directional interactions are strong enough to provide significant stabilization in aqueous medium and have been used for the buildup of supramolecular structures [69], or in molecular recognition [71].

Hamilton *et al.* [71, 77] reported an association constant for the guanidinium carboxylate ion pairs as high as 12000 M^{-1} in DMSO-d_6.

Benzamidine groups are attractive targets for complexation [72]. An important DNA binding benzamidine (pentamidine) drug is used for the treatment of *pneumocystis carinii* in AIDS patients [73]. In 1965, Mares-Guia and Shaw studied on "Active Center of Trypsin; the Binding of *Amidines* and Guanidines as Models of the Substrate Side Chain" [74]. They concluded that regarding the specificity requirements of the enzyme, amidines are good model systems for the arginine side chain (pKa = 12.48) [75] of trypsin substrate. Of the compounds studied, benzamidinium chloride (pKa = 11.41) [76] and p-aminobenzamidinium chloride (pKa = 12.69) [76] were the most effective. In fact, they were the most potent small molecular competitive inhibitors of trypsin reported.

By following these references, we thought that we could use MHA modified gold surfaces for the selective recognition of substituted amidines, bisbenzamidines and subsequent adsorption of biomolecules onto these bilayers.

The most important feature of the amidinium-carboxylate ion pair is that they can assemble and disassemble by changing the pH (Hydrogen and hydroxide ion concentration or strength surrounding them). *For the non-covalently adsorbed layer, this kind of switching function has never been exploited and we have achieved this by changing the pH from basic pH 9 to acidic pH 3 and vice-versa to regenerate the sensor platform* [20, 30-32].

3.12 Self-assembled monolayers of Mercaptohexadecanoic Acid (MHA)

As we have discussed in previous section regarding SAMs which contain high energy terminal group surfaces, one of the most interesting functions in this context is a carboxylic acid group. The -COOH terminated surfaces are of an interest for a wide range of applications in surface science, biology [41-42], sensor development [43], nanoparticles [44, 45], and for surface engineering [46-48].

In the first paper describing this particular type of organization, Nuzzo *et al.* [21] concluded from an IR investigation of SAMs made from mercaptohexadecanoic

acid (MHA), that the thin films exhibits a high degree of molecular orientation and that there is only a small number of carboxylic acid groups linked together by hydrogen bonds (Figure 3.7, Structure A). Nuzzo also proposed that about 50% of neighboring COOH groups are bound, by a single bond thus forming linear chains of hydrogen bonds (Figure 3.7 Structure B). Dannenberger *et al.* [49] and Himmel *et al.* [50, 51] revealed a highly disordered structure of the MHA SAM (Figure 3.7 Structure C, Figure 3.8, Structure 3). It was proposed that the disorder is linked to the high flexibility of the alkyl chain anchoring the carboxylic acid to the substrate or to the hydrogen-bond formation between neighboring carboxylic groups.
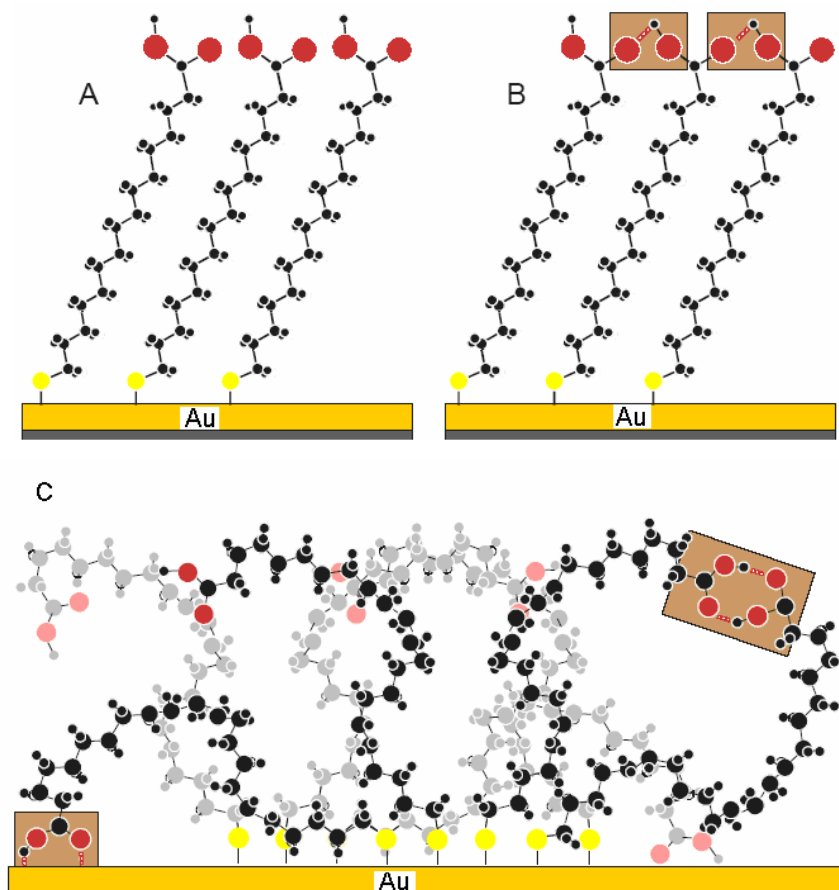
*Figure 3.7: Structure of MHA SAM without (A) and with (B,C) hydrogen bonds between the terminal carboxylic acid groups. {Adapted from Wöll et al. Langmuir, **2002**, 18, 3980.}*

To resolve these inconsistencies, Wöll *et al.* [29] carried out a detailed study of MHA SAMs assembled onto the Au(111) surface. As we intend to get well

ordered and rightly oriented MHA SAMs that contain only carboxylate (COO⁻) head groups at the ω- position (Figure 3.8,Structure 4), these negatively charged carboxylate ions could serve as host molecules for positively charged benzamidine molecules and subsequent adsorption of biomolecules onto them [31, 32].

With the highest purity of commercially available ethanol, the SAMs were found to contain a significant amount of deprotonated acid groups, yielding a characteristic carboxylate vibration (COO⁻ ~1450cm⁻¹) in the IR spectra (Figure 3.8,Structure 4).

Self-assembled monolayers prepared from dilute solutions (0.02 mM) [29] of MHA were found to exhibit a significantly higher degree of crystallinity and molecular orientation than films produced from concentrated (1 mM) solutions. The detailed study on the formation of MHA SAMs will be discussed in the following chapter.
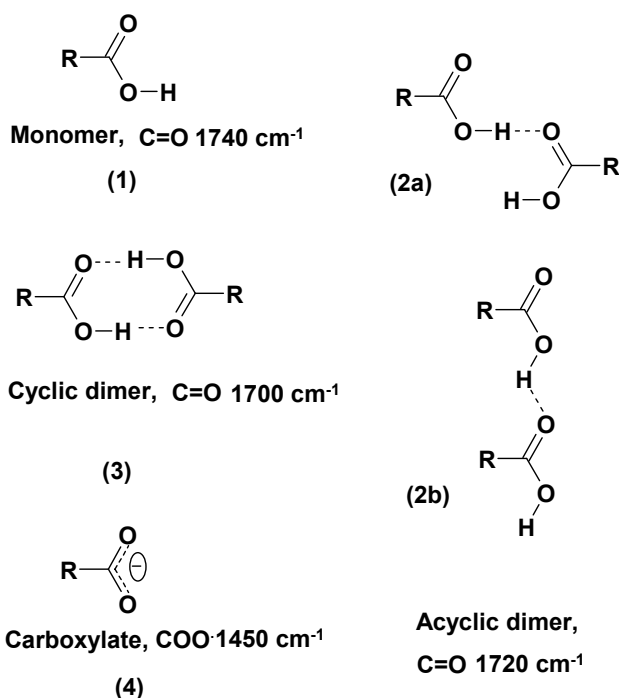
Figure 3.8: Variation of carboxylic acid (MHA) carbonyl band frequency with different type of interactions onto gold surfaces.

3.13   References

[1] Nuzzo, R. G., Fusco, F. A., Allara, D. L., *J. Am. Chem. Soc.* **1987,** 109, 2358.

[2] Hegner, M., Wagner, P., Semenza, G., *Surf. Sci.* **1993,** 291, 39.

[3] Chidsey, C. E. D., Loiacono, D. N., Sleator, T., Nakahara, S., *Surf. Sci.* **1988,** 200, 45.

[4] Porter, M. D., Bright, T. B., Allara, D. L., Chidsey, C. E. D., *J. Am. Chem. Soc.* **1987,** 109, 3559.

[5] Loiacono, D., Chidsey, C. E. D., *Langmuir,* **1990,** 6, 682.

[6] Green, J. B. D., McDermott, M. T., Porter, M. D., Siperko, L. M., *J. Phys. Chem.* **1995,** 99, 10960.

[7] Prime, K. L., Whitesides, G. M., *J. Am. Chem. Soc.* **1993,** 115, 10714.

[8] Pale-Grosdemange, C., Simon, E. S., Prime, K. L., Whitesides, G. M., *J. Am. Chem. Soc.* **1991,** 113, 12.

[9] Kim, T., Crooks, R. M., Tsen, M., Sun, L., *J. Am. Chem. Soc.* **1995,** 117, 3963.

[10] Hong, H. G., Mallouk, T. E., *Langmuir,* **1991,** 7, 2362.

[11] Yang, H. C., Aoki, K., Hong, H. G., Sackett, D. D., Arendt, M. F., Yau, S. L., Bell, C. M., Mallouk, T. E., *J. Am. Chem. Soc.* **1993,** 115, 11855.

[12] Evans, S. D., Ulman, A., Goppert-Berarducci, K. E., Gerenser, L. J., *J. Am. Chem. Soc.* **1991,** 113, 5866.

[13] Tillman, N., Ulman, A., Penner, T. L., *Langmuir,* **1989,** 5, 101.

[14] Schilling, M. L., Katz, H. E., Stein, S. M., Shane, S. F., Wilson, W. L., Buratto, W. S., Ungashe, S. B., Taylor, G. N., Putvinski, T. M., Chidsey, C. E. D., *Langmuir,* **1993,** 9, 2156.

[15] Dubois, L. H., Zegarski, B. R., Nuzzo, R. G., *J. Am. Chem. Soc.* **1990,** 112, 570.

[16] Laibinis, P. E., Bain, C. D., Nuzzo, R. G., Whitesides, G. M., *J. Phys. Chem.* **1995,** 99, 7663.

[17] Laibinis, P. E., Whitesides, G. M., *J. Am. Chem. Soc.* **1992,** 114, 1990.

[18] Bain, C. D., Troughton, E. B., Tao, Y. T., Evall, J., Whitesides, G. M,. Nuzzo,R. G., *J. Am. Chem. Soc.* **1989,** 111, 321.

[19] Delamarche, E., Michel, B., Biebuyck, H. A., Gerber, C., *Adv. Mater.* **1996,** 8, 719.

[20] Auer, F., Nelles, G., Sellergren, B., *Chem. Eur. J.* **2004,** 10, 3232.

[21] Nuzzo, R. G., Dubois, L. H., Allara, D. L., *J. Am. Chem. Soc.* **1990,** 112, 558.

[22] Wasserman, S. R., Tao, Y. T., Whitesides, G. M., *Langmuir,* **1989,** 5, 1074.

[23] Netzer, L., Sagiv, J., *J. Am. Chem. Soc.* **1983,** 105, 167.

[24] Tillman, N., Ulman, A., *Langmuir,* **1989,** 5, 1418.

[25] Nuzzo, R. G., Allara, D. L., *J. Am. Chem. Soc.* **1983,** 105, 4481.

[26] Kumar, A., Biebuyck, H. A., Whitesides, G. M., *Langmuir,* **1994,** 10, 1498.

[27] WardR, N., Duffy, D. C., Davis, P. B., Bain, C. D., *J. Phys. Chem.* **1994,** 98, 8536.

[28] Troughton, E. B., Bain, C. D., Whitesides, G. M., Nuzzo, R. G., Allara, D., Porter, M. D., *Langmuir,* **1988,** 4, 365.

[29] Arnold, R., Azzam, W., Terfort, A., Wöll, C., *Langmuir,* **2002,** 18, 3980.

[30] Sellergren, B., Swietlow, A., Arnebrant, T., Unger, K., *Anal. Chem.* **1996,** 68, 402.

[31] Sellergren, B., Auer, F., Arnebrant, T., *Chem. Comm.* **1999,** 19 , 2001.

[32] Auer, F., Schubert, D., Stamm, M., Arnebrant, T., Swietlow, A., Zizlsperger, M., Sellergren, B., *Chem. Eur. J.* **1999,** 5, 1150.

[33] Collinson, M., Bowden, E. F., Tarlov, M. J., *Langmuir,* **1992,** 8, 1247.

[34] Madoz, J., Kuznetzov, B. A., Medrano, F. J., Grcia, J. L., Fernandez, V. M., *J. Am. Chem. Soc.* **1997,** 119, 1043.

[35] Delamarche, E., Sundarababu, G., Biebuyck, H., Michel, B., Gerber, C., Sigrist, H., Wolf, H., Ringsdorf, H., Xanthopoulos, N., Mathieu, H. J., *Langmuir,* **1996,** 12, 1997.

[36] Wollman, E. W., Frisbie, C. D., Wrighton, M. S., *Langmuir, **1993,*** 9, 1517.

[37] Frisbie, C. D., Wollman, E. W., Wrighton. M. S., *Langmuir, 1995,* 11, 2563.

[38] Wolf, M. O., Fox, M. A., *J. Am. Chem. Soc.* **1995,** 117, 1845.

[39] Sayre, C. N., Collard, D. M., *Langmuir, 1995,* 11, 302.

[40] Willicut, R. J., McCarley, R. L., *Langmuir, 1995,* 11, 296.

[41] Franco, M., Nealey, P. F., Campbell, S., Teixeira, A. I., Murphy, C. J., *J. Biomed. Mater. Res. .* **2000**, *52*, 261.

[42] Chapman, R. G., Ostuni, E., Yan, L,, Whitesides, G. M., *Langmuir, 2000,* 16, 6927.

[43] Bertilsson, L., Potje-Kamloth, K., Liess, H. D., Liedberg, B., *Langmuir, 1999,* 15, 1128.

[44] Auer, F., Scotti, M., Ulman, A., Jordan, R., Sellergren, B., Garno, J., Liu, G Y., *Langmuir, 2000,* 16, 7554.

[45] Patil, V., Mayya, K. S., Sastry, M., *Thin Solid Films* **1997,** 307, 280.

[46] Lee, S. W., Laibinis, P. E., *J. Am. Chem. Soc.* **2000,** 122, 5395.

[47] Lee, S. W., Laibinis, P. E., *Isr. J. Chem.* **2000,** 40, 99.

[48] Huck, W. T. S., Yan, L., Stroock, A., Haag, R,, Whitesides, G. M., *Langmuir, 1999,* 15, 6862.

[49] Dannenberger, O., Weiss, K., Himmel, H-J., Jäger, B., Muck, M., Wöll, C., *Thin Solid Films* **1997,** 307, 183.

[50] Himmel, H-J., Weiss, K., Jäger, B., Dannenberger, O., Grunze, M., Wöll, C., *Langmuir, 1997,* 13, 4943.

[51] Himmel, H-J., Wöll, C., *Chem. Unserer Zeit.* **1998,** 6, 294.

[52] Löfas, A., Johnsson, B., *J. Chem. Soc. Chem. Comm.* **1990,** 1526.

[53] Abbot, N. L., Whitesides, G. M., *Langmuir, 1994,* 10, 1493.

[54] Sondag-Huethorst, J. A. M., Fokkink, L. G. J., *Langmuir, 1994,* 10, 4380.

[55] Mukae, F., Takemura, H., Takehara, K., *Bull. Chem. Soc. Jap.* **1996,** 69, 2461.

[56] Prime, K. L., Whitesides, G. M., *Science,* **1991,** 252, 1164.

[57] Motesharei, K., Myles, D. C., *J. Am. Chem. Soc.* **1994,** 116, 7413.

[58] Hickman, J. J., Ofer, D., Laibinis, P. E., Whitesides, G. M., Wrighton, M. S., *Science,* **1991,** 252, 688.

[59] Turner, A. F. P., in *Biosensors: Fundamentals and Applications*, ed. Turner, A. F. P., Karube, I. and Wilson, G. S., Oxford University Press, **1987,** pp. V–VIII.

[60] Byfield, M. P., and Abuknesha R. A., *Biosens. Bioelectron.,* **1994,** 9, 373.

[61] Lu, B., Smyth, M. R., and OAKennedy, R., *Analyst,* **1996**, 121, 29R.

[62] Collison, M., Bowden, E. F., and Tarlov, M. J., *Langmuir,* **1992,** 8, 1247

[63] Creager, S. E., and Olsen, K. G., *Anal. Chim. Acta,* **1995,** 307, 277.

[64] Haeussling, L., Ringsdorf, H., Schmitt, F.-J., Knoll, W., *Langmuir,* **1991,** 7, 1837.

[65] Schmitt, F.-J., H¨aussling, L., Ringsdorf, H.,Knoll, W., *Thin Solid Films,* **1992,** 210/211, 815.

[66] Hamilton, A. D., Linton, B., *Tetrahedron* **1999**, *55*, 6027.

[67] Sellergren, B., *Anal. Chem.* **1994**, *66*, 1578.

[68] Wulff, G., Gross, T., Schonfeld, R., *Angew. Chem., Int. Ed. Engl.* **1997**, *36*, 1961.

[69] Hosseini, M. W., Ruppert, R., Schaeffer, P., De, Cian. A., Kyritsakas, N., Fischer., *J. J. Chem. Soc. Chem.. Commun.* **1994,** 2135.

[70] Lehn, J.-M., *Supramolecular Chemistry: Concept and Perspectives, VCH, Verlagsgesellschaft mbH, Weinheim,* **1995**.

[71] Fan, E., Van Arman, S. A., Kincaid, S., Hamilton, A. D., *J. Am. Chem. Soc.* **1993,** 115, 369.

[72] Tidwell, R.R., Susan, Kilgore., *J. Med. Chem* **1990**, 33, 1252.

[73] Gluth, W. P., Kaliwoda, G., Dann, O. *J.*, *Chromatogr.* **1986,** 378, 183.

[74] Mares-Guja, M., Shaw, E., *J. Biol. Chem.* **1965,** 240, 1579.

[75] Pine, S. H., Hendrickson, J. B., Cram, D. J., Hammond, G. S., *Organic Chemistry*; McGraw-Hill: Tokyo, **1981**.

[76] Rogana, E., Nelson, D. L., Leite, L. F. F., Mares-Guia, M., *J. Chem. Res.* **1985**, 286.

[77] Hamilton, A. D., *Advancess in Supramolecular Chemistry;* Gokel, G. Ed. Jai Press. Greenwich, CT **1990**, Vol. 1.

[78] Lahann, J., Mitragotri, S., Tran, T. N., Kaido, H., Sundram, J., Choi, I. S., Hoffer, S., Somorjai, G. A., Langer, R., *Science*, **2003**. Vol. 299, 371.

[79] Borgmeir, F. M., *Doct. Dissertation,* Uni. Mainz. **1999**.

4 Results and Discussion

4.1 Synthesis of hetrofunctionalized amphiphiles

The main purpose of this work was to develop a biosensor platform in the form of self-assembled monolayers that would be re-usable. Previously we have demonstrated that α,ω-bis(4-amidinophenoxy)alkanes reversibly form mono and bi-layers on carboxylic acid functionalized thiol SAMs on gold [1]. We showed that once α,ω-bis(4-amidinophenoxy)alkanes form ordered monolayers on carboxylic acid terminated SAMs on gold, subsequently, they can be used for the selective recognition of oligonucleotides [2] proteins and phosphate molecules [3]. In order to extend the repertory of exposed head groups of the SAMs, our initial efforts were directed towards the synthesis of ω-functionalized α-(4-amidinophenoxy)alkanes molecules. Our further goal was to introduce different functionalities in the amphiphiles at the ω position which could lead to the different optical signal characteristics and also could give extra stability to the self-assembled layer.

The approaches taken towards the recognition of protein Streptavidin (**SA**) as well as the achievement of this doctoral research will be presented in this section. For the study of reversible version of self-assembled monolayers, the following molecules were synthesized in our laboratory.

1. α,ω-hetero-functionalized and α,ω-bis(4-amidinophenoxy)alkanes amphiphiles.
2. α,ω-bis(4-amidinophenylamine)alkanes amphiphiles.

Using modified literature procedure [4], we have successfully synthesized a series of ω-functionalized α-(4-amidinophenoxy)alkanes amphiphiles which contain different terminal functional groups with different polarity. This is displayed in Scheme 4.1.

The important steps in the synthesis of above molecules were the synthesis of 4-cyanophenoxyoctane-8 bromide (**1**) and the Pinner synthesis which converts -CN group into an amidinium group (**3**) [4].
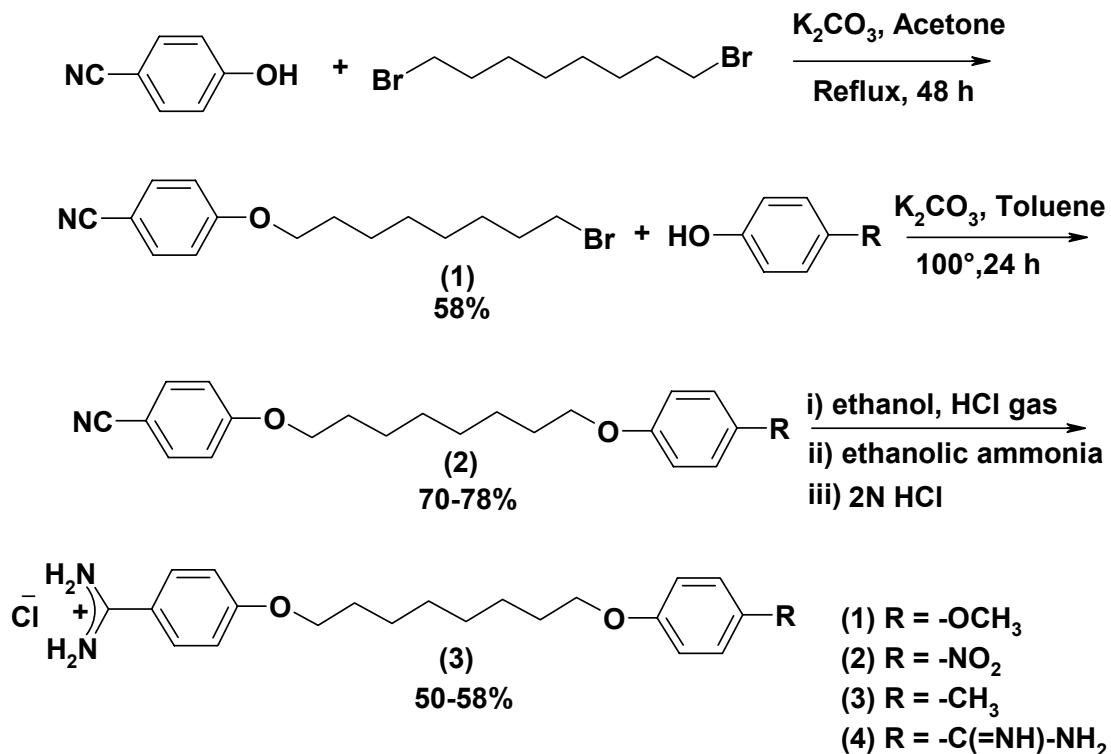
Scheme 4.1: Synthesis of amphiphiles.

4-cyanophenoxyoctane-8 bromide (**1**) was obtained by refluxing 4-cyanophenol with 1,8 dibromooctane in acetone for 48 h. A Large excess (20 eq.) of 1,8 dibromooctane was used and dropwise addition of 4-cyano phenol (dissolved in 5 mL acetone) was done. After aqueous workup, the crude product was purified by column chromatography and 4-cyanophenoxyoctane-8 bromide (**1**) was obtained in 58% yield.

4-cyanophenoxyoctane-8 bromide (**1**) was then heated at 100 °C with substituted phenols for 24 h to afford 70-78% of molecules (**2**)

Compound (**2**) was subjected to Pinner synthesis (HCl gas, ethanol) for the conversion of -CN groups to amidine groups. HCl gas was bubbled in the reaction mixture of (**2**) for 30 minutes and then the reaction mixture was sealed and stirred at room temperature for 2-3 days. This transforms the -CN groups into their corresponding imidate as intermediate products. The imidates were then heated at 50 °C in ethanolic ammonia and dry ethanol to afford the amidines (**3**). To make these molecules water soluble, they were crystallized from 2 N HCl and subsequently used for further study.

We anticipated that the above amphiphiles would form SAMs on acid functionalized surfaces exploring the ω-functionalized groups to the surrounding medium as depicted in Scheme 4.2.

4.2 Adsorption of single component amphiphiles on gold surfaces

Previous results from our group have shown that bisbensamidines with over eight carbon atoms in the mesogenic part formed ordered pH-switchable layers on ω-carboxyl functional thiol SAMs on gold [1, 14]. This tempted us to use eight carbons and above eight carbon atoms in the apolar part during our entire studies.

Our initial study focused on the interaction of the synthesized benzamidine molecules and mercaptohexadecanoic acid (MHA) SAMs which is represented in the schematic fashion in Scheme 4.2.

(1) R= -OCH$_3$
(2) R= -NO$_2$
(3) R= -CH$_3$
(4) R= -C(=NH)NH$_2$

d=25 Å (±2)
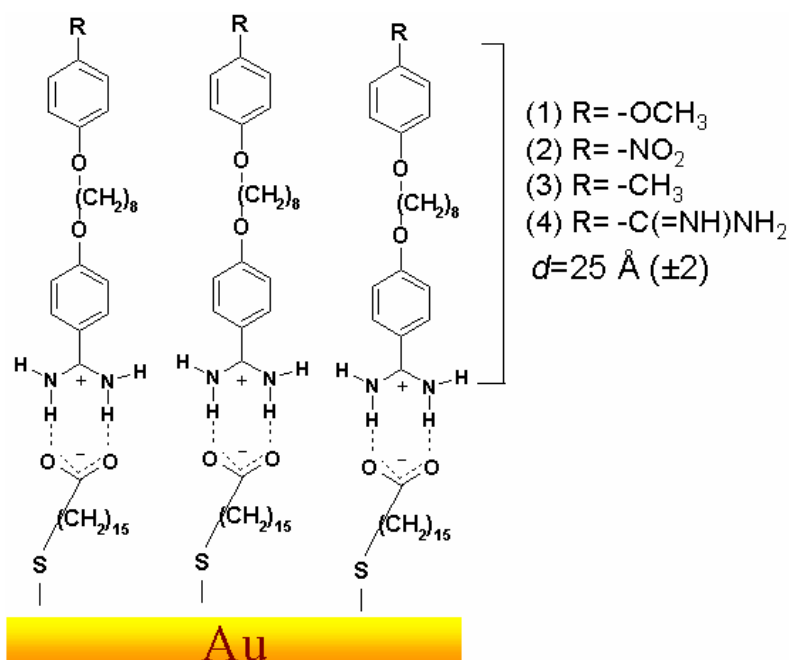
Scheme 4.2: Schematic representation of interaction between negatively charged carboxylate ions on a gold surface and positively charged amidinium ion.

4.2.1 *In-situ ellipsometry*

We have followed the actual adsorption kinetics or live formation of amphiphilic monolayers on acid terminated SAMs by *in situ* ellipsometry [9], shown in Figure 4.1.

All the *In-situ* ellipsometry measurements were carried out on gold surfaces which were prepared by vapor deposition of gold (2000 Å) onto glass slides containing adhesive layers (300 Å) of chromium. After deposition of the gold, these surfaces were cleaned by immersing them for 30 seconds in freshly prepared "piranha" solution (1:3 H_2O_2 (30%): H_2SO_4), which is followed by carefully several times rinsing with distilled water, ethanol and then drying them under the stream of nitrogen gas. Then, above clean gold plates were placed in solution of Mercaptohexadecanoic acid (0.002 M) [17] in ethanol for 16 hours for the chemisorptions of MHA.

The MHA modified gold surfaces were then immersed in a Teflon-coated cuvette containing 2 mL (0.01 M) sodium borate buffer (pH 9) prepared from boric acid. This cuvette was thermostated to 25 °C and equipped with a small magnetic stirrer and a pH electrode. The addition of amphiphiles (50 µM) was done after a stable base line was obtained. The adsorption of molecules was then monitored by *in-situ* ellipsometry using ELX-1 Precision ellipsometer (DRE-Ellipsometerbau, Ratzeburg, DE angle of incidence 70°, He Ne laser: $\lambda = 632.8$ nm).
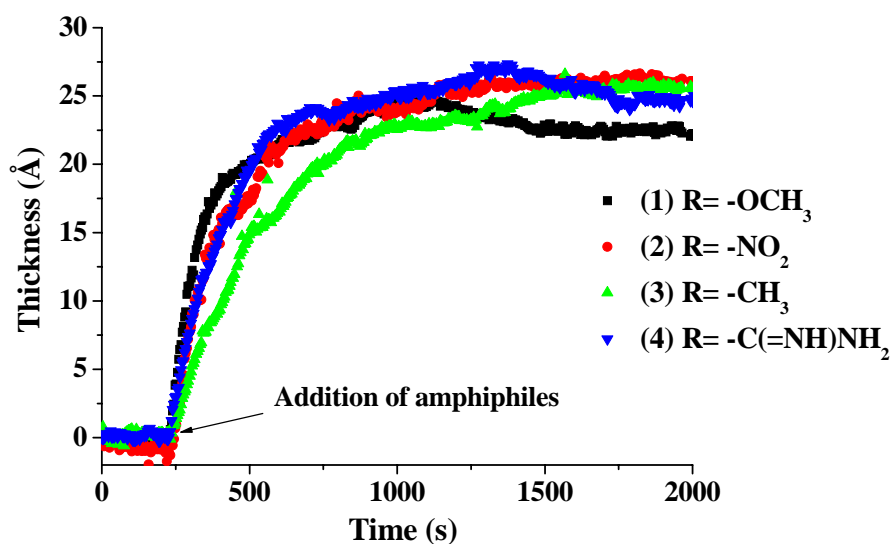
Figure 4.1: Film thickness versus time during adsorption of α,ω-hetero-functionalized substituted amphiphiles on MHA modified gold surfaces.

When we added different amphiphilic solutions at pH 9.0 on MHA SAMs (Figure 4.1), we anticipated that there would be an interaction between the negatively charged carboxylate ion surface and positively charged amidine which would result in the formation of stable hydrogen bonded amidinium-carboxylate ion pair [10, 11] (Figure 3.6, Scheme 4.2).

Similar to the previous reports from our group [1-3], after addition of the amphiphiles, rapid increase in thickness was observed which is shown in the Figure 4.1. A stable monolayer thickness of the amphiphiles was achieved after around 700 seconds and the rate of formation of monolayer for each amphiphile was similar. The processes of formation of amphiphilic monolayer transformed the negatively charged carboxylate (COO⁻) gold surface into the ω-functionalized α-(4-amidinophenoxy)alkanes and α,ω-bis(4-amidinophenoxy)alkanes surface.

After energy minimizations, with the help of CS Chem3D ultra software, we have estimated the molecular length of the synthesized amphiphiles and observed that the actual thickness (*d*) by *in-situ* ellipsometry and air ellipsometry, was in accordance with their molecular length, assuming a film refractive index of 1.45 [12] (in addition to the COOH monolayer). Interestingly, we have also observed

that these amphiphilic layers are stable after rinsing. This indicates the strong head group interaction between the host and guest molecules. The agreement between the maximum length of the amphiphiles and the observed increase in thicknesses upon addition of the same molecules, indicate that the amphiphililes are perpendicularly ordered related to the MHA terminated SAMs on the gold surface. The morphology of all these amidine layers was imaged using Atomic Force Microscopy (AFM) which we will discuss in coming section of this chapter. The order and crystalline like structure was confirmed via grazing angle FTIR method which will also be discussed in the next section.

4.2.2 Air ellipsometry

To compare the obtained results from *in-situ* ellipsometry, we have performed the air ellipsometry of the assembled bola-amphiphiles on MHA SAMs which are summarized in Table 4.1 for the air ellipsometric study; first of all, the amphiphiles were immobilized on MHA SAMs, and then the surfaces were dried with a stream of nitrogen before the measurements. For the rinsing experiment, first the surfaces were rinsed with borate buffer pH 9 and then flushed with nitrogen gas till dryness. The thickness values were obtained by ellipsometry of the SAMs in air. The values given in Table 4.1 are average values of 10 measurements at three different spots on each surface.

Sr.No.	Compounds	Estimated length ($\mathring{A}$)	Thickness before rinsing ($\mathring{A}$)	Thickness after rinsing ($\mathring{A}$)	Errors ($\mathring{A}$)
1	MHA	22	21	20	$\pm$ 2
2	(1) R= -OCH$_3$	24	26	24	$\pm$ 3
3	(2) R= -NO$_2$	24	27	26	$\pm$ 3
4	(3) R= -CH$_3$	25	27	22	$\pm$ 3
5	(4) R= -C(=NH)-NH$_2$	25	25	24	$\pm$ 2

Table 4.1: Ellipsometric air thickness of MHA SAMs and different amphiphiles assembled on MHA SAMs.

From the above table, it can be concluded that the layer thickness of the synthesized octamidine SAMs, measured by elliposmetry in air and by *in situ* ellipsometry, are in agreement with the estimated length of the molecules.

4.2.3 The influence of pH on the layer thickness

It is very unlikely that uncharged carboxylic acid group (-COOH) would form cyclic, stable hydrogen bonded ion pair with amidinium ion leading into cyclic carboxylate-amidinium structure. For such kind of stable non-covalent interactions, the carboxylic acid groups need to be charged. In return, the charged carboxylic acid groups (COO$^-$) are predominantly responsible for the anchoring of the amphiphilic head groups and they can form cyclic, stable hydrogen bonded carboxylate-amidinium ion pair [10]. By taking this observation into account, we changed the H$^+$ and OH$^-$ ion concentration surrounding the self-assembled monolayers on gold, which is discussed in detail in this section.

Completely ionized mercaptohexadecanoic acid surfaces were highly hydrophilic, showing a contact angle of 10° (±5°) (Table 3.1). As we have observed from the *in situ* ellipsometry measurements at pH 9, in 0.01 M sodium borate buffer that the negatively charged carboxylate ions (COO$^-$) form cyclic hydrogen bonds with its counterpart positively charged amidinium ions to form stable SAMs. This process occurs because at pH 9, the amidinium group is completely protonated and the carboxylic acid is deprotonated which leads to symmetry in amidinium proton donor (guest) and carboxylate ion proton acceptor (host) molecules.

In this section, we have observed that the acidification or lowering down the pH from 9 to 3 affords the protonation of carboxylate group (COO$^-$) on the gold surface into carboxylic acid (COOH) surfaces, which in turn reduces the head group electrostatic attraction between the amidinium and carboxylate ions, and disrupts the hydrogen bonding between them. This finally leads to the removal of amphiphilic monolayer from MHA SAMs which is shown in Figure 4.2. For changing the pH of the borate buffer *in situ*, we equipped the Teflon cuvette with two small needles. One of them can inject fresh buffer from the reservoir and at the same time second needle can take out the parent buffer solution from the

cuvette. This process was run using peristaltic pump. The pH electrode, which is already present in the Teflon cuvette, detects the change in the pH.
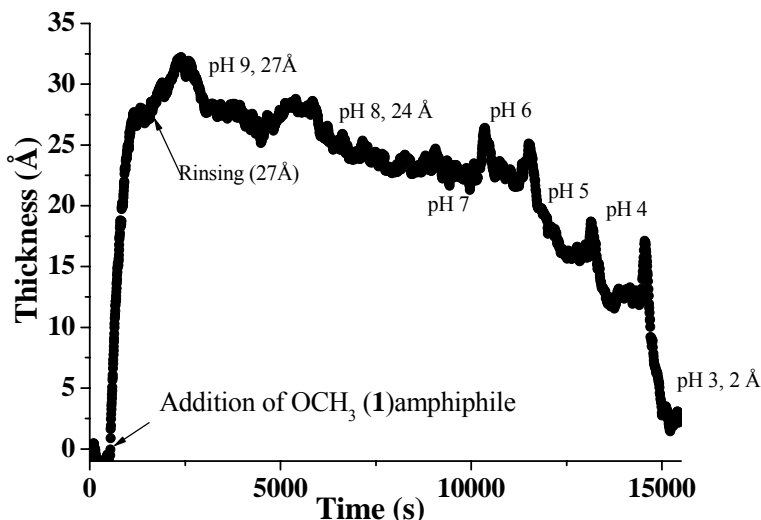
Figure 4.2: Film thickness, measured by in situ ellipsometry against time for a layer of OCH₃ (1) on MHA and subsequent influence of pH on the layer thickness.

After addition 4-methoxyphenoxy(4-amidinophenoxy)octane amphiphiles (**1**) on MHA SAMs at pH 9, we observed rapid increase in the layer thickness and the monolayer thickness of 27 Å was achieved. To confirm whether these formed monolayers are stable after rinsing or not, we have pumped in fresh buffer solution (pH 9) and at the same time the mother buffer solution of same pH was pumped off using peristaltic pump.

After rinsing, we observed that there was no change in the layer thickness (27 Å) hence these layers remains stable towards rinsing. When we decreased the pH from 9 to 8, we detected that there was small decrease in the layer thickness (24 Å). Interestingly, when we decreased the pH gradually from 8 till 6, we observed that the -OCH₃ (**1**) functionalized SAMs still attains monolayer thickness (22 Å). When these amphiphilic SAMs were further acidified till pH 3, we noticed that amphiphilic layer on MHA terminated SAMs was displaced. The influence of pH on NO_2 (**2**) functionalized SAM was also studied and is shown in Figure 4.3.
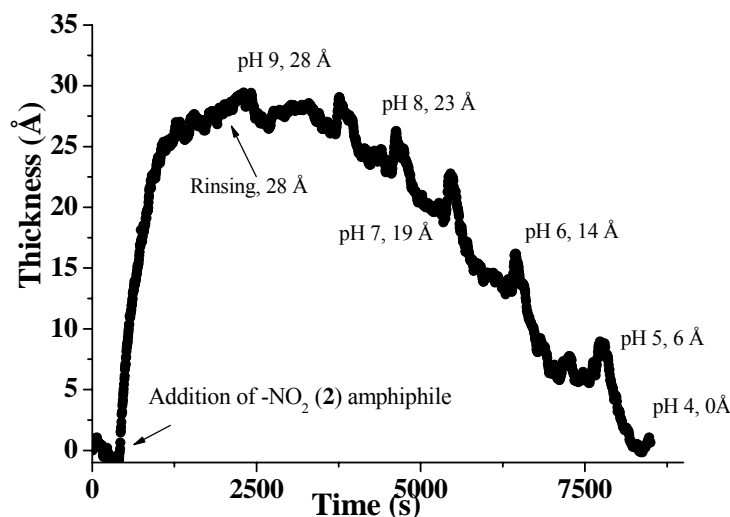
Figure 4.3: Film thickness, measured by in situ ellipsometry against time for a layer of NO_2 (2) on MHA and subsequent influence of pH on the layer thickness.

With reference to the previously reported results [3], here also we have observed that the layer thickness decreases with decreasing pH in a manner reflecting the degree of ionization of carboxylic acid surface. However, as seen in Figure 4.4, ω-functionalized terminated group also influence the stability of the assembled layer on MHA layer.

From the above observations, we can conclude that the thickness of the benzamidine layer on MHA terminated SAMs decreases to zero after acidification to pH 3. The process of changing the H^+ ion concentration surrounding the amidine layer transformed the 4-methoxyphenoxy(4-amidinophenoxy)octane (1), (Figure 4.2) and 4-nitrophenoxy(4-amidinophenoxy)octane (2) (Figure 4.3) SAMs surface into carboxylic acid (COOH) terminated SAMs surfaces. We have then reused the above surfaces after rinsing them with 0.1 M HCl, 0.1 M NaOH and then with pH 9 borate buffer.
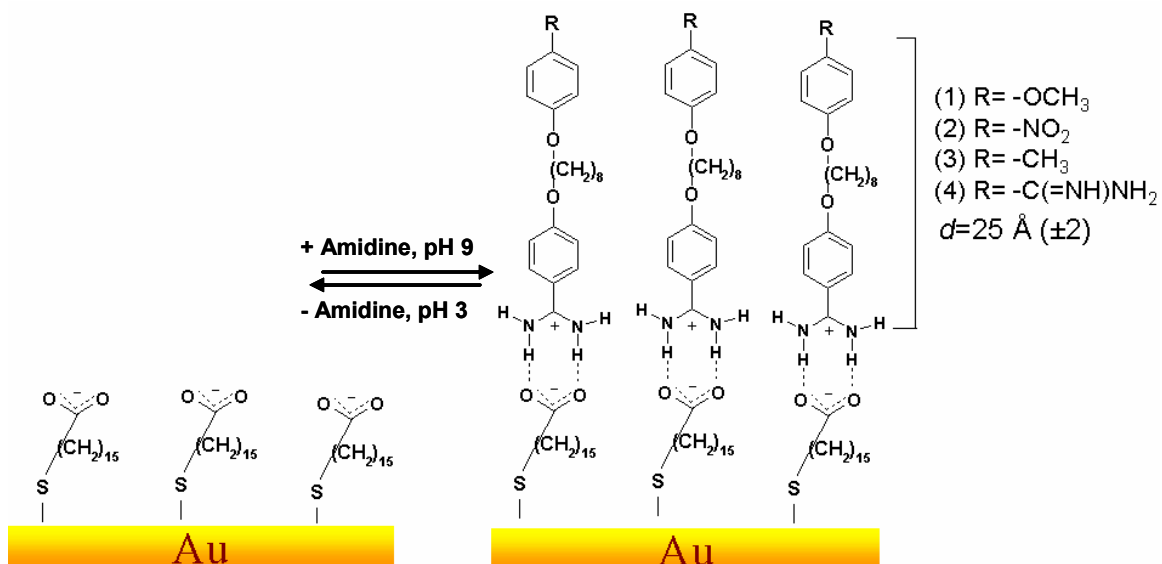
Scheme 4.3: Schematic representation of assembly-disassembly on mercaptohexadecanoic acid terminated SAMs on gold surfaces.

The above experiment was repeated for different amphiphiles which are summarized in Figure 4.4. When these amphiphiles were added on MHA terminated SAMs, we observed that the rapid increase in the thickness of respective amphiphiles and monolayer thicknesses were achieved after around 700 seconds. In this case also, there was agreement between the observed thickness increases upon addition of these molecules with respect to their maximum length calculated from CS Chem3D ultra programme.

We studied the effect of pH on the layer stability for four different amphiphiles shown in Scheme 4.3; we observed that all the layers were stable towards rinsing (Figure 4.4). Surprisingly we also observed that π electron rich amphiphile (**1**) tends to show more stable films by showing monolayer thickness (~23 Å) down to pH 6, but for the π electron poor amphiphile (**2**), they loose their monolayer thickness (~14 Å) at pH 6 itself.
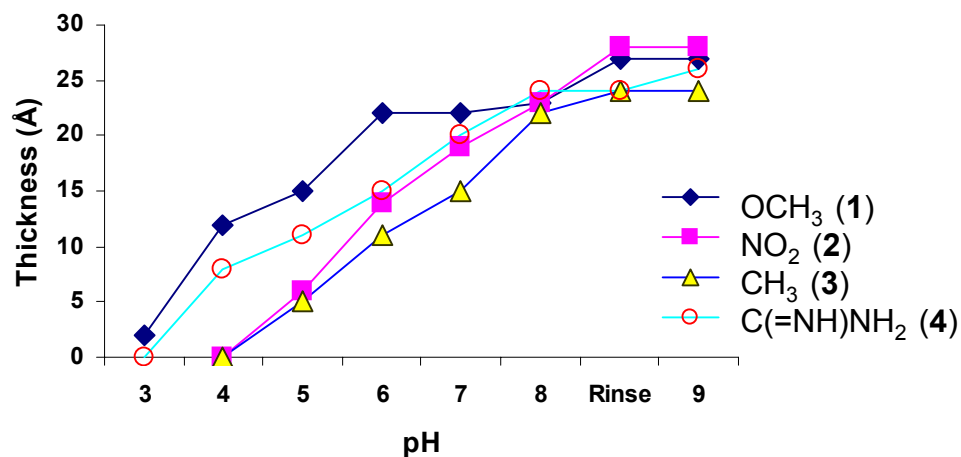
Figure 4.4: Influence of the pH on layer thickness for different amphiphiles.

The origin of these differences in stability is not clear. In view of the contact angle measured for ω-functionalized π electron rich amphiphile [OCH$_3$, (**1**)] and π electron poor amphiphile [NO$_2$, (**2**)] SAMs (Table 4.2), polarity and wettability do not seem to be the main factors influencing this behavior.

For all the synthesized amphiphiles which are immobilized on mercaptohexadecanoic acid SAMs, when we have subjected them to pH 3-4, we observed that the head group interaction of amidinium-carboxylate ion which held them together as a cyclic hydrogen bonded ion pair is weakened which in turn results in the removal of amphiphilic layer from the MHA surfaces to yield carboxylic acid terminated SAMs. After rinsing these surfaces with 0.1 M HCl, 0.1 M NaOH and pH 9 borate buffer solutions, we have reused the above surfaces several times with reproducible results.

4.2.4 Infrared reflection absorption spectroscopy (IRAS)

The orientation, order and crystalline like nature of the assembled monolayer on MHA SAMs were studied by **I**nfrared **R**eflection **A**bsorption **S**pectroscopy (**IRAS**). All the IRAS measurements were carried out on gold surfaces which were prepared by vapor deposition of gold (2000 Å) onto glass slides containing adhesive layers (300 Å) of chromium. Before the chemo adsorption of MHA, these surfaces were cleaned by immersing them for 30 seconds in freshly prepared "piranha" solution (1:3 H_2O_2 (30%): H_2SO_4) which is followed by carefully rinsing with distilled water several times and ethanol and drying them under the stream of nitrogen gas. From IRAS spectroscopy, we could characterize the molecules which are present on the gold surface.

Immobilized MHA SAM surfaces were characterized first to see the order and crystalline like nature of the layer. As we have discussed the synthesis of MHA SAMs in our introduction part, we have synthesized MHA SAMs based on the procedure reported by Wöll *et al* [17]. This procedure involved formation of SAMs from dilute solution of Mercaptohexadecanoic acid (MHA, 0.002 M) in ethanol, which leads to well ordered and crystalline like SAMs on the gold surface. Interestingly, these layer yields the deprotonated form of the carboxylic acid [carboxylate ion (COO$^-$] on the surface in upward oriented fashion. Wöll *et al.* also mentioned that the deprotonation of the carboxylic acid occurs due to presence of small amount of water and Na^+ ions present in ethanol.

After following the above procedure for the construction of MHA SAMs on freshly prepared gold surfaces, we observed in the high frequency region of the IRAS the asymmetric -CH stretch band at 2917cm^{-1} position (Figure 4.5). This indicates a crystalline like order of the layer alkyl chains [17, 18], present in an all trans extended conformation of the alkyl chain methylenes [1-3].
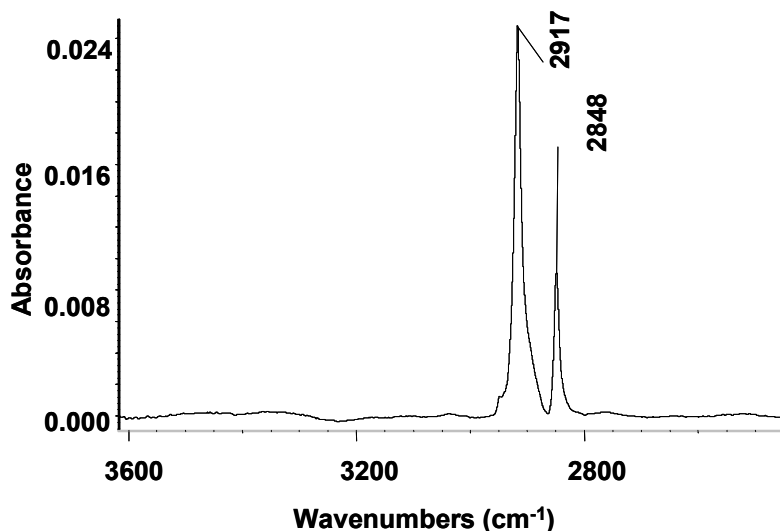
Figure 4.5: Baseline corrected IRAS spectra of high frequency region of MHA SAMs on gold surface.

When terminal carboxylic acid groups are not deprotonated, they show a strong band at ~1740 cm^{-1} which is characteristic band for carbonyl group, and when they form cyclic dimer with each other, a strong peak at ~1700 cm^{-1} appears in IRAS [17].

In the low frequency region of the same spectra, the peak at ~1450 cm^{-1} corresponds to the deprotonated form of carboxylic acid (COO^{-}). This is responsible for anchoring of benzamidine groups via cyclic hydrogen bonded ion pairs.

After carefully following the same preparation procedure for the immobilization of MHA SAMs, we observed in the low frequency region of the IRAS, the presence of a strong band at ~1450 cm^{-1}, which indicates the presence of carboxylate (COO^{-}) group terminated SAMs (Figure 4.6).
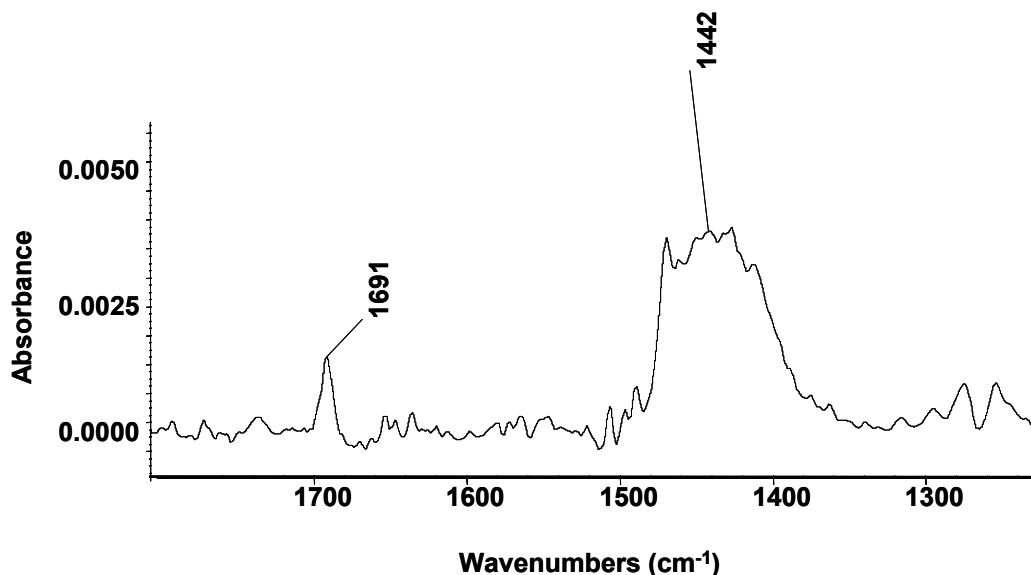
Figure 4.6: Low frequency region of the baseline corrected IRAS spectra of MHA SAMs.

After the spectroscopic confirmations of the presence of MHA SAMs on surface, the benzamidine amphiphiles were allowed to adsorb onto these SAMs. Subsequently, the surfaces were carefully rinsed with pH 9 borate buffer (0.01 M), dried under a stream of nitrogen and then the surfaces were characterized in air by IRAS.

A carefully comparison of the IRAS of different amphiphiles with their transmission spectrum (KBr pellets), clearly revealed the peaks characteristic for the amidine amphiphiles were clearly seen on all surfaces which is shown from the Figure 4.7 to Figure 4.13.

As we have recorded all the IRAS spectra after rinsing them with pH 9 borate buffer and they show all the characteristic peaks for the amidines, we conclude that these layers are stable after rinsing providing additional confirmation for the result observed by *in-situ* ellipsometry and air ellipsometry (Table 4.1, Figure 4.4).
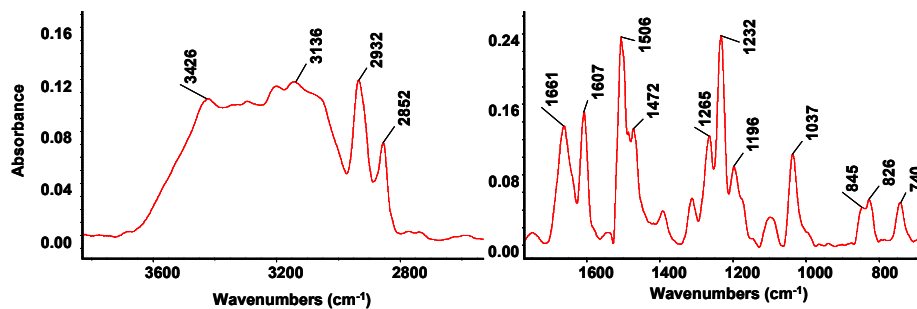
*Figure 4.7: FTIR spectrum (KBr) of OCH₃ functionalized amphiphile (**1**).*
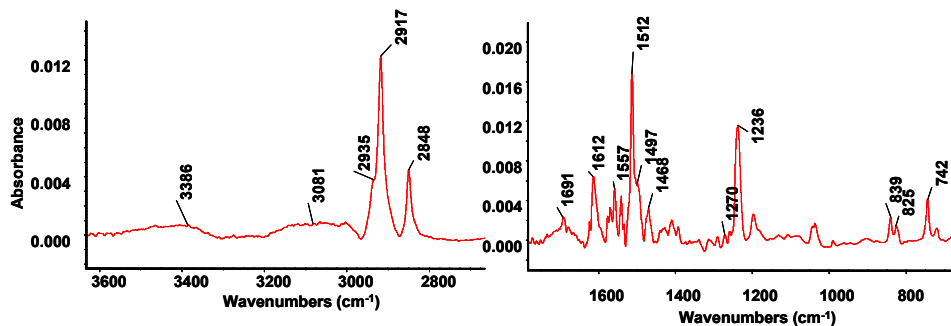
*Figure 4.8: Baseline corrected Infrared reflection absorption spectrum of amphiphiles (**1**).*
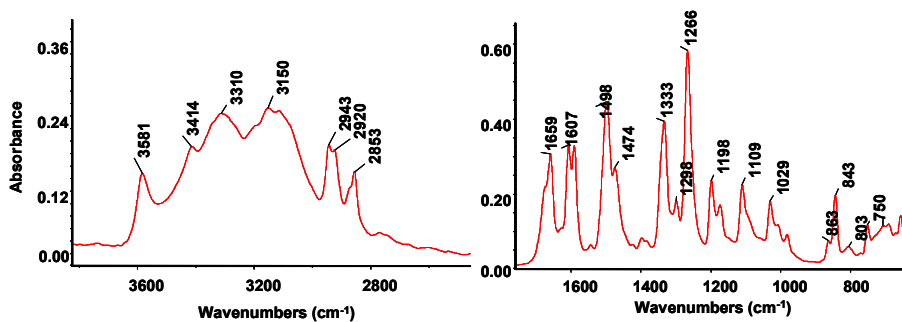
*Figure 4.9: FTIR spectrum (KBr) of NO₂ functionalized amphiphile (**2**).*
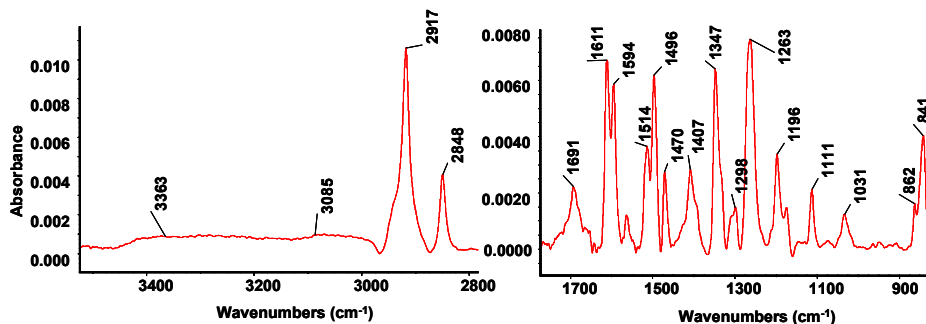
*Figure 4.10: Baseline corrected Infrared reflection absorption spectrum of amphiphile (**2**).*

53
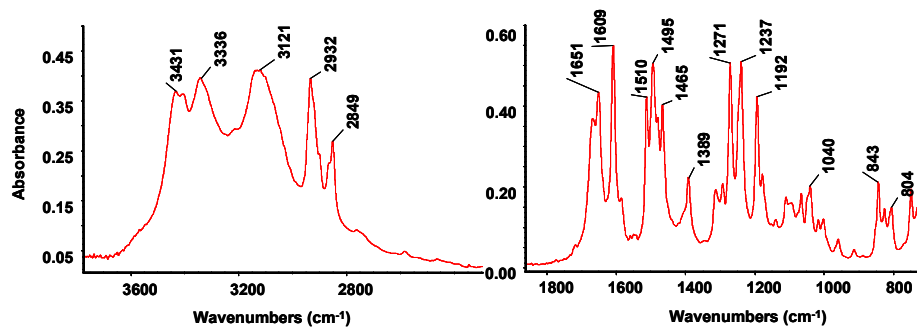
Figure 4.11: FTIR spectrum (KBr) of CH₃ functionalized amphiphile (3).
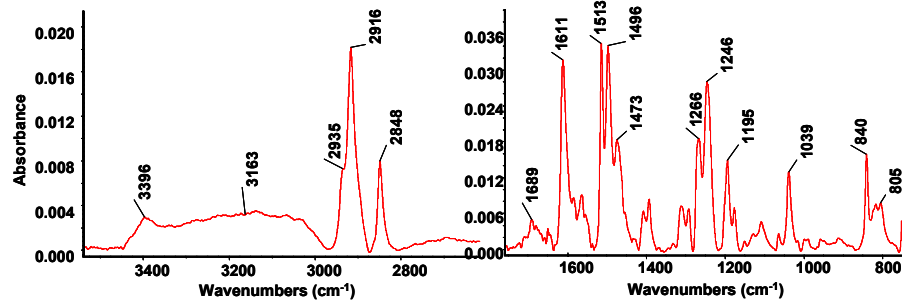
Figure 4.12: Baseline corrected Infrared reflection absorption spectrum of amphiphile (3).
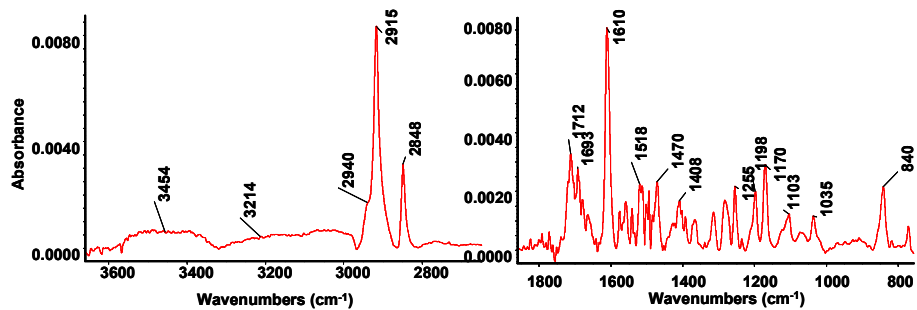
Figure 4.13: Baseline corrected Infrared reflection absorption spectrum of amphiphile (4).
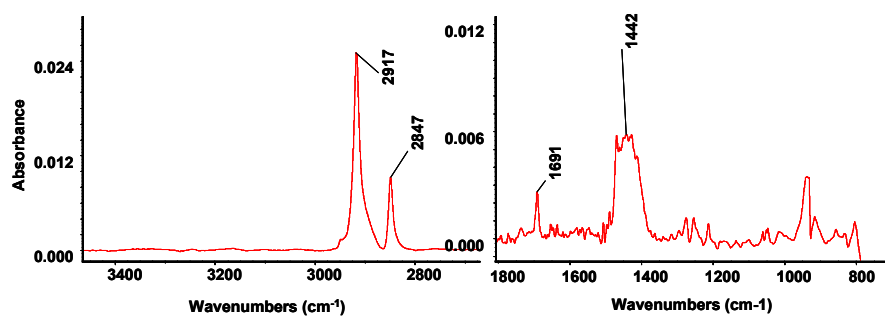
Figure 4.14: Baseline corrected Infrared reflection absorption spectra of MHA Sams on gold surface.

54

Careful inspection of the spectra of all amphiphile modified SAMs leads to identification of all significant peaks present in the transmission spectrum. This is evidence for the presence of the amidine amphiphiles on the acid monolayer. However, compared to the transmission spectrum, a number of additional features were seen. In Figure 4.8, Figure 4.10, Figure 4.12 and Figure 4.13, we can see the CH asymmetric stretch band at ~ 2917 cm^{-1}, symmetric band at 2848-2850 cm^{-1}, and also the CH band characteristic for the amidines at around 2937 cm^{-1} was observed.

The peak at 2917 cm^{-1} for CH asymmetric stretch of amphiphiles indicates a crystalline like order of the layer of alkyl chain on MHA SAMs, which also indicates the formation of an ordered layer. When this band (2917 cm^{-1}) is observed at higher frequencies (2920 cm^{-1} and above) it corresponds to a more disordered structure. This is accordance with the earlier reported observations for well ordered and crystalline like assembly of these amphiphilic layers on MHA SAMs [17, 19].

Low frequency region of the spectrum shown in Figure 4.8 reveals the presence of strong bands at 1512 cm^{-1} and at 1236 cm^{-1} which correspond to the Ph-OCH$_3$ stretch of the amphiphile (**1**).

For NO$_2$ (**2**) amphiphile, the low frequency region (Figure 4.10), shows all the functional groups which were present in the transmission spectrum of the amphiphile. NO$_2$ asymmetric stretch was observed at 1594 cm^{-1} and NO$_2$ symmetric stretch was detected at 1347 cm^{-1}.

The benzene ring C=C stretching mode (around 1610-1613 cm^{-1} and ~1494-1497 cm^{-1}), benzene CH out of plane mode (~ 840 cm^{-1}) and the COC stretch mode at 1266-1270 cm^{-1} were also detected in the IRAS spectrum of all the amphiphiles.

Figure 4.15 shows all the characteristic bands for amidine functionalities and also CH$_2$ symmetric and CH$_2$ asymmetric stretch at 2848 and 2917 cm^{-1} respectively.
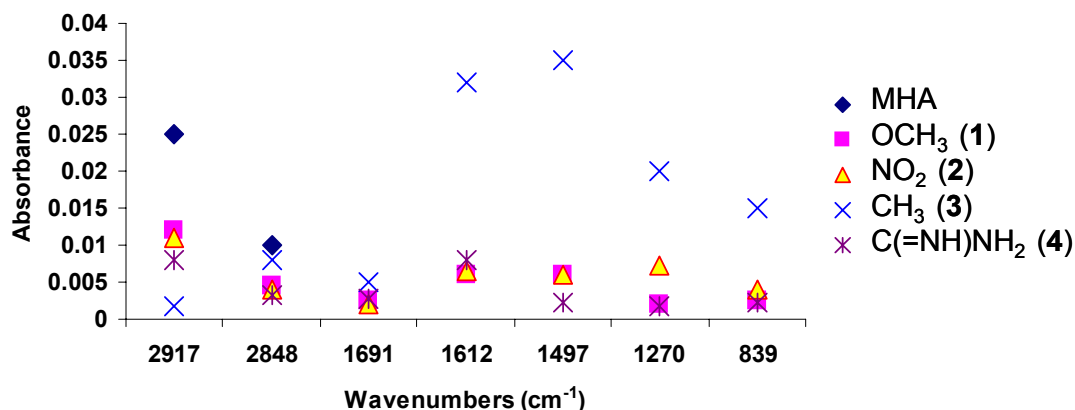
Figure 4.15: Band position and absorption intensities of all amphiphilic SAMs on MHA surfaces.

The broad bands between 3100 cm^{-1} to 3400 cm^{-1}, are indicative of interaction between the positively charged amidine head group and negatively charged carboxylate ion on the surface.

The grazing angle IR spectroscopy is thus found to be a better analytical tool for the structural studies of SAMs on the surfaces. The IRAS study of the amphiphiles assembled on mercaptohexadecanoic acid (MHA) reveals that the amphiphilic SAMs are stable to rinsing with pH borate buffer 9.

4.2.5 Contact angle measurements

The surface modification and its effects on wettability were analyzed using contact angle measurements. They were performed with a contact angle measuring system G10 by Krüss GmbH (Hamburg, Germany). The contact angle measurements were performed on air-dried sample by placing a borate buffer (pH 9) drop on the SAM surface. The measured contact angles were the advancing and receding angle between the surface and the buffer drop.

Sr. No.	Amphiphiles	Contact angles θ (°) Advancing	Contact angles θ (°) Receding
1	MHA	15	10
2	(1) R= -OCH$_3$	76	68
3	(2) R= -NO$_2$	78	71
4	(3) R= -CH$_3$	80	72
5	(4) R= -C(=NH)-NH$_2$	55	49

Table 4.2: Advancing and receding contact angles of MHA SAMs and subsequent immobilization of all amphiphiles on MHA SAMs.

The values given in the above Table are averages based on the mean measurements at three different spots on each surface.

From Table 4.2, originally highly hydrophilic MHA functionalized surfaces (contact angle 15°) converted into hydrophobic surfaces can be seen.

4.3 Mixed self-assembled monolayers of OCH$_3$ (1) and NO$_2$ (2) functionalized amphiphiles

Mixed SAMs on gold have widely been used to study the biocompatibility of the surfaces [22] and in the development of biosensors and in cell biology [23-26]. Mixed SAMs are the ideal system for studying the competiation of adsorption between two different molecules on the surface.

Ulman *et al.* [27, 28], extensively studied the formation of mixed monolayers of 4-substituted-4-mercaptobiphenyls on gold surfaces using different solvents. In their first study, they used 4-trifluoromethyl-4-mercaptobiphenyl and 4-methyl-4-mercaptobiphenyl, both having molecular dipoles relatively small for construction of mixed SAMs and observed that both dipole moment of the adsorbing 4-substituted-4-mercaptobiphenyls, and the solvent polarity, control the composition of mixed SAMs at equilibrium [28].

In their second study for the formation of mixed SAMs on gold surfaces, the extent of dipole interactions on adsorption of mixed SAMs was studied for the two dipolar molecules having significantly larger dipole moments [27]. The two p-substituents that were used for the same study were the nitro (NO$_2$) and dimethylamino (CH$_3$)$_2$N groups. They represent a strong electron withdrawing, and electron donor group, respectively. This paper reported that above two molecules tend to form 1:1 in stoichiometry.

In line with the work by Ulman, we have synthesized amphiphiles that have a π electron donor [OCH$_3$ (**1**)] and a π electron acceptor [NO$_2$ (**2**)] group at ω-position in ω-functionalized α-(4-amidinophenoxy)alkane amphiphile.

In analogy with the reported work [27, 28], we wanted to know whether π electron donor [OCH$_3$ (**1**)] and a π electron acceptor [NO$_2$ (**2**)] complementary head groups of mixed SAMs of these constituents influence their preferred stoichiometry and mixing tendency.

Schematic representation of mixed ω-functionalized SAMs on gold surfaces is shown in Scheme 4.4.
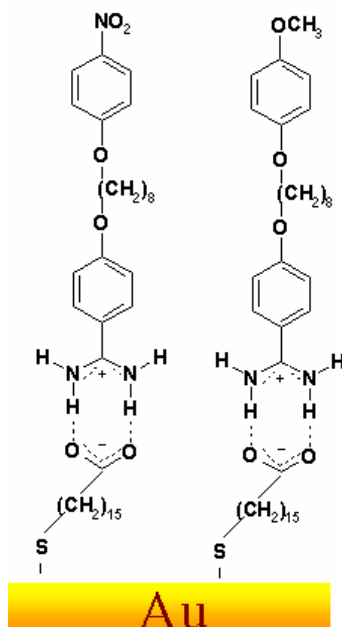
Scheme 4.4: Schematic representation of mixed monolayers of ω-functionalized amphiphiles on mercaptohexadecanoic acid terminated SAMs on gold surface.

4.3.1 In-situ ellipsometry of mixed SAMs

In situ ellipsometry experiments were performed on the mixed monolayers in order to gain an insight into the real time amphiphilic film thickness on MHA SAMs. These measurements were carried out on gold surfaces prepared by vapor deposition of gold (2000 Å) onto glass slides containing adhesive layers (300 Å) of chromium. MHA (0.002 M) was then immobilized on the above surfaces and then the MHA modified gold surfaces were immersed in a Teflon-coated cuvette containing 2 mL (0.01 M) sodium borate buffer (pH 9). Cuvette was thermostated at 25 °C and equipped with a small magnetic stirrer and a pH electrode. The addition of mixed amphiphiles (50 µM) was done after obtaining a stable base line in five different compositions of amphiphiles, 100:0% {R= -NO$_2$ (**2**) : R= -OCH$_3$ (**1**)}, 75:25%, 50:50%, 25:75%, and 0:100%.

Layer formation was monitored by *in situ* ellipsometry. As in the single component amphiphilic *in situ* ellipsometric kinetics shown in our previous section (Figure 4.1.), here also we anticipated that there would be an interaction between the negatively charged carboxylate ion surfaces and positively charged

mixed amidinium amphiphiles which would result in the stable, cyclic amidinium-carboxylate complex shown in Scheme 4.4.
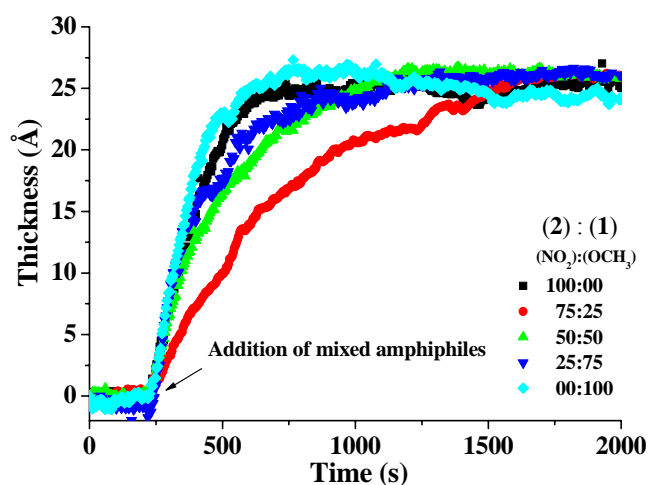
Figure 4.16 : Film thickness versus time during adsorption of α,ω-hetero-functionalized substituted amphiphiles on MHA modified gold surfaces.

Similar to the previous experimental observations (Figure 4.1) for the formation of single component amphiphiles on MHA SAMs, after the addition of the mixed amphiphiles in different composition, we observed the formation of monolayer with different rate of adsorption which is shown in the Figure 4.16. The monolayer thickness for the mixed SAMs was achieved which transforms the originally negatively charged carboxylate ion surface on gold into ω-functionalized α-(4-amidinophenoxy)alkanes surface.

When we studied all above kinetic spectra carefully, we noticed that the mixed SAMs (75:25%, 50:50% and 25:75% SAMs) show slower rate of adsorption for the formation of amphiphilic monolayer on MHA surface as compared to their single counterparts (non mixed) which are 100:0% and 0:100%.

75:25% composition of NO_2: OCH_3 was the slowest in kinetics. In Figure 4.16, we can see that, as the concentration of -NO_2 (**2**) decreases from 75% to 25%, the rate of monolayer formation in mixed SAMs increases. While pure 4-nitrophenoxy(4-amidinophenoxy)octane (**2**) and 4-methoxyphenoxy(4-amidinophenoxy)octane (**1**) show faster kinetics and rapid increase in the monolayer thickness.

60

4.3.2 The influence of pH on the layer thickness of mixed self-assembled monolayers
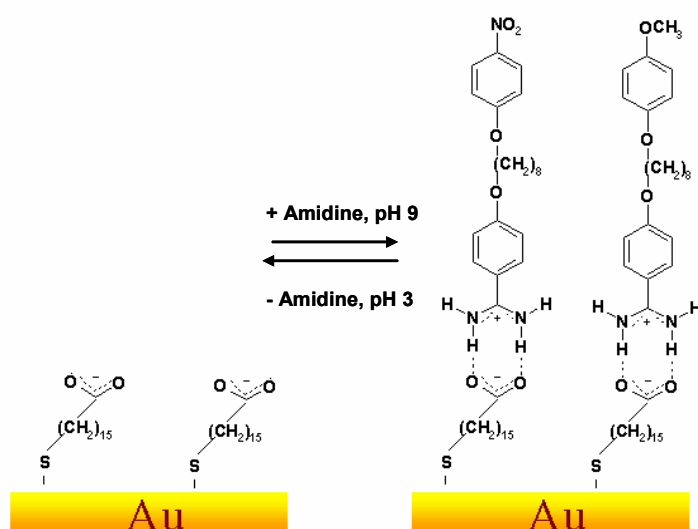
Scheme 4.5 : Schematic representation of assembly-disassembly of mixed monolayers on mercaptohexadecanoic acid terminated SAMs on gold surfaces.

Our main objective for studying the influence of pH on the layer thickness was to find out whether the different ratios of mixed amphiphiles added on MHA surfaces would result in different pH stability curves.

Lowering the pH leads to the protonation of carboxylate group (COO-) into carboxylic acid (COOH), surface which in turn reduces the head group attraction between the amidinium and carboxylate ions. This disrupts the hydrogen bonding between them, and finally removal of amphiphilic monolayer from MHA SAMs to yield ω-functionalized carboxylic acid gold surfaces. These surfaces can be reused after rinsing with 0.01 M HCl, 0.1 M NaOH and pH 9 borate buffer solutions.
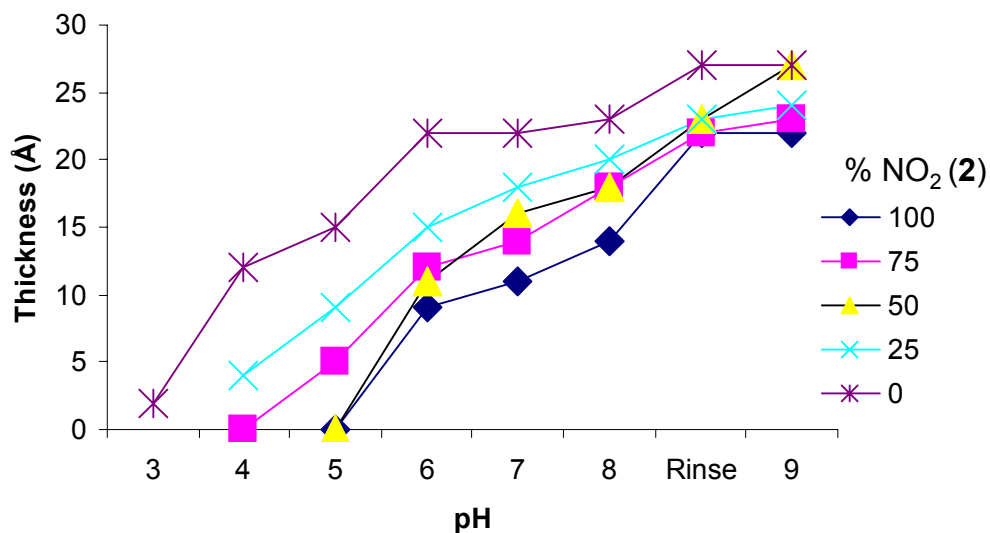
Figure 4.17 : The Influence of pH on layer thickness for mixed monolayers.

From Figure 4.16, we could conclude that the single component amphiphiles assemble faster in kinetics as compared to the mixed component amphiphiles. From Figure 4.17, we can say that as with the single component system, mixed monolayers are also stable to rinsing with pH 9, borate buffer and then layer thickness of the mixed amphiphiles decreases with decreasing pH. At pH 3, all the amphiphilic layers were ripped off from the surface yielding the carboxylic acid terminated SAMs.

4.3.3 IRAS of mixed SAMs of 4-nitrophenoxy and 4-methoxyphenoxy (4-amidinophenoxy)octane amphiphiles

We have performed the IRAS study on the mixed SAMs which we will discuss in this section.

For the IRAS study, we have used the same type of substrates which we have used for the *in situ* ellipsometry. Here, instead of only five compositions of mixed monolayers which were used in *in situ* ellipsometry study, we have used a total of nine compositions to gain more insight into the packing, orientation, order and crystalline like nature structure of mixed SAMs on MHA modified gold surfaces.

After following the same preparation procedure for the construction of MHA SAMs on freshly prepared gold surfaces, the mixed benzamidine amphiphiles {4-nitrophenoxy(4-amidinophenoxy)octane (**2**) and 4-methoxyphenoxy(4-amidinophenoxy)octane (**1**)} in nine different compositions (100, 87.5, 75, 63.5, 50, 37.5, 25, 12.5, 0%) were allowed to adsorb onto MHA modified gold surfaces for 16 hours. After that, the surfaces were carefully rinsed with pH 9 borate buffer (0.01 M), dried under a stream of nitrogen and then surfaces were characterized in air by IRAS.

Careful observation of the spectra obtained from IRAS leads to identification of all significant peaks present in the transmission spectrum (prepared from KBr pellets), which in turn tells us that the mixed amidine amphiphilic layer is present on the MHA monolayer and that these mixed amidine layers are stable after rinsing.

Figure 4.18 shows the high frequency region of the baseline corrected IR reflection absorption spectra of mixed SAMs of 4-nitrophenoxy(4-amidinophenoxy)octane (**2**) and 4-methoxyphenoxy(4-amidinophenoxy)octane (**1**) in nine different compositions. The first spectrum (bottom) is of MHA SAMs and the concentration of nitro terminated amphiphiles increases from bottom to top. (i.e. 0%, 12.5, 25, 37.5, 50, 63.5, 75, 87.5 and 100% respectively above the MHA SAMs).
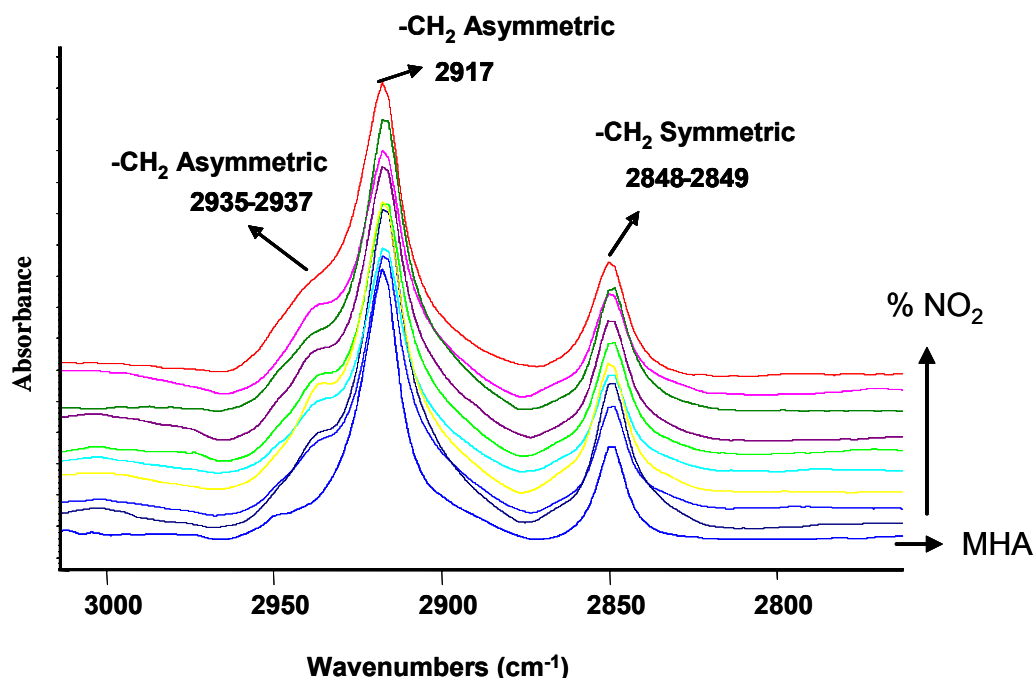
Figure 4.18: Baseline corrected IRAS spectra of high frequency region of different compositions of mixed amphiphiles on MHA SAMs. The compositions of each monolayer (NO₂) are from bottom to top in the orders: 0%.12.5, 25, 37.5, 50, 63.5, 75, 87.5, and 100% NO₂ (2).

The band at 2917 cm^{-1} corresponds to the CH_2 (C-H) asymmetric stretch, which indicates the crystalline like order of the assembled mixed and single component layers on MHA SAMs. The band at 2935- 2937 cm^{-1} was assigned to the CH_2 (C-H) asymmetric stretch characteristic of the amidines which is typical for the methylene CH close to the electronegative substituents [29]. The peak at 2848-2849 cm^{-1} represents the CH_2 (C-H) symmetric stretch.
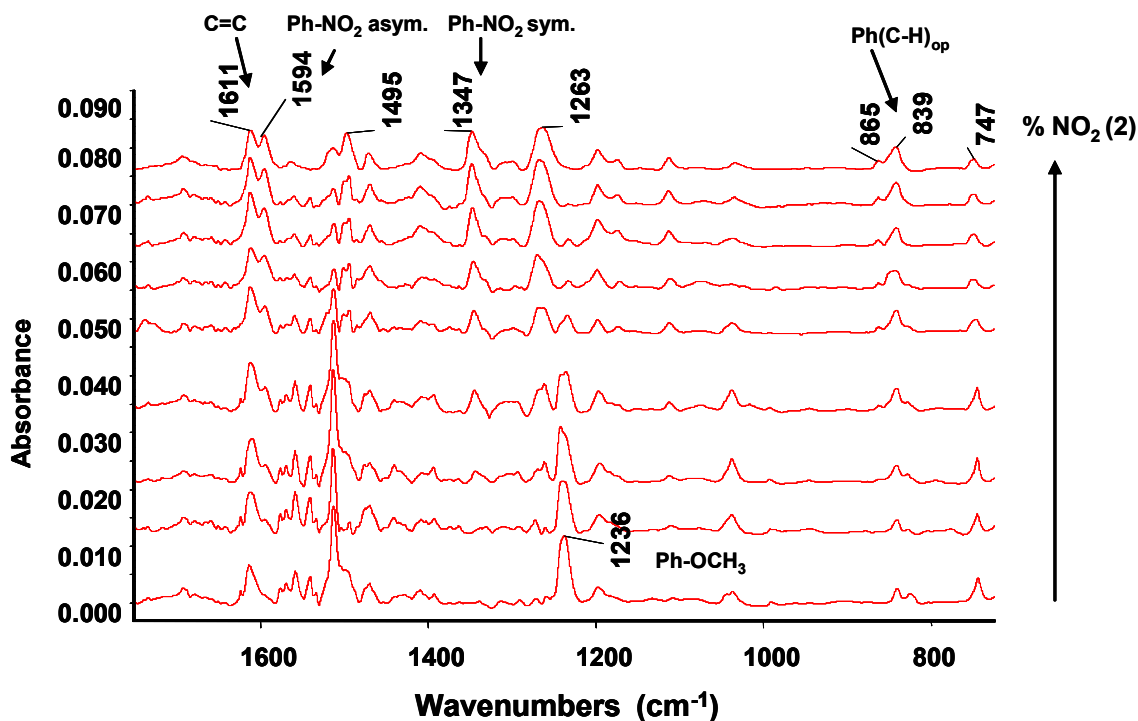
Figure 4.19: Baseline corrected IRAS spectra of low frequency region of different compositions of mixed amphiphiles on MHA SAMs. The compositions of each monolayer are from bottom to top 0%.12.5, 25, 37.5, 50, 63.5, 75, 87.5, and 100% of NO₂ (2) amphiphiles.

Figure 4.19 shows the low frequency region of the assembled mixed amphiphiles on MHA terminated SAMs on gold surfaces.

As with the high frequency region of SAMs, here also we have observed all significant peaks present in the low frequency region of the transmission spectrum like benzene C=C stretch at 1611 to 1614 cm^{-1} and C-O-C stretch at 1263-1272 cm^{-1}, Ph C-H stretch at 839- 842 cm^{-1} (out of plane). We have also observed the amphiphilic NO$_2$ symmetric stretch around 1340-1347 cm^{-1} and NO$_2$ asymmetric stretch at 1594 cm^{-1}. The OCH$_3$ stretches at 1236-1238 cm-1 and at 1511 cm-1 were also present in SAMs.

From Figure 4.19 and Figure 4.20 we can see that the intensities of benzamidine groups were constant where as, those of the bands characteristic for -OCH$_3$ (**1**) and -NO$_2$ (**2**) head group (Figure 4.23 and Figure 4.24) changes as the concentration of these amphiphile changes.
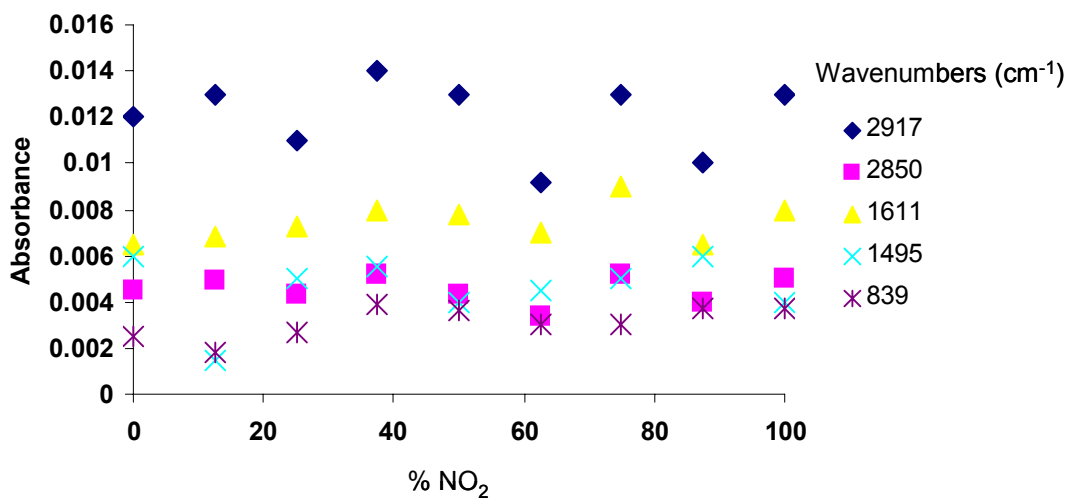
Figure 4.20: Band position and absorption intensities of mixed amphiphiles of NO₂ and OCH₃ SAMs on MHA surfaces.

While preparing these mixed SAMs, we have used one electron withdrawing group (NO$_2$) (**2**) and one electron donating group (OCH$_3$) (**1**) at ω- position of the amphiphiles in SAMs. These two functional groups in self-assembled monolayers appear very strongly in IRAS. A separate plot of the NO$_2$ band at around 1340-1347 cm^{-1} [27], and the OCH$_3$ band at ~1236 cm^{-1} is shown in the Figure 4.21 and Figure 4.23 respectively.
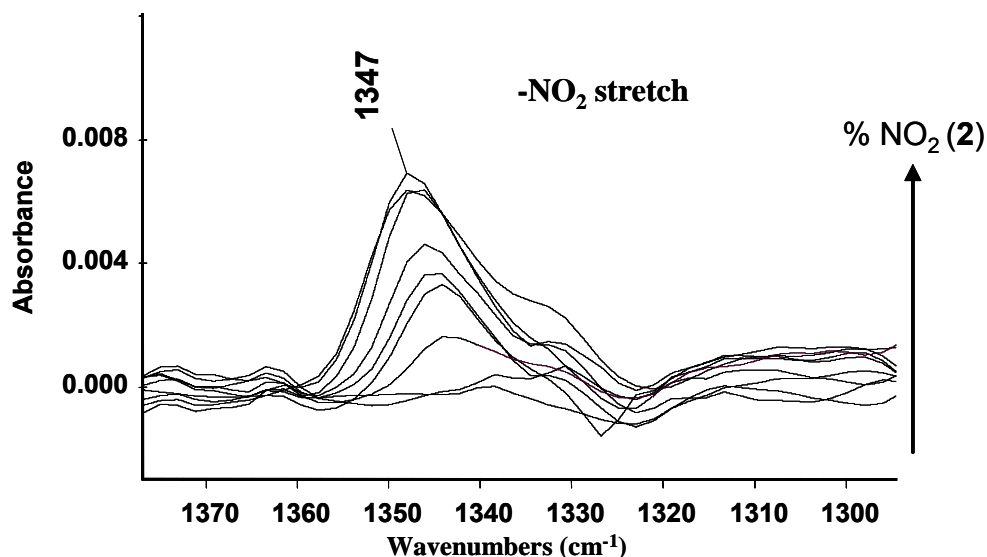
Figure 4.21: Baseline corrected IRAS spectra of the –NO₂ band at ~ 1347cm⁻¹ for the mixed SAMs with OCH₃.(composition is from bottom to top 0%.12.5, 25, 37.5, 50, 63.5, 75, 87.5, and 100% -NO₂).

66

As displayed in Figure 4.21, the peak intensity of NO_2 band increases with the increasing amounts of added NO_2 amphiphile (bottom to top). Interestingly, we have not only observed the increase in the intensity of NO_2 band upon addition of same amphiphile, but also observed that there is an optically induced band shift (1340 cm^{-1} to 1347cm^{-1}) as the concentration of NO_2 amphiphile increases in the mixed monolayer gradually. When we compared the position of the NO_2 symmetric band (1333 cm^{-1} in transmission mode, KBr pellets) with the absorption spectra (1347 cm^{-1} in IRAS, on surface) of assembled SAMs on MHA gold surface, we observed that the band maxima are shifted to higher energy from transmission spectrum to IRAS spectrum which is shown in Figure 4.22.
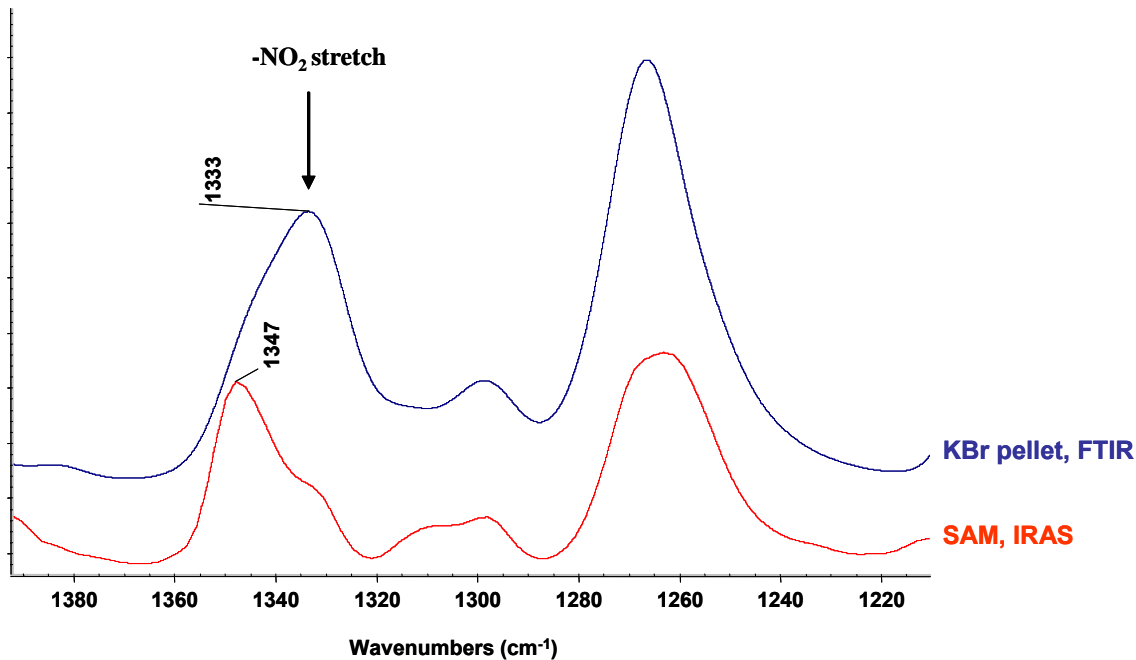
Figure 4.22: Comparison between transmission infrared spectrum of NO_2 band (Top, KBr pellet) and the absorption spectra (IRAS, SAM, bottom) of assembled SAMs on MHA gold surface.

Ulman *et al* [30] carried out detailed investigation on the formation of a mixed monolayer consisting of 4-trifluoromethyl-4-mercaptobiphenyl (strongly electron withdrawing head group) and 4-methyl-4-mercaptobiphenyl (electron donating head group) molecules on gold surface. They observed that the transmission spectrum of the 4-trifluoromethyl-4-mercaptobiphenyl molecule showed a broad

band at ~ 1327 cm^{-1} where as the IRAS showed narrow and well resolved band at ~ 1340 cm^{-1}. They concluded that the intermolecular interactions were different in SAM (IRAS) and in solid (KBr pellets).

We have also detected the same observation that the FTIR spectrum (4.22) of NO_2 amphiphile (**2**) shows (KBr pellet, top spectrum) a broad band as compared to the SAM of the same amphiphile (bottom spectrum) and even we have observed the optical shift of the same band from 1333 cm^{-1} in FTIR mode to 1347 cm^{-1} in IRAS mode. These observations lead to the conclusion that the intermolecular interactions present in the solid (transmission spectrum) seem to be absent in the well ordered SAMs, one would expect the molecular interactions to be minimized in oriented monolayer assemblies. This is fully supported by the observation of the bandwidth of the symmetric NO_2 stretch shifted from 1333 cm^{-1} in transmission mode to 1347 cm^{-1} in a SAM.

When we mixed ω-functionalized NO_2 (**2**) and OCH_3 (**1**) amphiphiles in different concentrations, we not only observed the decrease in the peak intensity but also observed the change in the optical shift in the peak position from 1347cm^{-1} to 1340 cm^{-1} (Figure 4.21). In literature [31], following three factors that could be responsible for the change in the peak positions of adsorbed molecule have been identified. (1)The blue shift due to mechanical renormalization, (2) chemical effects due to surface bonding and (3) lateral interactions between neighboring oscillators (vibrational coupling).

Coverage-dependent frequency shift can be caused due to the vibrational coupling effect [32]. Since the vibrational frequencies for NO_2 (**2**) and OCH_3 (**1**) are widely different, they should show coverage dependent frequency shift. This could be the reason that we are detecting the concentration-dependent peak shift in IRAS spectra of mixed SAMs.

Interestingly, we also observed the concentration dependent peak shift for the OCH_3 (**1**) amphiphile which was very less as compared to NO_2 (**2**) and is displayed in the Figure 4.23 along with NO_2 symmetric peak at ~1347 cm^{-1}.
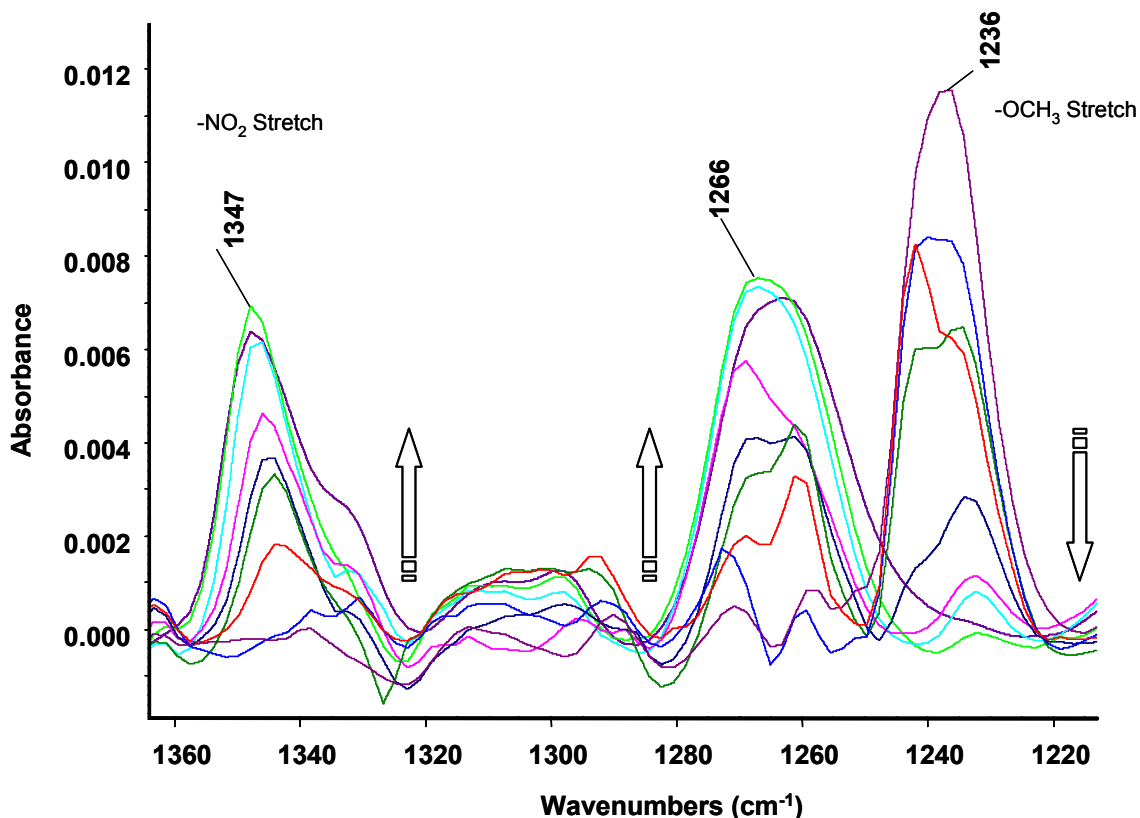
Figure 4.23: Baseline corrected IRAS spectra of the -NO$_2$ band at ~ 1347cm^{-1} and -OCH$_3$ band at ~ 1236 cm^{-1} for the mixed SAMs.(composition is from bottom to top 0%.12.5, 25, 37.5, 50, 63.5, 75, 87.5, and 100% -NO$_2$).

Figure 4.23 reveals the IRAS region between 1220-1360 cm^{-1} of mixed SAMs of OCH$_3$ (**1**) and NO$_2$ (**2**) at different compositions. The peak at ~ 1347 cm^{-1} assigned for NO$_2$ symmetric stretch and peak at 1236 cm^{-1} was assigned for OCH$_3$ stretch. Arrows indicate the change in intensity with increasing NO$_2$ content from bottom to top.

When we plotted the integrated area of NO$_2$ and OCH$_3$ bands for different compositions, we observed that there is a direct relationship between the peaks integrated area and the amount of added amphiphile on the SAMs. In Figure 4.24, it is visualized that when the concentration of NO$_2$ amphiphile in mixed monolayer increases from 0% to 100%, then the peak integrated area of the same functional group increases as well. The same observed for the OCH$_3$ amphiphile in the mixed monolayer. It is also seen that there was clear tendency of -OCH$_3$ (**1**) layer to stay on the MHA surface.
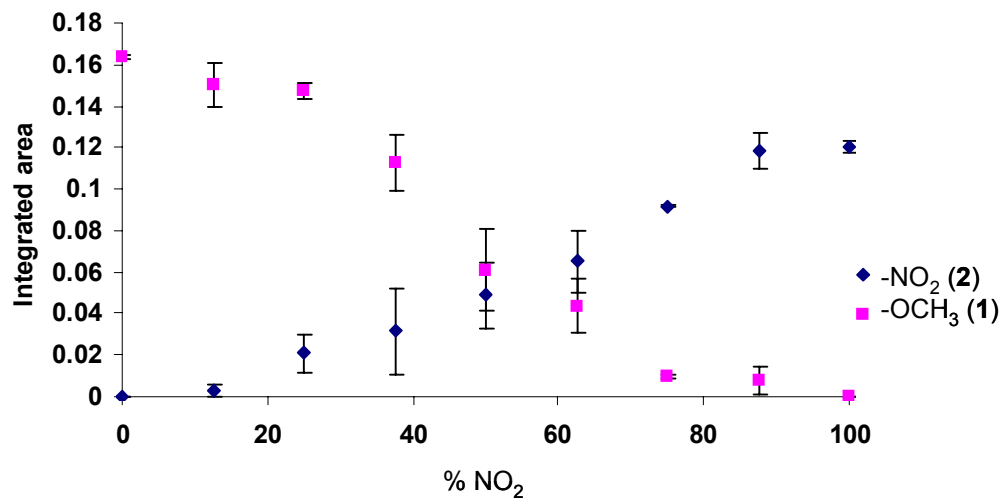
*Figure 4.24: Plot of the integrated area under -NO$_2$ (**2**) (~1347cm^{-1}) and -OCH$_3$ (**1**) (~1236 cm^{-1}) bands at different concentratiosn in the mixed monolayers on MHA SAMs.*

4.3.4 Contact angle measurements

As with the single component amphiphiles, the surface wettability was also studied for the ω-functionalized mixed component amphiphiles (Figure 4.25). The contact angle measurements were performed on air-dried sample by placing a borate buffer (pH 9) drop on the SAM surface. The measured contact angles were the advancing and receding angle between the surface and the buffer drop.
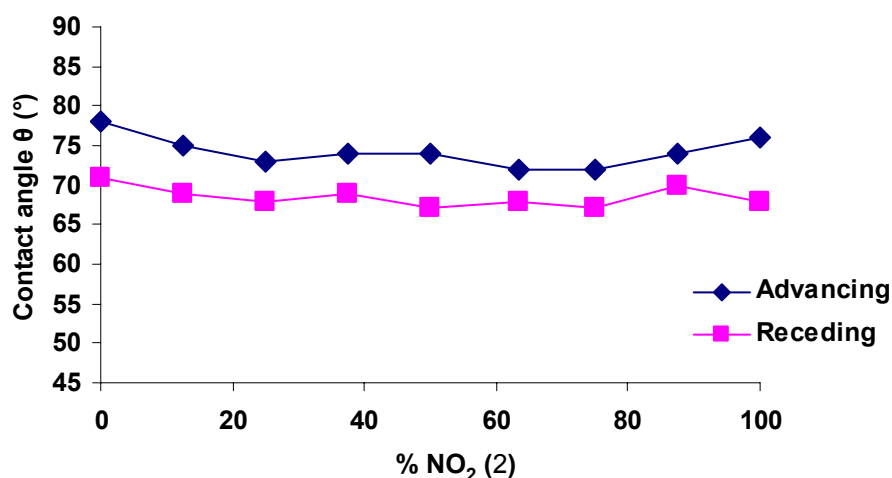
Figure 4.25: Plot of the advancing and receding contact angle of NO₂ and OCH₃ amphiphiles at different concentrations in the mixed monolayers on MHA SAMs.

The contact angle of the mercaptohexadecanoic acid SAMs was 10° (± 5°) [35]. Figure 4.25 shows the advancing and receding contact angle of the assembled ω-functionalized -OCH$_3$ (**1**) and -NO$_2$ (**2**) mixed amphiphiles on MHA SAMs. We can conclude from the above figure that, after the adsorption of these amphiphiles, originally hydrophilic MHA SAM surfaces were converted into less polar surfaces reading contact angles between 70° and 80°. Notably, the contact angle of OCH$_3$ (**1**) terminated SAMs agrees with the literature value [55, 56] (Table 3.1).

4.4 Mixed self-assembled monolayers of 4-methoxyphenoxy(4-amidinophenoxy)octane and 4-bis(amidinophenoxy)octane

We have also performed the mixed monolayer study on 4-methoxyphenoxy(4-amidinophenoxy)octane (**1**) and 4-bis(amidinophenoxy)octane (**4**) which is displayed in Scheme 4.6.
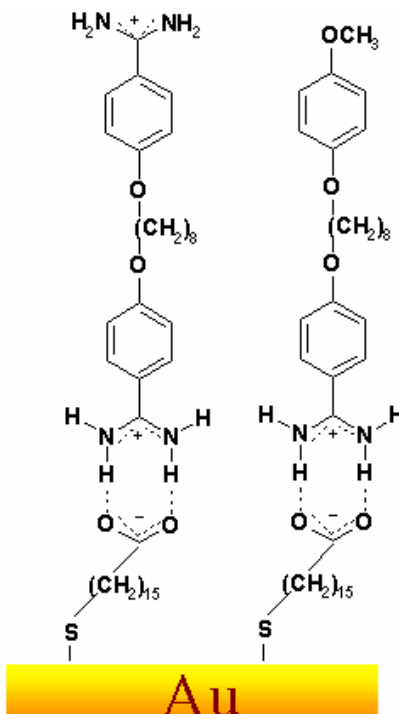
Scheme 4.6: Schematic representation of mixed monolayers of ω- functionalized amphiphiles on mercaptohexadecanoic acid terminated SAMs on gold surface.

To gain more knowledge about the arrangement, ordered like structure, and wetting properties of another set of mixed self-assembled monolayers and to achieve the chemical foundation of surface properties, we have extensively studied the phenomenon of formation of mixed monolayers of 4 amidinophenoxy (**4**) and 4-methoxyphenoxy(4-amidinophenoxy)octane (**1**) amphiphile by adsorption and desorption process using *in situ* ellipsometry, which will be discussed in the following paragraph of this chapter.

4.4.1 *In-situ ellipsometry*

We have mixed 4-methoxyphenoxy (**1**) and 4-bis(4-amidinophenoxy)octane (**4**) amphiphiles in five different proportions for *in situ* ellipsometry study; {100:0% (-OCH$_3$: -C(=NH)NH$_2$), 75:25%, 50:50%, 25:75%, and 0:100%}. The sample preparation and immobilization of MHA were done identical to the procedure described for the *in situ* ellipsometry studies in section 4.2.1.

When the above prepared amphiphiles were added on MHA terminated SAMs, we observed increase in layer thickness upon time for all the compositions of mixed molecules which is shown in Figure 4.26.
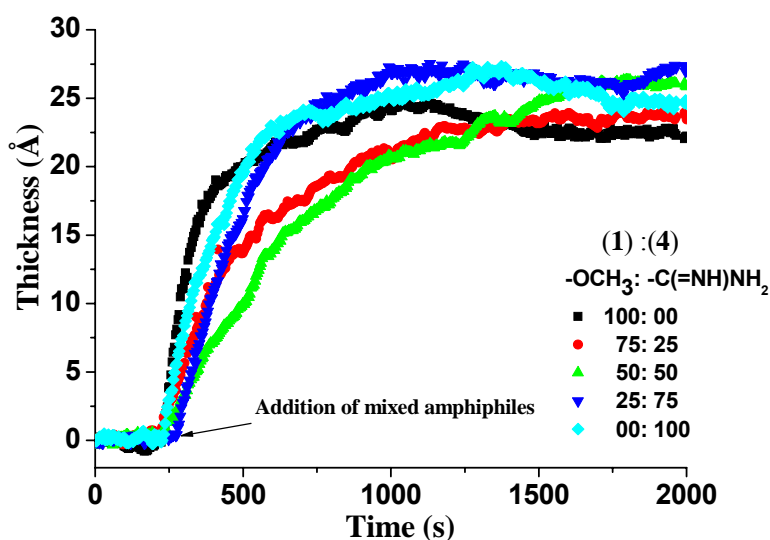
Figure 4.26: Film thickness versus time during adsorption of ω-functionalized amphiphiles on MHA modified gold surfaces.

From Figure 4.26, it is observed that as in the case of single component amphiphiles, mixed amphiphiles also achieve monolayer thickness upon addition of them on MHA terminated SAMs but more slowly as compared to their single component amphiphiles. When we look into the above Figure 4.26 carefully, we can also detect that 1:1 composition (50:50) of these mixed monolayers tends to acquire monolayer thickness more slowly as compared to their single component counterparts. The agreement between the observed thickness (*in situ* ellipsometry) upon addition of mixed amphiphilic solution on MHA SAMs and

calculated maximum length of the molecule (using Chem 3D ultra 6.0) suggest that the mixed component system also forms closely packed monolayers on the carboxylate surface.

4.4.2 The influence of pH on mixed self-assembled monolayers

In our entire study, the degree of ionization of the surface of carboxylic acid was the controlling factor for the assembly-disassembly of amphiphilic molecules on MHA terminated surfaces.

For the mixed self-assembled monolayers of 4-methoxyphenoxy (**1**) and 4-bis(4-amidinophenoxy)octane (**4**) amphiphiles, we have carried out the same investigations which we studied in our previous part of the chapter (section 4.3.2). The formation of mixed monolayer assembly, (at pH 9) and disassembly of the same layer (pH 3) were studied to achieve the reusable sensor surface. Figure 4.27 displays the influence of pH on mixed monolayer thickness. Importantly, all the mixed assembled monolayers on MHA surfaces were stable after rinsing.
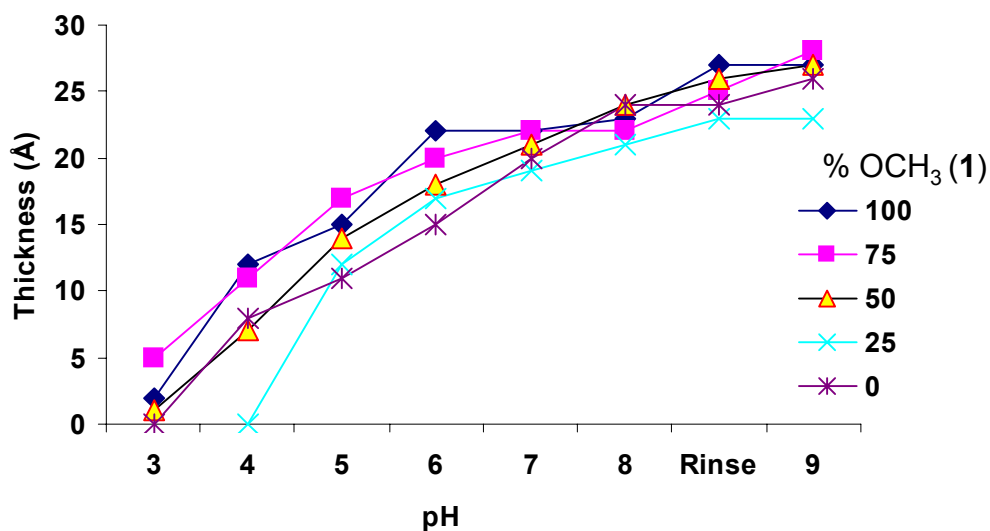
Figure 4.27: Influence of the pH on layer thickness for mixed monolayers.

Mixed monolayers of 4-methoxyphenoxy (**1**) and 4-bis(4-amidinophenoxy)octane (**4**) amphiphiles retain their monolayer thickness upon decrease in pH till 6-7. However, below pH 6 till pH 3, the state of ionization of carboxylate surface changes and hence disrupts the intermolecular head group hydrogen bonding between carboxylate ion of acid surface and amidinium ion of amphiphiles. This leads to the removal of mixed amphiphilic layer from the acid surface to yield the reusable form of carboxylic acid surfaces to construct more layer assemblies on the same sensor platform. When we compared the stability of above mixed SAMs upon changing the pH, with the layer stability for the mixed monolayers of 4-nitrophenoxy (4-amidinophenoxy)octane (**2**) amphiphile and 4-methoxyphenoxy (4-amidinophenoxy)octane (**1**) amphiphile, we observed that 4-methoxyphenoxy (**1**) and 4-bis(4-amidinophenoxy)octane (**4**) amphiphiles were more stable towards the treatment of pH until 6-7 (these mixed SAMs retained their monolayer thickness till pH 6-7) but mixed amphiphiles of (**1**) and (**2**) were less stable to lower pH (pH 6) and below pH 6. In both mixed SAMs, submonolayer thicknesses were recorded.

When the above surfaces were further acidified till pH 3, the amphiphilic layer was taken away from the surface. After removal of amphiphilic layer from the acid surfaces, the same surfaces were subjected to 0.1 M HCl and 0.1 M NaOH rinsing followed by rinsing with buffer pH 9 and then they were subsequently reused several times with reproducible results.

4.4.3 Infrared reflection absorption spectroscopy of mixed SAMs of 4-methoxyphenoxy and 4-bis(4-amidinophenoxy)octane amphiphiles

The peak position of the CH_2 asymmetric stretch at 2916 cm^{-1} indicates the crystallinity and order of the mixed self-assembled monolayers on MHA terminated SAMs, which is displayed in Figure 4.28.
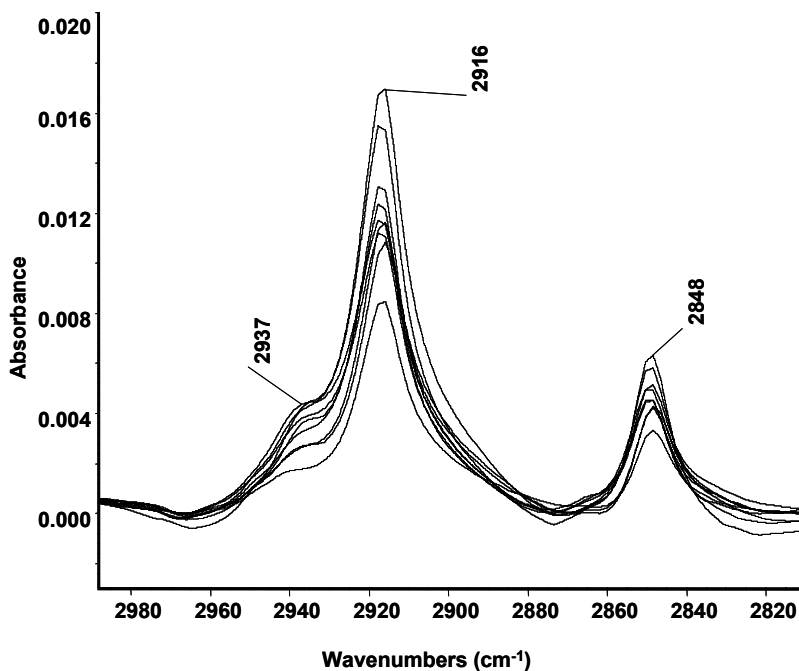
Figure 4.28: Baseline corrected IRAS spectra of high frequency region of mixed amphiphiles on MHA SAMs.

Apart from CH_2 asymmetric stretch at 2916 cm^{-1}, we have also detected the CH_2 asymmetric stretch at 2937 cm^{-1}, which corresponds to the typical characteristic peak for the amidines. This indicates the presence of mixed amphiphilic amidine layers on acid functionalized surfaces. The CH_2 symmetric stretch was also observed at 2848 cm^{-1}.
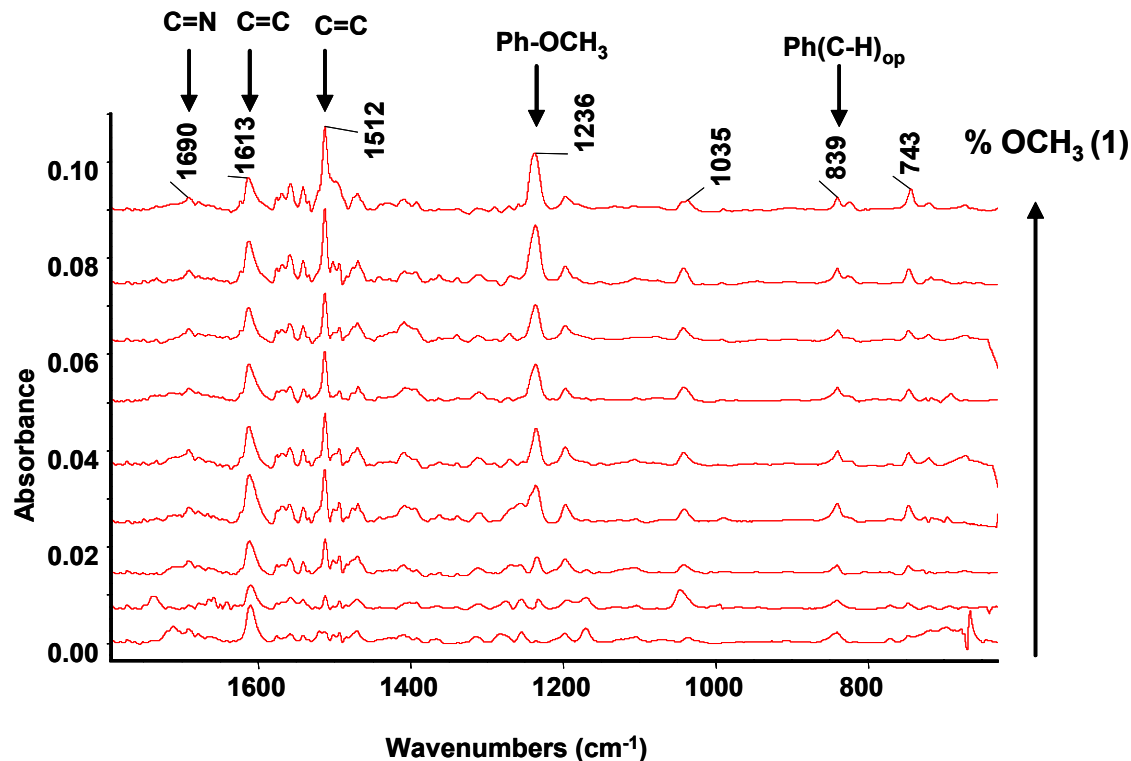
Figure 4.29 Baseline corrected IRAS spectra of high frequency region of mixed amphiphiles on MHA SAMs.

When we looked carefully into the low frequency region of these mixed amphiphiles (Figure 4.29), we observed a peak at ~ 1512 cm^{-1} and peak at ~ 1236 cm^{-1}, which corresponds to the Ph-OCH$_3$ stretch of amphiphile (**1**). C=C stretch of benzene ring and Ph (C-H) out of plane were detected at 1613 $cm^{-1}$and 839 cm^{-1} respectively.

The presence of all functionalities in the IRAS spectrum further confirms the presence of amphiphilic layers on acid functionalized SAMs. The relative intensities of the corresponding bands are drawn in Figure 4.30.
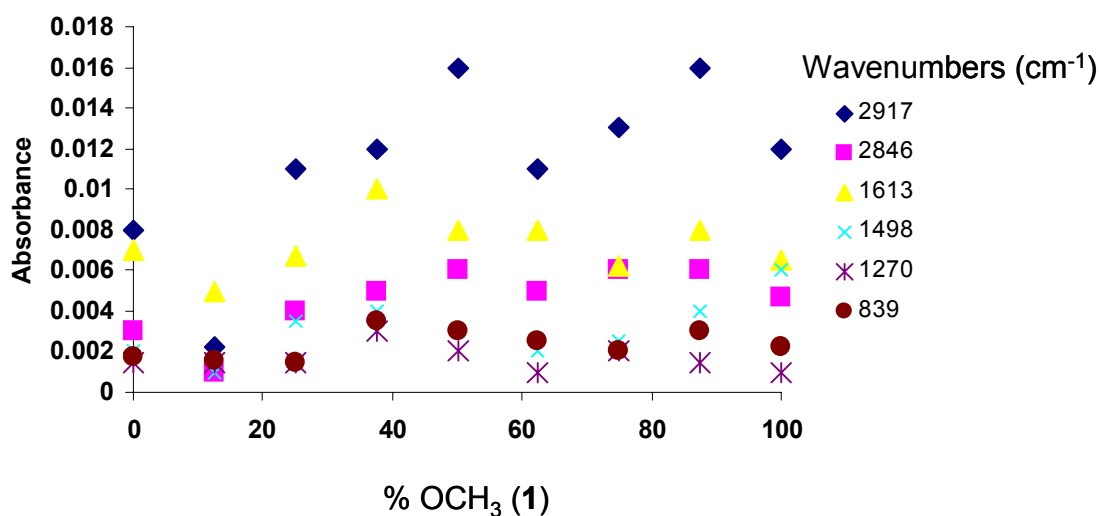
*Figure 4.30: Band position and absorption intensities of mixed amphiphiles of OCH$_3$ (**1**) and C(=NH)NH$_2$ (**4**) SAMs on MHA surfaces.*

The peaks at ~1236 cm^{-1} and at ~1512 cm^{-1} which correspond to the Ph-OCH$_3$ stretch of 4-methoxyphenoxy (4-amidinophenoxy)octane (**1**) were distinct and are drawn in Figure 4.31 and Figure 4.32 respectively.
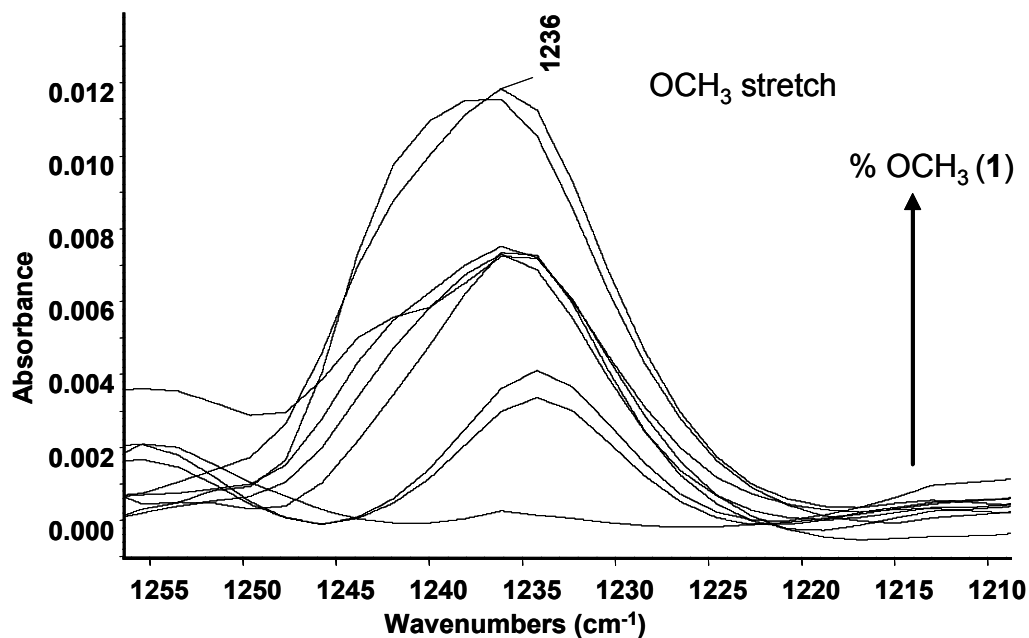
*Figure 4.31: Baseline corrected IRAS spectra of the –OCH$_3$ band at 1236 cm^{-1} for the mixed SAMs with bisbenzamidine (**4**).*
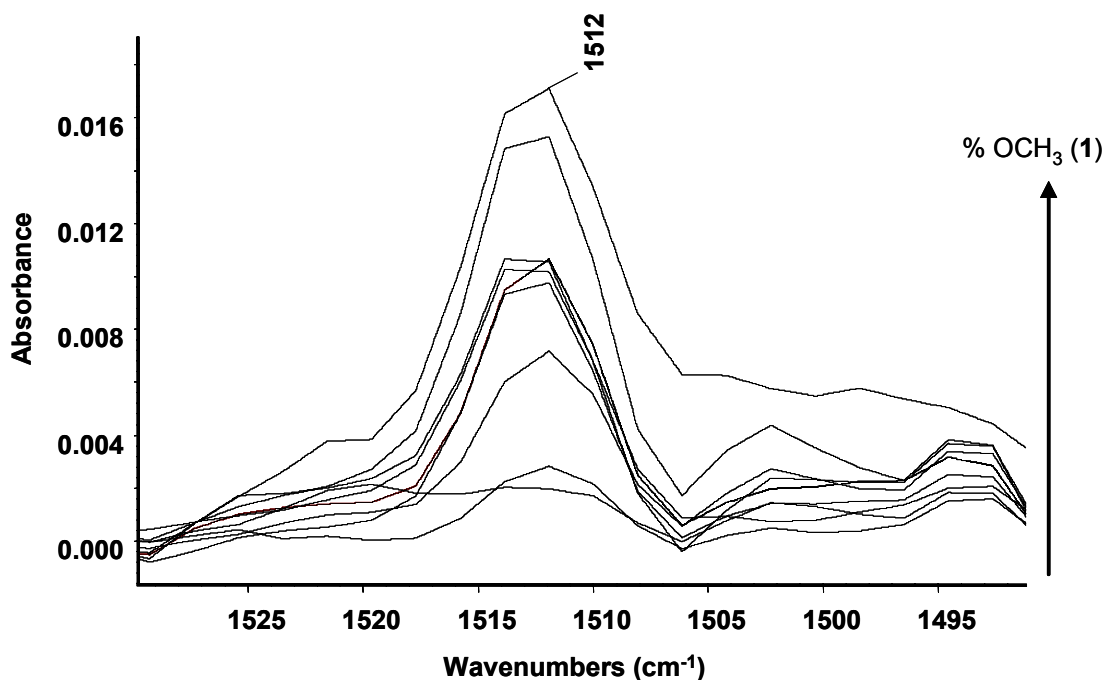
Figure 4.32: Baseline corrected IRAS spectra of the $-OCH_3$ band at 1511 cm^{-1} for the mixed SAMs with bisbenzamidine (4).

We have also plotted the peak intensity of OCH_3 (**1**) band in mixed self-assembled monolayers at different concentrations which is shown in Figure 4.33. From the same Figure, we can see that the peak intensity increases with respect to the concentration of added amphiphiles in mixed layer compositions.
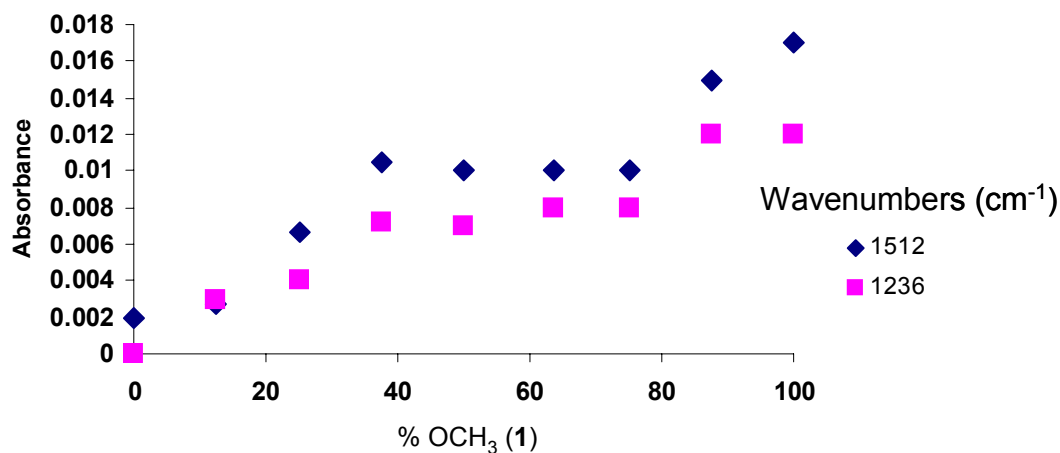
Figure 4.33: Plot of the intensities of OCH_3 (1512 cm^{-1} and 1236cm^{-1}) bands at different concentrations in the mixed monolayers on MHA SAMs.

As compared to the mixed monolayers of 4-nitrophenoxy (4-amidinophenoxy)octane (**2**) and 4-methoxyphenoxy (4-amidinophenoxy)octane (**1**) amphiphile, we observed that 4-methoxyphenoxy (**1**) and 4-bis(4-amidinophenoxy)octane (**4**) amphiphiles appear to form randomly mixed monolayers. This is also confirmed by the contact angle measurements which are shown in Figure 4.34.

4.4.4 Contact angle measurements

To gain more information about the ordered arrangement of mixed amphiphilic amidine layers on acid terminated SAMs, and to detect the wetting property of the same surfaces, we have carried out detailed investigation by contact angle measurements.

Advancing and receding contact angles of mixed monolayers of 4-methoxyphenoxy (**1**) and 4-bis(4-amidinophenoxy)octane (**4**) (Figure 4.34), reveals that as the concentration of OCH_3 (**1**) amphiphile increases, the wettability of the surfaces decreases. At 0% OCH_3 concentration, this means that at 100% amidine terminated SAMs, the advancing and receding contact angles were 55 and 49° respectively. As the concentration of OCH_3 (**1**) amphiphile increases from 0% to 100%, we detected a continuous increase in the advancing and receding contact angles and at 100% concentration of OCH_3, the contact angles were detected 78 and 71° respectively. This in turn tells us that the continuously decreasing wetting property of the surface was achieved with increasing concentration of the OCH_3 component, which is a reference to a well arranged layer with complete head group exposition of the amphiphiles on acid terminated surfaces. The linear independency in the following figure indicates good mixing of mixed SAMs.
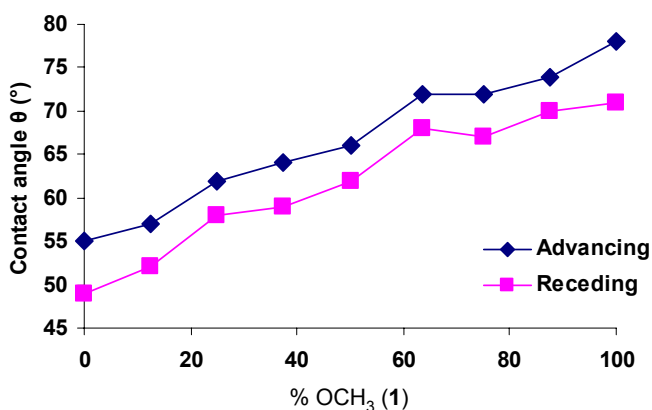
*Figure 4.34: Plot of the advancing and receding contact angle of OCH_3 (**1**) and –C(=NH)NH$_2$ (**4**) terminated amphiphiles at different concentration levels in the mixed monolayers on MHA SAMs.*

4.5 Atomic force microscopy (AFM)

Morphological information of assembled SAMs was obtained by **A**tomic **F**orce **M**icroscopy (**AFM**) measurements. Assembled single and mixed component amphiphiles on acid terminated surfaces were characterized by AFM.

While performing an AFM measurement, it is important to have flat gold surface or flat gold region on the gold surface. This allows one to investigate the height differences from gold to acid terminated self-assembled monolayers and subsequently the height differences between the gold and added amphiphile on MHA SAMs as well as to obtain information about the lateral homogeneity of the SAM surface [19, 33]. Initially, our efforts were in the direction of achieving the crystalline like layer structure of MHA SAMs and then, if possible, the further crystalline like ordered structure of the amidine amphiphile on the acid terminated SAMs.

Initial experiments were done using home-made gold evaporated surfaces. For that, onto the freshly cleaved mica surfaces, gold (2000 Å) was vapor deposited containing adhesive layer (300 Å) of chromium. Before the chemoadsorption of MHA, these surfaces were annealed at 400 °C in the oven for 3 hours and were immediately placed in solution of Mercaptohexadecanoic acid (0.002 M) in ethanol for 16 hours.

2000 Å of gold deposited substrates were also bought readymade from "Ssenes" Netherlands. These surfaces were flame annealed (time duration of flame annealing was 15 to 30 seconds as after 30 seconds of flame annealing, the gold from the surface was completely evaporated).

Figure 4.35 shows the AFM image of a freshly evaporated gold surface. These gold surfaces were too rough for the immobilization of MHA SAMs because of the degree of roughness they posses in terms of height and width distances. We can see in the same figure that there are small particles of gold (gold balls) around 20-30 nm in height and spread throughout the surface which are responsible for the roughness of the gold surface.
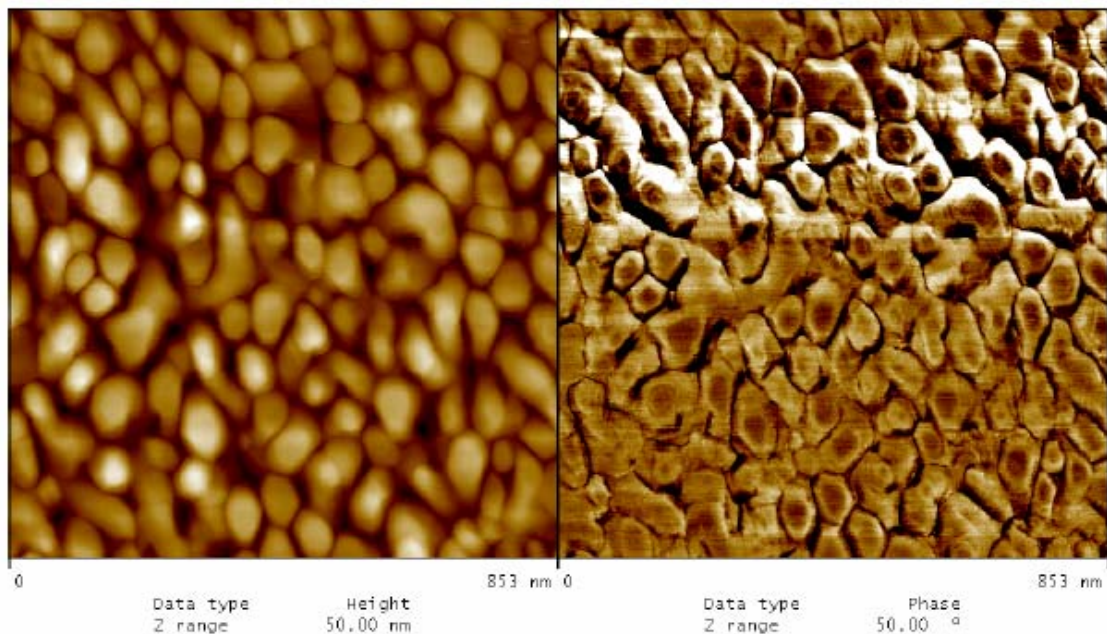
Figure 4.35: AFM image of surface section (853 nm X 843 nm) of freshly prepared gold on mica surface.

When we annealed the same gold surfaces with short flame treatment (15 to 30 seconds), we observed that 2 to 4 nm height gold particles were converted into ~ 0.148nm roughness (flatness) of the surface shown in Figure 4.36.

Onto these flat gold surfaces, we have immobilized mercaptohexadecanoic acid in ethanol for 16 hours and then these surfaces were characterized by AFM.

The packing and orientation in a SAM affects the surface chemistry and is responsible for particular applications such as molecular recognition and sensor activity of the surface [34].

All the AFM measurements were accomplished on a Multimode Scanning Probe Microscope (Digital Instruments Santa Barbara, CA) using an E-Scanner (15µm). All images were obtained applying tapping mode in air with Non-Contact High frequency Point probes (NCHR-W, NanoSensors) with backside reflex coating. Tips with Nominal force constants of 42 N/m were used at driving frequencies ranging from 300 to 330 kHz. Height and phase images of sample regions between 0.5 and 5.0 µm were acquired with resolutions of 512×512 pixels and scan frequencies between 0.4 and 2.0 Hz. All measurements were carried out at room temperature.
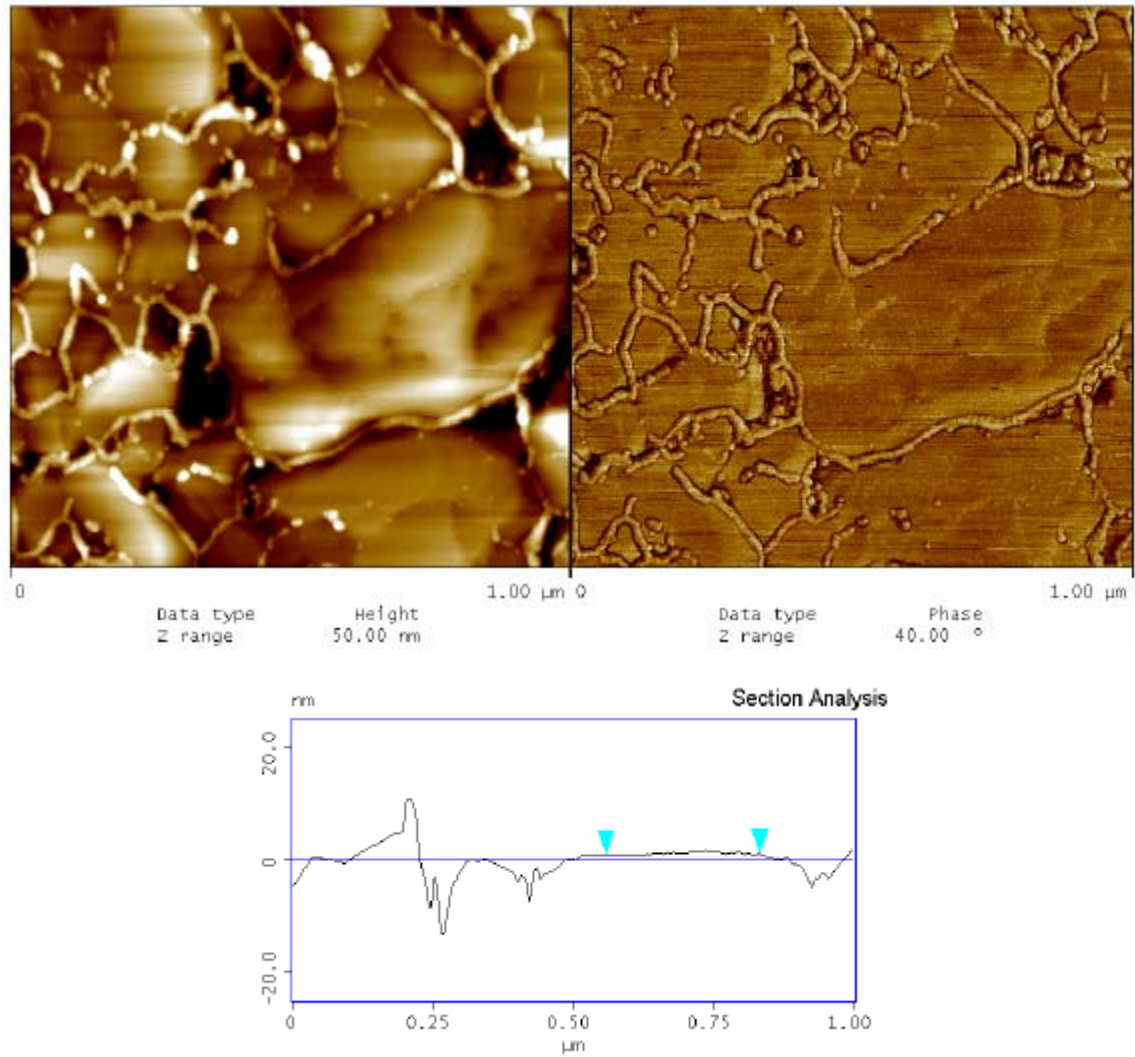
Figure 4.36: AFM image of surface section (1µm X 1 µm) of flame annealed gold on mica surface.

4.5.1 Atomic Force Microscopy (AFM) of single component monolayers

Butt H. J and Ringsdorf H. reported [33] that it was possible to obtain a good contrast image on carboxy terminated thiols by measuring in water using 1 mM $CaCl_2$ solution. We tried to obtain the same image applying the tapping in air method and observed that (Figure 4.37) the height differences between the gold and acid terminated SAMs match with the estimated length of the acid monolayer and also with the obtained air ellipsometry results (20 to 23 Å). We have also observed that these acid terminated SAMs tend to form isolated 30 to 50 nm size islands.

When we added ω-functionalized amphiphiles [-NO_2 (**2**) and -OCH_3 (**1**)] onto these acid terminated SAMs, we observed that the whole surface is completely covered with the added molecules and a few defects in those layers show the height differences from the gold surface to the amphiphiles which is displayed in Figure 4.38.
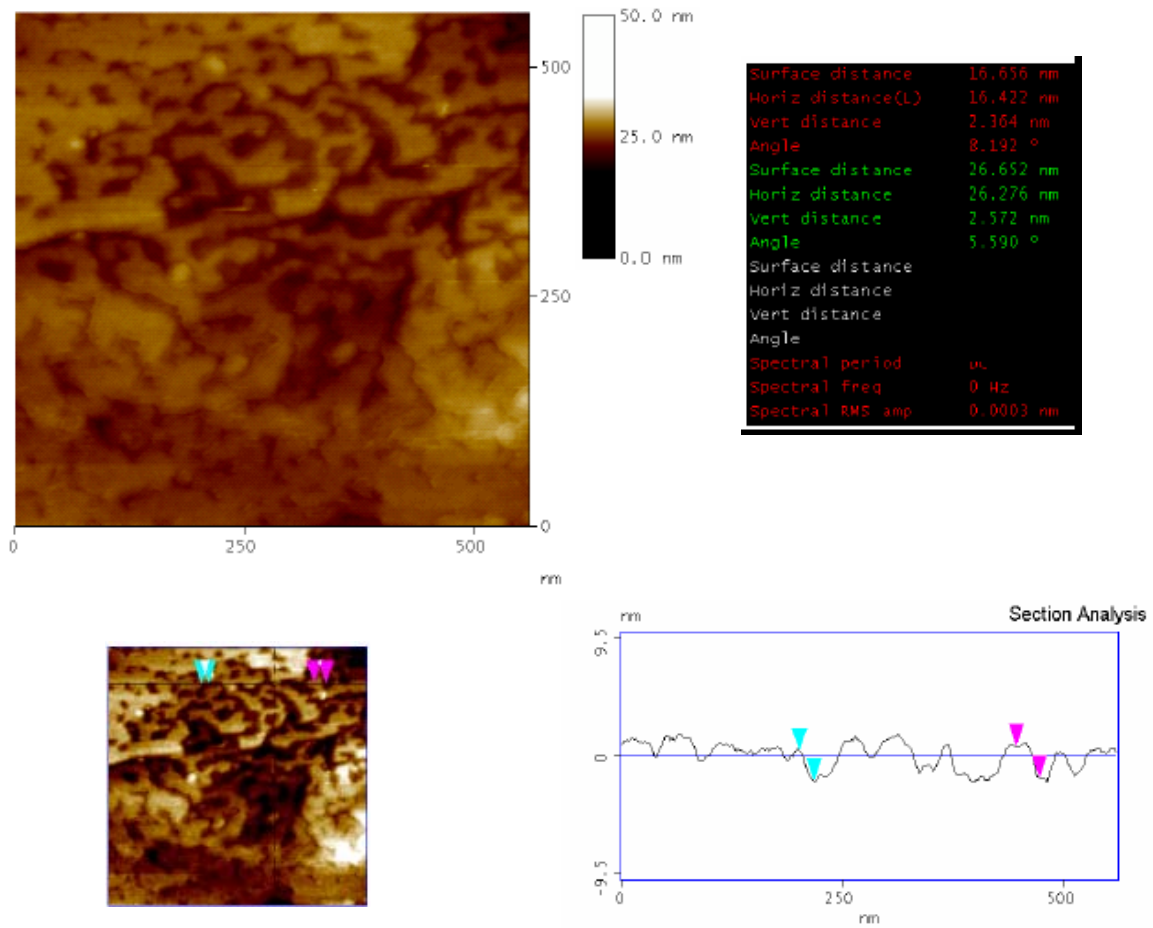
Figure 4.37: AFM image of mercaptohexadecanoic acid (MHA) terminated SAMs on annealed gold surface.

	MHA	MHA + NO$_2$	MHA + OCH$_3$

pH 9

$\Delta d \sim$ 20-22 Å $\Delta d \sim$ 40-45 Å $\Delta d \sim$ 40-45 Å

pH 8

$\Delta d \sim$ 30-40 Å $\Delta d \sim$ 30-40 Å

pH 3

$\Delta d \sim$ 15-20 Å $\Delta d \sim$ 12-15 Å $\Delta d \sim$ 12-18 Å
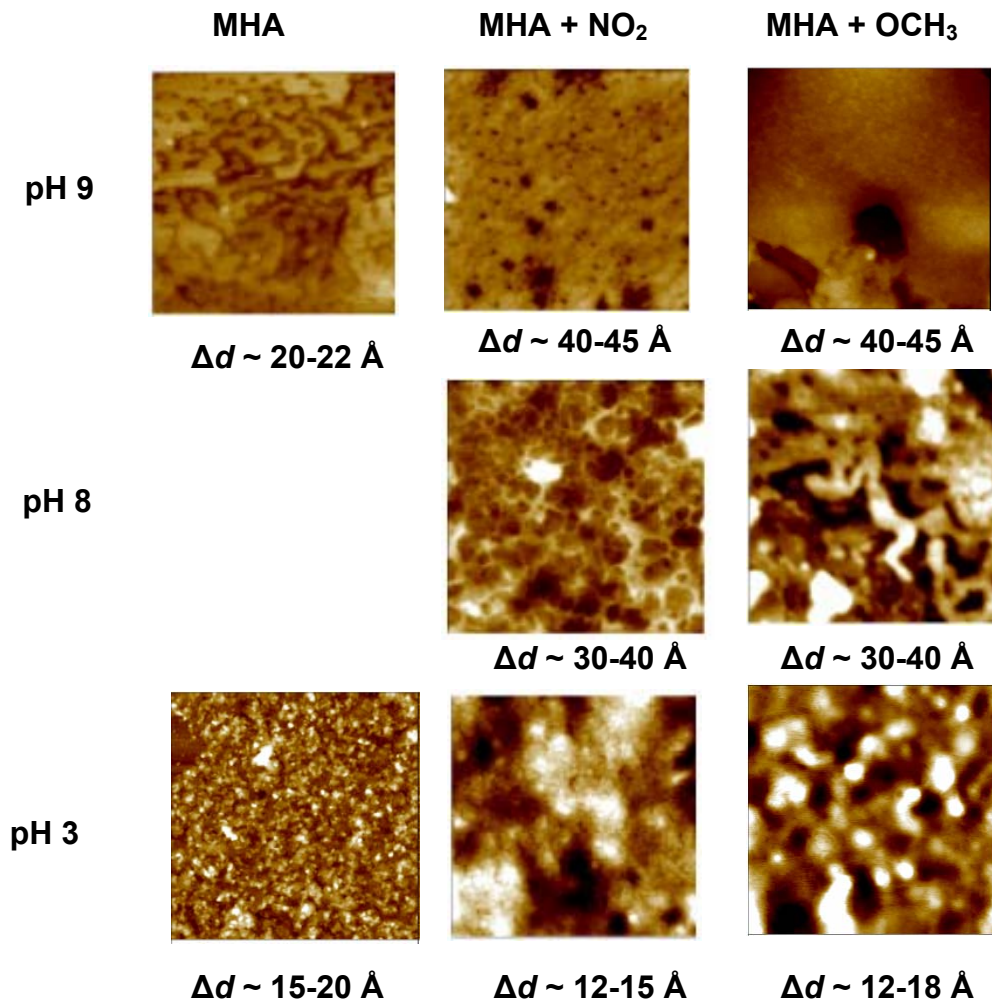
Figure 4.38: AFM images (500 × 500 nm) of mercaptohexadecanoic acid (MHA) SAM on gold, subsequent immobilization of -NO$_2$ and -OCH$_3$ substituted bipolar amphiphiles onto them and effect of different pH on the thickness of assembled amphiphiles.

As expected, the height differences were increased upon addition of ω-functionalized amphiphiles on acid terminated SAMs from originally 20-22 Å (MHA) thickness to 40-45 Å thickness (MHA + ω-functionalized amphiphiles). Figure 4.39 and Figure 4.40 shows the AFM images and section analysis for -OCH$_3$ (**1**) and -NO$_2$ (**2**) amphiphiles respectively.
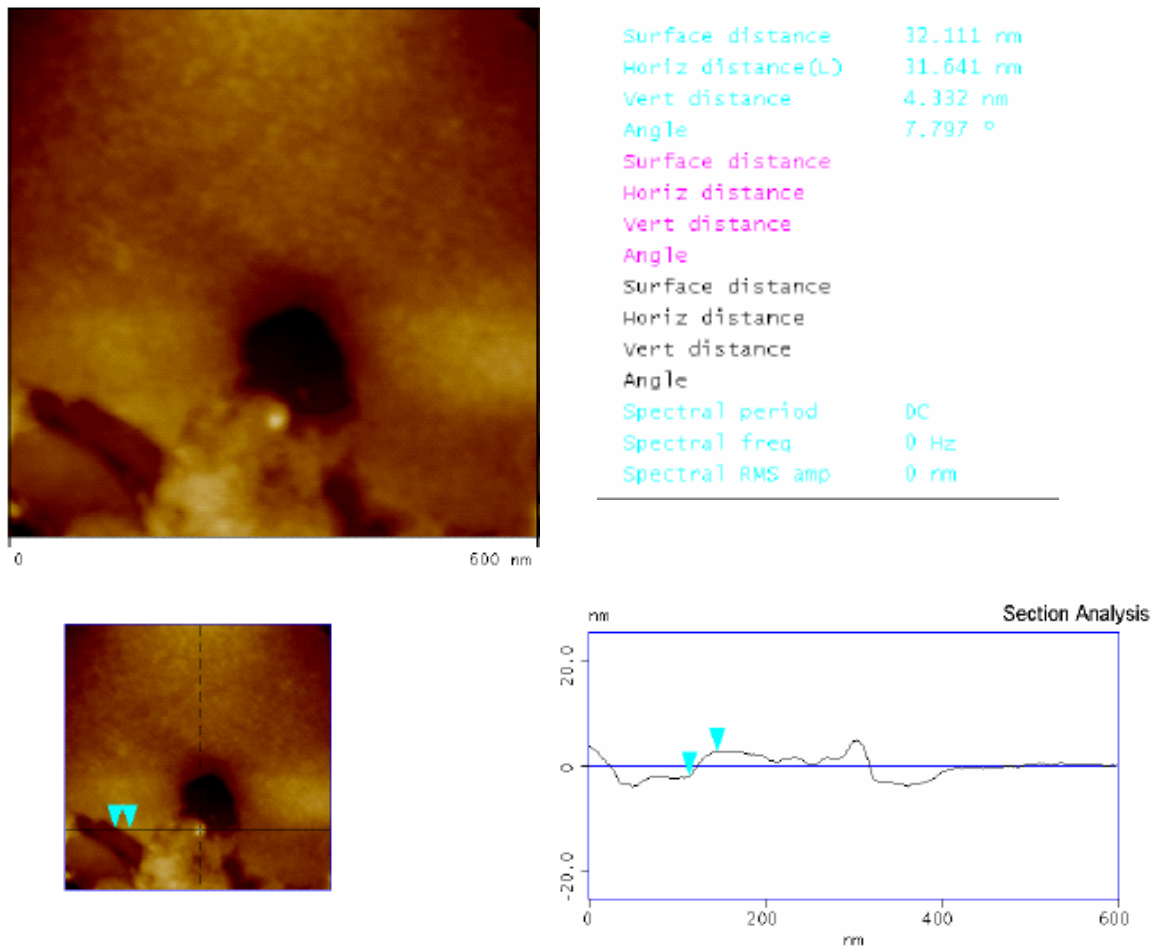
Figure 4.39: AFM image of SAMs of –OCH₃ (**1**) amphiphile on MHA functionalized SAMs on gold surface.
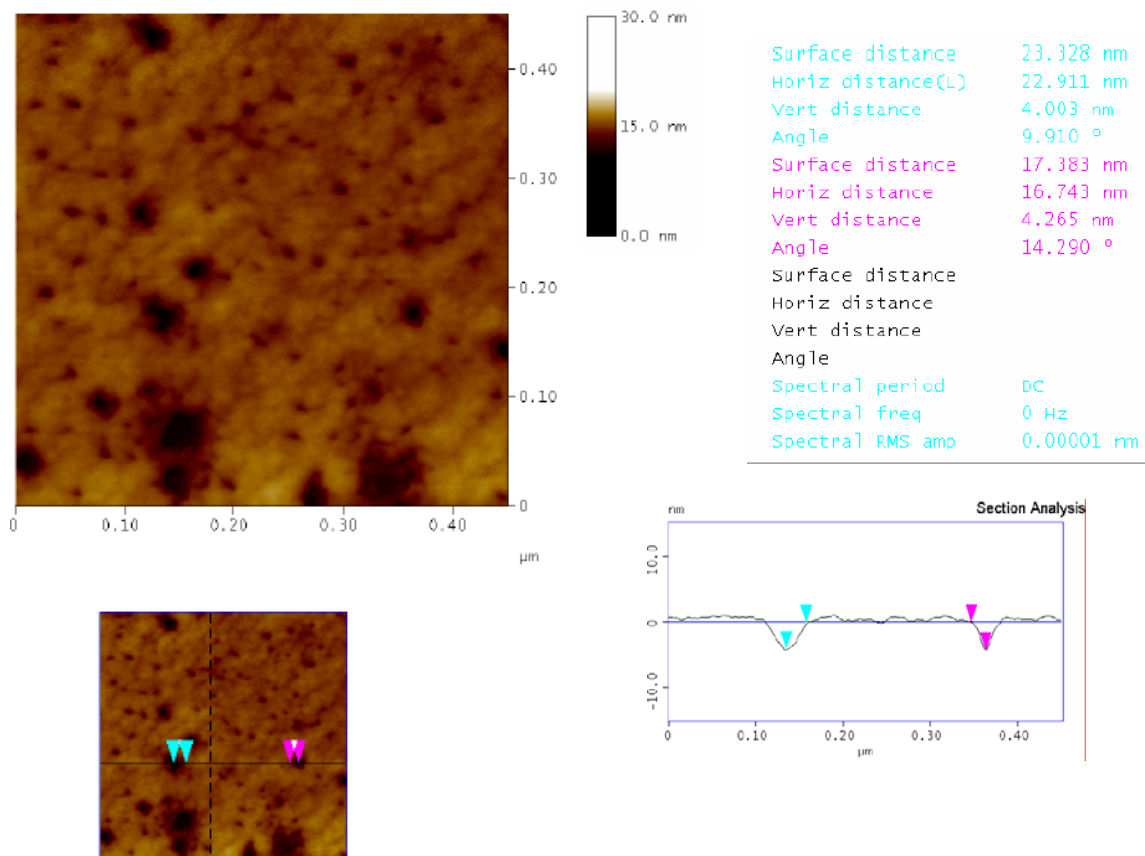
*Figure 4.40: AFM image of SAMs of -NO$_2$ (**2**) amphiphile on MHA functionalized SAMs on gold surface.*

As we have observed from the pH titration study in our previous sections of this chapter (4.2.3), the assembled amphiphiles on MHA SAMs lose their monolayer thickness upon decrease in the pH from 9 to 3. At pH 3, the amphiphilic layer was removed from the acid surfaces yielding again carboxylic acid terminated SAMs. We have carried out the same investigation here as well to see the decrease in the height differences upon decreasing the pH from 9 to 3 which is displayed in Figure 4.38.

For pH treatments, samples were removed from the AFM instrument and exposed to corresponding buffer solutions. Then the samples were rinsed with distilled water, dried under a stream of nitrogen and replaced in the AFM apparatus. After pH 8 treatment, we observed that, ω-functionalized -NO$_2$ (**2**) surface was covered with a defined fractal pattern and height difference were

marginally decreased from 40-45 Å to 30-40 Å. These structures might be interpreted as "partially detachment" of -NO$_2$ amphiphile layer from the surface.

In contrast, the surfaces of -OCH$_3$ amphiphile did not indicate any considerable change in topology, but again, the height difference decreases from 40-45 Å to 30-40 Å.

These samples exhibit equal feature of layers containing height differences from gold surface of about 12 to 20 Å depth after treatment at pH 3 (Figure 4.41).
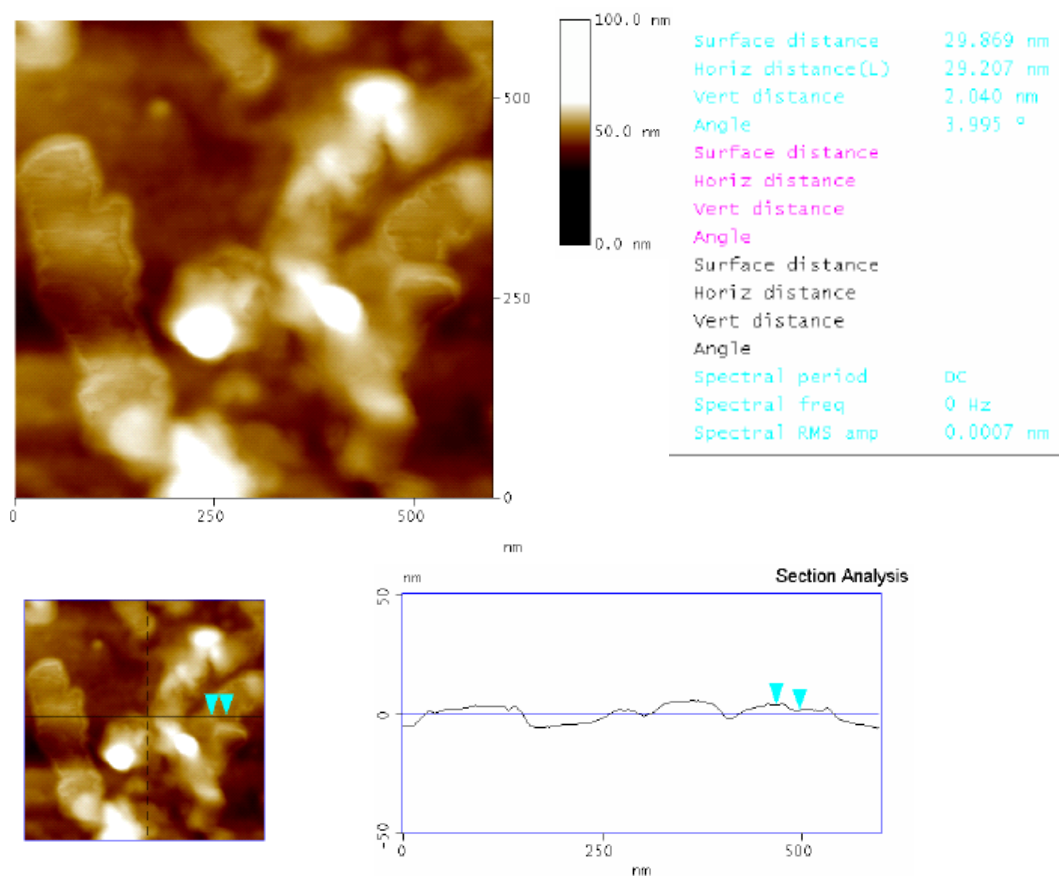
*Figure 4.41: AFM image of SAMs of -NO$_2$ (**2**) amphiphile at pH 3 on acid functionalized SAMs.*

4.5.2 Atomic Force Microscopy (AFM) of mixed component monolayers

AFM study was also carried out on mixed monolayers (1:1 composition) of -OCH$_3$ (**1**) and -NO$_2$ (**2**) functionalized amphiphile which is shown in Figure 4.42. The height differences recorded in case of mixed monolayers were in between 15 to 20 Å.
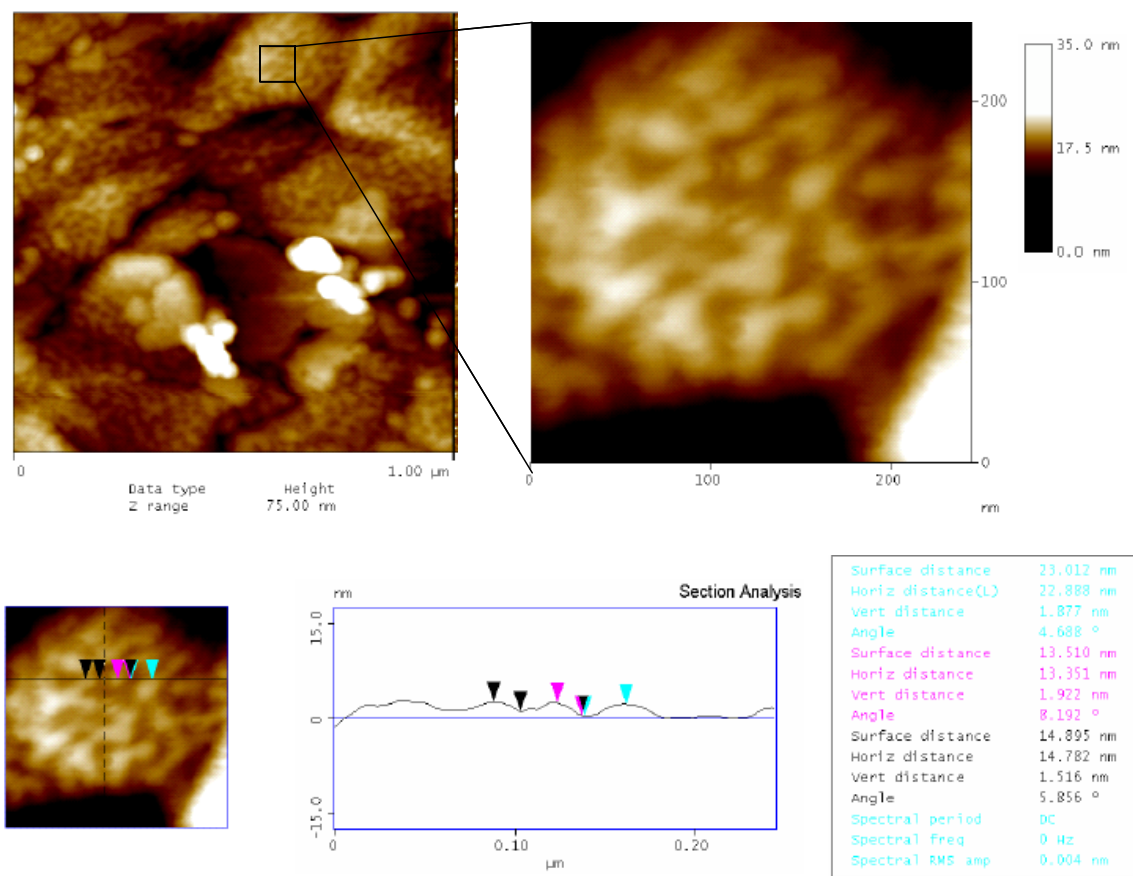
*Figure 4.42: AFM image of mixed monolayers of OCH$_3$ (**1**) and -NO$_2$ (**2**) amphiphile at 1:1 composition on MHA functionalized SAMs.*

The pattern of the AFM image sown in the Figure 4.42 may be an indication of domain formation between two different components contrary to what was observed for single component amphiphiles.

Table 4.3 reveals the amphiphilic thickness measured from three different methods (Air ellipsometry, *In situ* ellipsometry and AFM).

Compounds	Estimated length (Å)	Thickness by air ellipsometry (Å)	Thickness by in situ ellipsometry (Å)	Thickness by AFM (Å)
MHA	22	20 ± 2	----	$18\text{-}22 \pm 4$
(1) R= -OCH$_3$	24	26 ± 3	24 ± 3	$20\text{-}24 \pm 3$
(2) R= -NO$_2$	24	25 ± 2	26 ± 3	$20\text{-}24 \pm 4$
(4) R= Amidine	25	25 ± 3	24 ± 2	$22\text{-}25 \pm 3$

Table 4.3: Thickness of MHA SAMs and different amphiphiles assembled on MHA SAMs by ellipsometry and AFM methods.

4.5.3 Conclusions

A series of ω-functionalized amphiphiles with the ability to form stable and ordered layer with pH switchable function on mercaptohexadecanoic acid on gold surface were studied. The pH switching ability of these amphiphiles leads to the regeneration of single sensor surface.

In situ ellipsometric studies of single component and mixed component ω-functionalized amphiphiles on MHA SAMs showed the agreement between the observed thickness upon addition of amphiphiles and the maximum length of the molecules (maximum length of the molecule was calculated from Chem3D Ultra 6.0). This also suggested that the positively charged amidinium head group of amphiphiles forms closely packed monolayer on acid terminated SAMs by forming strong, cyclic directed hydrogen bonded pair with negatively charged carboxylate ions.

Rinsing of the amphiphilic SAMs with pH 9 borate buffer indicated that the layers were stable after rinsing. We also observed that the decrease of the pH of the borate buffer from 9 to pH 3 leads to the removal of amphiphilic layer from acid terminated SAMs yielding carboxylic acid terminated SAMs on gold surface. After treatment with 0.1 M HCl, 0.1 M NaOH solution and then rinsing with pH 9 borate buffer, the same sensor plates were reused several times.

By following the procedure reported by Wöll et al [17], we have constructed the mercaptohexadecanoic acid (MHA) surfaces which were used in our study. These sensor surfaces were fully characterized by air ellipsometry, IRAS, contact angle measurements and by atomic force microscopy. IRAS measurements of the acid terminated SAMs showed that the formed layer is crystalline like and ordered in nature (CH_2 asymmetric stretch peak at 2917 cm^{-1}) and peak at ~ 1450 cm^{-1} indicates the formation of negatively charged (COO^-) carboxylate surfaces on gold.

IRAS study of the single component and mixed component amphiphilic SAMs showed the characteristic peaks for all functionalities in SAMs as by their transmission spectrum (KBr pellets), which indicates the presence of amphiphilic layer on acid terminated SAMs. For all the added amphiphiles on MHA terminated SAMs, a peak at ~ 2917 cm^{-1} was observed, which indicates the highly crystalline like nature of the assembled layer.

Coverage-dependent frequency shift for the NO_2 group was observed (Figure 4.21) which could be caused by the vibrational coupling effect [32]. As the vibrational frequencies for NO_2 and OCH_3 terminated SAMs are widely different, they could show coverage dependent frequency shift [30].

Contact angle of MHA SAM was ~10° (±5) [35], which indicates the formation of highly hydrophilic acid terminated surfaces. The addition of NO_2 (**2**) and OCH_3 (**1**) ω-functionalized amphiphiles onto highly hydrophilic MHA SAMs leads to the formation of more hydrophobic surfaces measuring contact angles in between 70° and 80°. In case of OCH_3 (**1**) and -C(=NH)NH_2 (**4**) mixed monolayer, we have detected continuous decrease in the wetting property of the surface as the concentration of OCH_3 layer increases. This indicates the presence of a well arranged layer with all head groups exposed on the surface. (The switching of the surface from hydrophobic to hydrophilic was visualized using contact angle measurements).

Atomic Force Microscopy was used to characterize the pH-dependent adsorption-desorption process and also to gain more insight into the thickness information of added amphiphiles on acid terminated SAM on gold. AFM images

of the SAM of MHA reveals that over 30-50 nm of islands separated by the flatter region with height differences from gold to acid were ~ 20-22 Å. Addition of amphiphiles onto the acid terminated SAMs revealed very densely packed amphiphilic layer which resulted in very flat region on the same surface.

The height differences (peak-to-valley height) for both the acid SAMs (20-23 Å) and the amidine layers (40-45 Å) were found to be in close agreement with the thickness estimated by air and *in situ* ellipsometry. The amphiphilic layer was taken off by acidification (pH 3) leading again to acid terminated SAMs.

4.6 Introducing bioaffinity ligands at ω-position of the amphiphiles

In the study of organic surfaces and thin films, the process of self-assembly of multilayer structures has attracted a great deal of interest during the last decade. Recently, there have been several reports on the formation of Self-assembled multilayers using biological components [36-40]. SAMs have been widely used in studying the biocompatibility of materials, in the development of *biosensors* and in cell biology [41-45].

While constructing the self-assembled multilayer platform on gold surfaces to construct the biosensors, one should very well consider which functional groups could be introduced at the ω- position. These should either resist the nonspecific adsorption of added proteins or they should promote the biospecific adsorption of specific proteins [38].

We have seen in the previous sections (4.2.1) of this chapter that α,ω-hetero-functionalized amphiphiles form stable, ordered and switchable self-assembled monolayer on MHA terminated SAMs. The formation of assembly and disassembly of the α,ω-hetero-functionalized amphiphiles occurs in the aqueous medium (buffer pH 9 and pH 3) and most of the biological processes happen also in aqueous environment. This gave us an idea to use these platforms for recognizing some biological molecules at the interface.

For the effective recognition of biomolecules on the surfaces, a suitable binding system has to be chosen; hence our initial efforts were concentrated on the synthesis of ω-functionalized biotinylated amphiphiles for the selective binding of streptavidin.

Biotin is a vitamin having molecular weight 244 dalton, found in tissue and blood which binds with high affinity to streptavidin. In fact, the streptavidin-biotin interaction is the strongest known non-covalent biological interaction (Ka = 10^{15} M^{-1}) [46] between protein and ligand. The bond formation between streptavidin and biotin is rapid and essentially non-reversible, unaffected by most extremes of pH, organic solvents, and denaturing reagents. The streptavidin-biotin interactions

have found extensive use as a research tool. Each streptavidin (a tetramer) molecule possesses four biotin binding sites positioned as two pairs on opposite faces on the protein molecule.

4.6.1 Synthesis of ω-functionalized biotinylated amphiphiles

For the synthesis of ω-functionalized biotinylated amphiphile, we developed a synthetic procedure revealed in Scheme 4.7.
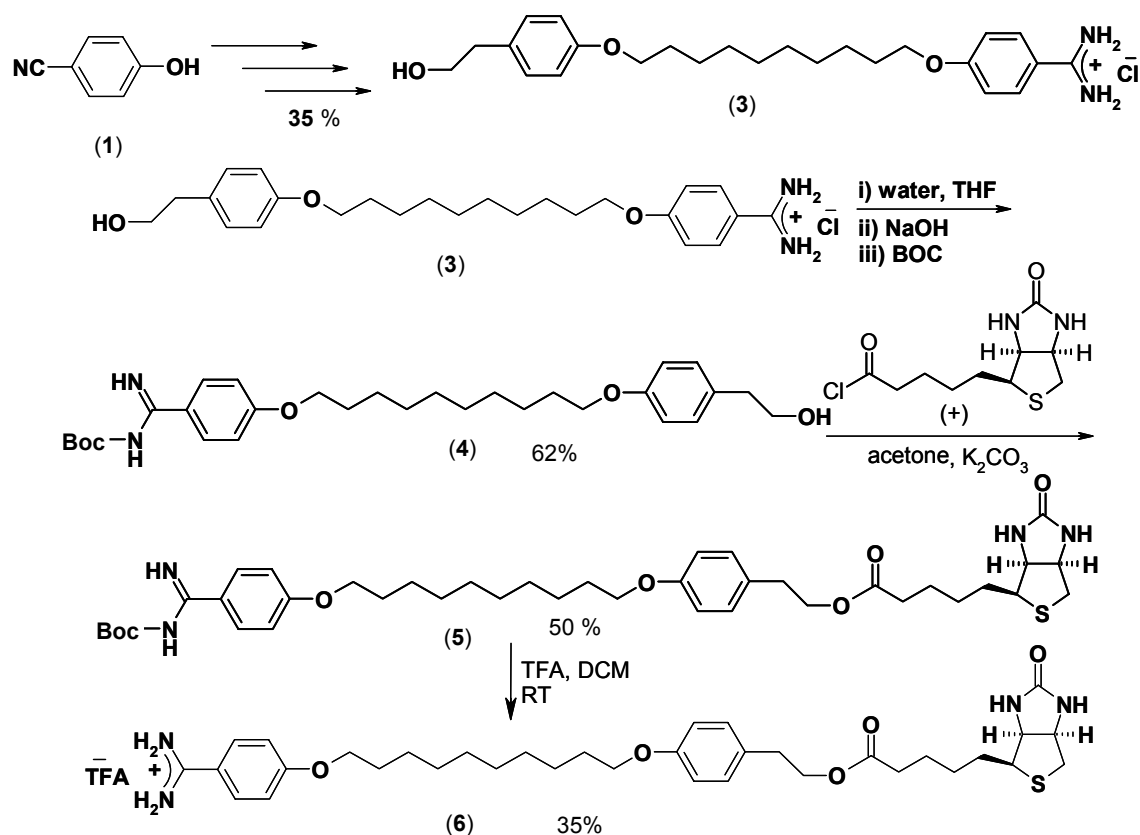
Scheme 4.7: Synthesis of biotinylated amphiphile.

The important steps in the synthesis of above molecule were the Pinner synthesis [4] which converts -CN group into the amidinium group (**3**) and the protection of amidinium group [54] by protecting agent -BOC(**4**) (di-tert-butyldicarbonate).

After the amidine protection, biotin chloride was coupled [51b] with the protected molecule yielding ω-functionalized biotin at one end and protected amidine at the other end (**5**).

The ω-functionalized biotin amphiphile (**6**) was obtained in 35% yield by deprotecting the -BOC group by Trifluroacetic acid (TFA) at room temperature and subsequent crystallization using ethanol.

Scheme 4.7 reveals the synthesis of ω-functionalized biotinylated amphiphile molecule (**6**) and ω-functionalized hydroxy (**3**) amphiphile.

The formation of self-assembled monolayers by using single and mixed ω-functionalized α-(4-amidinophenoxy)alkanes are discussed in the following paragraph.

The amphiphiles which are used in the following studies are

1. 4-{10-[4-(2-Hydroxy-ethyl)-phenyoxy]-decyloxy}-benzamidine hydrochloride (**3**)

2. 5-(2-Oxo-hexahydro-thieno[3,4-*d*]imidazol-6-yl)-pentanoic acid 2-{4-[10-(4-carbamimidoyl-phenoxy)-decyloxy]-phenyl}-ethyl ester triflouro acetic acid. [Biotinylated amphiphile (**6**)].

4.6.2 In situ ellipsometry

Our initial studies focused on the interaction of synthesized biotinylated and hydroxyl terminated amphiphiles (**6** and **3**, Scheme 4.7 and Scheme 4.8) with mercaptohexadecanoic acid (MHA) SAMs.

The interaction between the acid functionalized gold surfaces and synthesized amphiphiles is represented schematically in Scheme 4.8.
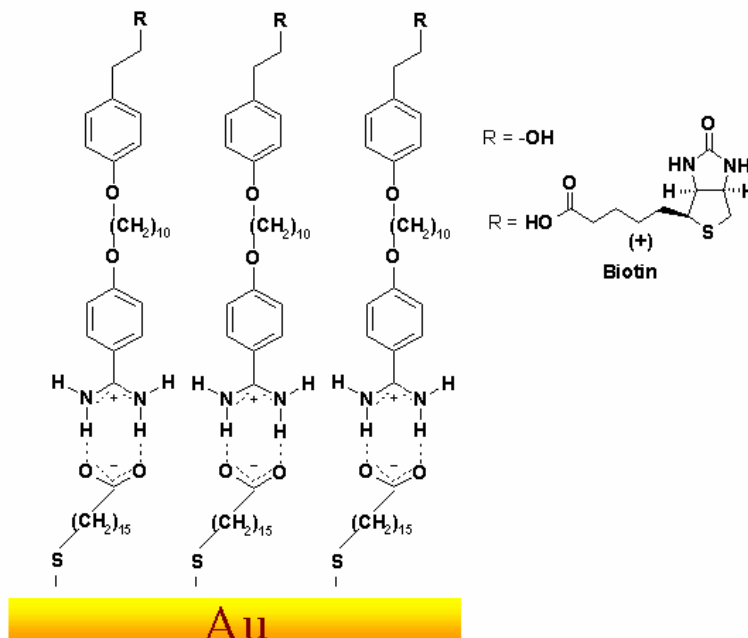
Scheme 4.8: *Schematic representation of interaction between negatively charged carboxylate ion gold surfaces and positively charged amidinium amphiphiles.*

For the adsorption of hydroxyl terminated (**3**) and biotin terminated (**6**) molecules, acid terminated substrates were prepared as described in the previous section of this chapter (4.2.1). The MHA modified gold surfaces were then immersed in a Teflon-coated cuvette containing 2 mL (0.01 M) sodium borate buffer (pH 9) prepared from boric acid. This cuvette was thermostated at 25 °C and was equipped with a small magnetic stirrer. The addition of the amphiphiles (**3** and **6**, 50 µM each) was done after obtaining a stable base line.

After addition of the amphiphiles, we observed increase in the layer thickness which is displayed in Figure 4.43. The increase in layer thickness was attributed to the non-covalent interaction between the negatively charged carboxylate (COO⁻) and positively charged amidinium ions.
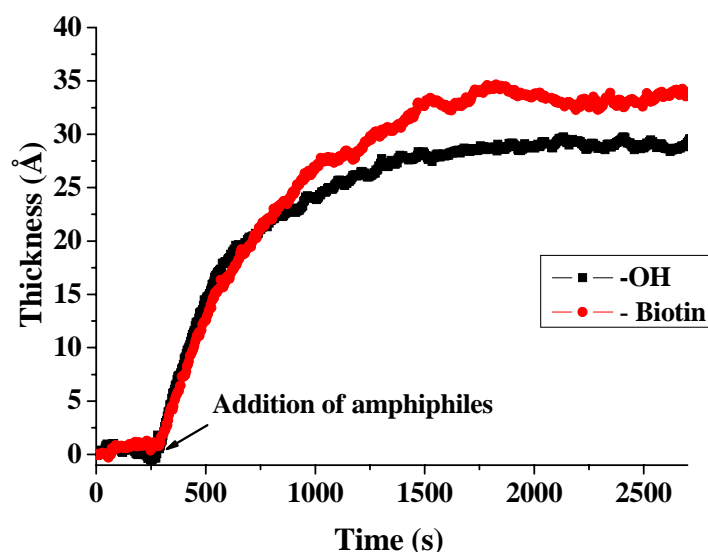
*Figure 4.43: Film thickness versus time during adsorption of OH (**3**) and biotin (**6**)-functionalized amphiphiles on MHA modified gold surfaces.*

After the formation of a stable monolayer on the acid terminated SAMs, we observed that there was an agreement between the observed thickness by *in situ* ellipsometry, air ellipsometry and the estimated length of the molecules calculated by the Chem3D Ultra 6.0 as depicted in Table 4.4.

Amphiphiles	Estimated length (Å)	Thickness by air ellipsometry (Å)	Thickness by in situ ellipsometry (Å)
R= OH (**3**)	28	29 ± 2	29 ± 3
R= Biotin (**6**)	32	34 ± 3	33 ± 3

*Table 4.4: air and in situ ellipsometric thicknesses of assembled SAMs of the amphiphiles **3** and **6** on MHA SAMs.*

4.6.3 Infrared reflection absorption spectroscopy (IRAS) of SAMs of hydroxy (3) and biotin (6) amphiphiles

Biotin (**6**) and hydroxy (**3**) functionalized SAM surfaces were then characterized by IRAS in air. The IRAS spectrum obtained after the immobilization of hydroxy (**3**) and biotin (**6**) terminated SAMs on acid surfaces also confirms the presence of above amphiphiles. When we compared the IRAS spectrum of the assembled amphiphiles with the transmission spectrum (KBr pellets, Figure 4.44) of the same amphiphiles, we observed the presence of all functional groups in the IRAS spectrum. The CH_2 asymmetric stretch at 2918-2919 cm^{-1} indicated the presence of highly crystalline and ordered amphiphilic layer on the surfaces as shown in the IRAS spectrum in Figure 4.45.

The broad band between 3000 cm^{-1} and 3400 cm^{-1} in Figure 4.45 indicates that the amphiphilic amidine head groups form hydrogen bonding [47] to the carboxylic acid SAM surfaces. We assigned the 2933-2936 cm^{-1} band to the typical amidine asymmetric CH_2 stretch [29].
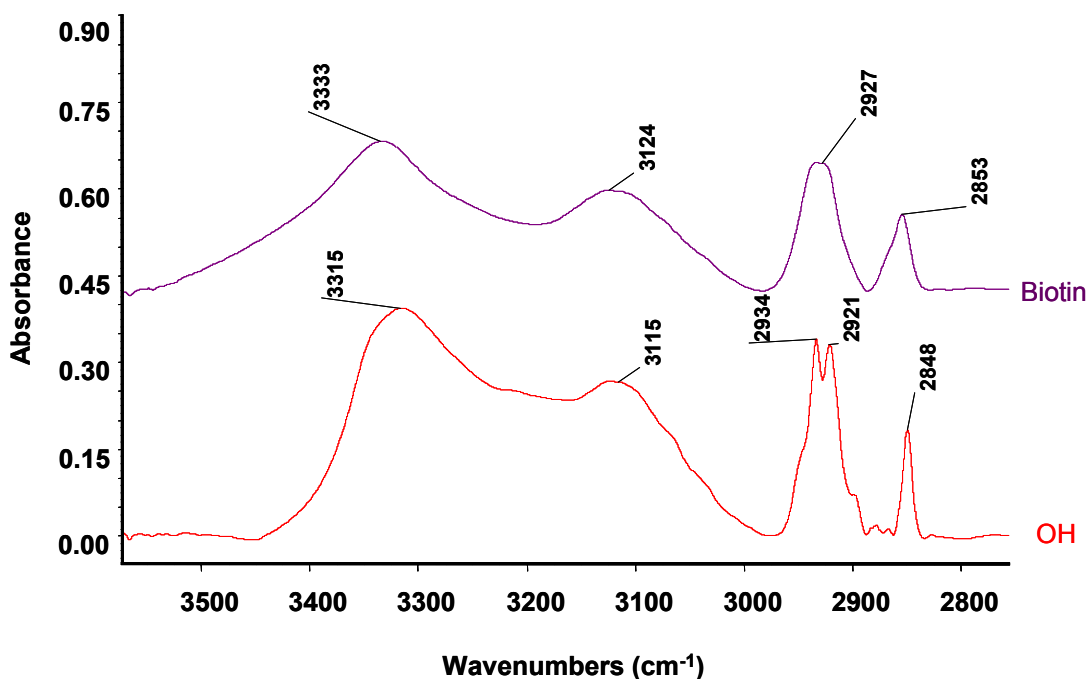
Figure 4.44: FTIR spectrum (KBr) of high frequency region of amphiphile OH (3) and biotin (6).
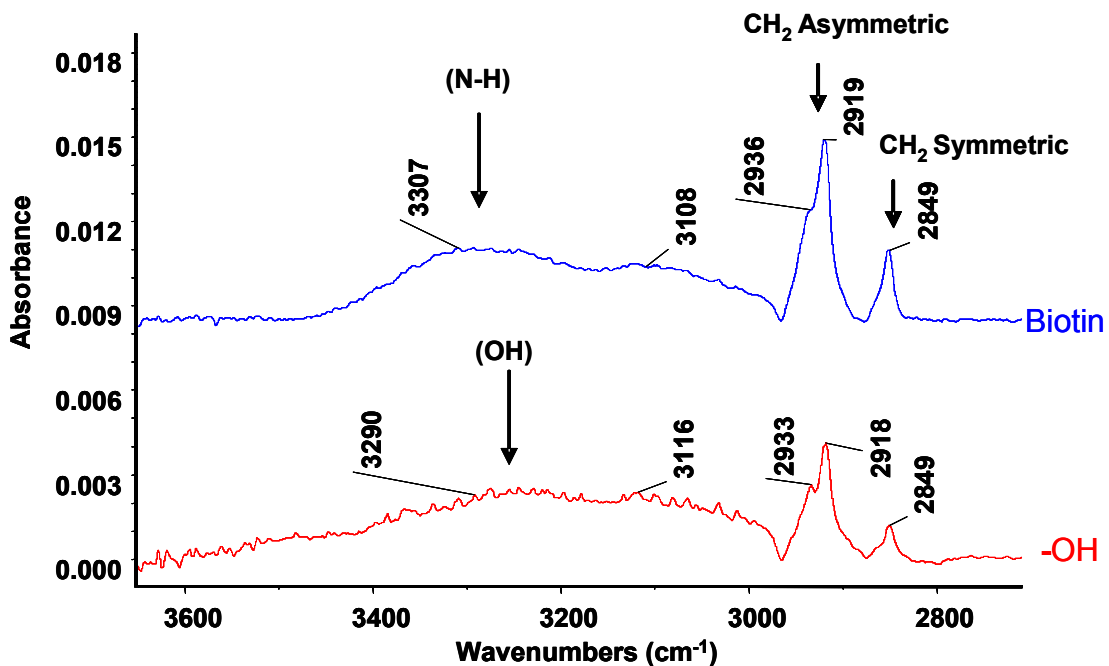
*Figure 4.45: Baseline corrected IRAS spectra of high frequency region of OH (**3**) and biotin (**6**) terminated SAMs on MHA gold surface.*

The low frequency region (Figure 4.47) of the IRAS spectra of the amphiphiles (**3**) and (**6**) reveals the characteristic peaks for all functionalities in the SAMs as observed in their corresponding transmission spectra (KBr pellets, Figure 4.46). This indicates the presence of amphiphilic layer on the acid terminated SAMs. The peak at ~ 1726 cm^{-1} was assigned to the carbonyl group of the biotin amphiphile.
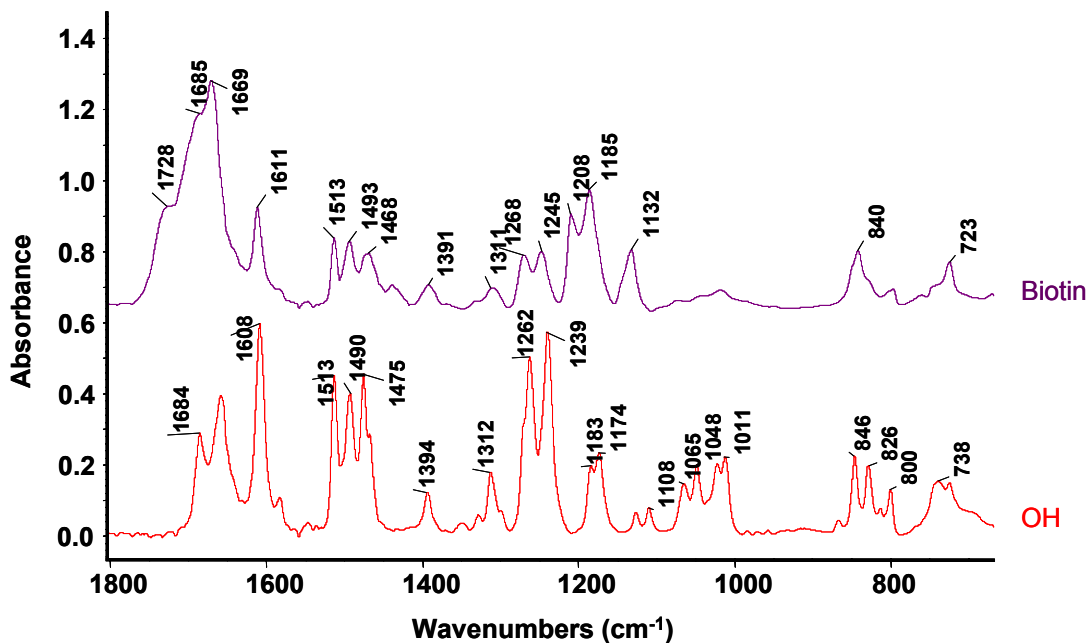
Figure 4.46: FTIR spectrum (KBr) of low frequency region of amphiphile OH (3) and biotin (6).
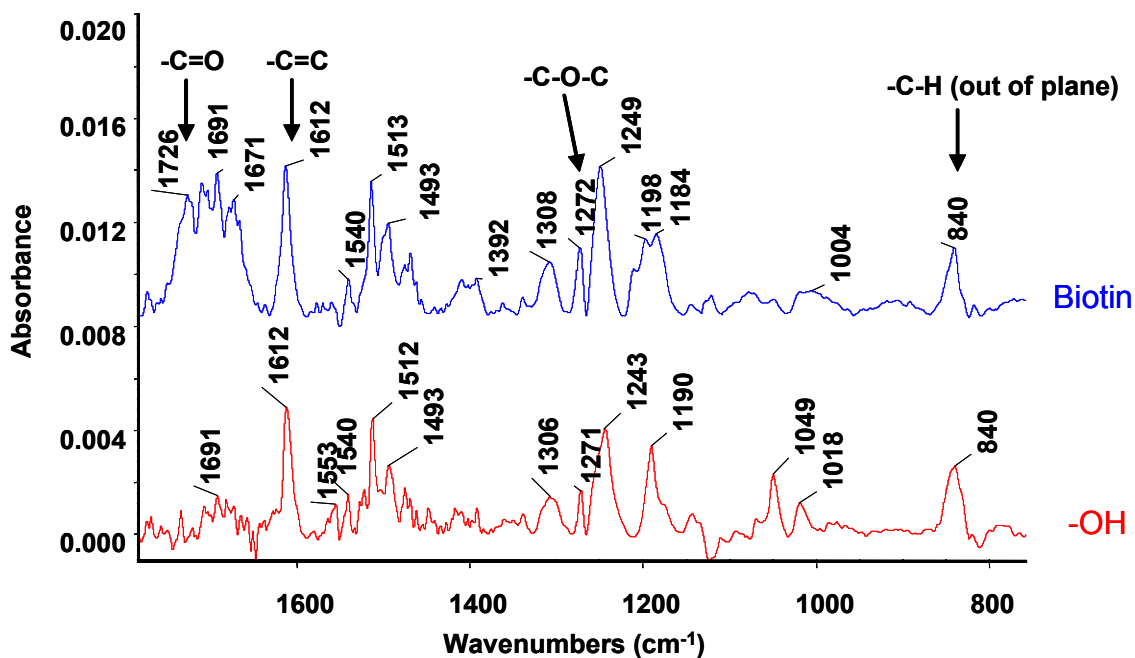
Figure 4.47: Baseline corrected IRAS spectra of low frequency region of OH (3) and biotin (6) terminated SAMs on MHA gold surface.

The benzene C=C stretching mode (1612 cm^{-1} and 1493 cm^{-1}) of the amidine group and COC (1270-1270 cm^{-1}) was detected. The benzene CH out of plane

bending mode was seen at 840cm^{-1}. The characteristic band at 1726 cm^{-1} was observed for the carbonyl group of the biotin terminated amphiphile (**6**).

All the above IRAS spectrra were obtained after rinsing the surfaces with borate buffer (pH 9). This indicates the stability of amphiphilic layers upon rinsing.

4.7 Mixed self-assembled monolayers of 4-hydroxyphenoxy(4-amidinophenoxy)decane (3) and 4- biotinphenoxy(4-amidinophenoxy)decane (6) amphiphiles

The strength and reliability of the streptavidin- biotin interaction underlies its importance for biotechnological applications and its use as a model for high-affinity receptor-ligand interactions. These facts prompted us to choose the streptavidin- biotin system for our study [41-45].

In an attempt to build new, sensitive, easy to handle and most significantly *reusable* biosensor platform, our initial investigations were directed towards the assembly of mixed self-assembled monolayers of (**3**) and (**6**) in different concentrations.

It is well reported in literature that oligo(ethylene glycols) and hydroxyl terminated self-assembled monolayers resist the non specific adsorption of protein from the surfaces [51]. Whitesides *et al.* reported that single-component SAMs that present oligo(ethylene glycol) groups are not unique in their ability to resist adsorption of proteins, however, mixed SAMs containing as little as 50% of $HS(CH_2)_{11}$-EG_6OH (mixed with $HS(CH_2)_{11}CH_3$) show good resistance to the adsorption of proteins [38, 52].

From the previous studies by Ringsdorf and Knoll *et al* [36, 48], it is known that the content of Biotin is important for achieving the maximum surface density on the surface. To achieve the same density of synthesized ω-functionalized biotin (**6**) molecule for streptavidin recognition and also to prevent non-specific interaction of the streptavidin layer, we have mixed the above amphiphiles in five (100%, 75, 50, 25, and 0% of biotin) different compositions with -OH (**3**) functionalized amphiphile.
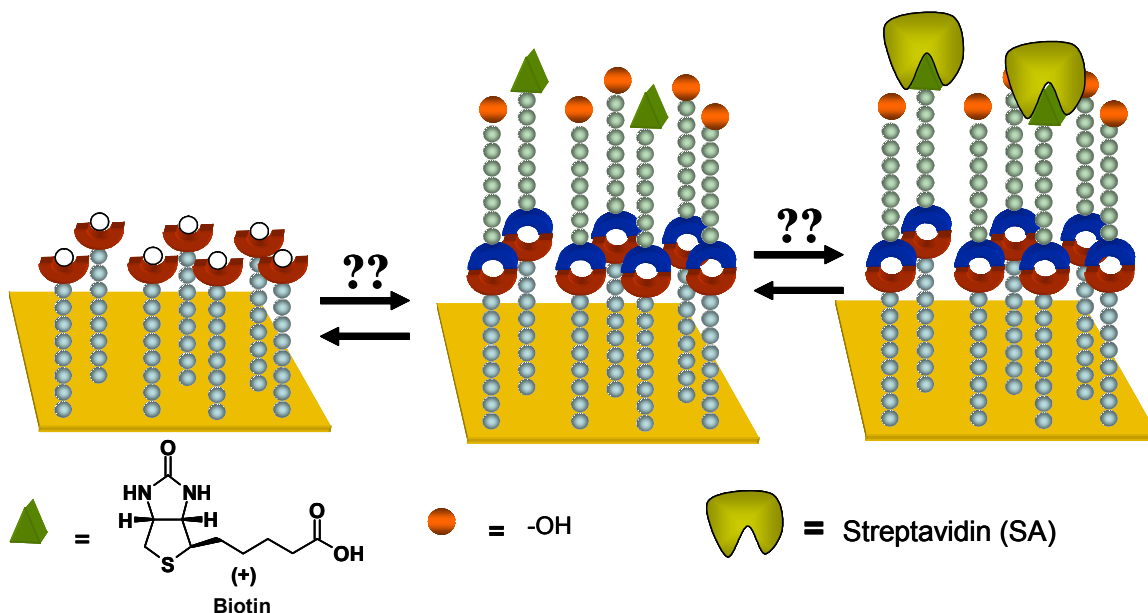
Scheme 4.9: Schematic representation of interaction between negatively charged carboxylate ion gold surfaces and positively charged amidinium amphiphiles (3) and (6) and subsequent immobilization of streptavidin on these layers.

Scheme 4.9 shows the concept involved in the construction of reversible biosensor platform.

4.7.1 *Air ellipsometry*

We have investigated the formation of mixed self-assembled monolayers of amphiphiles (**3**) and (**6**) and the subsequent immobilization of streptavidin (**SA**) by air ellipsometry. The observed layer thicknesses of the various samples by air ellipsometry are summarized in Table 4.5.

First, the above mentioned mixed amphiphiles were immobilized on MHA SAMs and then the surfaces were rinsed with borate buffer (pH 9). The surfaces were then flushed with nitrogen gas till dryness. After taking the ellipsometric thicknesses of the above assembled amphiphiles, we immersed the same surfaces in 500 nM solution of streptavidin for 16 hours [48]. The surfaces were again rinsed with borate buffer (pH 9) and dried under a flush of nitrogen gas till dryness. The ellipsometric thicknesses were calculated by considering the refractive index of the protein layer being 1.45 [36, 48].

The values given in Table 4.5 are the average thicknesses (~± 3 Å) based on 10 measurements at three different spots on each surface.

Sr. No.	Compounds	Estimated length (Å)	Amphiphilic layer thickness (Å)	Amphiphilic + SA layer thickness (Å)	Difference (Å)
1	MHA	21	20 (±2)	9	9 (±2)
2	100%Biotin	32	33 (±2)	63	30 (±2)
3	75%Biotin	–	34 (±2)	66	32 (±2)
4	50%Biotin	–	30 (±3)	67	37 (±3)
5	25%Biotin	–	28 (±2)	75	47 (±4)
6	0%Biotin	28	27 (±2)	37	10 (±2)
7	Bare Gold	–		8	8 (±2)

Table 4.5: Air ellipsometric thicknesses of mixed SAMs of (3) and (6) and subsequent adsorption of SA onto them.

From the above Table, we can conclude that there is very little binding of the protein molecules on the mercaptohexadecanoic acid (MHA) surfaces, on hydroxy (**3**) terminated SAMs and on clean bare gold surfaces. We also observed the maximum binding of **SA** (47 Å ± 4 Å) on biotinylated SAMs at a biotin content of 25%. When **SA** binds with biotin with right orientation, the reported size of **SA** molecule is 45-50 Å [36, 48] which is observed in our studies at biotin content of 25%.

There was gradual decrease in the thickness of adsorbed streptavidin film as the concentration of biotin was increased.

For the streptavidin, the above observation of gradual decrease in the thickness indicates that the specific binding requires the full insertion of the biotin ligand into the protein **SA** and at the same time the biotin molecule should be uprightly oriented. In order to achieve this, we have diluted the biotinylated (**6**) layer with OH (**3**) functionalized SAMs and detected the similar type of results which Ringsdorf and Knoll *et al.* observed [36, 48]. This indicated the formation of closely packed protein layer.

The obtained layer thickness of the protein (**SA**) molecule on hydroxy (**3**) terminated SAMs, on MHA terminated SAMs and on clean bare gold surfaces shows that the nonspecific binding of **SA** was less.

The above surfaces were allowed to stand in pH 3, which destabilized the bond between carboxylate surfaces and amidinium group of the amphiphiles. This leads to the removal of amphiphilic layer with the protein molecule from the gold surfaces. The IRAS spectrum of the gold surface [100% Biotin (**6**) + **SA** at pH 3] shown in Figure 4.48, reveals that the amphiphilic layer was removed from the surface with the protein **SA** leaving behind the acid functionalized SAMs on the gold surface (Figure 4.5 and Figure 4.6).

The above surfaces were then rinsed with 0.1 M HCl, 0.1 M NaOH and finally with borate buffer (pH 9, 0.01 M). Then, the surfaces were *reused* in subsequent experiments.
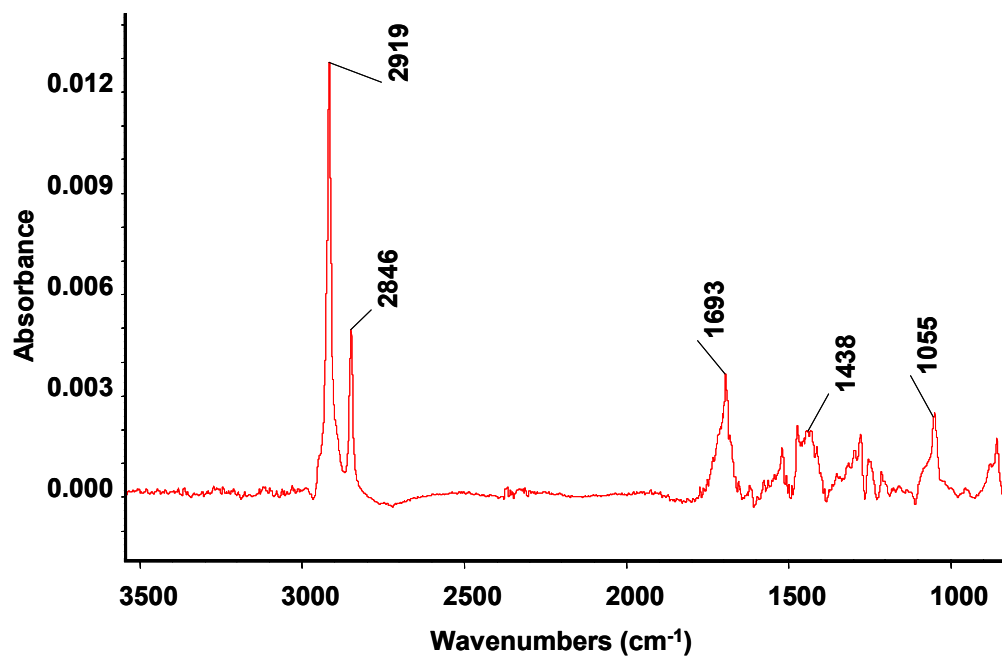
*Figure 4.48: IRAS spectrum of 100% biotin (**6**) + **SA** after pH 3 treatment.*

4.7.2 Infrared reflection absorption spectroscopy (IRAS) of mixed SAMs of ω-functionalized hydroxy (3) and biotin (6) amphiphiles

To further confirm the presence of mixed monolayers of amphiphiles (**3**) and (**6**) in different compositions on acid terminated SAMs, we have carried out detailed investigations using IRAS (Figure 4.49 and Figure 4.51). The crystalline like nature of all assembled mixed SAMs were confirmed by the presence of a peak at ~2919 cm^{-1}. The typical peak for the asymmetric CH_2 stretch for amidine amphiphiles was also detected at 2936 cm^{-1} in all the compositions.
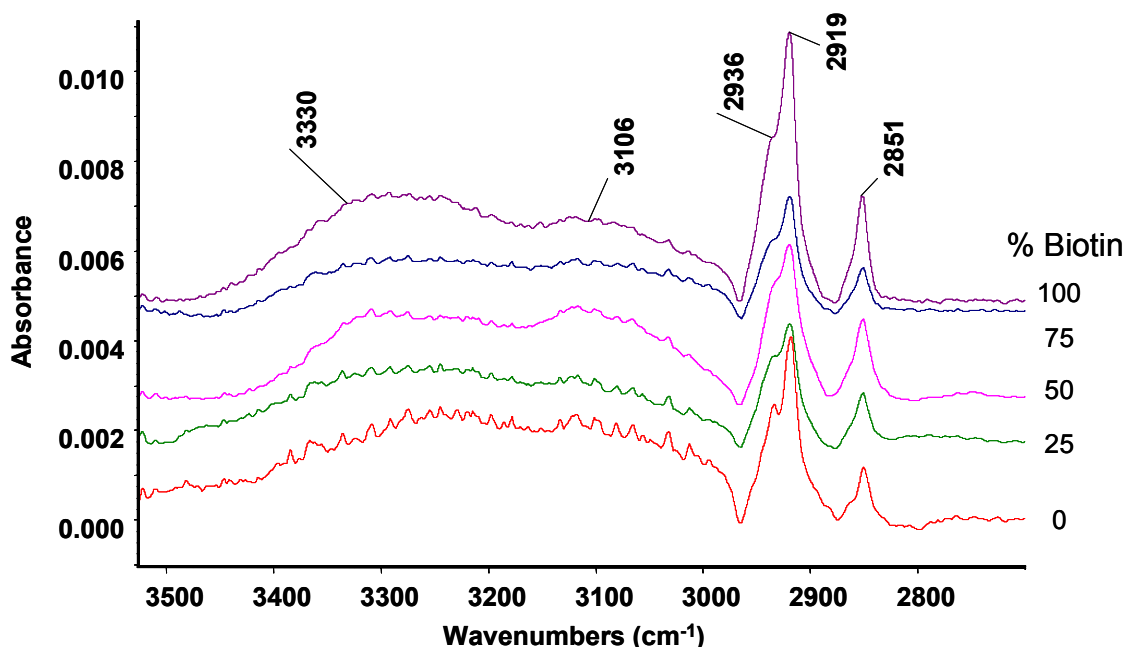
*Figure 4.49: Baseline corrected IRAS spectra of high frequency region of OH (**3**) and biotin (**6**) terminated mixed SAMs on MHA gold surface.*

A broad band between 3000 cm^{-1} and 3400 cm^{-1} indicates the presence of polar head groups like urea of the biotin molecule (**6**) and hydroxide of the -OH terminated amphiphile molecule (**3**).

The low frequency region of the same spectra (Figure 4.50 and Figure 4.51) shows the presence of all functional groups which were present in the transmission spectrum (KBr pellets, Figure 4.44 and Figure 4.46) of the amphiphiles (**3**) and (**6**), which further proves the presence of mixed amphiphilic amidine layers on the acid terminated SAMs.
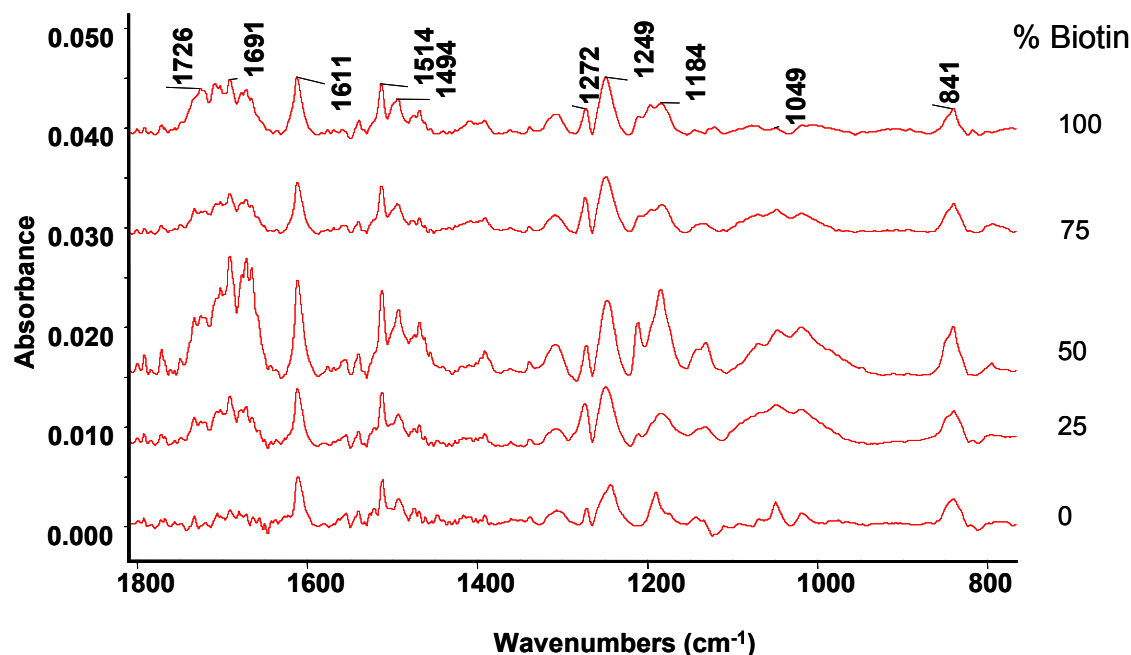
Figure 4.50: Baseline corrected IRAS spectra of low frequency region of OH (**3**) and biotin (**6**) terminated mixed SAMs on MHA gold surface.
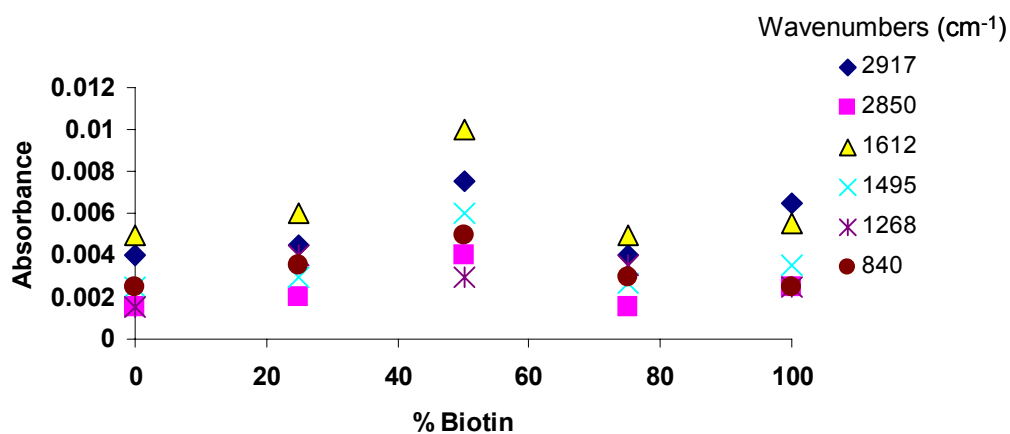
Figure 4.51: Band position and absorption intensities of mixed amphiphiles of OH (**3**) and biotin (**6**) SAMs on MHA surfaces.

Figure 4.52 reveals the plot of integrated area between 1650 cm^{-1} and 1750 cm^{-1} as a function of biotin (**6**) content in the mixed monolayer study of hydroxy (**3**) and Biotin (**6**) functionalized SAMs.

108

*Figure 4.52: Plot of integrated area vs. biotin (**6**) content mixed with hydroxy (**3**) terminated SAMs on acid functionalized monolayers.*

4.7.3 IRAS study of the adsorption of streptavidin (SA) on mixed SAMs of hydroxy (3) and biotin (6) amphiphiles

We have observed in the air ellipsometry measurements (Table 4.5) that the addition of streptavidin (**SA**) on hydroxyl (**3**) and biotin (**6**) terminated mixed SAMs led to a gradual increase in the layer thickness of the added molecule as the concentration of biotin decreases from 100% to 25%. To further confirm the presence of the **SA** layer on mixed amphiphiles, we have carried out a detailed investigation on mixed SAMs by IRAS in air.

For the IRAS measurements, first the different compositions of mixed benzamidine amphiphiles (**3**) and (**6**) were allowed to adsorb onto the acid functionalized SAMs. After this, the surfaces were carefully rinsed with pH 9 borate buffer (0.01 M), dried under a stream of nitrogen and then the surfaces were characterized in air by IRAS for the presence of amphiphilic molecules on the surfaces. After the characterization, the surfaces were immersed in a 500 nM streptavidin solution [36, 48] for 16 hours and then the surfaces were again rinsed with borate buffer pH 9 and flushed with nitrogen gas till dryness.

Based on the recorded IRAS spectrum of the adsorbed protein (**SA**) molecule after rinsing of the surfaces on OH (**3**) and biotin (**6**) terminated SAMs (Figure

4.53 and Figure 4.54), the assembled amphiphilic layers appeared stable with respect to the exchange by protein.

The presence of polar functional groups (Figure 4.53) of the amphiphile [(**3**) and (**6**)] on the surfaces were confirmed by the presence of a broad band in between 3000 and 3400 cm^{-1}. Ordered and stable nature of the assembled layer was also confirmed by the presence of a peak at 2918 cm^{-1} in all the spectra for the CH$_2$ asymmetric stretch. A peak at 2937 cm^{-1} was assigned to the CH$_2$ asymmetric stretch for the amidine amphiphiles.
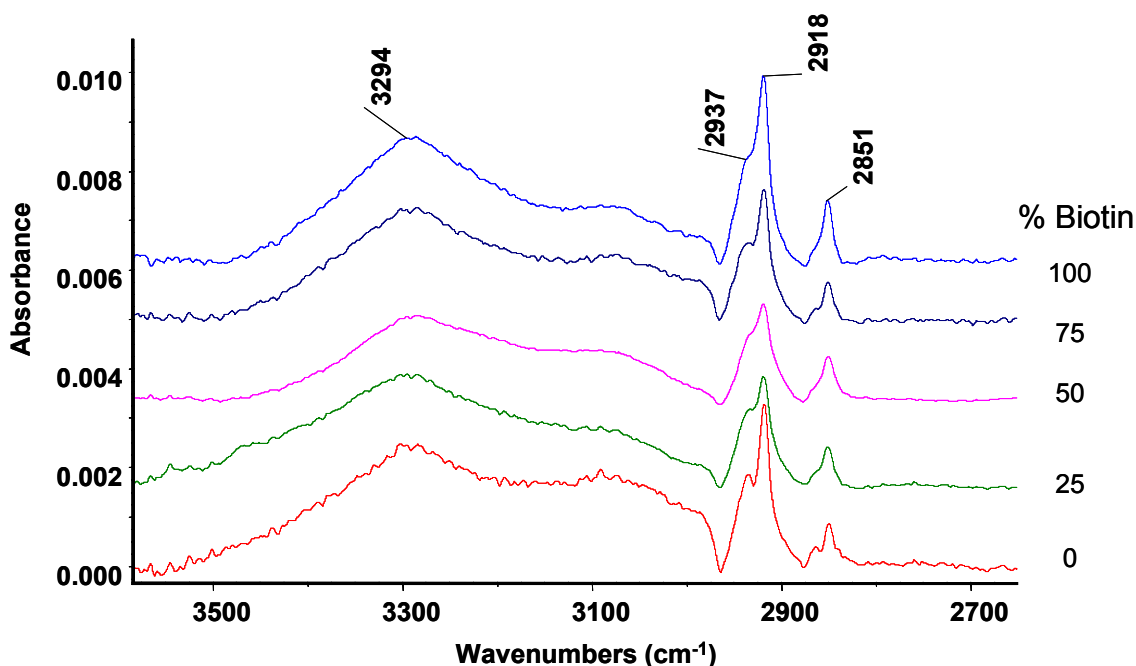
*Figure 4.53: Baseline corrected IRAS spectra of high frequency region of added Streptavidin (**SA**) on OH (**3**) and biotin (**6**) terminated mixed SAMs on MHA gold surface.*

The low frequency region of the IRAS (Figure 4.54) of the added streptavidin (**SA**) on different compositions of OH (**3**) and Biotin (**6**) terminated SAMs showed the presence of all functional groups which were present before the adsorption of the protein **SA** onto them. Apart from these functional group peaks, we have also observed important bands at ~ 1670, 1637 cm^{-1} and ~ 1560 cm^{-1} which were not present before the adsorption of **SA** and we assigned them to the amide I and

amide II vibrations of the **SA** protein [49-50] and was consequently confirmed that the streptavidin **SA** was immobilized on the surface.
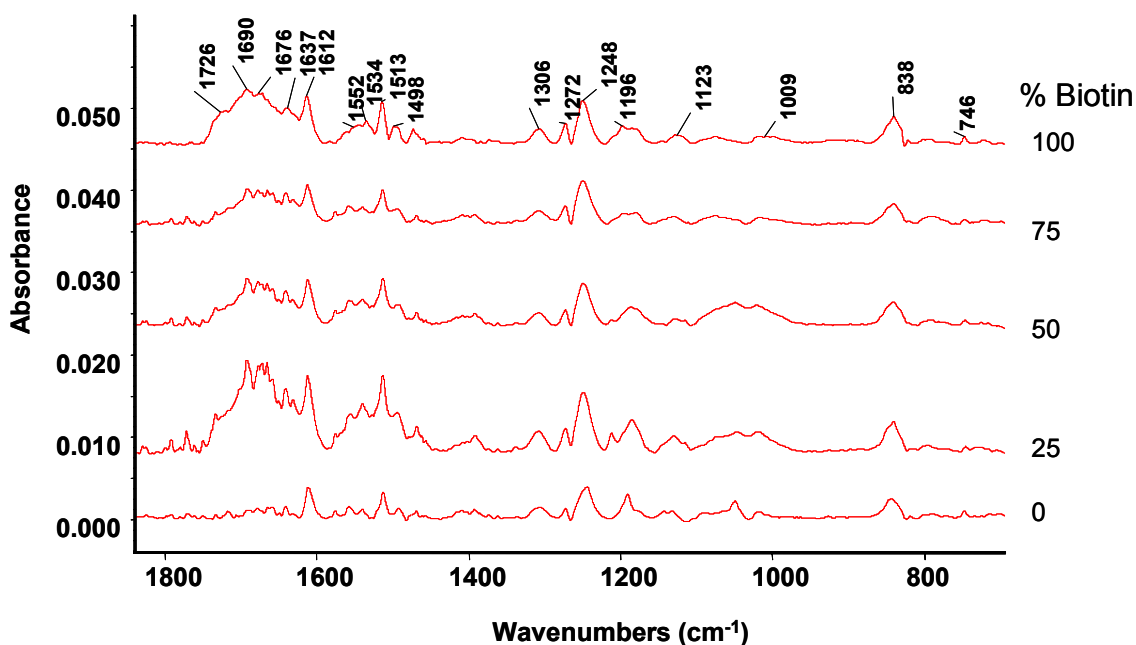
*Figure 4.54: Baseline corrected IRAS spectra of low frequency region of added Streptavidin (**SA**) on OH (**3**) and biotin (**6**) terminated mixed SAMs on MHA gold surface.*

Figure 4.55 shows the IRAS intensities of mixed monolayers of (**3**) and (**6**) after the addition of protein streptavidin (**SA**). As we have recorded all these IRAS spectra after rinsing with pH 9 borate buffer (Figure 4.54 and Figure 4.55), we concluded that the assembled amphiphilic layers were stable towards the rinsing in presence of **SA**.
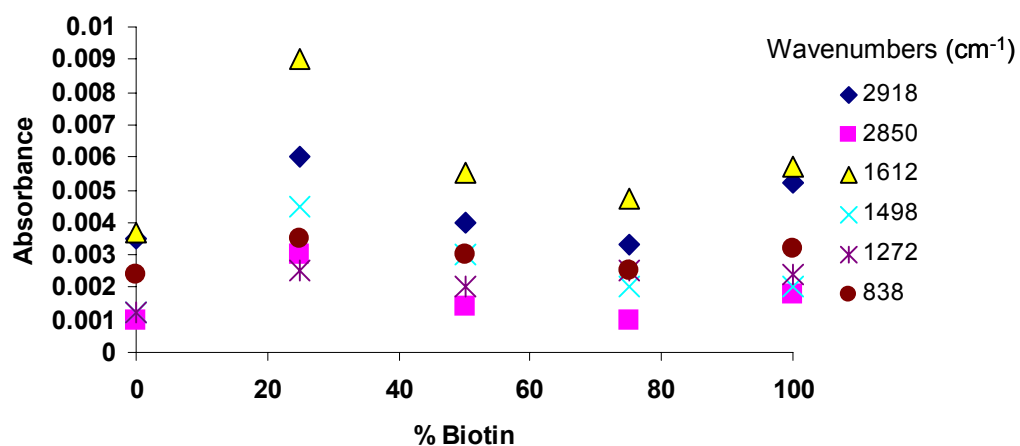
*Figure 4.55: Band position and absorption intensities of mixed amphiphiles of OH (3) and biotin (6) SAMs in the presence of protein **SA** on MHA surfaces.*

Figure 4.56 shows the low frequency region of the stepwise formation of self-assembled monolayers on MHA terminated SAMs. Upon addition of biotin amphiphile (**6**), the originally ω-functionalized acid terminated SAMs transformed into the ω-functionalized biotin terminated self-assembled monolayers via carboxylate-amidine interactions. A peak at ~1726 cm^{-1} indicates the presence of the biotin amphiphile on the acid terminated surface as we have assigned the above peak to carbonyl group of biotin amphiphilic layer. Further, the adsorption of protein molecule **SA** on the ω-functionalized biotin SAMs leads to the formation of multilayer system. Additional peaks at ~ 1670, 1637 and ~ 1560 cm^{-1} were assigned to the amide I and amide II vibrations of the SA protein [49-50].
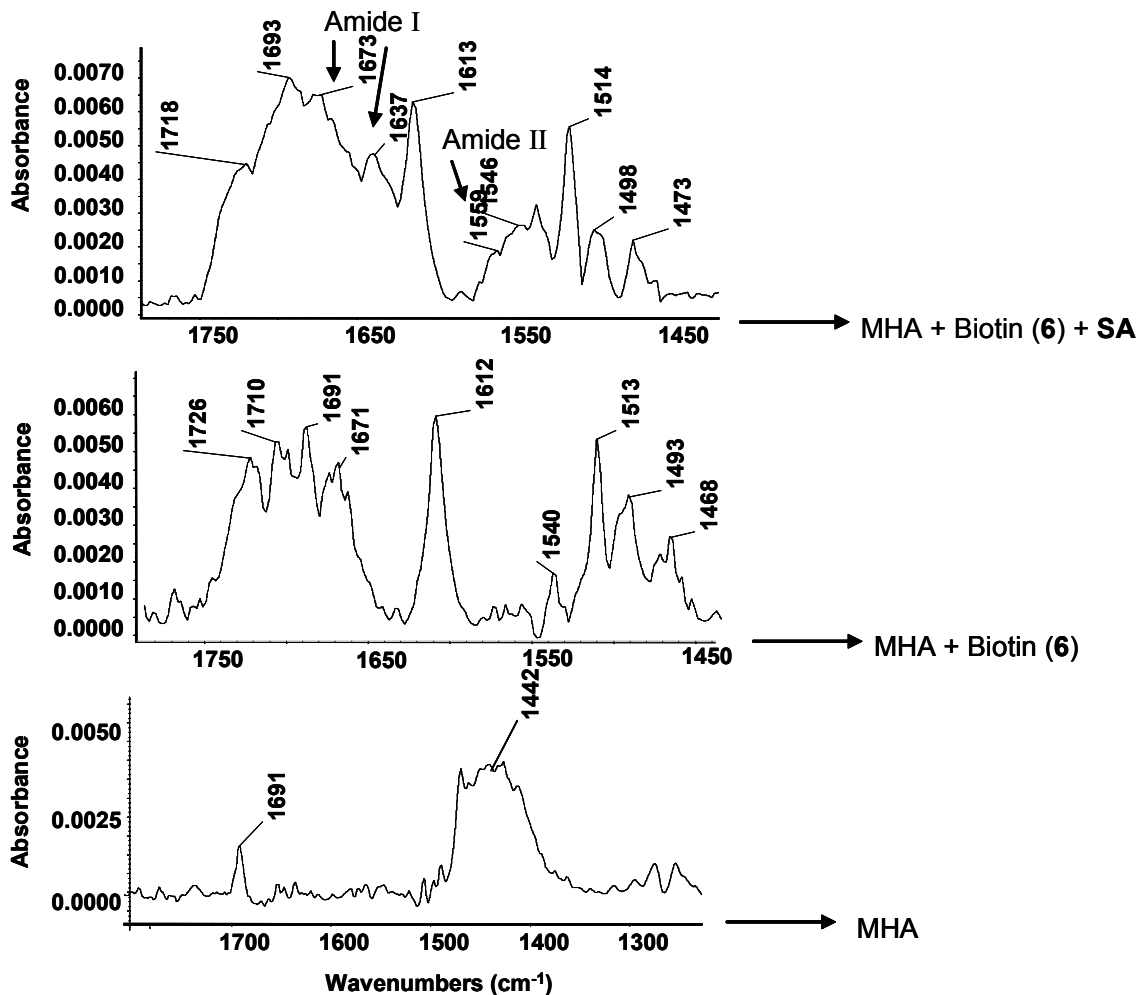
*Figure 4.56: Baseline corrected IRAS spectra of low frequency region of added Streptavidin (**SA**) on biotin (**6**) terminated SAMs at 100% content of biotin on MHA surface.*

We have seen that at 25% content of biotin (**6**) amphiphile mixed with 75% of hydroxy (**3**) functionalized SAMs, the adsorption of protein **SA** was maximum (47 ± 4 Å) (Table 4.5) which also agrees with the reported literature values [36, 48].

From Figure 4.57 we can see that at 25% biotin content, there was maximum difference in the integrated area [{Integrated area of mixed SAMs of biotin + OH + **SA** (Figure 4.54)} – {integrated area of biotin + OH (Figure 4.50)} amphiphiles].as compared to the other mixed monolayer compositions.
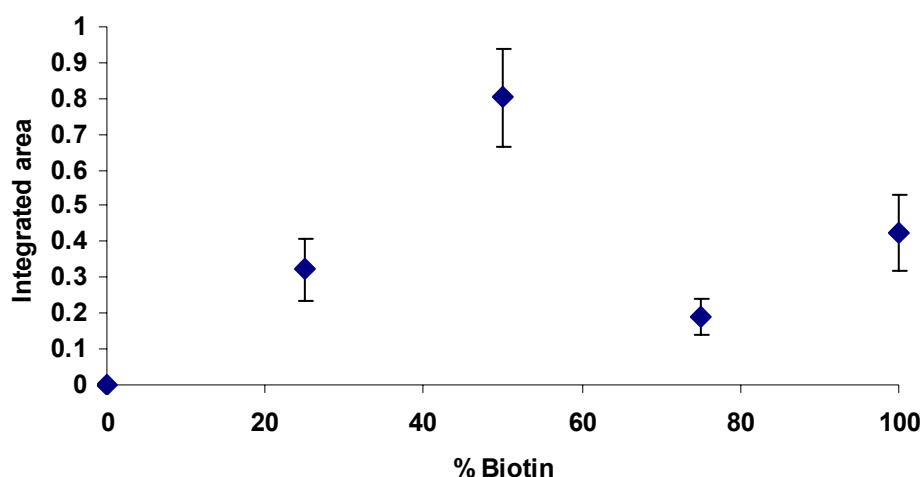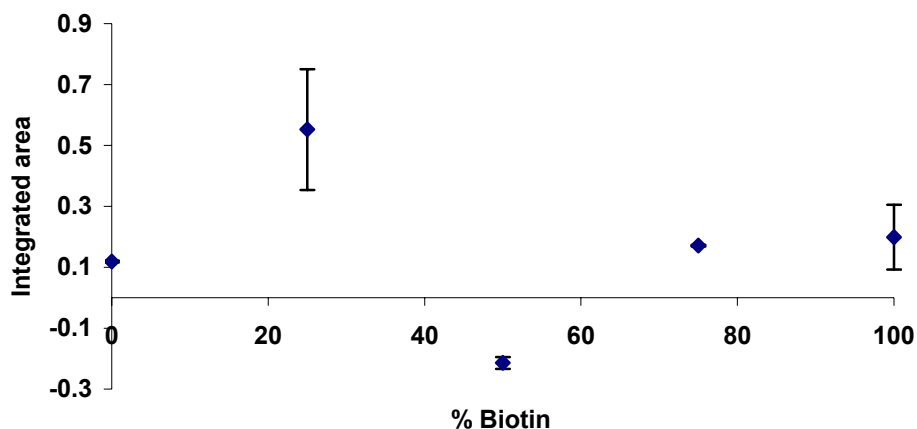
*Figure 4.57 Plot of integrated area vs. biotin (**6**) content mixed with hydroxy (**3**) terminated SAMs on acid functionalized monolayers.*

In Figure 4.58, the intensities of amide I and amide II bands at 25% content of biotin were higher as compared to the rest of the mixed monolayer compositions can be seen.
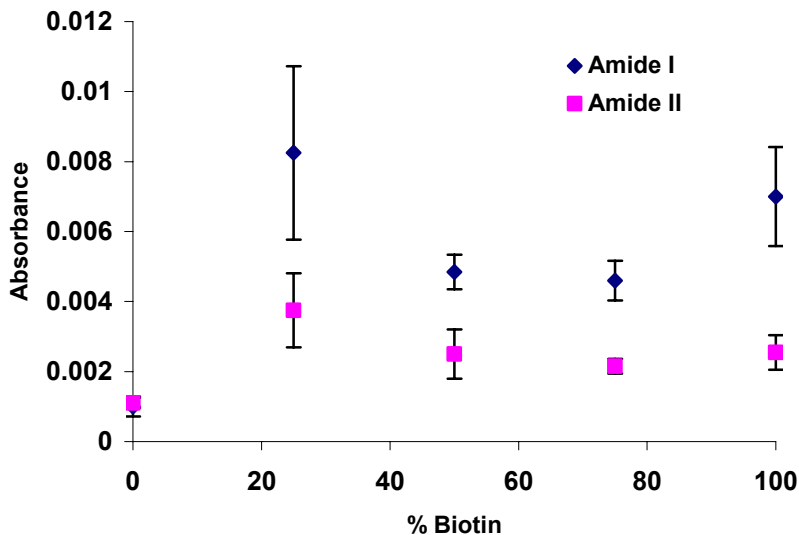
*Figure 4.58: Plot of the absorption intensities of amide I (~1670 cm^{-1}) and amide II (~1560 cm^{-1}) bands of **SA** at different compositions of biotin (**6**) amphiphile with mixed monolayers of hydroxy (**3**) functionalized SAMs.*

114

4.7.4 Conclusions

A stepwise approach was followed to generate the biosensor platform from the acid terminated self-assembled monolayers on the gold surfaces. Molecular recognition of a protein (**SA**), from solution, by a self-assembled monolayer of ω-functionalized biotin receptor molecule on acid terminated SAMs is described in this part of the thesis. Self assembly and disassembly was achieved by changing the pH of the parent system from 9 to 3 and hence to regenerate the sensor surfaces for subsequent measurements.

Air ellipsometric measurements have shown that the nonspecific binding of **SA** on clean bare gold surfaces, hydroxy (**3**), and carboxylic acid terminated SAMs was very less. The maximum surface density of the biotin molecule for the molecular recognition of **SA** was obtained at 25% content of Biotin (**6**) in the mixed self-assembled monolayers with hydroxy (**3**) terminated SAMs.

The CH stretch band at ~ 2918 cm^{-1} indicates the ordered self-assembled layer and strong absorption at 3100-3400 cm^{-1}, which could be due to the hydrogen bonding between the head groups (carboxylate and amidinium ions). Characterization of the layers by means of IRAS supported a layer structure composed of closely packed amphiphilic layers on the acid terminated SAMs. These layers were stable towards rinsing and the regeneration of the same surface was achieved by acidification to pH 3. Peaks at ~ 1670, 1637 cm^{-1} and ~ 1560 cm^{-1} were assigned to the amide I and amide II vibrations of the **SA** protein (Figure 4.56) which also confirms the presence of the protein layer on the mixed SAMs.

We have also observed the strong bands characteristic of the other corresponding functionalities.

4.8 Switchable assembly of α,ω-bis(4-amidinophenylamine)alkanes

As a part of the ongoing project for the self-assembly of fluorescence amphiphiles on acid terminated self-assembled monolayers [1-3], we have synthesized three α,ω-bis(4-amidinophenylamine)alkane amphiphiles by following the same reaction procedure reported by Tidwell *et al.* [4] which are displayed in Scheme 4.10. This part of the work was carried out to evaluate the formation of single component monolayers of these synthesized fluorescence amphiphiles on acid (MHA) terminated SAMs.

We have seen in our previous study of ω-functionalized(4-amidinophenoxy)alkanes, that these amphiphiles form switchable, stable and ordered molecular layers on the acid functionalized SAMs. Here also we were curious to know whether the α,ω-bis(4-amidinophenylamine)alkanes form stable and switchable layers on the acid terminated SAMs. In order to characterize the formation of self-assembled monolayers of the above molecules, we have performed *in situ* ellipsometry, IRAS studies and contact angle measurements and these will be discussed in this section.
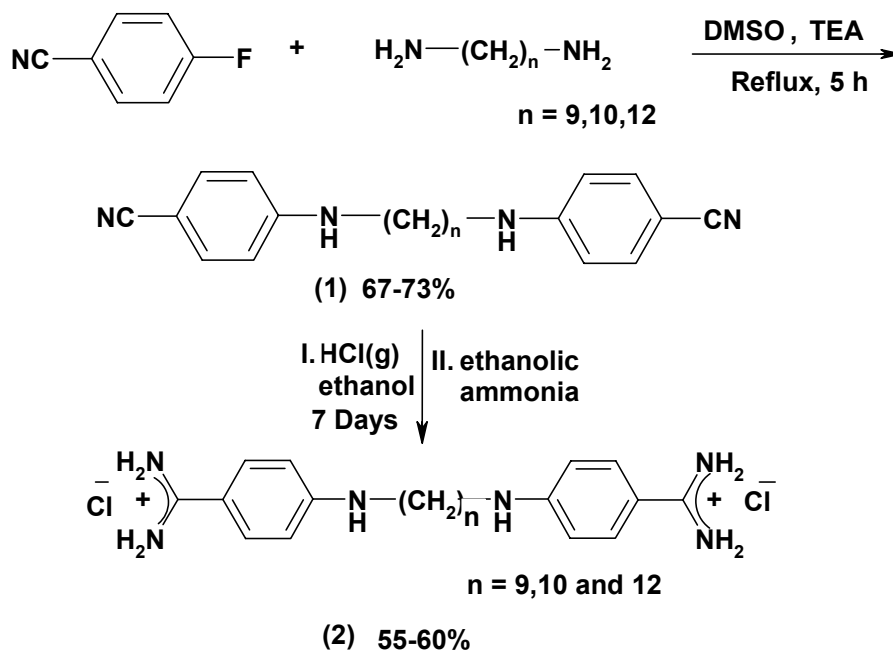
Scheme 4.10: Synthesis of α,ω-bis(4-amidinophenylamine)alkanes.

4.8.1 In situ ellipsometry of α,ω-bis(4-amidinophenylamine)alkanes

Scheme 4.11 reveals the interaction between the positively charged bis-benzamidine amphiphiles and negatively charged acid surfaces on gold.
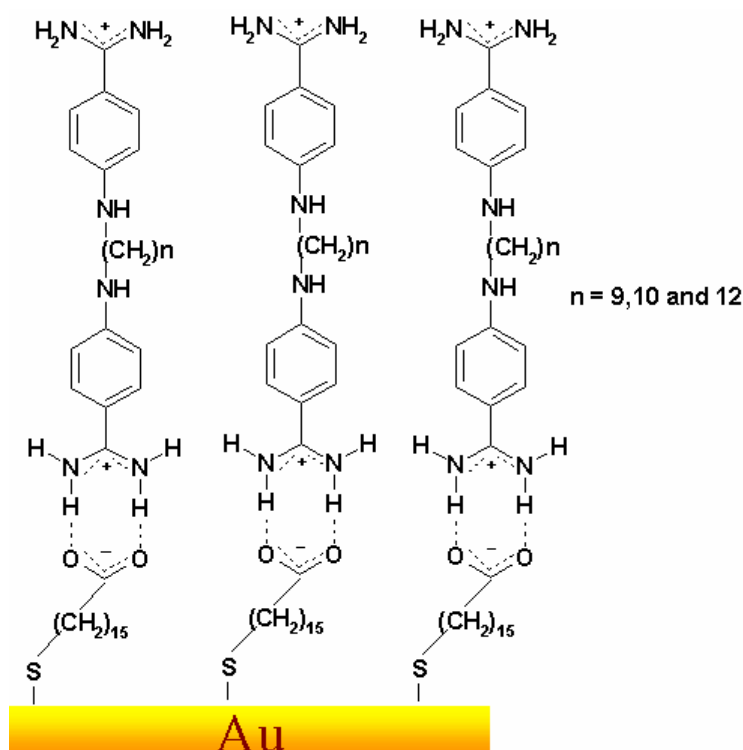
Scheme 4.11: Schematic representation of interaction between negatively charged carboxylate ion on the gold surface and positively charged amidinium ions of the synthesized amphiphiles.

The *in-situ* ellipsometry measurements were carried out on a freshly prepared gold surface. The surfaces were prepared as described in the previous section of this chapter (4.2.1).
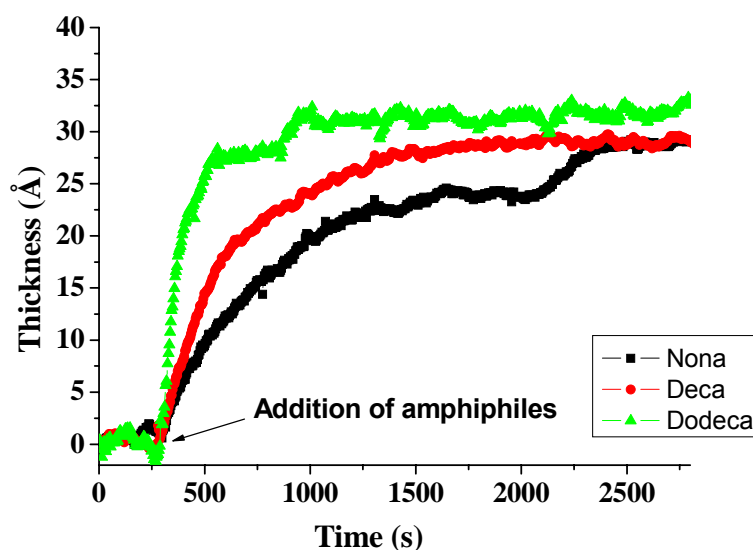
Figure 4.59: Film thickness versus time during adsorption of para-bisbenzamidine amphiphiles on MHA modified gold surfaces.

The MHA modified gold surfaces were then immersed in a Teflon-coated cuvette containing 2 mL of a 0.01 M sodium borate buffer (pH 9) prepared from boric acid. This cuvette was thermostated to 25 °C and equipped with a small magnetic stirrer. The addition of amphiphiles (50 µM) was done after obtaining a stable base line. The adsorption of bisbenzamidine molecules were then monitored by *in situ* ellipsometry from ELX-1 Precision ellipsometer (DRE-Ellipsometerbau, Ratzeburg, DE, angle of incidence 70°, He Ne laser: λ = 632.8 nm).

As displayed in Figure 4.59, upon addition of amphiphiles, we have observed an increase in layer thickness and monolayer thickness of the corresponding amphiphiles was achieved on acid functionalized gold surfaces. We have estimated the length of the molecules using CS Chem3D Ultra software. Unlike the ω-functionalized(4-amidinophenoxy)alkane amphiphiles, α,ω-bis(4-amidinophenylamine)alkanes also form stable self-assembled monolayers on acid (MHA) terminated SAMs on gold surfaces. The presence of amphiphilic self-assembly was further supported from air ellipsometry investigations which are summarized in Table 4.6.

Sr. No.	Amphiphiles	Estimated length (Å)	Thickness by air ellipsometry (Å)	Thickness by in- situ ellipsometry (Å)
1	Nonamidine	27	28 ± 2	27 ± 2
2	Decamidine	29	30 ± 3	29 ± 2
3	Dodecamidine	31	33 ± 2	34 ± 3

Table 4.6: Ellipsometric air and in situ thickness of assembled SAMs of bisbenzamidine amphiphiles on MHA SAMs.

From the Table 4.6, we can see the close agreement between the estimated length of the synthesized amphiphiles and the observed thickness by *in situ* ellipsometry and air ellipsometry (±3 Å) which suggests that the amphiphiles form a closely packed monolayer on the acid terminated SAMs on gold surfaces.

Instead of adding 50 µM amphiphilic solution, in few experiments we have added 100 µM of amphiphiles and observed the layer formation by *in situ* ellipsometry which is shown in Figure 4.60. A sharp increase in the layer thickness was observed after the addition of 100 µM of dodecamidine on the MHA functionalized SAMs on gold surfaces.
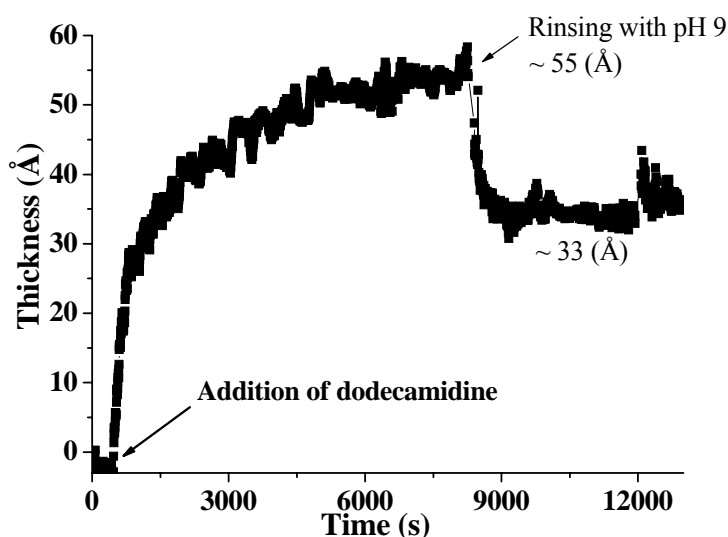
Figure 4.60: Film thickness versus time during adsorption of para-bisdodecamidine amphiphile on MHA modified gold surfaces.

In the previous study from this laboratory [1,19], it was observed that the longer chain para-substituted amidines tended to adsorb on acid functionalized surfaces in two distinct steps. A rapid initial step to reach a thickness of 20 to 30 Å followed by a slower step with the final thickness leveling off at ~ 50- 55 Å. This corresponds to bilayer thickness of the added amphiphile. The reason for the above observation may be amidine-amidine hydrogen bonding [53] between the formed amphiphilic monolayer on acid terminated SAMs and excess of amidine amphiphile in the solution, or even the bridging of the amidine head groups by the buffer anions may be responsible for the formation of amphiphilic bilayer on acid terminated SAMs. The second layer was susceptible to rinsing and after rinsing with borate buffer pH 9, monolayer thickness (~ 33 Å) of the corresponding amphiphile was achieved which is shown in Figure 4.60.

4.8.2 Infrared reflection absorption spectroscopy (IRAS) of α,ω-bis(4-amidinophenylamine)alkanes

IRAS spectroscopy was employed in order to investigate the presence of amphiphilic layers on the acid functionalized SAMs. Before the IRAS air measurements, all substrates were rinsed with pH 9 borate buffer and dried under a stream of nitrogen gas. When we compared the obtained IRAS with FTIR spectrum (Figure 4.61), we observed all the significant peaks which were present in the later. High frequency region (Figure 4.62) of the assembled amphiphiles shows a peak at ~ 2919 cm^{-1} which we have assigned to the CH_2 asymmetric stretch. This confirms the crystalline like nature of the alkyl chain of the amphiphilic layer [17,18]. The broad band at 3100 to 3400 cm^{-1} indicates the intermolecular hydrogen bonding between the head groups (amidinium-carboxylate interaction). Low frequency region of the IRAS is shown in the Figure 4.63.
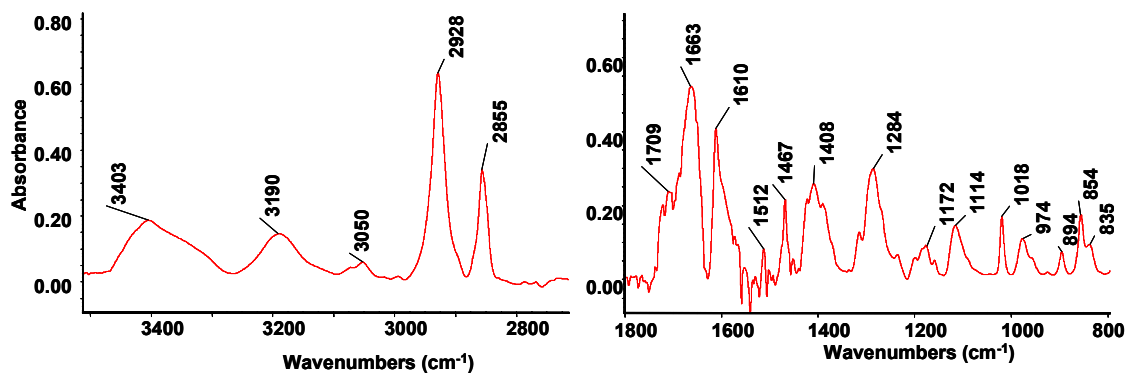
Figure 4.61: FTIR spectrum (KBr) of Dodecamidine.
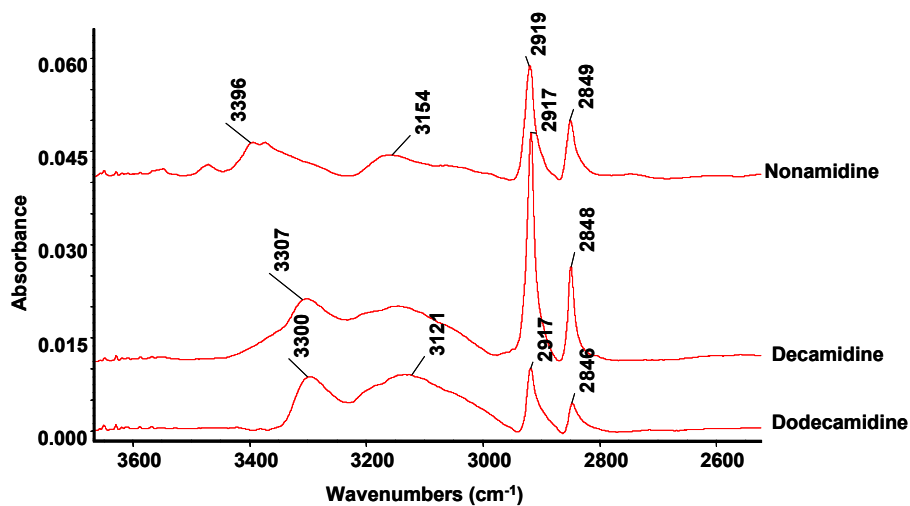
Figure 4.62: Baseline corrected IRAS spectra of high frequency region of added α,ω-bis(4-amidinophenylamine)alkanes SAMs on MHA gold surface.
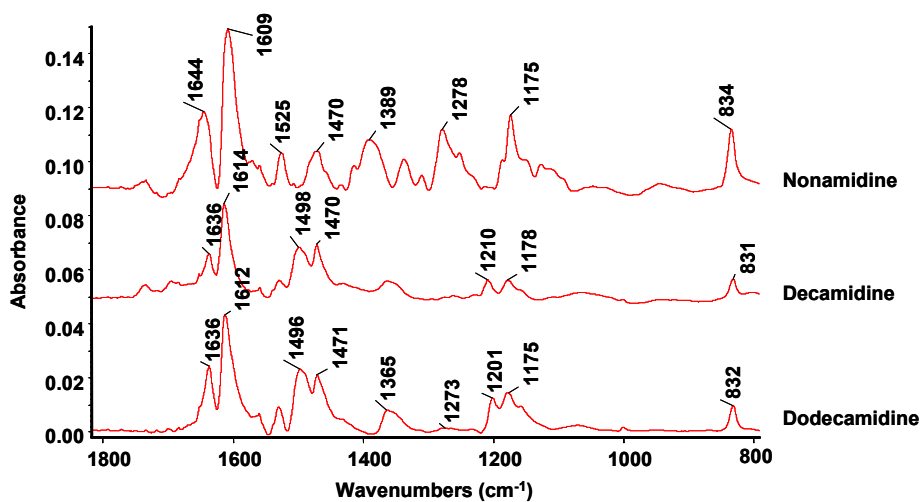
Figure 4.63: IRAS spectra of low frequency region of added α,ω-bis(4-amidinophenylamine)alkanes SAMs on MHA gold surface.

121
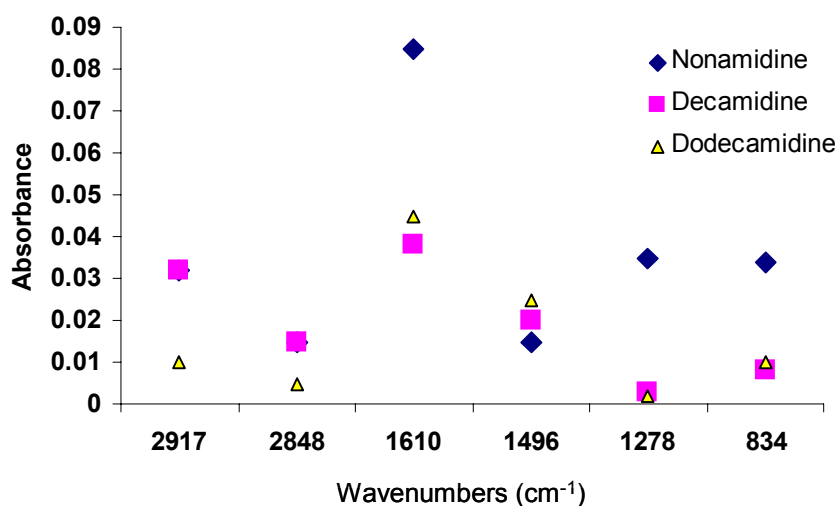
Figure 4.64: Band position and absorption intensities of amphiphiles on MHA surfaces.

4.8.3 Contact angle measurements

Contact angle measurements were recorded on the instrument G10 by Krüss GmbH (Hamburg, Germany). These measurements were performed on air-dried sample by placing a borate buffer (pH 9) drop on the SAM surface. The measured contact angles were the advancing and receding angle between the surface and the buffer drop. (Table 4.7)

Sr. No.	Amphiphiles	Contact angles θ (°) Advancing	Contact angles θ (°) Receding
1	Nonamidine	59	51
2	Decamidine	54	49
3	Dodecamidine	58	53

Table 4.7 Advancing and receding contact angles of the α,ω-bis(4-amidinophenylamine)alkanes amphiphiles on MHA SAMs.

122

4.8.4 Conclusions

Like the *α,ω*-bis(4-amidinophenoxy)alkanes amphiphiles, the synthesized *α,ω*-bis(4-amidinophenylamine)alkanes amphiphiles also forms stable, switchable assembled layers on acid terminated SAMs. An IRAS investigation of the assembled layer confirms the presence of amphiphilic molecules on the acid terminated SAMs. Amphiphilic bilayer formation was also observed although the second layer was not stable to rinsing experiment and finally gave the monolayer thickness of the corresponding amphiphiles on acid functionalized SAMs. These amphiphiles also exhibit fluorescence activity which may be used to monitor the adsorption of fluorescence amphiphile on acid surfaces.

4.9 Introducing amide linkages in the amphiphiles for lateral hydrogen bonding
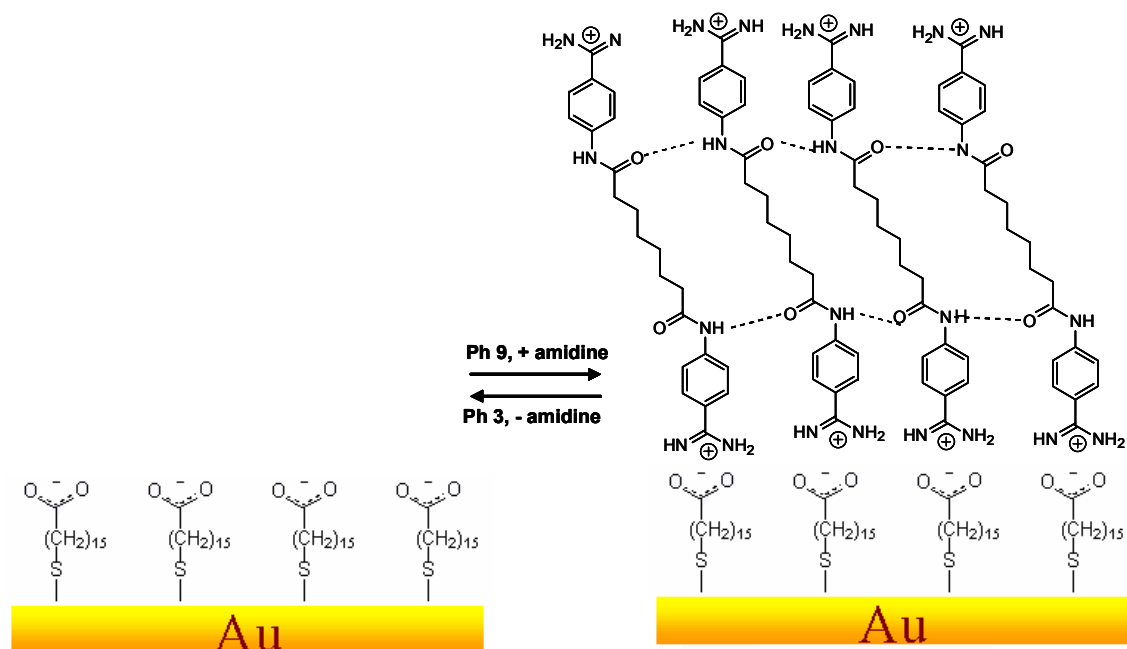
Scheme 4.12: Schematic representation of amide amphiphiles assembled on MHA SAMs.

With an effort to further stabilize the bisbenzamidine layer by lateral hydrogen bonding, our further efforts were directed towards the synthesis of amidinoamidine amphiphiles which is shown in Scheme 4.13

The key step in the preparation of following amphiphile was the protection of 4-aminobenzamidine group by protecting agent (BOC)$_2$O {(di-tert-butyldicarbonate)}. The BOC protection was performed according to the reported literature procedure [54] to obtain protected amidine (**1**) in 82% yield

Octanedioyl dichloride (**2)** was reacted) (dropwise addition at 0 °C) with protected amidine (**1**) at room temperature for 3 h to afford the molecule (**3**) which was deprotected by TFA at room temperature to yield the final product (**4**)as white solid.
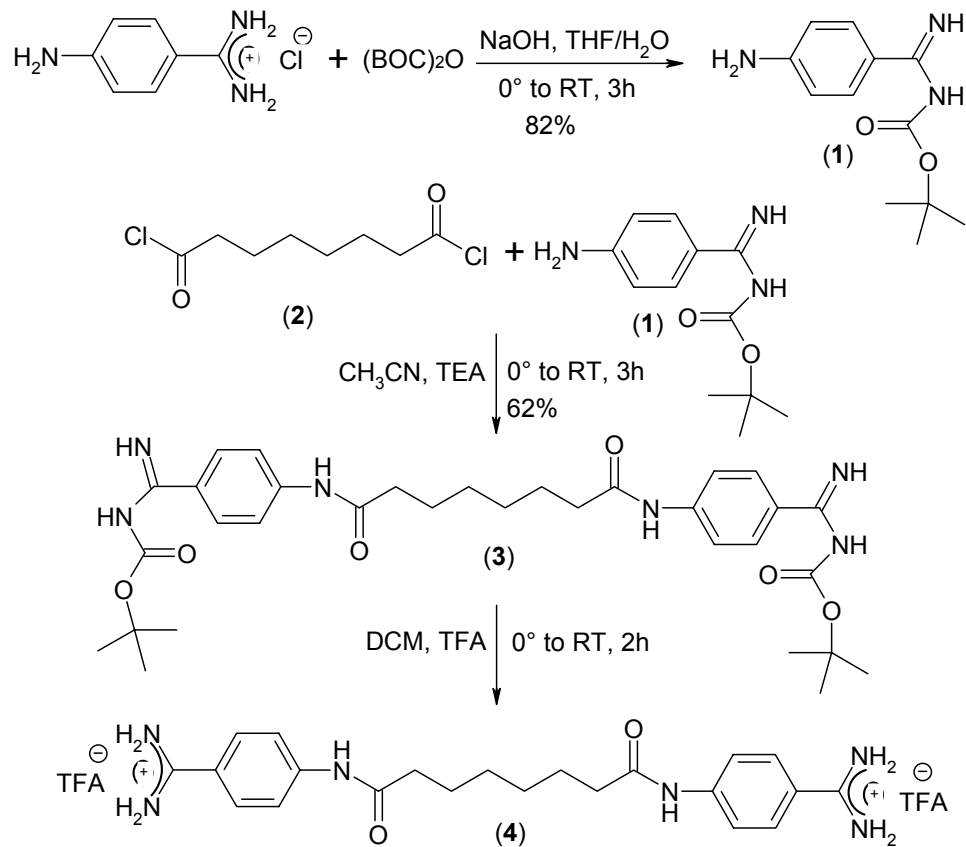
Scheme 4.13: Synthesis of amidinoamidine amphiphile.

4.10 References

[1] Auer, F., Schubert, D., Stamm, M., Arnebrant, T., Swietlow, A., Zizlsperger, M., Sellergren, B., *Chem. Eur. J.* **1999,** 5, No.4 1150.

[2] Sellergren, B., Auer, F., Arnebrant, T.*, Chem. Comm.* **1999,** 2001.

[3] Sellergren, B., Swietlow, A., Arnebrant, T.*,* Unger, K., *Anal. Chem.* **1996,** 68, 402.

[4] Tidwell, R.R., Susan, K., *J. Med. Chem* **1990**, 33, 1252.

[5] Gluth, W. P., Kaliwoda, G., Dann, O., *J. Chromatogr.* **1986,** 378, 183.

[6] Mares-Guja, M., Shaw, E., *J. Biol. Chem.* **1965,** 240, 1579.

[7] Pine, S., H., Hendrickson, J., B., Cram, D. J., Hammond, G. S., *Organic Chemistry*; McGraw-Hill: Tokyo, **1981**.

[8] Rogana, E., Nelson, D. L., Leite, L. F. F., Mares-Guia, M., *J. Chem. Res.* **1985**, 286.

[9a] Arnebrant, T., Nylander, T., *J. Colloid. Interface Sci.* **1986**, *111*, 529.

[9b] Wahlgren, M., Arnebrant, T., *J. Colloid. Interface Sci.* **1991**, *142*, 503.

[9c] Azzam, R., M., Bashara, N. M., *Ellipsometry and Polarized Light*; North-Holland: Amsterdam, **1977**.

[10a] Wang, J., Frostman, L. M., Ward, M. D., *J. Phys. Chem.* **1992**, *96*, 5224.

[10b] Lee, R. T., Carey, R. I., Biebuyck, H., A., Whitesides, G. M., *Langmuir* **1994**, *10*, 741.

[11a] Walker, J., *J. Chem. Soc., Chem. Commun.* **1949**, 1996.

[11b] Hosseini, M. W., Schaeffer, P.. De Cian, A., Kyritsakas, N., Fischer, J., *J. Chem. Soc., Chem. Commun.* **1994**, 2135.

[12] Whitesides, G. M., Ferguson, G. S., Allara, D., Scherson, D., Speaker, L., Ulman, A., *Crit. Rev. Surf. Chem.* **1993**, *3*, 49.

[12a] Nuzzo, R. G., Allara, D. L., *J. Am. Chem. Soc.* **1983**, *105*.

[12b] Porter, M. D., Bright, T. B., Allara, D. L., Chidsey, C. E. D., *J. Am. Chem. Soc.* **1987**, *109*, 3559.

[13] Sellergren, B., Swietlow, A., Arnebrant, T.*,*Unger, K., *Anal. Chem.* **1996,** 68, 402.

[14] Auer, F., Nelles, G., Sellergren, B., *Chem. Eur. J.* **2004,** 5, 10, 3232.

[15] Auer, F., Sellergren, B., Swietlow, A., Offenhauser, A., *Langmuir,* **2000,** 5936.

[16] Sellergren, B., Auer, F., Arnebrant, T., *Chem. Commun.* **1999,** 19, 2001.

[17] Arnold, R., Azzam, W., Terfort, A., Wöll, C., *Langmuir,* **2002,** 18, 3980.

[18] Nuzzo, R. G., Dubois, L. H., Allara, D. L., *J. Am. Chem. Soc.* **1990**, 112, 558.

[19] Auer, F., Nelles, G., Sellergren, B., *Chem. Eur. J.* **2004,** 5, 10, 3232.

[20] Debe, M. K., *J. Appl. Phys.* **1984,** 55, 3345.

[21] Chang, S. C., Chao, I., Tao, Y.T., *J. Am. Chem. Soc.* **1994**, 116, 6792.

[22] Mrksich, M., Whitesides, G.M., *Annu. Rev. Biophys. Biomol. Struct.* **1996**, *25*, 55.

[23] Lo´pez, G. P., Albers, M. W., Schreiber, S. L., Carroll, R. W., Peralta, E., Whitesides, G. M., *J. Am. Chem. Soc.* **1993**, *115*, 5877.

[24] Chen, C. S., Mrksich, M., Huang, S., Whitesides, G. M., Ingber, D. E., *Science* **1997**, *276*, 1425.

[25] Tidwell, C. D., Ertel, S. I., Ratner, B. D., *Langmuir* **1997**, *13*, 3404.

[26] Green, R. J., Tasker, S., Davies, J., Davies, M. C., Roberts, C. J., Tendler, S. J. B., *Langmuir* **1997**, *13*, 6510.

[27] Kang, J. F., Ulman, A., Liao. S., Jordan, R., *Langmuir.* **1999**, *15*, 2095.

[28] Kang, J. F., Ulman, A., Liao,. S., Jordan, R., *J. Am. Chem. Soc.* **1998**, *120*, 9662.

[29] Colthup, N. B., Daly, L. H., Wiberly, S. E., *Introduction to IR and Raman spectroscopy,* Academic press, New York **1990.**

[30] Kang, F. J., Ulman, A., Jordan, R., *Langmuir.* **1999,** 15, 5555.

[31] Bradshaw, A. M., Schweizer, E., In *Advances in Spectroscopy. Spectroscopy of Surfaces;* Hester, R. E., Clark, R. J. H., Eds.; Wiley: New York, **1988,** Vol. 16, pp 413.

[32] Willis, R. F., Lucas, A. A., Mahan, G. D., *The Chemical Physics of Solid Surfaces and Heterogeneous Catalysis*; King, D. A. Woodruff D. P. Eds. Elsevier Amsterdam, **1981,** Vol. 2, pp 67.

[33] Nelles, G., Schönherr, H., Jaschke, M., Wolf, H., Schaub, M., Küther, J., Tremel, W., Bamberg, E., Ringsdorf, H., Butt, H. J., *Langmuir.* **1998,** 14, 808.

[34] Willner, I., Blonder, R., Dagan, A., *J. Am. Chem. Soc.* **1994**, *116*, 9365.

[34a] Spinke, J., Liley, M., Schmitt, F.-J., Guder, H.-J., Angermaier, L., Knoll, W., *J. Chem. Phys.* **1993**, *99*, 7012.

[35] Ulman, A., *An Introduction to ultrathin organic films from Langmuir-Blodgett to self-assembly.* Academic press inc. San Diego. CA **1991**.

[36] Herron, J. N., Müller, W., Paudler, M., Riegler, H., Ringsdorf, H., Suci, P. A., *Langmuir* **1992,** 8, 1413.

[37] Sigal, G.B., Bamdad, C., Barberis, A., Stominger, J., Whitesides, G. M., *Anal. Chem.* **1996,** 68, 490.

[38] Chapman, R. G., Lin Yan, E. O., Whitesides, G. M., *Langmuir* **2000,** 16, 6927.

[39] Prime, K.L., Whitesides, G. M., *Science* **1991**, 252, 1164.

[40] Prime, K.L., Whitesides, G. M., *J. Am. Chem. Soc.* **1993**, *115*, 10714.

[41] Mrksich, M., Whitesides, G. M., *Annu. Rev. Biophys. Biomol. Struct,* **1996,** 25, 55.

[42] Whitesides, G. M., *Chimia* **1990**, *44*, 310.

[43] Nishimura, T., *Polymer Materials for Blood Purification*, Nishimura, T., Ed.; CRC Press: Boca Raton, FL, **1993**.

[44] Chen, C. S., Mrksich, M., Huang, S., Whitesides, G. M., Ingber, D. E., *Science* **1997**, *276*, 1425.

[45] Göpel, W., Heiduschka, P., *Biosens. Bioelectron.* **1995,** 10, 853.

[45a] Green, N. M., *Methods Enzymol*. **1990,** 184, 51.

[45b] Wilchek, M., Bayer, E.A., *Anal. Biochem.* **1988,** 171, 1.

[46] Chaiet, L., Wolf, F., *J. Arch. Biochem. Biophys*. **1964,** 106, 1.

[47] Sasaki, D.Y., Kurihara, K., Kunitake, T., *J. Am. Chem. Soc.* **1991**, *113*, 9685.

[48] Spinke, J., Liley, M., Guder, H. J., Angermaier, L., Knoll, W., *Langmuir* **1993,** 9, 1821.

[49] Pradier, C. M., Salmain, M., Methivier, C., *Surf. Interface Anal.* **2002**, 34, 67.

[50] Krimm, S., Bandekar, J., *Adv. Protein Chem*., **1986,** 38, 181.

[51a] Chapman, R. G., Ostuni, E., Shuichi, T., Holmlin ,R. E., Yan, L., Whitesides, G. M., *J. Am. Chem. Soc.* **2000**, *122*, 8303.

[51b] Kim, K., Yang, H., Jon, S., Kim, E., Kwak, J., *J. Am. Chem. Soc.* **2004**, *126*, 15368.

[52] Deng, L., Mrksich, M., Whitesides, G. M., *J. Am. Chem. Soc.* **1996**, *118*, 5136.

[53] Halliday, J. D., Symons, E. A., Binder, P. E., *Can. J. Chem.* **1978,** 56, 1470.

[54] Pons, J. F., Fauchere, J. F., Lamaty, F., Molla, A., Lazaro, R., *Eur. J. of Org. Chem,* **1998**, 853.

[55] Laibinis, P. E., Bain, C. D., Nuzzo, R. G., Whitesides, G. M., *J. Phys. Chem.* **1995,** 99, 7663.

[56] Bain, C. D., Troughton, E. B., Tao, Y. T., Evall, J., Whitesides, G. M., Nuzzo, R. G., *J. Am. Chem. Soc.* **1989,** 111, 321.

5 Experimental part

5.1 Synthesis of α,ω-hetero-functionalized amphiphiles

5.1.1 Synthesis of 4-cynophenoxyoctane-8 bromide

Reaction:
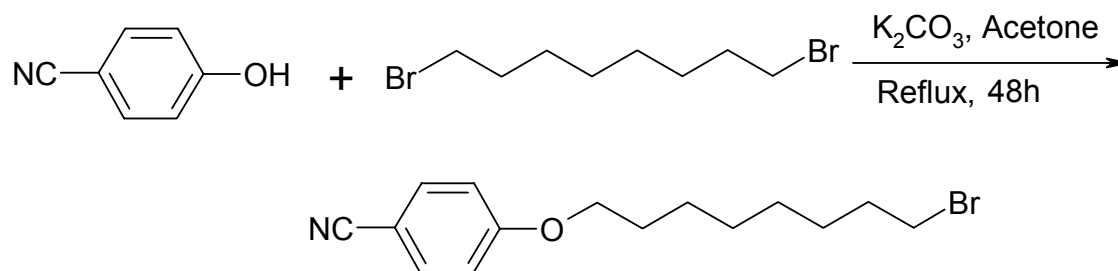
Procedure:

4-cyanophenol (5g, 42 mmol) was dissolved in 25 mL of dry acetone, 1.8, dibromooctane (115 mL, 420 mmol) was added drop wise over 30 minutes into the above reaction mixture. Then mild base, K_2CO_3 (11.5 g, 83.3 mmol) was added and reaction mixture was refluxed (56 °C) for 48 h. (reaction was monitored by TLC)

Reaction mixture was allowed to come at room temperature and inorganic (K_2CO_3) was filtered off and washed with 50 mL of acetone. Filtrate (acetone) was concentrated on rotavapour. 100 mL of chloroform was added in the obtained residue and it was washed twice (50x2 mL) with water. Organic layer was again concentrated on rotavapour to give crude product. Pure compound was obtained by column chromatography using cyclohexane: ethyl acetate (1:9) as a solvent mixture to afford 58% of the final product as (4-cyanophenoxyoctane-8 bromide).

Characterizations:

^{1}H NMR (CDCl$_3$): 200 MHZ, δ (ppm): 1.3-1.8 (m, 12H), 3.5 (t, 2H), 4.0 (t, 2H), 7.08-7.7 (m, Aromatic)

^{13}C NMR (CDCl$_3$), 200 MHz)δ : 25.6, 29.2,, 29.7, 30.6, 33.4, 34.5, 73.2, 103.7, 115.2, 119.4, 134.0, 162.5

Mass (M/e), (EI) Exact Mass: 309.07 Found: 309.0

5.1.2 Synthesis of 4-methylphenoxy (4-cynophenoxy)octane

Reaction:
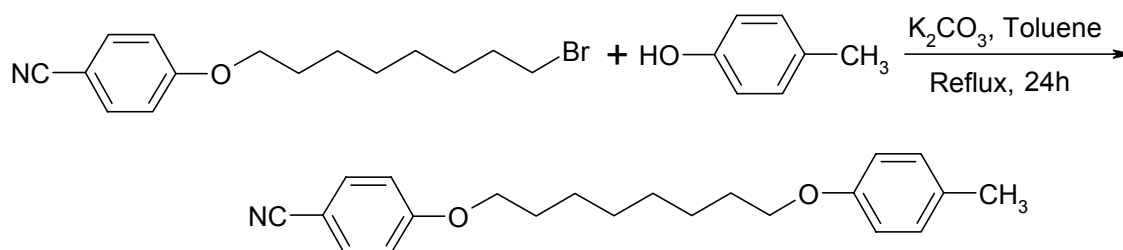
Procedure:

4-cynophenoxyoctane-8 bromide (1 g, 3.23 mmol) was heated at 100 °C with 4-methyl phenol (0.34 mL, 3.3 mmol) in toluene (25 mL) and K$_2$CO$_3$ (2.5 g, 18.11 mmol) for 24 h. after aqueous workup; the crude product was obtained and was purified by column chromatography to give the 4-methylphenoxy (4-cynophenoxy)octane (0.85 g, 78%) as a white solid.

Characterizations:

^{1}H NMR (CDCl$_3$): 400 MHZ, δ (ppm): 1.3-1.8 (m, 12H), 3.2 (s –CH$_3$), 3.8 (t, 2H), 4.0 (t, 2H), 6.70-7.7 (m, Aromatic)

^{13}C NMR (CDCl$_3$), 400 MHz)δ : 20.4, 25.8, 30.3, 30.8, 33.4, 73.2, 104.7, 114.7, 115.3, 116.9, 129.4, 129.9, 133.5, 155.4, 162.5

Mass (M/e), (EI) Exact Mass: 337.20 Found: 337.0

5.1.3 Synthesis of 4-methylphenoxy(4-amidinophenoxy)octane hydrochloride
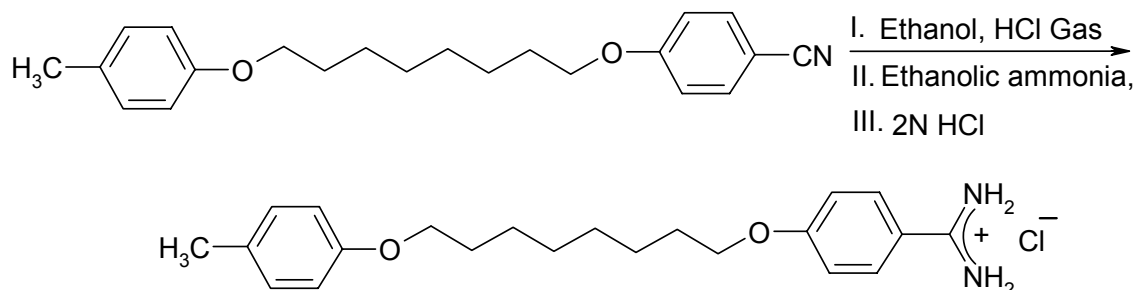
Reaction:

Procedure

4-methylphenoxy (4-cynophenoxy)octane (0.5 g, 14.83 mmols) was dissolved in 50 mL of dry benzene and 5 mL of dry ethanol. The above reaction mixture was cooled to 0-5 °C and HCl gas was passed through the reaction mixture for 30 minutes. Reaction mixture was then saturated with HCl gas and allowed to warm to room temperature (*Pinner synthesis*). The above reaction mixture was stirred at room temperature for 3 days. After 3 days, reaction mixture was concentrated under reduced pressure and 100 mL of dry diethyl ether was added to precipitate the intermediate product as imidate. This imidate was filtered and washed with 50 mL of dry ether and dried under nitrogen. The solid was dissolved in 50 mL of dry ethanolic ammonia and dry ethanol (50 mL) and was heated to 60 °C for 6 h. After 6 hours, the volume of the reaction mixture was reduced to one-half, and ether was added to precipitate the product as a white solid.

The solid was recrystallized from 2 N HCl to give 0.29 g (55%) of 4-methylphenoxy(4-amidinophenoxy)octane as a white solid.

Characterizations:

^{1}H NMR (DMSO-d$_6$): 200 MHZ, δ (ppm): 1.30-1.66 (m, 12H), 2.162(s, 3H), 3.83-3.86 (t, 2H), 4.01-4.04(t, 2H), 6.72-7.77(m, 8H, Aromatic), 8.79(s, 2H –NH$_2$), 9.10 (s, 2H –NH$_2$)

Mass: (EI) 54.5 (18.67), 69.1(16.35) 91.1(10.81) 108.1(100), 120.1(16.34), 149.1(13.87) 205.2(13.19), 337.2(35.77), 355.3(6.34)

5.1.4 Synthesis of 4-nitrophenoxy(4-cynophenoxy)octane

Reaction:
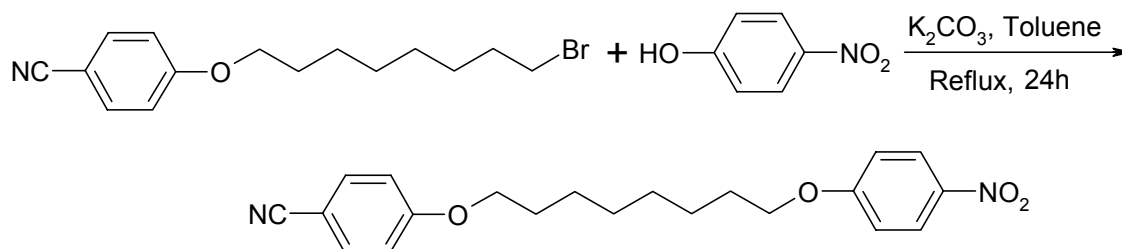
Procedure:

4-cynophenoxyoctane-8 bromide (1 g, 3.23 mmol) and *p*-nitro phenol (0.45 g, 3.23 mmol) was heated to 100 °C in the presence of K_2CO_3 (2.5 g, 18.11 mmol) and 25mL of toluene for 24 h. After the aqueous workup, the crude product was obtained and was purified by column chromatography to give the 4-nitrohenoxy (4-cynophenoxy)octane (0.87 g, 73%) as a white solid.

Characterizations:

^{1}H NMR (CDCl$_3$): 200 MHZ, δ (ppm): 1.35-1.79 (m,12H), 3.94-3.97 (t, 2H) 3.99-4.02 (t, 2H), 6.87-6.90 (m, 4H Aromatic), 7.52-7.54 (m, 2H Aromatic), 8.14-8.16(m,2H Ar-H).

^{13}C NMR (CDCl$_3$), 200 MHz)δ : 26.5, 30.5, 39.5, 72.4, 104.2, 114.7, 115.3, 116.7, 124.4, 134.2, 141.2, 163.4, 164.3

Mass: (EI) 54.5 (56.28), 69 (100), 81.1 (10.55), 102.0 (13.77), 119.0 (23.86) 368 (49.64)

5.1.5 Synthesis of 4-nitrophenoxy(4-amidinophenoxy)octane hydrochloride

Reaction:
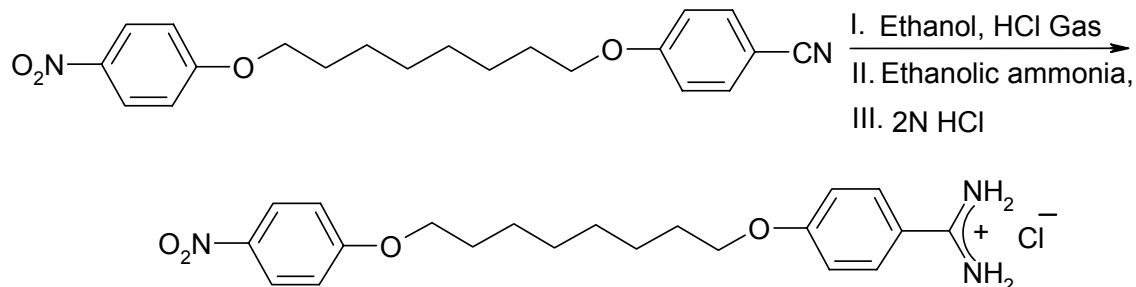
Procedure:

The compound was synthesized according to the procedure described for the synthesis of molecule, 4-methylphenoxy(4-amidinophenoxy)octane hydrochloride (**5.1.3**).

0.61 g (58%) of final product, 4-nitrophenoxy(4-amidinophenoxy)octane was obtained as a white solid.

Characterizations:

^{1}H NMR (DMSO-d$_6$): 400 MHZ, δ (ppm): 1.30-1.71 (m,12H), 4.01-4.02 (t,2H), 4.06-4.08(t,2H), 7.07-7.09(m,4H, Aromatic), 7.77-7.79 and 8.13-8.15(m,4H, Aromatic), 8.93(s,2H –NH$_2$), 9.15 (s, 2H –NH$_2$).

^{13}C NMR (DMSO-D$_6$), 400 MHz)δ : 25.5, 28.8, 39.5, 68.3, 68.8, 115.2, 126.1, 130.4, 140.9, 163.2, 164.3, 164.9

^{1}H NMR (D$_2$O) 400 MHz)δ: 1.25-1.67 (m, 12H), 3.98-4.01 (t, 2H), 4.03-4.05(t, 2H), 7.04-7.06(m, 4H, Aromatic), 7.70-7.73 and 8.11-8.13(m, 4H, Aromatic).

Mass: (EI) 119.0(2.21) 139.0(5.25) 265.0(20.41) 285.0(57.58) 368(100) 386(7.84)

5.1.6 Synthesis of 4-methoxyphenoxy(4-cynophenoxy)octane
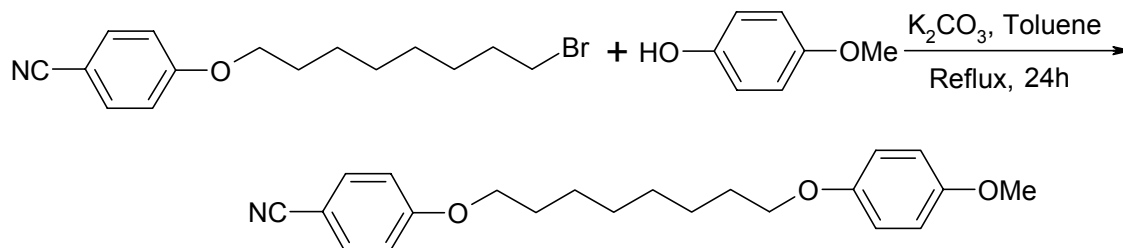
Reaction:

Procedure:

4-methoxy phenol (0.4 g 3.23 mmol) and 4-cynophenoxyoctane-8 bromide (1 g, 3.23 mmol) were heated at 100 °C in presence of K_2CO_3 for 24 h in toluene as a solvent. After the reaction is over, the inorganic was filtered off and residue was washed with 25 mL toluene. Organic layer was concentrated under reduced pressure to afford the crude product. The pure product (0.85 g, 74%) was obtained as a white solid by column chromatography using petroleum ether and ethyl acetate as a eluting mixture (80:20)

Characterizations:

^{1}H NMR (CDCl3): 400 MHZ, δ (ppm): 1.34-1.78 (m,12H), 3.72 (s OCH3), 3.85-3.88(t, 2H), 3.93-3.97(t,2H), 6.78-6.90 and 7.52-7.54 (m, 8H. Aromatic).

Mass: (EI) 69.0(3.43, 109.0(11.31) 124.1(96.00) 353.1(100)

5.1.7 Synthesis of 4-nitrophenoxy(4-amidinophenoxy)octane hydrochloride

Reaction:
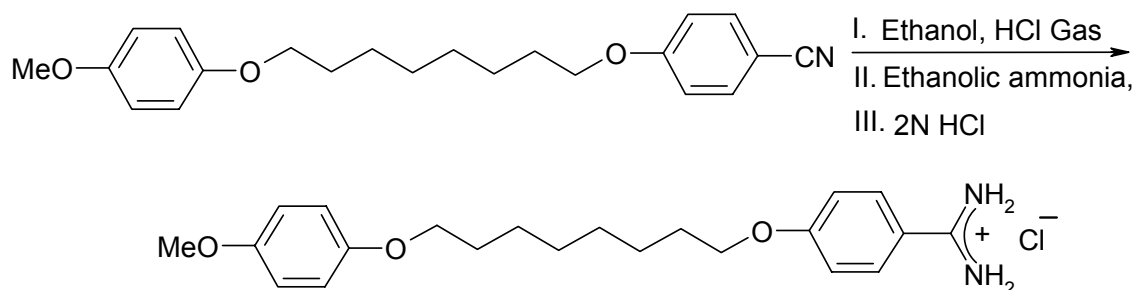
Procedure:

The compound 4-methoxyphenoxy (4-amidinophenoxy)octane was synthesized according to the procedure described for the synthesis of molecule, 4-methylphenoxy(4-amidinophenoxy)octane hydrochloride (**5.1.3**).

0.27 g (52%) of final product, 4-methoxyphenoxy(4-amidinophenoxy)octane was obtained as a white solid.

Characterizations:

^{1}H NMR (DMSO-d$_6$): 400 MHZ, δ (ppm): 1.29-1.70 (m, 12H), 3.62(s, 3H) 3.80-3.83(t, 2H), 4.008-4.04(t, 2H), 6.78-7.78(m, 8H, Aromatic), 8.90(s, 2H –NH$_2$), 9.14(s, 2H –NH$_2$).

^{13}C NMR (DMSO-D$_6$, 400 MHz)δ : 29.0, 39.3, 68.0, 114.8, 115.5, 130.4, 152.9, 153.4, 163.3, 164.9.

Mass: (EI)%**:** 109.1(26.41) 120.1(17.18) 124.1(95.03) 136.0(18.87) 247.1(12.68) 353.1(100) 371.2(13.57)

5.2 Synthesis of α,ω-bis(4-amidinophenylamine)alkanes

5.2.1 Synthesis of 1,9-bis (4-cyanophenylamine) nonane (Nonamidine)

Reaction:
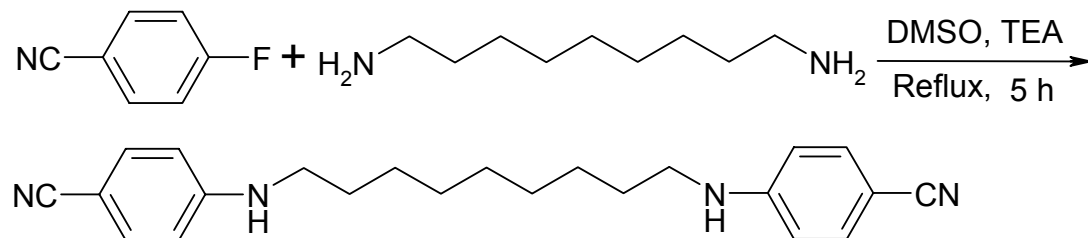
Procedure:

A mixture of 4 flurobenzonitrile (2.75 g 0.022 moles) 1,9-diaminononane (1.8 g, 0.011 moles), Triethyl amine (TEA) (2.5 mL,0.024 moles) and 50 mL of dry dimethyl sulfoxide (DMSO) was heated at 150 °C with stirring for 4 h. The mixture was poured into 100 mL of iced water and the precipitate was collected by filtration. The solid was recrystallized from DMSO/H_2O (8:2) filtered and washed with water to give 2.4 g (67%) of 1,9-bis (4-cyanophenoxy) nonane as a white solid.

Characterizations:

^{1}H NMR (DMSO-d$_6$): 400 MHZ, δ (ppm): 1.20-1.52 (m, 14H), 2.95-3.00 (m, 4H), 6.54- 6.57 (m, 4H, Aromatic), 6.60-6.63 (t, 2H, -NH_2), 7.35-7.30 (m, 4H, Aromatic)

Mass: (EI)%: Exact mass: calculated: 402.2 Mass found: 402.2

5.2.2 Synthesis of 1,9-bis (4-amidinophenylamine) nonane dihydrochloride (Nonamidine)

Reaction:
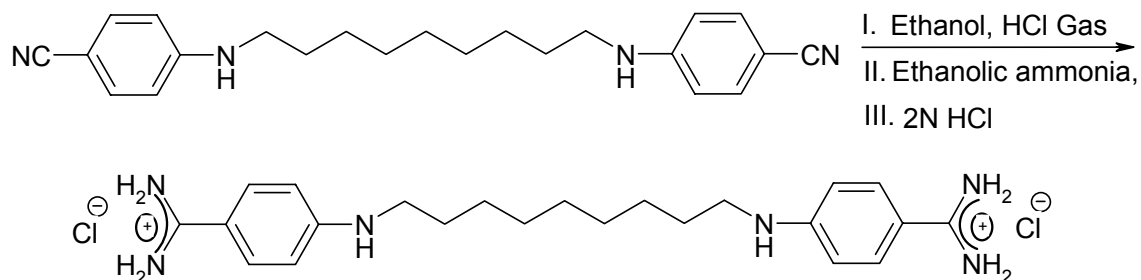
Procedure:

A solution (1 g, 0.0027 moles) of 1,9-bis (4-cyanophenoxy) nonane in 100 mL of dry dioxane and 40 mL of dry methanol was saturated with HCl gas. The sealed reaction mixture was allowed to stir at room temperature for 7 days. (After 7 days, IR of the aliquot indicates the absence of dinitrile group.) During those 7 days, the reaction mixture was saturated 2 times with the HCl gas.

After reaction is over, the reaction mixture was concentrated under reduced pressure. 100 mL of dry diethyl ether was added to precipitate the intermediate product as imidate. This imidate was filtered and washed with 50 mL of dry ether and dried under nitrogen. The solid imidate was dissolved in 50 mL of dry ethanol and 50 mL ethanolic ammonia and heated to 60 °C for 4 h. The volume of the reaction mixture was reduced to one-half, and ether was added to precipitate the product as a white solid.

The solid was filtered and recrystallized from 2 N HCl to give 0.64 g (59%) of 9-bis (4-amidinophenoxy) nonane (Nonamidine)

Characterizations:

^{1}H NMR (DMSO-d$_6$): 400 MHZ, δ (ppm): 1.30-1.70 (m, 14H), 4.05-4.10 (m, 4H), 6.60-6.63 (t, 2H, -NH$_2$), 7.12 (m, 4H Aromatic) 8.05 (m, 4H Aromatic), 11.0 (s, 4H), 11.80 (s, 4H)

^{13}C NMR (DMSO-D$_6$, 400 MHz)δ : 26.1, 26.7, 28.1, 30.6, 32.8, 53.2, 111.7, 123.7, 124.7, 153.4, 163.7.

5.2.3 Synthesis of 1,10-bis (4-cyanophenylamine) decane (decamidine)

Reaction:
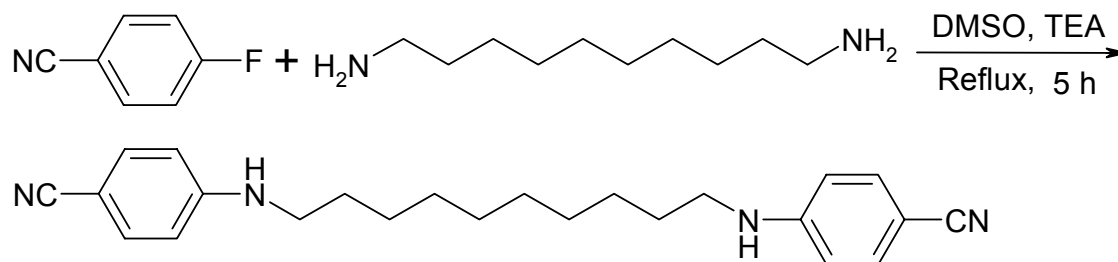
Procedure:

The synthesis of 1,10-bis (4-cyanophenoxy) decane (Decamidine) was achieved in 70% yield by using the same reaction procedure described for the synthesis of 1,9-bis (4-cyanophenoxy) nonane (**5.2.1**)

Characterization:

^{1}H NMR (DMSO-d$_6$): 400 MHZ, δ (ppm): 1.20-1.52 (m, 14H), 2.95 (m, 4H), 6.54 (m, 4H, Aromatic), 6.60 (t, 2H, -NH$_2$), 7.40 (m, 4H, Aromatic)

5.2.4 Synthesis of 1,10-bis (4-amidinophenylamine) decane dihydrochloride (decamidine)

Reaction:
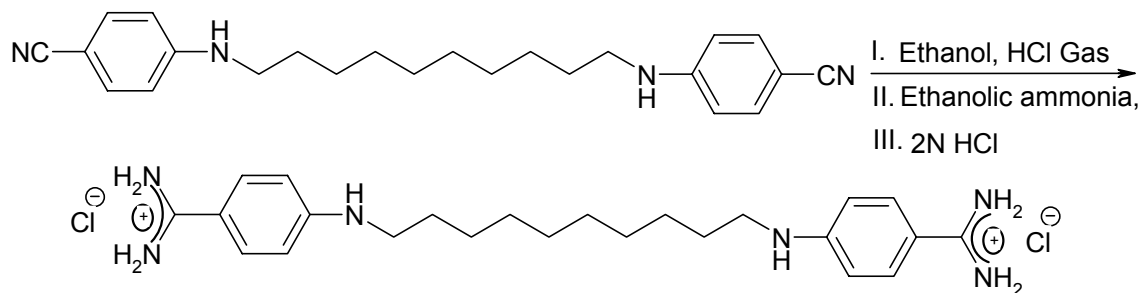
Procedure:

The synthesis of 1,10-bis (4-amidinoophenoxy) decane (Decamidine) was achieved in 57% yield by using the same reaction procedure described for the synthesis of 1,9-bis (4-amidinophenoxy) nonane (**5.2.2**)

Characterization:

^{1}H NMR (DMSO-d_6): 400 MHZ, δ (ppm): 1.20-1.52 (m, 16H), 3.00 (m, 4H), 6.50 (t, 2H, -NH$_2$), 6.60 (m, 4H, Aromatic), 7.60 (m, 4H, Aromatic), 8.70 (s, 4H), 8.90 (s, 4H).

5.2.5 Synthesis of 1,12-bis (4-cyanophenylamine) dodecane (dodecamidine)

Reaction:
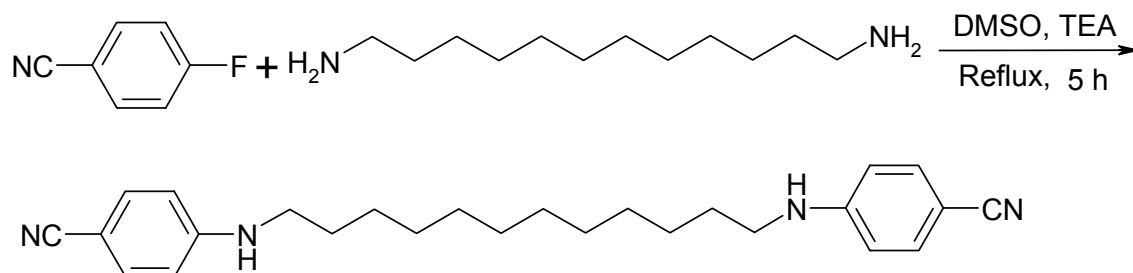
Procedure:

The synthesis of 1,12-bis (4-cyanophenoxy) dodecane (Dodecamidine) was achieved in 73% yield by using the same reaction procedure described for the synthesis of 1,9-bis (4-cyanophenoxy) nonane (**5.2.1**).

Characterization:

^{1}H NMR (DMSO-d$_6$): 400 MHZ, δ (ppm): 1.20-1.52 (m, 20H), 3.00 (m, 4H), 6.54 (m, 4H, Aromatic), 6.60 (t, 2H, -NH$_2$), 7.60 (m, 4H, Aromatic)

5.2.6 Synthesis of 1,12-bis (4-amidinophenylamine) dodecane dihydrochloride (dodecamidine)

Reaction:
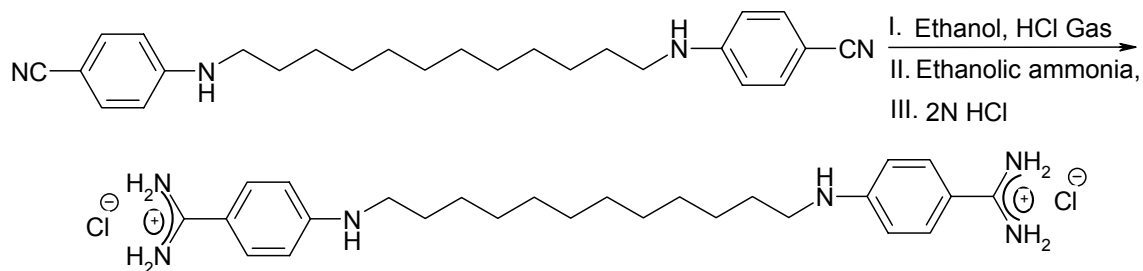
Procedure:

The synthesis of 1,12-bis (4-amidinophenylamine) decane (Decamidine) was achieved in 55% yield by using the same reaction procedure described for the synthesis of 1,9-bis (4-amidinophenylamine) nonane (**5.2.2**).

Characterizations*:*

^{1}H NMR (DMSO-d$_6$): 400 MHZ, δ (ppm): 1.20-1.52 (m, 20H), 3.00 (m, 4H), 6.54 (m, 4H, Aromatic), 6.60 (t, 2H, -NH$_2$), 7.60 (m, 4H, Aromatic), 8.6(s, 4H), 8.8 (s, 4H).

^{13}C NMR (DMSO-D$_6$, 400 MHz)δ : 26.2, 26.7, 29.5, 30.6, 31.7, 52.4, 111.5, 121.6, 125.7, 153.5, 164.13.

5.2.7 Synthesis of 1,8-bis (4-cyanophenylamide)
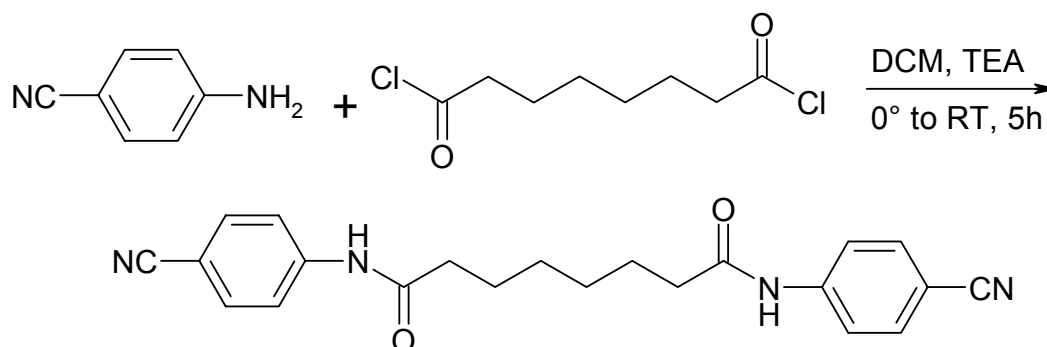
Reaction:

Procedure:

4-amino benzonitrile (1 g, 0.0084 moles) was dissolved in 50 mL of dichloromethane. Triethylamine (1 mL) was added and addition of octanedioyl dichloride (0.9 mL, 0.0042 moles) was done at 0 °C. Reaction mixture was allowed to stir at room temperature for 5 h. solid (HCl salt) was filtered off and the organic layer was washed with water (25X2) mL

The organic layer was concentrated under reduced pressure to afford the 1,8-bis (4-cyanophenylamide) as a white solid.

Characterization:

^{1}H NMR (DMSO-d$_6$): 400 MHZ, δ (ppm): 1.25 (m, 4H), 1.55 (m, 4H), 2.30 (t, 4H), 7.70 (m, 8H, Aromatic), 10.25(s, 2H, -NH$_2$)

5.2.8 Synthesis of 1,9-bis (4-cyanophenylamide)

Reaction:
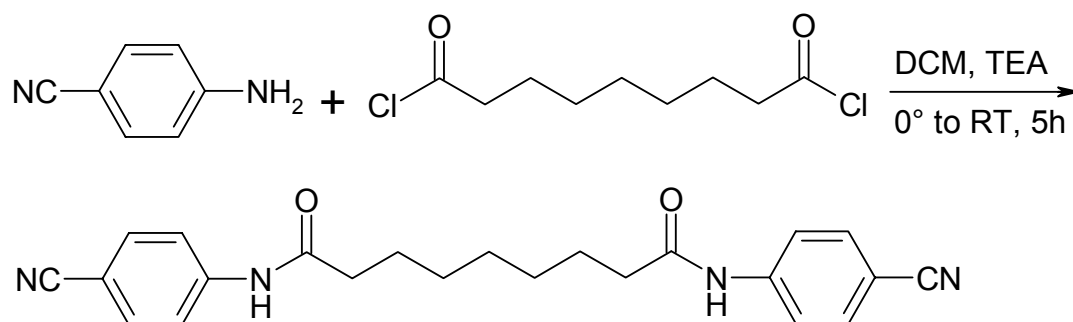
Procedure:

1,9-bis (4-cyanophenylamide) was synthesized in 66% yield by following the same procedure as described for the synthesis of molecule 1,8-bis (4-cyanophenylamide) (**5.2.7**).

Characterization*:*

^{1}H NMR (DMSO-d$_6$): 400 MHZ, δ (ppm): 1.25 (m, 6H), 1.6(m, 4H), 2.30 (t, 4H), 7.70 (m, 8H, Aromatic), 10.25(s, 2H, -NH$_2$)

5.2.9 Synthesis of 1,8-bis (4-amidinophenylamide) octane dihydrochloride

Reaction:
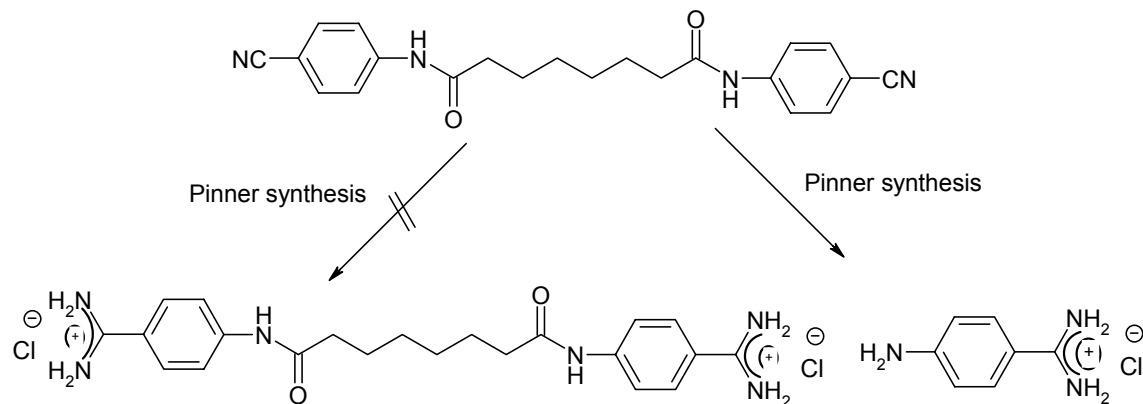
Procedure:

For the synthesis of 1,8-bis (4-amidinophenylamide) octane dihydrochloride, same procedure was adopted which we have used for the synthesis of 4-methylphenoxy(4-amidinophenoxy)octane hydrochloride(**5.1.3**). We observed that amide groups were acid labile to pinner conditions and instead of affording the final product as 1,8-bis (4-amidinophenylamide) octane dihydrochloride, we always got the final product as 4-aminobenzamidine hydrochloride as a white solid.

5.2.10 Synthesis of [Amino-(4-amino-phenyl)-methyl]-carbamic acid tetra-butyl ester

Reaction:
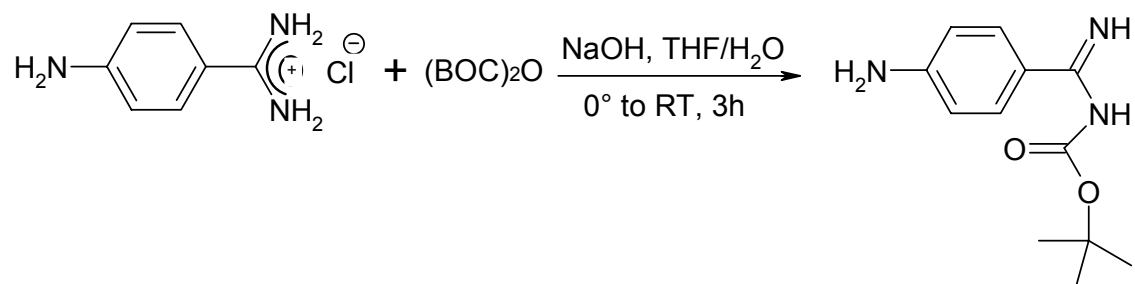
Procedure:

4-aminobenzamidine hydrochloride (1 g, 0.0048 moles) was dissolved in 50 mL of distilled water. 3 N NaOH (4 mL) was added in the above reaction mixture followed by the addition of 20mL of tetrahedron furan (THF). The reaction mixture was cooled to 0 °C.

BOC (di-tert-butyldicarbonate, 1.1 g, 0.0050) was dissolved in 5 mL of THF and was subsequently dropwise added into the above reaction mixture. The reaction mixture was stirred at room temperature for 3 hours and 2 phases were then separated.

The organic layer was concentrated to dryness and the white solid was taken up in ethyl acetate (100 mL). The resulting solution was washed twice with water (2 X 30 mL) and dried over sodium sulphate. The organic layer was concentrated to dryness to afford 0.85 g of pure product as a yellow solid in 82% yield.

Characterizations*:*
^{1}H NMR (CDCl$_3$): 400 MHZ, δ (ppm): 1.4 (s, 9H), 4.5 (bs, 3H), 6.6 (d, 2H), 7.6 (d, 2H)
Mass: (FAB/LR) Exact Mass: 236.15 Found: 236.16.

5.2.11 Synthesis of octanedioic acid bis- [(4-carbamimidoyl-phenyl)-amide]
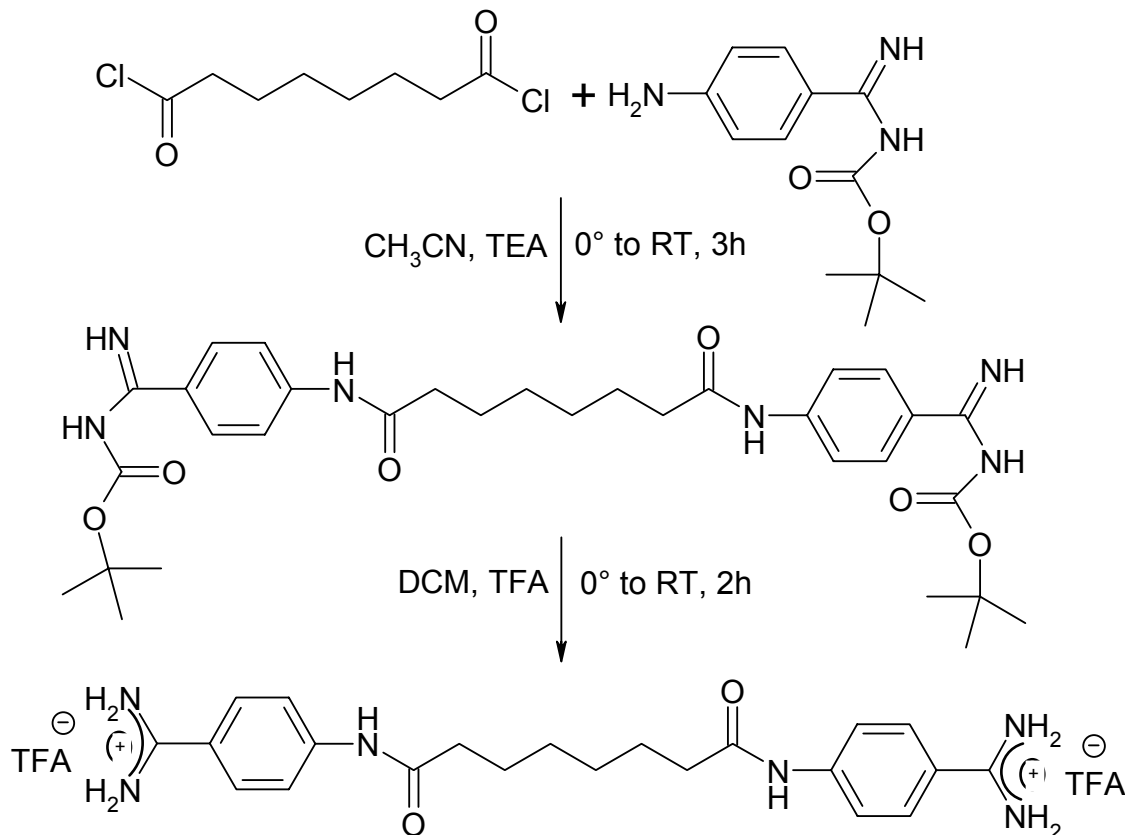
Reaction:

Procedure:

BOC protected 4-aminobenzamidine (1.0 g, 0.0042 moles) was dissolved in 25 mL of dry acetonitrile (CH_3CN) followed by the addition of Triethyl amine (TEA, 0.45 mL, 0.0044 moles). The above reaction mixture was ice cooled and dropwise addition of octanedioyl dichloride (0.50 mL, 0.0022 moles) was done. The reaction mixture was stirred at room temperature for 3 hours.

The solid was filtered off and the organic layer was concentrated under reduced pressure to afford light yellow gummy crude product. This yellow product was dissolved in 25 mL of chloroform ($CHCl_3$) and washed twice with water (2 X 10 mL) and dried over sodium sulphate. The organic layer was concentrated to dryness to yield 0.83 g of product as yellow oil in 62% yield. This oil was

immediately dissolved in 25 mL of dry DCM and reaction mixture was ice cooled. Slowly drop wise addition of Trifluro acetic acid (TFA) 1 mL was done and reaction mixture was allowed to stir at room temperature for further 2 hours.

After 2 hours, reaction mixture was concentrated to dryness under reduced pressure. The yellowish solid was crystallized using 20 mL of ethanol to afford the crude product

Characterization*:*

Mass: (FAB/LR): Exact Mass: 408.22, Found: 408.30

5.2.12   Synthesis of nonanedioic acid bis- [(4-carbamimidoyl-phenyl)-amide]

Reaction:
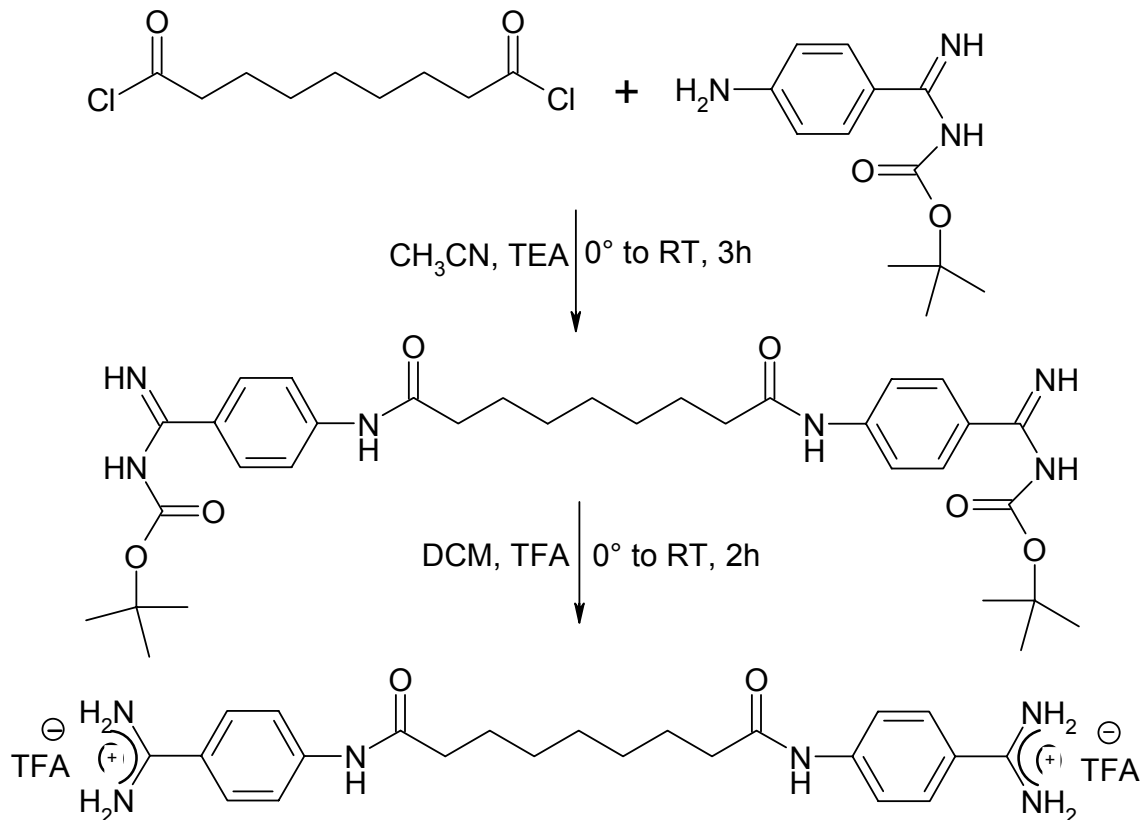
Procedure:

Synthesis of nonanedioic acid bis- [(4-carbamimidoyl-phenyl)-amide] was done following the same procedure described for the synthesis of octanedioic acid bis-[(4-carbamimidoyl-phenyl)-amide] (**5.2.11**).

Characterization:

Exact mass: Calculated: 422.24 Found (LRMS): 422.40

5.3 Synthesis of Biotinylated amphiphile

5.3.1 Synthesis of 2-[4-(8-Bromo-octyloxy)-phenyl]-ethanol

Reaction:
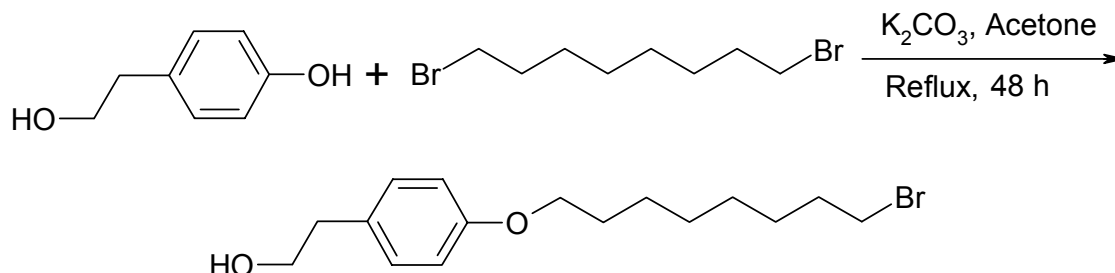
Procedure:

4-(2-Hydroxy-ethyl)-phenol (5 g, 0.032 moles) was dissolved in 100 mL of dry acetone in the presence of 32 g (0.23 moles) of K_2CO_3. Slowly drop wise addition of 1,8 dibromo octane (48 g, 0.176 moles) was done over 30 mints. And reaction mixture was kept refluxing for 48 hours.

K_2CO_3 was filtered off and the organic layer was concentrated under reduced pressure to give the crude product which was dissolved in 100 mL of chloroform and washed twice with 50 mL of water. The organic layer was dried over anhydrous sodium sulphate and then concentrated to dryness. Column chromatography was done (Ethyl acetate (1): Petroliumether (9) to afford the 1.9 g(49% yield) of 2-[4-(8-Bromo-octyloxy)-phenyl]-ethanol as white solid.

Characterizations:

^{1}H NMR (CDCl$_3$): 400 MHZ, δ (ppm): 1.3 (m, 8H), 1.6 (m, 2H), 1.8 (m, 2H), 2.8 (t, 2H), 3.4 (t, 2H), 3.8 (t, 2H), 3.9 (t, 2H), 6.8 (m, 2H), 7.1 (m, 2H)

^{13}C NMR (CDCl$_3$), 400 MHz)δ : 26.1, 28.9, 29.5, 30.1, 30.8, 33.2, 34.5, 38.5, 67.3, 72.5, 114.9, 129.8, 130.1, 157.6.

Mass: (EI/LR) Exact Mass: 328.10, Found: 328.00

5.3.2 Synthesis of 4-{8-[4-(2-Hydroxy-ethyl)-phenoxy]-octyloxy}-benzonitrile
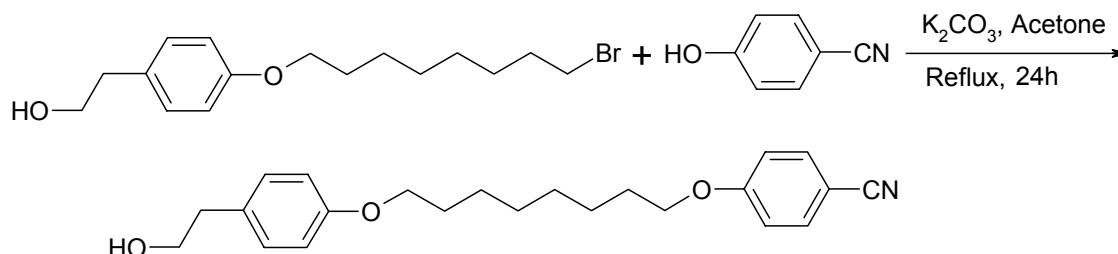
Reaction:

Procedure:

2-[4-(8-Bromo-octyloxy)-phenyl]-ethanol (1 g, 0.0030 moles) was dissolved in 25 mL of dry acetone and (0.4 g, 0.0033 moles) of 4-cyanophenol. K_2CO_3 (1 g, 0.0072) was added as a base and reaction mixture was refluxed for 24 hours. Inorganic was filtered off and acetone was concentrated on rotary evaporator to give the crude product. The pure product was obtained after performing column chromatography using ethyl acetate and cyclohexane as a elute solvents (2:8) to afford the 4-{8-[4-(2-Hydroxy-ethyl)-phenoxy]-octyloxy}-benzonitrile in 77% yield (0.63 g) as a white solid.

Characterizations:

^{1}H NMR (CDCl$_3$): 400 MHZ, δ (ppm): 1.30 (m, 8H), 1.7 (m, 4H), 2.7 (t, 2H), 3.75 (t, 2H), 3.85 (t, 2H), 3.95 (t, 2H), 6.7 (d, 2H), 6.8(d, 2H), 7.05 (d, 2H), 7.50 (d, 2H)

5.3.3 Synthesis of 4-(10-Bromo-decyloxy)-benzonitrile.
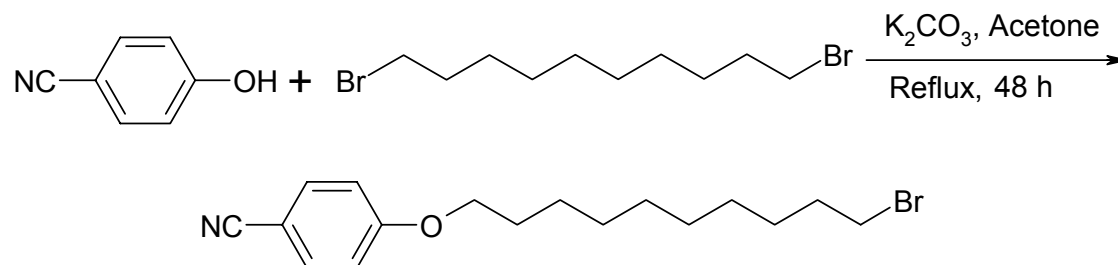
Reaction:

Procedure:

The synthesis of 4-(10-Bromo-decyloxy)-benzonitrile was achieved in 55% yield by using the same reaction procedure which we have used for the synthesis of the molecule 4-cynophenoxyoctane-8 bromide. (**5.1.1**)

Characterizations:

^{1}H NMR (CDCl$_3$): 400 MHZ, δ (ppm): 1.30 (m, 12H), 1.80 (m, 4H), 3.4 (t, 2H), 4.0 (t, 2H), 6.90 (d, 2H), 7.60 (d, 2H).

^{13}C NMR (CDCl$_3$), 400 MHz)δ : 25.4, 27.8, 29.5, 30.2, 30.5, 33.1, 34.2, 72.5, 103.4, 115.1, 132.4, 162.3

Mass: Exact Mass: 337.10 Found: 337.12

5.3.4 Synthesis of 4-{10-[4-(2-Hydroxy-ethyl)-phenoxy]-decyloxy}-benzonitrile.
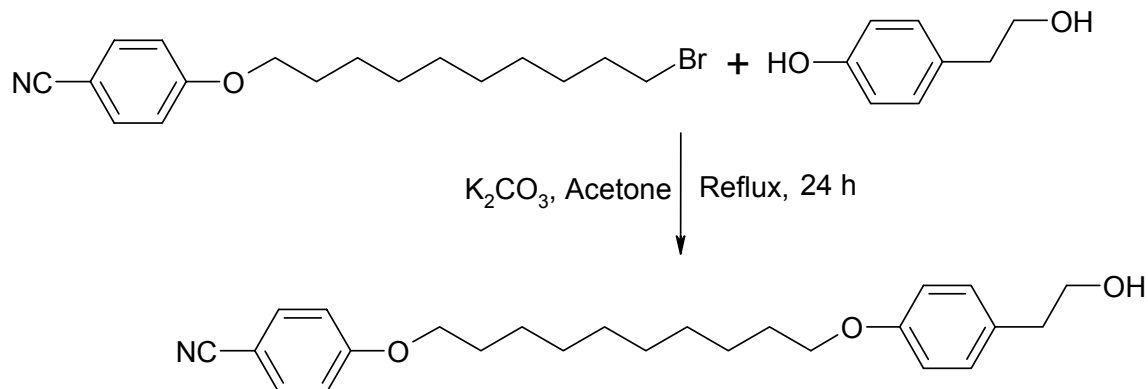
Reaction:

Procedure:

The synthesis of 4-{10-[4-(2-Hydroxy-ethyl)-phenoxy]-decyloxy}-benzonitrile was achieved in 73% yield by the same reaction procedure which is described above for the Synthesis of 4-{8-[4-(2-Hydroxy-ethyl)-phenoxy]-octyloxy}-benzonitrile. (**5.3.2**)

Characterizations

^{1}H NMR (CDCl$_3$): 400 MHZ, δ (ppm): 1.30 (m, 12H), 1.80 (m, 4H), 2.80 (t, 2H), 3.80 (t, 2H), 3.90 (t, 2H), 4.0 (t, 2H), 6.80 (d, 2H), 6.90 (d, 2H), 7.10 (d, 2H), 7.60 (d, 2H),

^{13}C NMR (CDCl$_3$), 400 MHz)δ : 26.5, 29.4, 30.2, 38.5, 65.2, 72.5, 103.6, 114.2, 114.6, 116.2, 128.7, 131.5, 132.3, 156.3, 163.2.

Mass: (EI/LR) Exact Mass: 395. 25, Found: 395.23.

5.3.5 Synthesis of 4-{10-[4-(2-Hydrody-ethyl)-phenyoxy]-decyloxy}-benzamidine hydrochloride
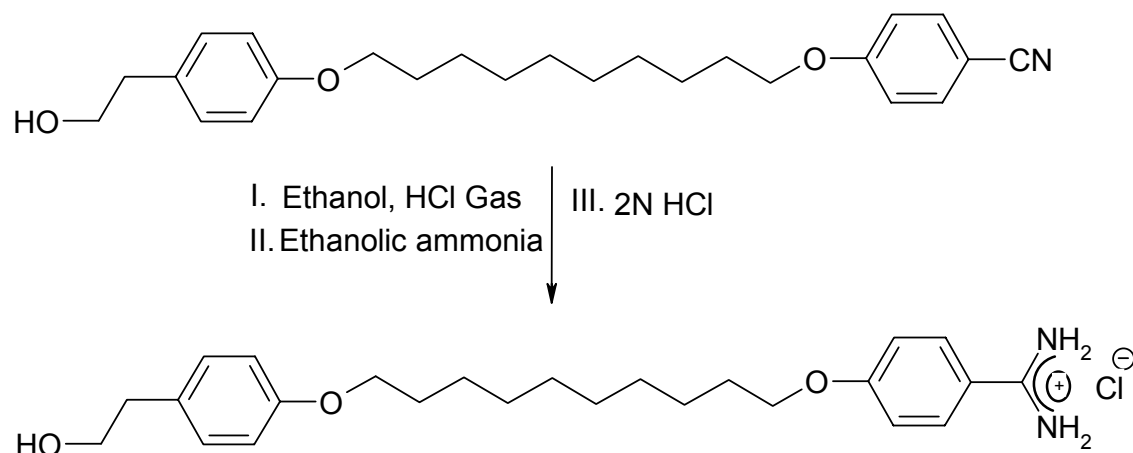
Reaction:

Procedure:

We have followed the same reaction procedure for the synthesis of 4-{10-[4-(2-Hydrody-ethyl)-phenyoxy]-decyloxy}-benzamidine hydrochloride which we have described previously for the synthesis of 4-methylphenoxy (4-amidinophenoxy)octane hydrochloride (**5.1.3**). This gave us 57% of the hydrochloride salt of the molecule

Characterizations:

^{1}H NMR (DMSO-d$_6$): 400 MHZ, δ (ppm): 1.3 (m, 12H), 1.8 (m, 4H), 2.6 (t, 2H), 3.5 (t, 2H), 3.9 (t, 2H), 4.0 (t, 2H), 6.7 (d, 2H), 7.0 (d, 2H), 7.1 (d, 2H), 7.7 (d, 2H), 8.8, (s, 2H), 9.1 (s, 2H).

^{13}C NMR (DMSO-d$_6$), 400 MHz)δ : 26.5, 30.5, 38.4, 65.3, 72.6, 114.2, 124.3, 126.2, 128.3, 131.6, 156.3, 160.1, 163.2, 164.3, 166.4

Mass: Exact Mass: 412.2, Found: 412.2

5.3.6 Synthesis of [(4-{10-[4-(2-Hydroxy-ethyl)-phenoxy]-decyloxy}-phenyl)-imino-methyl]-carbamic acid tert-butyl ester.

Reaction:
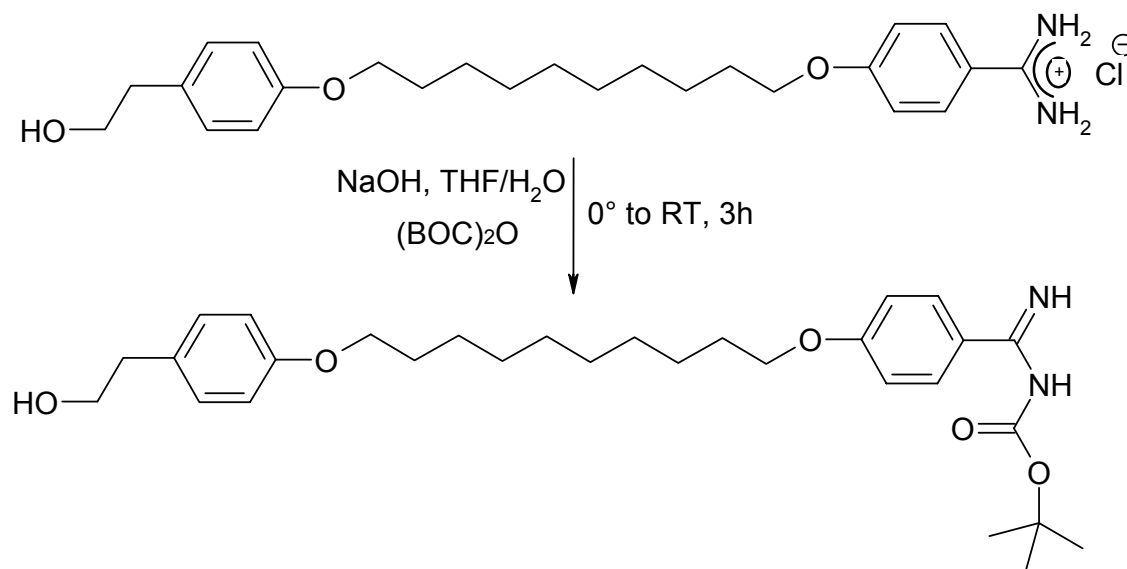
Procedure:

For the synthesis of above molecule, we have repeated the same reaction procedure which we have described for the synthesis of [Amino-(4-amino-phenyl)-methyl]-carbamic acid tetra-butyl ester (**5.2.10**). The final product was obtained as a white solid in 62% yield.

Characterizations:

^{1}H NMR (DMSO-d$_6$): 400 MHZ, δ (ppm): 1.3 (m, 12H), 1.4 (s, 9H), 1.70 (m, 4H), 2.6 (t, 2H), 3.5 (t, 2H), 3.9 (t, 2H), 4.0 (m, 2H), 6.8 (d, 2H), 7.0 (d,2H), 7.1 (d, 2H), 7.7 (d, 1H, 1H), 7.9 (d, 1H).

Mass: (FAB/LR) Exact Mass: 512.33, Found: (M+H), 513.30

5.3.7 Synthesis of 5-(2-Oxo-hexahydro-thieno[3,4-d]imidazol-6-yl)-pentanoic acid 2-{4-[10-(4-carbamimidoyl-phenoxy)-decyloxy]-phenyl}-ethyl ester triflouro acetic acid. (Biotinylated amphiphile)

Reaction:
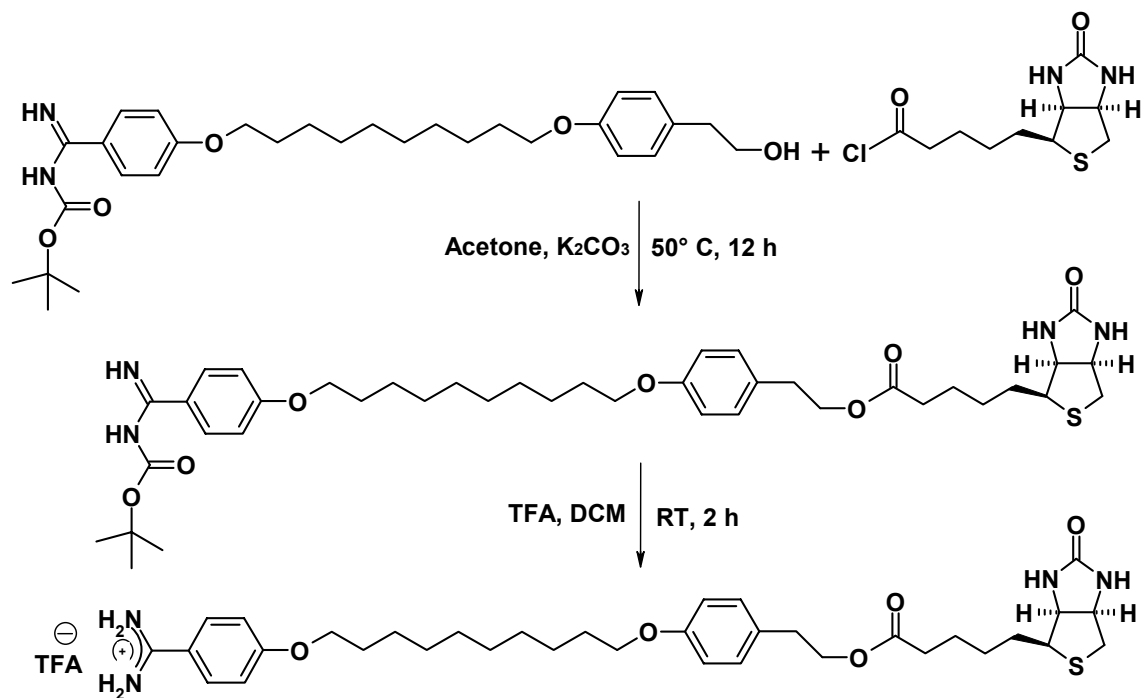
Procedure:

Protected benzamidine, [(4-{10-[4-(2-Hydroxy-ethyl)-phenoxy]-decyloxy}-phenyl)-imino-methyl]-carbamic acid *tert*-butyl ester (0.40 g, 0.00079 moles) was dissolved in the mixture of dry acetone 10mL and dry toluene 10 mL. Addition of biotin chloride (5-(2-Oxo-hexahydro-thieno[3,4-*d*]imidazol-6-yl)-pentanoyl chloride), 0.21 g, 0.00078 moles was done followed by the addition of anhydrous K_2CO_3 (1 g, 0.0072 moles). Reaction mixture was warmed up to 50 °C and stirred at the same temperature for 12 hours. After reaction is over (monitored by TLC), the inorganic K_2CO_3 was filtered off and organic layer was concentrated under reduced pressure to yield the crude product in 52% (0.21 g) yield. This crude product was immediately dissolved in 10 mL of dry DCM and then the reaction mixture was ice cooled. In the above ice cooled reaction mixture, drop

wise addition of 3 mL of trifluro acetic acid (TFA) was done very slowly to give faint orange color reaction mixture which was further stirred at room temperature for 2 more hours.

The reaction mixture was concentrated to dryness on rotary evaporator to give the slightly yellowish solid product which was then crystallized by 20 mL ethanol to afford 0.06 g, 35% yield of final product as a slightly yellowish solid.

Characterizations:

^{1}H NMR (DMSO-d$_6$): 400 MHZ, δ (ppm): 1.30 (m, 14H), 1.60 (m, 6H), 2.20 (t, 2H), 2.80 (m, 4H), 3.30 (d, 2H), 3.80 (t, 2H), 4.10 (2t, 4H), 4.20 (t, 2H), 6.32 (s, 1H, -NH Biotin), 6.40 (s, 1H, -NH biotin), 6.80 (d, 2H), 7.10 (2d, 4H), 7.75 (d, 2H), 8.70 (s, 2H, -NH$_2$ amidine), 9.10 (s, 2H, -NH$_2$ amidine).

Mass: (FAB/LR) Exact Mass: 638.35 Found: 638.33

6 Characterization of substrates by different methods

6.1 Ellipsometry for thin-film and surface analysis

The term ellipsometry was coined in 1944, the principle of ellipsometry was first applied by Paul Drude in Germany and Lord Rayleigh in Great Britain studied the polarization state of light reflected from thin film coated solid and liquid surfaces, respectively.

When a polarized light bean reflects from any specular surface, changes occur in both the amplitude and phase of the oscillating parallel and perpendicular vector components of the electric field associated with the beam, As shown in Figure 6.1, p and s refer to the spatial directions parallel and perpendicular to the plane of incidence, which contains both incident and reflected beams. The goal of an ellipsometry experiment is to measure these amplitude and phase changes, which provide researcher with information about the reflecting surfaces [1]. Since the general polarization state of polarized light reflected from a surface is elliptical, the term *ellipsometer* was chosen. The most important application of ellipsometry is to study thin film. In the context of ellipsometry a thin film is one that ranges from essentially zero thickness to several thousand Angstroms.

In Figure 6.1, the incident beam is linearly polarized at an angle with respect to the p and s directions, with p and s electric field vector components that are in phase. The planes indicated by the dotted lines represent the planes of polarization of the beam just before and just after reflection from the surface. Because of the different and amplitude changes that the p and s electric field components incur upon reflection, the direction of the liner polarization changes in the manner shown qualitatively in the figure.

These two angles give the phase shift between the parallel and perpendicular components (Δ), and the change in the ratio of the amplitudes of the two components ($\tan\Psi$) which is shown in equation 1.

$$\rho = \frac{r_p}{r_s} = \frac{\dfrac{E_{rp}}{E_{ip}}}{\dfrac{E_{rs}}{E_{is}}} = \tan\psi \exp(i\Delta)$$

Incident   Equation 1   **Reflected**
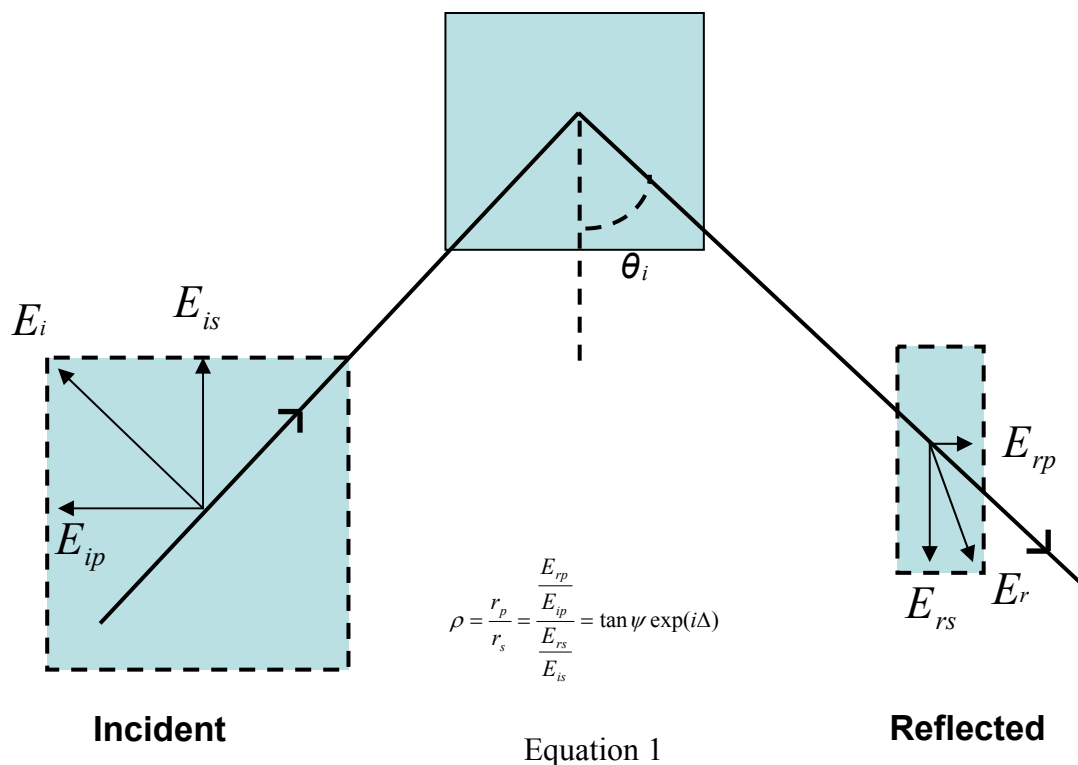
Figure 6.1 The geometry of reflection and the definition of ψ and Δ

Ellipsometer consist of a laser (commonly a 632.8nm helium/neon laser), a polarizer and a quarter wave plate which provide a state of polarization which can be varied from linearly polarized light to elliptically polarized light to circularly polarized light by varying the angle of polarizer. The beam is reflected off the layer of interest and then analyzed with the analyzer which is displayed in Figure 6.2. Ellipsometry can determine both the thickness and the refractive index of the sample. Usually the material chemist uses the value of 1.45 to 1.50 as the refractive index for organic monolayers [2]. This value is suggested on the basis that the provided monolayer is crystalline in nature similar to the polyethylene [3]. Within the realm of the tools available for surface and thin-film characterization, ellipsometry fills a special place. Its primary advantage is that it can be applied to study surface in real time in variety of adverse environments.
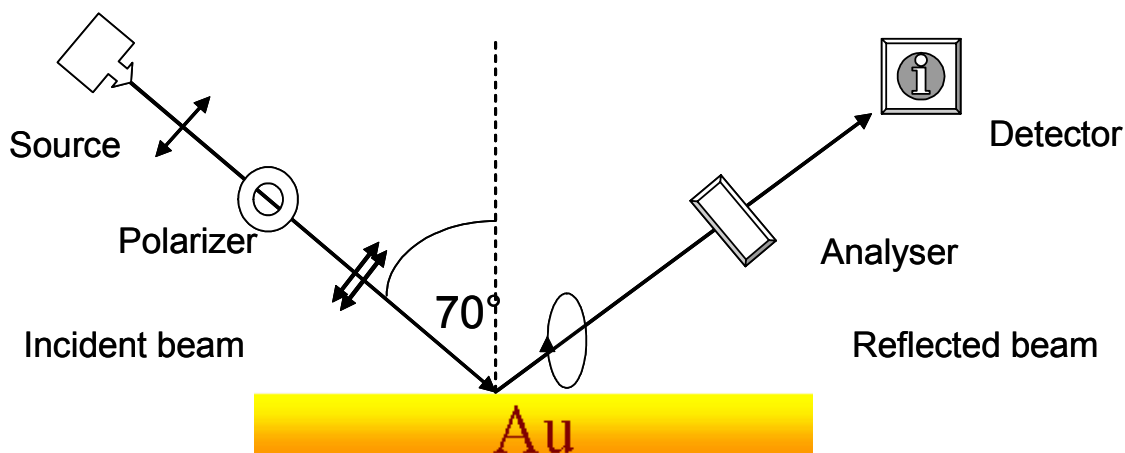
Figure 6.2 Schematic drawing of an ellipsometer

6.2 Infrared Reflection Absorption Spectroscopy (IRAS)

Infrared spectroscopy is the everyday tool for the study of molecular packing and orientation in ultra thin organic films. There are two main spectroscopic methods to detect the orientation of an organic film 1. Grazing-angle (GA), and 2. Attenuated total reflection (ATR) spectroscopy. During my research work, I have been using grazing-angle (**I**nfrared **R**eflection **A**bsorption **S**pectroscopy, **IRAS**). Reflection-absorption spectroscopy is very important and useful technique which gives information about the direction of transition dipole in a sample.

The reflection absorption spectrum is measured efficiently at high angles of incidence, and the condition is that only the component of incident light that is parallel to the plane of incidence gives measurable absorption [4].

It is very important to note the direction of the different transition dipoles. In case of the alkyl thiol molecule on gold surface, the symmetric and asymmetric methylene vibrations are parallel to the gold plane, but the symmetric and asymmetric vibrations of the methylene groups have components that are perpendicular to the metal surface. The methylene groups which are all-trans alkyl chain will not be detected by p-polarized light. And when the alkyl chain of the methylene molecule tilts from the plane, both asymmetric and symmetric vibrations appears in the infrared reflection absorption spectra.
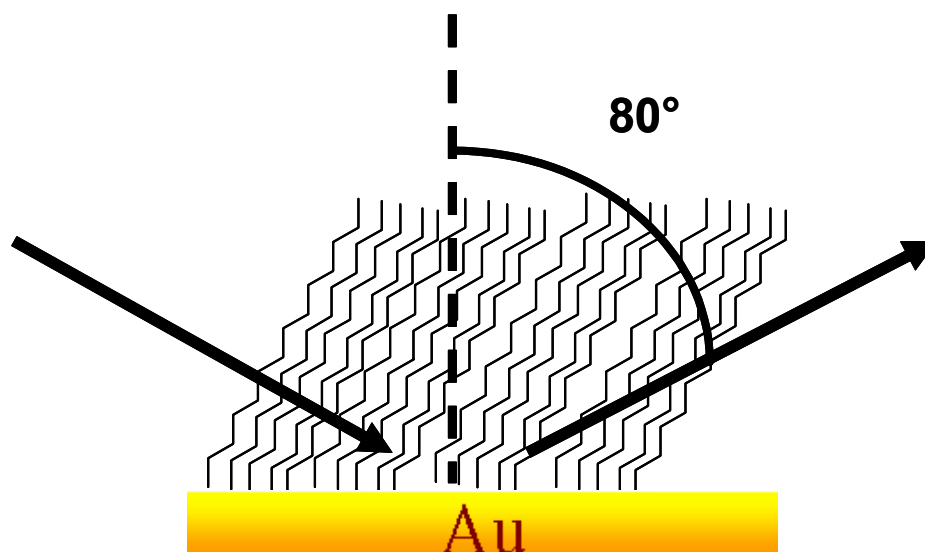
Figure 6.3 Schematic diagram of the grazing-angle IR instrument.

From the intensity of the methylene vibrations, we can calculate the molecular orientation of the molecule on the gold surface. The intensity of peak is a direct function of the tilt angle. The important work of alkanethiol monolayer on gold by grazing-angle spectroscopy was reported by Porter *et.al*. [5]

Snyder *et.al*. [6, 7] suggested that the asymmetric vibrations tend to come at higher peak frequencies as the length of the alkyl chain decreases. They reported $2920cm^{-1}$ for the asymmetric vibration for the CH_2 mode in crystalline polyethylene which is 8 cm^{-1} lower than the peak position in the liquid state (2928 cm^{-1}). For the symmetric vibration of CH_2, they did report that the crystalline polyethylene comes at $2850cm^{-1}$ as compared to the liquid state ($2856cm^{-1}$)

IRAS study helps to establish the different degree of packing (e.g. liquid like and solid like) in different parts of the monolayer, due to different type of interactions between the different functional groups.

In our studies, we have used Nexus FTIR instrument which has OMNIC software. The MCTA detector was cooled with liquid nitrogen prior to use. The angle of incidence was 80° and for the SAMs, 1000 scans were recorded for each spectrum at the resolution of 2 cm^{-1}. For the solid samples, 32 scans were recorded (KBr pellets).

6.3 Contact angle measurements

Self-assembled monolayers of derivatized alkanethiols on gold surfaces provide a useful tool for the surface engineering. *Contact Angle measurements'* are a very popular methodology for the evaluation of wetting and adhesion properties and calculation of surface energies and the critical surface tension of solids. When a liquid does not wet a surface completely, it forms an angle *θ*, the contact angle with the surface. In the following Figure 6.4, typical hydrophobic and hydrophilic surfaces are shown.

Hydrophobic surface   Hydrophilic surface
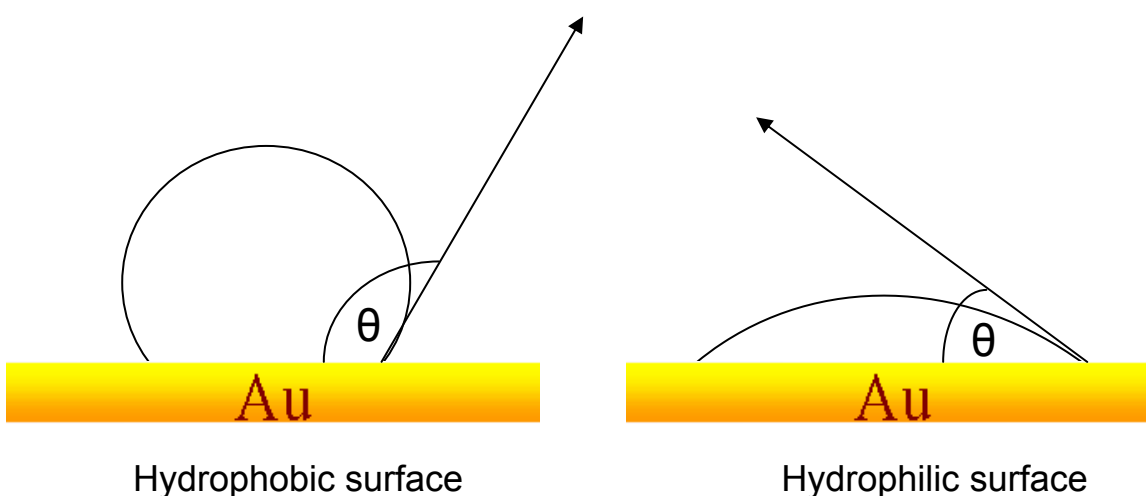
Figure 6.4 Schematic diagram of the contact angles.

The work of adhesion between a solid surface and liquid drop is defined as

$$W \, SL = \gamma \, SL + \gamma LV + \gamma \, SL,$$

Where *W* is the work, γ is the surface interfacial tension, and LV, SV, and SL refer to liquid-vapor, solid-vapor, and solid-liquid interfaces, respectively.

By the principle of the virtual work, we get the free energy of the surface and unique contact angle *θ*. Thomas young described the following equation for measuring the contact angle measurement called as Young's equation [8].

$$\gamma \, LV \, COS \, \theta = \gamma \, SV - \gamma SL$$

6.4 Atomic Force Microscopy (AFM)

The atomic force microscopey (AFM) is a very powerful microscopey invented by Binnig, Quate and Gerber in 1986. The AFM consist of a cantilever with a sharp tip at its end, typically composed of silicon or silicon nitride with tip sizes on the order of nanometers (Figure 6.5). The tip is brought into the close proximity of a sample surface. The Van der Waals force between the tip and the sample leads to a deflection of the cantilever. This deflection is measured by laser spot reflected from the top of the cantilever into an array of photodiodes.

There are several mode of operation of the AFM. The primary modes of operation are contact mode, non-contact mode, and dynamic contact mode. Dynamic contact mode was developed by Zhong *et.al*. [9] In dynamic contact mode, the cantilever is oscillated such that it comes in contact with the sample with each cycle, and then enough force is applied to detach the tip from the sample.

We have measured our self-assembled monolayer samples on gold surfaces which were prepared by gold deposition (200nm) onto a freshly cleaved atomically flat mica surface. AFM measurments were done on a multimode Scanning Probe Microscope (Digital Instrument Santa Barbara, CA) using E-scanner (15 μm). Images were obtained applying the tapping in air with non contact high frequency point probes (NCHR-W, nanosensors) with backside reflex coating. Tips with the nominal force constant of 42 N/m were used at driving frequencies ranged from 300 to 330 KHZ. Height and phase images of sample regions between 0.5 and 5.0 μm were acquired with resolution of 512 X 512 pixels and scan frequencies between 0.4 and 2.0 HZ. All measurements were carried out at room temperature.
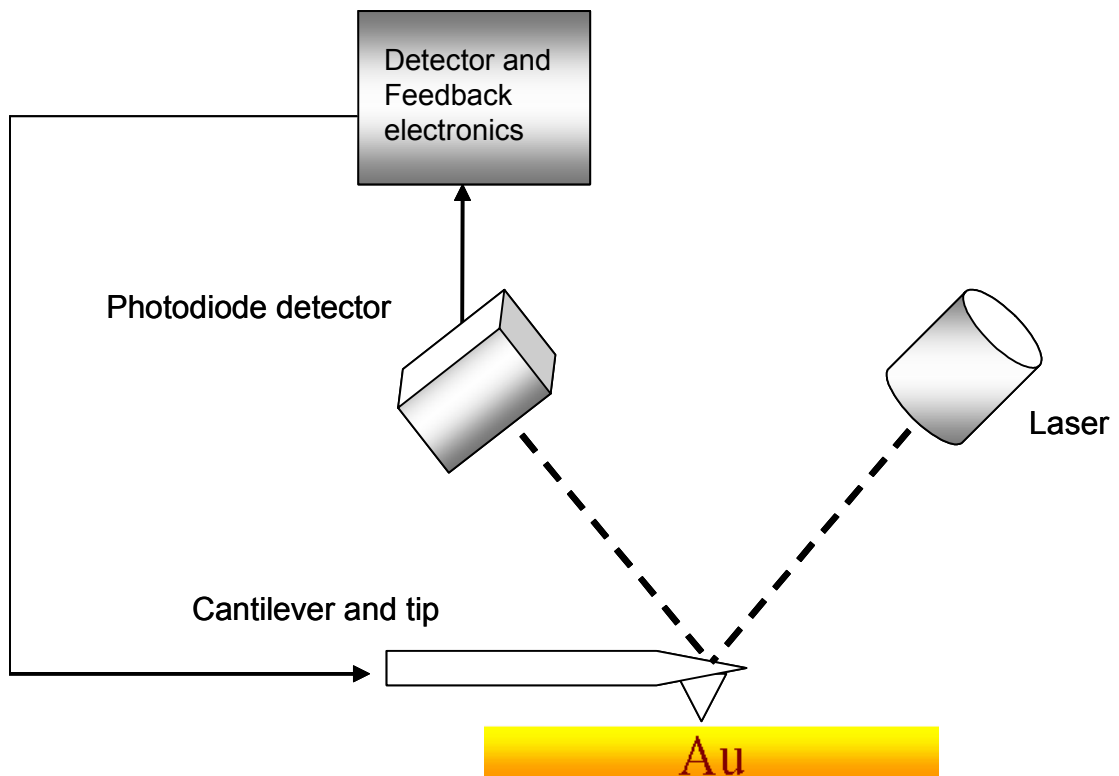
Figure 6.5 Concept of AFM and a cantilever touching a sample.

6.5 References

1. Ellipsometry and polarized light; Azzam, R.M.A, Bashara, N.M., North-Holland Amsterdam 1977

2. Allara, D. L., Nuzzo, R. G., *Langmuir* **1985**, 1, 45

3. Brandrup, J., Polymer Handbook; John willy: New York **1975**, v13-v22

4. Blanke, J. F., Vincent, S.E., Overend, J., *Spectrochem. Acta*, Part A **1976**, 32, 163

5. Porter, M. D., Bright, T. B., Allara, D. L., Chidsey, C. E. D., *J. Am. Chem. Soc.* **1987,** 109, 3559

6. Snyder, R., G., Strauss, H., Ellinger, C. A., *J.Phys. Che*. 1982, 86, **5145**

7. Snyder, R. G., Maroncelli, M., Strauss, H., Hallmark, V. M., *J. Phys. Chem.* **1986**, 90, 5623

8. Young, T., *Miscellaneous works*; Peacock G., Ed.; Murray: London, 1855, Vol. 1, p. 418

9. Zhong, Q., Innis, D., Kjoller, K., Elings, V.B., *Surf. Sci. Lett*. **1993** 290, L688

7 Appendix

Appendix contains information about the abbreviations used in this thesis, details about chemicals and solvents used during this work, as well as the IRAS intensities of mixed monolayers of OCH_3: NO_2, OCH_3: $C(=NH)NH_2$, Biotin: OH, and Biotin: Streptavidin (**SA**) system.

7.1 List of Abbreviations

AFM	Atomic Force Microscopy
BOC	Di-tert-butyldicarbonate
CA	Contact Angle
DCM	Dichloromethane
DMSO	Dimethyl sulfoxide
DMF	Dimethyl formamide
EtOH	Ethanol
FTIR	Fourier Transform Infrared Reflection
HRMS	High Resolution Mass Spectroscopy
IRAS	Infrared Reflection Absorption Spectroscopy
LRMS	Low Resolution Mass Spectroscopy
MHA	Mercaptohexadecanoic acid
MeOH	Methanol
NMR	Nuclear Magnetic Resonance
QCM	Quartz Crystal Microbalance
SAM	Self-Assembled Monolayers
SA	Self-Assembly
SPR	Surface Plasmon Resonance
THF	Tetrahydrofurane
TEA	Triethylamine
TFA	Trifluoroacetic acid
TLC	Thin Layer Chromatography

7.2 Chemicals and Solvents

7.2.1 Chemicals and solvents for synthesis

Chemicals and solvents were provided by the following sources:

Acetone, p.a.	Merck KGaA, Darmstadt, Germany
4-aminobenzamidine Hydrochloride	Across, Geel, Belgium
4-amino benzonitrile	Sigma-Aldrich, Steinheim, Germany
BOC (di-tert-butyldicarbonate)	Merck KGaA, Darmstadt, Germany
Boric Acid	Merck KGaA, Darmstadt, Germany
Benzene (dry)	Merck KGaA, Darmstadt, Germany
Biotin	Acros Chemicals, Geel, Belgium
Chloroform, p.a.	Merck KGaA, Darmstadt, Germany
Chloroform, (dry).	Merck KGaA, Darmstadt, Germany
Cyclohexene	Acros Chemicals, Geel, Belgium
4-Cyanophenol	Acros Chemicals, Geel, Belgium
4-Methoxy phenol	Acros Chemicals, Geel, Belgium
1,8, Dibromooctane	Sigma-Aldrich, Steinheim, Germany
1,10, Dibromooctane	Sigma-Aldrich, Steinheim, Germany
1,9-Diaminononane	Sigma-Aldrich, Steinheim, Germany
1,10-Diaminononane	Sigma-Aldrich, Steinheim, Germany
1,12-Diaminononane	Sigma-Aldrich, Steinheim, Germany
Dimethyl formamide	Merck KGaA, Darmstadt, Germany
Dimethyl sulfoxide	Merck KGaA, Darmstadt, Germany
Dichloromethane, (dry)	Fluka, Deisenhofen, Germany
Ethanol, p.a.	Merck KGaA, Darmstadt, Germany
Ethanol, (dry)	Merck KGaA, Darmstadt, Germany
Ethyl Acetate	Merck KGaA, Darmstadt, Germany
4 flurobenzonitrile	Fluka, Deisenhofen, Germany
4-(2-Hydroxy-ethyl)-phenol	Sigma-Aldrich, Steinheim, Germany
Methanol, p.a.	Merck KGaA, Darmstadt, Germany
4-methyl phenol	Acros Chemicals, Geel, Belgium

Methanol, (dry)   Merck KGaA, Darmstadt, Germany

Magnesium sulphate   Fluka, Deisenhofen, Germany

p-nitro phenol   Acros Chemicals, Geel, Belgium

Octanedioyl dichloride   Acros Chemicals, Geel, Belgium

Potassium carbonate   Acros Chemicals, Geel, Belgium

Sodium hydroxide   Merck KGaA, Darmstadt, Germany

Streptavidin   Sigma-Aldrich, Steinheim, Germany

Tetrahydrofuran, (dry)   Fluka, Deisenhofen, Germany

Toluene, p.a.   Merck KGaA, Darmstadt, Germany

Toluene, (dry).   Merck KGaA, Darmstadt, Germany

Triethylamine   Sigma-Aldrich, Steinheim, Germany

Trifluoroacetic acid   Aldrich, Steinheim, Germany

7.2.2 Solvents for NMR spectroscopy

Chloroform, d_1 ($CDCl_3$)   Deutero GmbH, Kastellaun, Germany

Deuterated water (D_2O)   Merck KGaA, Darmstadt, Germany

Dimethylsulfoxide, d_6 (DMSO-d_6)   Deutero GmbH, Kastellaun, Germany

7.3 Infrared Reflection Absorption Spectroscopy

7.3.1 Peak intensities of mixed monolayers of -NO₂ (2) and -OCH₃ (1) amphiphiles at different compositions

Amphiphiles	NH₂+OH str		NH₂+=NH str.		α,ω–CH₂ asym.		CH₂ asym.		CH₂ sym.		N-C=N asym.		(C=C)₁,₄ str.		NO₂ (sym.)		C-C str. (OCH₃)	
NO₂:OCH₃	cm⁻¹	Abs.	cm⁻¹	Abs.	cm⁻¹	Abs.	cm⁻¹	Abs.	cm⁻¹	Abs.	cm⁻¹	Abs.	cm⁻¹	Abs.	cm⁻¹	Abs.	cm⁻¹	Abs.
100	3366	0.0002	3196	0.0010	2937	0.0035	2917	0.013	2848	0.005	1691	0.0027	1611	0.008	1594	0.0062	1512	0.0022
87.5	3381	.0005	3076	0.0005			2917	0.010	2848	0.0040	1694	0.0020	1612	0.0065	1594	0.0057	1512	0.0035
75	3365	0.0012	3124	0.0006	2937	0.0040	2917	0.013	2849	0.0052	1690	0.002	1612	0.009	1594	0.0052	1511	0.0035
63.5	3458	0.0010	3102	0.0010	2936	0.0028	2917	0.0092	2848	0.0034	1691	0.002	1611	0.007	1595	0.0055	1511	0.0030
50	3364	0.0010	3176	0.0007	2936	0.0045	2917	0.013	2849	0.0043	1691	0.002	1612	0.0078	1594	0.0040	1511	0.0075
37.5	3528	0.0005	3064	0.0010	2935	0.0050	2917	0.014	2848	0.0052	1691	0.002	1611	0.008	1594	0.0032	1511	0.016
25	3414	0.001	3041	0.002	2935	0.0047	2917	0.011	2848	0.0043	1692	0.002	1609	0.0073	1594	0.0030	1512	0.019
12.5	3239	0.001	3009	0.001	2935	0.0044	2917	0.013	2848	0.0049	1692	0.002	1612	0.0068	1594	0.0018	1513	0.014
0:100	3358	0.0005	3004	0.0006	2935	0.004	2917	0.012	2849	0.0045	1691	0.0025	1613	0.0065	----	----	1511	0.017

Amphiphiles	C=C str		NO₂ Sym. Str.		C-O-C str		OCH₃ Str.		(C-N)		CH op		CH op			
NO₂:OCH₃	cm⁻¹	Abs.	cm⁻¹	Abs.	cm⁻¹	Abs.	cm⁻¹	Abs.	cm⁻¹	Abs.	cm⁻¹	Abs.	cm⁻¹	Abs.	cm⁻¹	Abs.
100	1498	0.0040	1347	0.007	1266	0.0078	----	------	862	0.0010	840	0.0037	----	------	748	0.0015
87.5	1495	0.0060	1347	0.0064	1262	0.0070	1234	0.0002	861	0.0015	840	0.0037	----	-----	748	0.0015
75	1494	0.005	1346	0.0062	1266	0.0070	1232	0.0008	862	0.0008	840	0.003	824	0.0001	748	0.0017
63.5	1494	0.0045	1346	0.0046	1268	0.0058	1232	0.0012	861	0.0010	845	0.003	826	0.0005	751	0.0016
50	1494	0.0040	1344	0.0037	1268	0.0045	1234	0.0028	862	0.0007	840	0.0036	827	0.0010	747	0.0020
37.5	1498	0.0055	1344	0.0033	1261	0.0035	1234	0.0064	861	0.001	841	0.0039	827	0.0012	744	0.0035
25	1497	0.005	1343	0.0013	1261	0.0032	1234	0.0073	863	0.0005	841	0.0027	826	0.0012	744	0.0040
12.5	1493	0.0015	1339	0.0004	1270	0.0015	1236	0.0084	862	0.0002	840	0.0018	825	0.0005	744	0.0027
0:100	1498	0.006	----	------	1271	0.0005	1236	0.012	----	----	839	0.0025	825	0.0015	742	0.0045

Table 7.1: IRAS intensities of the mixed monolayers of ω-functionalized –OCH₃ (1) and NO₂ (2) amphiphiles assembled on MHA SAMs.

7.3.2 Peak intensities of mixed monolayers of -NO$_2$ (2) and -OCH$_3$ (1) amphiphiles at different compositions (Repeat)

Amphiphiles NO$_2$:OCH$_3$	NH$_2$+OH str cm^{-1}	Abs.	NH$_2$+=NH str cm^{-1}	Abs.	α,ω–CH$_2$ asym cm^{-1}	Abs.	CH$_2$ asym cm^{-1}	Abs.	CH$_2$ sym cm^{-1}	Abs.	N-C=N asym cm^{-1}	Abs.	(C=C)$_{1,4}$ str cm^{-1}	Abs.	NO$_2$ (sym.) str. cm^{-1}	Abs.	C-C str. OCH$_3$ cm^{-1}	Abs.
100	3364	0.0005	3115	0.0005	2937	0.003	2917	0.009	2850	0.0035	1692	0.0015	1612	0.007	1595	0.0060	1513	0.0032
87.5	3332	0.0002	3049	0.0020	2936	0.0050	2917	0.014	2850	0.0060	1691	0.0040	1612	0.013	1592	0.0060	1511	0.013
75	3361	0.0005	3162	0.0005	2937	0.0030	2916	0.011	2848	0.0052	1691	0.002	1612	0.0072	1594	0.0050	1511	0.0055
63.5	3337	0.0010	3074	0.0010	2937	0.0030	2917	0.010	2850	0.0045	1691	0.003	1612	0.0080	1594	0.0030	1511	0.010
50	3361	0.0010	3160	0.0007	2936	0.0040	2917	0.011	2849	0.0055	1691	0.002	1613	0.008	1594	0.0020	1513	0.015
37.5	3365	0.001	3048	0.0010	2935	0.0045	2917	0.014	2849	0.0060	1691	0.002	1614	0.010	1593	0.0018	1513	0.022
25	3314	0.002	3047	0.002	2935	0.0070	2917	0.018	2849	0.008	1695	0.004	1613	0.010	1593	0.0015	1511	0.024
12.5	3361	0.0015	3050	0.001	2935	0.0040	2917	0.015	2848	0.0060	1691	0.002	1614	0.009	1594	0.0012	1513	0.019
0:100	3356	0.001	3098	0.001	2936	0.0045	2916	0.014	2849	0.0065	1691	0.0030	1611	0.0077	----	--------	1511	0.014

Amphiphiles NO$_2$:OCH$_3$	C=C str cm^{-1}	Abs.	NO$_2$ Sym. Str. cm^{-1}	Abs.	C-O-C str cm^{-1}	Abs.	OCH$_3$ Str. cm^{-1}	Abs.	(C-N) cm^{-1}	Abs.	CH op cm^{-1}	Abs.	CH op cm^{-1}	Abs.	cm^{-1}	Abs.
100	1498	0.0045	1347	0.0080	1266	0.0075	------	------	861	0.0015	842	0.0030	828	0.0010	751	0.0015
87.5	1494	0.0090	1344	0.0078	1266	0.010	1232	0.0005	861	0.0015	840	0.0050	826	0.0015	747	0.0030
75	1494	0.0045	1345	0.0062	1265	0.0070	1232	0.0016	861	0.0012	840	0.0030	828	0.0008	748	0.0015
63.5	1498	0.0050	1343	0.0030	1266	0.0047	1235	0.0044	856	0.0013	840	0.0025	828	0.0008	746	0.0023
50	1498	0.0055	1342	0.0015	1266	0.0032	1235	0.0062	855	0.0001	840	0.0020	825	0.0012	746	0.0027
37.5	1498	0.0070	1342	0.0007	1267	0.0028	1236	0.0070	854	0.0005	840	0.0025	825	0.001	745	0.0025
25	1498	0.009	1342	0.0005	1266	0.0030	1236	0.095	856	0.0005	840	0.0030	823	0.0012	746	0.0040
12.5	1497	0.0060	1340	0.0001	1272	0.0020	1236	0.009	855	0.0005	840	0.0020	827	0.0010	745	0.0030
0:100	1497	0.0050	----	------	1267	0.0028	1236	0.0010			840	0.0025	824	0.0013	746	0.0025

7.3.3 Peak intensities of mixed monolayers of –OCH₃ (1) and C(=NH)NH₂ (4) amphiphiles at different compositions

Amphiphiles	NH₂+OH str		NH₂+=NH str		α,ω–CH₂ asym		CH₂ asym		CH₂ sym		N-C=N asym		(C=C)₁,₄ str	
OCH₃: Amidine	cm⁻¹	Abs.	cm⁻¹	Abs.	cm⁻¹	Abs.	cm⁻¹	Abs.	cm⁻¹	Abs.	cm⁻¹	Abs.	cm⁻¹	Abs.
100	3399	0.001	3090	0.001	2935	0.0040	2917	0.012	2846	0.0047	1690	0.0025	1613	0.0065
87.5	3469	0.001	3105	0.001	2935	0.004	2916	0.016	2848	0.006	1691	0.002	1612	0.008
75	3517	0.001	3172	0.001	2937	0.004	2917	0.013	2849	0.006	1691	0.002	1611	0.0062
63.5	3339	0.001	3147	0.001	2935	0.004	2917	0.011	2849	0.005	1691	0.003	1611	0.008
50	3496	0.0005	3138	0.001	2935	0.004	2916	0.016	2849	0.006	1692	0.003	1612	0.008
37.5	3491	0.0005	3186	0.0015	2936	0.0045	2917	0.012	2847	0.005	1691	0.003	1612	0.010
25	3404	0.001	3134	0.001	2935	0.003	2916	0.011	2847	0.004	1692	0.0025	1612	0.0067
12.5	3285	0.006	3065	0.002	---	-----	2916	0.0022	2846	0.001	----	-----	1610	0.005
0:100	3452	0.001	3069	0.001	2940	0.002	2916	0.008	2848	0.0030	----	-------	1610	0.007

Amphiphiles	C-C str. (OCH₃)		C=C str		C-O-C str		(OCH₃) str.		CH op		C=C str			
OCH₃:ami	cm⁻¹	Abs.	cm⁻¹	Abs.	cm⁻¹	Abs.	cm⁻¹	Abs.	cm⁻¹	Abs.	cm⁻¹	Abs.	cm⁻¹	Abs.
100	1512	0.017	1498	0.006	1270	0.001	1263	0.012	839	0.0022	824	0.0015	743	0.0042
87.5	1512	0.015	1494	0.004	1269	0.0015	1236	0.012	839	0.003	825	0.0012	746	0.0025
75	1512	0.010	1493	0.0025	1271	0.0020	1236	0.0073	838	0.002	824	0.0005	746	0.0020
63.5	1513	0.010	1493	0.002	1272	0.001	1236	0.0074	839	0.0025	826	0.0010	746	0.0025
50	1512	0.010	1493	0.0030	1272	0.002	1236	0.0074	839	0.003	820	0.0007	747	0.0025
37.5	1513	0.0105	1493	0.0040	1268	0.003	1235	0.0072	840	0.0035	827	0.0007	746	0.0032
25	1511	0.0067	1494	0.0035	1268	0.0015	1234	0.0034	840	0.0015	821	0.0002	746	0.0014
12.5	1511	0.0027	1492	0.001	1274	0.0015	1232	0.0018	839	0.0016	817	0.0001	746	0.0012
0:100	1513	0.0020	1493	0.002	1283	0.0015	----	----	840	0.0018				

Table 7.2: IRAS intensities of the mixed monolayers of ω-functionalized –OCH₃ (1) and C(=NH)NH₂ (4) amphiphiles assembled on MHA SAMs.

7.3.4 Peak intensities of mixed monolayers of Biotin and Hydroxide amphiphiles at different compositions

Amphiphiles	NH$_2$+OH str		NH$_2$+=NH str		α,ω–CH$_2$ asym		CH$_2$ asym		CH$_2$ sym		-C=O str.		N-C=N asym		(C=C)$_{1,4}$ str			
Biotin-OH	cm^{-1}	Abs.	cm^{-1}	Abs.	cm^{-1}	Abs.	cm^{-1}	Abs.	cm^{-1}	Abs.	cm^{-1}	Abs.	cm^{-1}	Abs.	cm^{-1}	Abs.	cm^{-1}	Abs.
100	3303	0.0025	3117	0..0020	2935	0.0040	2919	0.0065	2850	0.0025	1726	0.0045	1691	0.0055	1611	0.0055	1514	0.0050
75	3306	0.002	3115	0.002	2935	0.0025	2919	0.0040	2850	0.0018	1733	0.0025	1691	0.0040	1612	0.0055	1513	0.0050
50	3308	0.004	3115	0.0042	2933	0.0055	2919	0.0075	2849	0.0040	1733	0.0055	1691	0.012	1612	0.010	1512	0.0080
25	3273	0.0025	3118	0.0025	2934	0.0030	2919	0.0040	2850	0.0401	1733	0.0029	1691	0.0050	1612	0.0060	1512	0.0055
0	3247	0.0025	3117	0..0025	2933	0.0025	2917	0.0040	2850	0.0012	-----	------	1690	0.0015	1612	0.0047	1512	0.0045

Amphiphiles	C=C str		C-O-C str				CH op	
Biotin: OH	cm^{-1}	Abs.	cm^{-1}	Abs.	cm^{-1}	Abs.	cm^{-1}	Abs.
100	1494	0.0035	1272	0.0025	1049	0.0005	841	0.0025
75	1494	0.0030	1272	0.0020	1046	0.0020	839	0.0025
50	1493	0.006	1272	0.003	1046	0.0042	840	0.0045
25	1494	0.0030	1272	0.002	1048	0.003	838	0.0025
0	1492	0.0025	1272	0.0017	1049	0.0023	839	0.0025

Table 7.3: IRAS intensities of the mixed monolayers of ω-functionalized Biotin and Hydroxy amphiphiles assembled on MHA SAMs.

7.3.5 Peak intensities of mixed monolayers of Biotin and Hydroxide amphiphiles at different compositions (Repeat)

Amphiphiles	NH_2+OH str		$NH_2+=NH$ str		$\alpha,\omega-CH_2$ asym		CH_2 asym		CH_2 sym		-C=O str.		N-C=N asym		$(C=C)_{1,4}$ str			
Biotin: OH	cm^{-1}	Abs.	cm^{-1}	Abs.	cm^{-1}	Abs.	cm^{-1}	Abs.	cm^{-1}	Abs.	cm^{-1}	Abs.	cm^{-1}	Abs.	cm^{-1}	Abs.	cm^{-1}	Abs.
100	3364	0.0030	3231	0..0025	2933	0.0045	2919	0.006	2850	0.0030	1726	0.0055	1693	0.0095	1612	0.0065	1514	0.0052
75	3291	0.0015	3079	0.002	2931	0.0027	2917	0.0052	2848	0.0015	1737	0.0023	1688	0.0030	1610	0.0057	1513	0.0055
50	3329	0.0025	3067	0.0020	2936	0.0020	2917	0.0075	2848	0.0036	1725	0.0060	1691	0.011	1612	0.0071	1513	0.0055
25	3309	0.0015	3114	0.0015	2935	0.0025	2918	0.0045	2851	0.0016	1732	0.0037	1688	0.0062	1612	0.0048	1513	0.0039
0	3312	0.0030	3113	0..0025	2935	0.003	2917	0.0052	2850	0.0025	-----	------	1690	0.0045	1611	0.0060	1513	0.0047

Amphiphiles	C=C str		C-O-C str				CH op	
Biotin: OH	cm^{-1}	Abs.	cm^{-1}	Abs.	cm^{-1}	Abs.	cm^{-1}	Abs.
100	1499	0.0052	1272	0.0037	1074	0.0050	839	0.0030
75	1492	0.0037	1272	0.0050	1048	0.0035	845	0.0037
50	1495	0.005	1271	0.0035	1047	0.0030	840	0.0045
25	1494	0.0023	1273	0.0022	1052	0.0037	839	0.0025
0	1492	0.0027	1272	0.0025	1049	0.0012	841	0.0030

7.3.6 Peak intensities of mixed monolayers of Biotin and Hydroxide amphiphiles after the addition of SA at different compositions

Amphiphiles (%)	NH$_2$+OH str.		NH$_2$+=NH str.		α,ω–CH$_2$ asym.		CH$_2$ asym.		CH$_2$ sym.		-C=O str.		N-C=N asym.		Amide I		Amide I	
Biotin-SA	cm^{-1}	Abs.	cm^{-1}	Abs.	cm^{-1}	Abs.	cm^{-1}	Abs.	cm^{-1}	Abs.	cm^{-1}	Abs.	cm^{-1}	Abs.	cm^{-1}	Abs.	cm^{-1}	Abs.
100	3294	0.0035	3078	0..0017	2937	0.0030	2918	0.0052	2851	0.0018	1718	0.0040	1690	0.0070	1637	0.0042	1673	0.0060
75	3284	0.0030	3074	0.0015	2935	0.0020	2917	0.0033	2850	0.0010	1717	0.0020	1692	0.0042	1641	0.0039	1676	0.0042
50	3303	0.004	3094	0.0020	2934	0.0030	2919	0.0040	2850	0.0014	1733	0.0020	1692	0.057	1640	0.0041	1677	0.0052
25	3286	0.0055	3093	0.0030	2934	0.0040	2919	0.0060	2850	0.0030	1733	0.0045	1691	0.011	1641	0.0075	1671	0.010
0	3298	0.0025	3091	0..0020	2936	0.0020	2917	0.0035	2850	0.0010	------	--------	----	-------	1638	0.001	1662-	0.0012

Amphiphiles (%)	(C=C)$_{1,4}$ Str.		Amide II		C=C str.		C-O-C str.		CH op.	
Biotin: SA	cm^{-1}	Abs.	cm^{-1}	Abs.	cm^{-1}	Abs.	cm^{-1}	Abs.	cm^{-1}	Abs.
100	1613	0.0057	1546	**0.0022**	1498	0.0020	1272	0.0024	838	0.0032
75	1612	**0.0047**	1558	**0.0023**	1493	**0.0020**	1273	0.0025	840	0.0025
50	1612	0.0055	1557	0.0030	1493	0.0030	1272	0.0020	839	0.0030
25	1612	0.009	1556	0.0045	1493	0.0045	1272	0.0025	840	0.0035
0	1611	0.0037	1560	0.0012	1492	0.0012	1272	0.0012	843	0.0024

Table 7.4: IRAS intensities of the mixed monolayers of ω-functionalized Biotin and Hydroxy amphiphiles after addition of SA on MHA SAMs.

7.3.7 Peak intensities of mixed monolayers of Biotin and Hydroxide amphiphiles after the addition of SA at different compositions (Repeat)

Amphiphiles (%)	NH$_2$+OH str		NH$_2$+=NH str		α,ω–CH$_2$ asym		CH$_2$ asym		CH$_2$ sym		-C=O str.		N-C=N asym		Amide I	
Biotin-SA	cm^{-1}	Abs.	cm^{-1}	Abs.	cm^{-1}	Abs.	cm^{-1}	Abs.	cm^{-1}	Abs.	cm^{-1}	Abs.	cm^{-1}	Abs.	cm^{-1}	Abs.
100	3279	0.0025	3071	0..0025			2916	0.0060	2849	0.0022	1728	0.0060	1690	0.0070	1666	0.008
75	3281	0.0025	3095	0.0010	2934	0.0015	2916	0.0050	2848	0.0030	1734	0.0025	1691	0.0060	1677	0.005
50	3273	0.0025	3031	0.0020	2932	0.0020	2917	0.0057	2849	0.0028	1733	0.0022	1692	0.039	1673	0.0045
25	3292	0.0025	3064	0.0020	2934	0.0021	2917	0.0060	2848	0.0030	1733	0.0020	1693	0.0045	1673	0.0065
0	3298	0.0025	3091	0..0020	2939	0.0017	2918	0.0032	2850	0.0010	----------	-	----		1677	0.0008

Amphiphiles (%)	(C=C)$_{1,4}$ str		Amide II		C=C str		C-O-C str		CH op	
Biotin: SA	cm^{-1}	Abs.	cm^{-1}	Abs.	cm^{-1}	Abs.	cm^{-1}	Abs.	cm^{-1}	Abs.
100	1611	0.0060	1557	0.0029	1498	0.0030	1273	0.0030	839	0.0048
75	1612	0.0057	1560	0.0020	1494	0.0035	1271	0.0030	839	0.0027
50	1611	0.0062	1560	0.0020	1498	0.0040	1270	0.0035	839	0.0035
25	1612	0.0065	1575	0.0030	1497	0.0035	1271	0.0035	839	0.0035
0	1611	0.0045	1558	0.001	1493	0.0025	1273	0.0033	842	0.0015

7.3.8 Peak intensities of amineamidines

Amphiphile	NH$_2$+OH str		NH$_2$+=NH str		CH$_2$ asym		CH$_2$ sym		N-C=N asym		(C=C)$_{1,4}$ str		C=C str		C-O-C str		CH op	
	cm^{-1}	Abs.	cm^{-1}	Abs.	cm^{-1}	Abs.	cm^{-1}	Abs.	cm^{-1}	Abs.	cm^{-1}	Abs.	cm^{-1}	Abs.	cm^{-1}	Abs.	cm^{-1}	Abs.
NONA	3396	0.01	3154	0.007	2919	0.032	2848	0.015	1682	0.005	1609	0.087	1482	0.015	1278	0.035	834	0.034
DECA	3307	0.01	3141	0.010	2917	0.032	2848	0.015	1695	0.007	1614	0.038	1498	0.020	1263	0.003	831	0.0080
DODECA	3300	0.0008	3121	0.009	2917	0.010	2846	0.005			1612	0.0045	1496	0.0025	1273	0.002	832	0.0010

Table 7.5 IRAS intensities of the amineamidines.

7.4 Ellipsometric Δ and Ψ values of the assembled amphiphiles on acid terminated SAMs

7.4.1 Single component amphiphiles

Amphiphiles	Molecular length (Å)	Δ_{start} (°)	Ψ_{start} (°)	Δ_{end} (°)	Ψ_{end} (°)	Layer thickness (Å)
-OCH$_3$ (1)	24	105.710 ± 0.010	44.1434 ± 0.005	102.9893 ± 0.009	44.0388 ± 0.006	24
NO$_2$ (2)	24	106.437 ± 0.002	44.1719 ± 0.003	103.627 ± 0.006	44.1017 ± 0.001	26
CH$_3$ (3)	25	106.485 ± 0.010	44.198 ± 0.007	103.6326 ± 0.015	44.127 ± 0.013	23
Amidine (4)	25	106.0038 ± 0.008	44.2001 ± 0.002	103.3839 ± 0.006	44.1099 ± 0.005	24
MHA	21	106.092 ± 0.010	44.03 ± 0.003	104.047 ± 0.003	44.127 ± 0.006	20

Table 7.6 Ellipsometric Δ and Ψ values for single component amphiphiles.

7.4.2 Mixed amphiphiles

Amphiphiles -OCH$_3$ (1): NO$_2$ (2) %	Molecular length (Å)	Δ_{start} (°)	Ψ_{start} (°)	Δ_{end} (°)	Ψ_{end} (°)	Layer thickness (Å)
100	24	105.710 ± 0.010	44.1434 ± 0.005	102.9893 ± 0.009	44.0388 ± 0.006	24
75	----	105.854 ± 0.002	44.2104 ± 0.003	103.417 ± 0.006	44.1217 ± 0.001	25
50	----	105.682 ± 0.010	44.1875 ± 0.007	103.2146 ± 0.015	44.0750 ± 0.013	23
25	**----**	107.7250 ± 0.008	44.1502 ± 0.002	103.1347 ± 0.006	44.0799 ± 0.05	26
0	24	106.437 ± 0.002	44.1719 ± 0.003	103.627 ± 0.006	44.1017 ± 0.001	26

Ellipsometric Δ and Ψ values for mixed component amphiphiles.

Amphiphiles	Molecular length (Å)	Δ_{start} (°)	Ψ_{start} (°)	Δ_{end} (°)	Ψ_{end} (°)	Layer thickness (Å)
Biotin	32	103.3072 ± 0.012	42.4121 ± 0.009	100.4708 ± 0.006	42.3172 ± 0.007	34
-OH	28	103.5383 ± 0.002	42.4306 ± 0.003	101.0166 ± 0.006	42.6724 ± 0.011	27

7.5 Atomic Force Microscopy

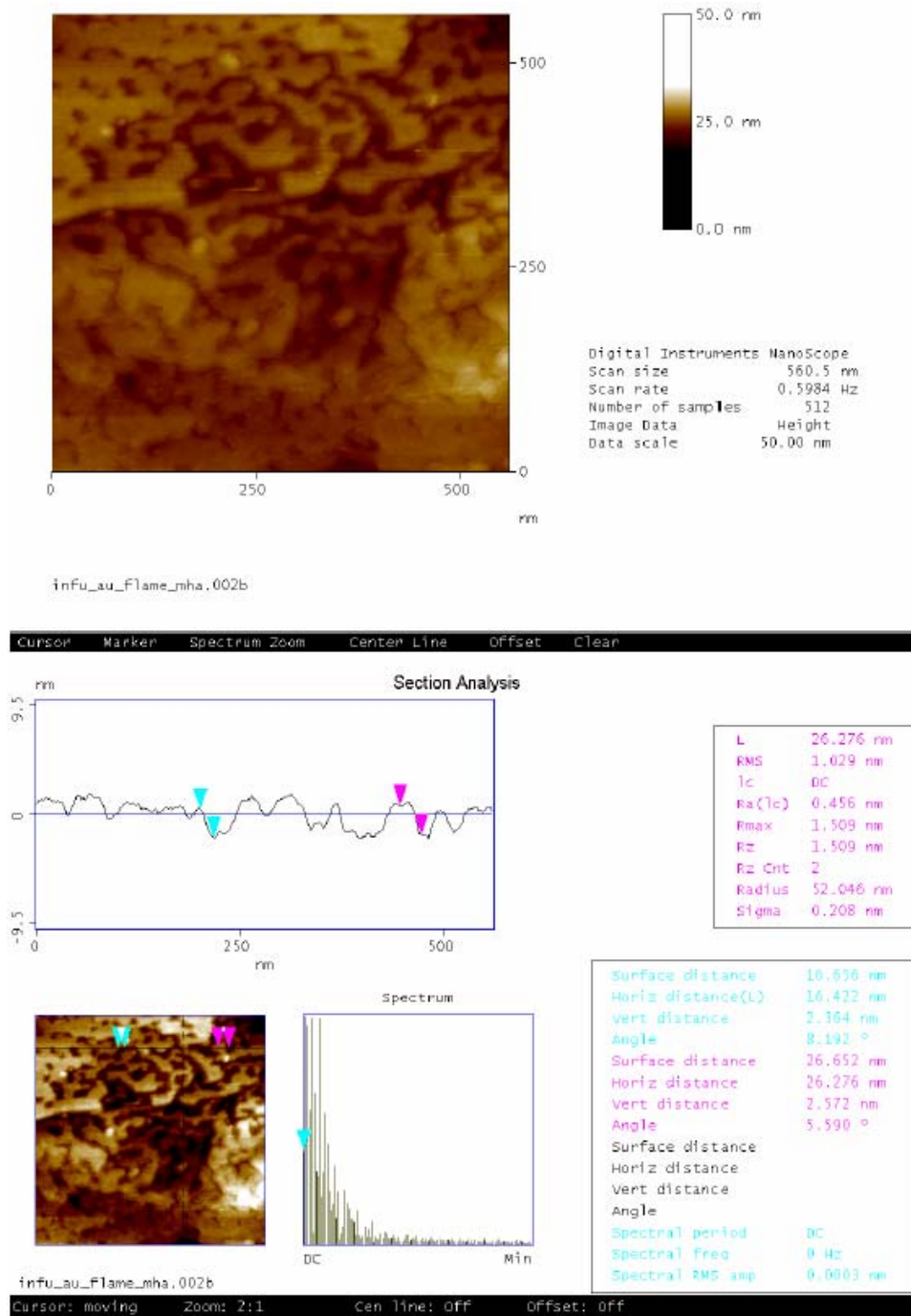### 7.5.1 AFM of MHA SAMs

Figure 7.1: AFM image of mercaptahexadecanoic acid (MHA) terminated SAMs on annealed gold surface at pH 9.

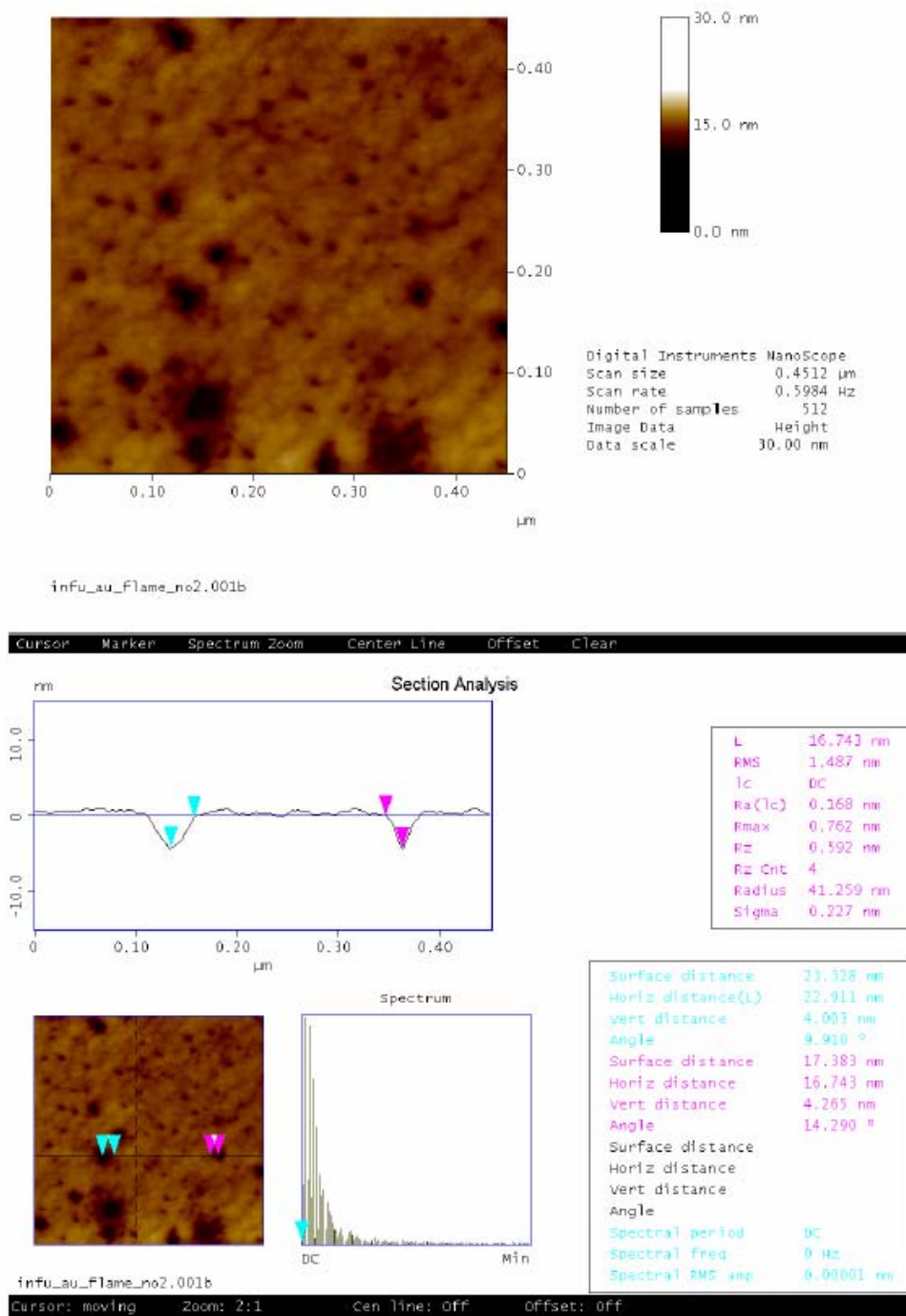### 7.5.2 AFM of -NO₂ amphiphilic SAMs on acid functionalized surface

Figure 7.2: AFM image of –NO₂ (2) amphiphile immobilized SAMs on mercaptohexadecanoic acid surface at pH 9.
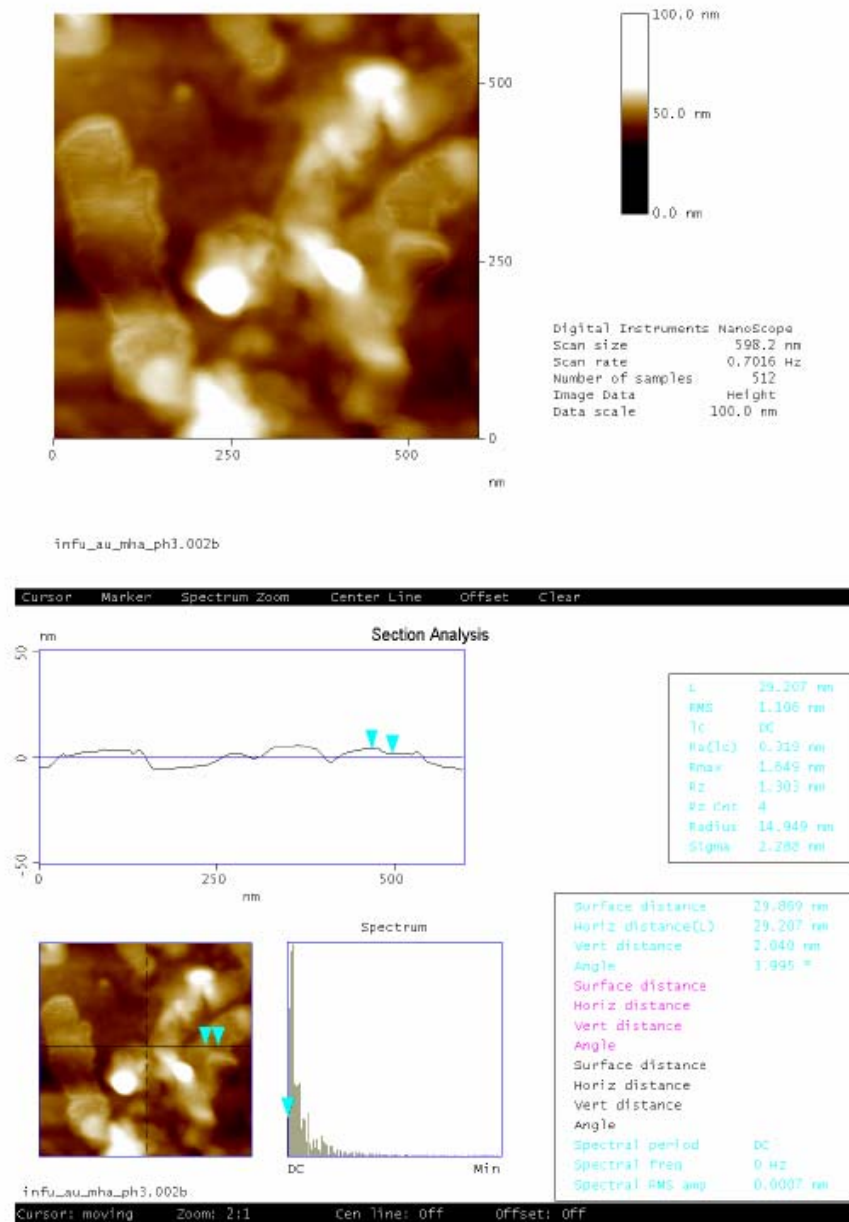
7.5.3 AFM of acid functionalized surface at pH 3

Figure 7.3: AFM image -NO$_2$ SAMs after PH 3 treatment.

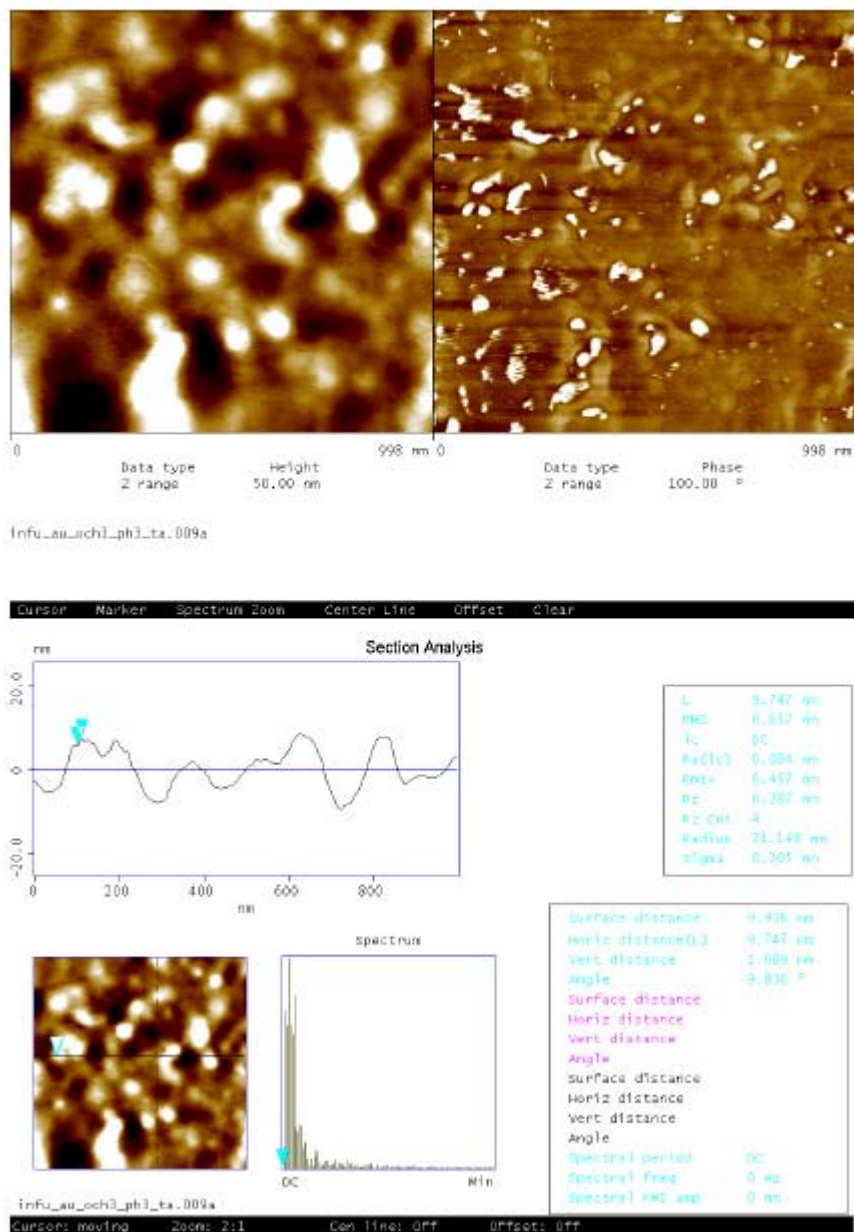### 7.5.4 AFM of –OCH$_3$ SAMs on acid functionalized surface at pH 3

Figure 7.4: image of –OCH$_3$ (1) amphiphile immobilized SAMs on mercaptohexadecanoic acid surface ftert pH 3.treatment